UNIVERSIDADE ESTADUAL DE CAMPINAS
FACULDADE DE ENGENHARIA QUÍMICA

ÁREA DE CONCENTRAÇÃO
DESENVOLVIMENTO DE PROCESSOS QUÍMICOS

Desenvolvimento e Avaliação de Microreatores: Aplicação para Produção de Biodiesel

AUTOR: EDGAR LEONARDO MARTÍNEZ ARIAS
ORIENTADOR: Prof. Dr. RUBENS MACIEL FILHO

Dissertação de Mestrado apresentada à Faculdade de Engenharia Química como parte dos requisitos exigidos para obtenção do titulo de Mestre em Engenharia Química.

Campinas - São Paulo
Julho de 2010

FICHA CATALOGRÁFICA ELABORADA PELA
BIBLIOTECA DA ÁREA DE ENGENHARIA E ARQUITETURA - BAE - UNICAMP

M366d

Martínez Arias, Edgar Leonardo
Desenvolvimento e avaliação de microreatores: aplicação para produção de biodiesel / Edgar Leonardo Martínez Arias. --Campinas, SP: [s.n.], 2010.

Orientador: Rubens Maciel Filho.
Dissertação de Mestrado - Universidade Estadual de Campinas, Faculdade de Engenharia Química.

1. Processos químicos. 2. Reatores químicos. 3. Biodiesel. 4. Fluidodinâmica computacional. 5. Espectroscopia no infravermelho próximo. I. Maciel Filho, Rubens. II. Universidade Estadual de Campinas. Faculdade de Engenharia Química. III. Título.

Título em Inglês: Development and assessment of microreactors applied to biodiesel production
Palavras-chave em Inglês: Chemical processes, Chemical reactors, Biodiesel, Computational fluid dynamics, Near-infrared spectroscopy
Área de concentração: Desenvolvimento de Processos Químicos
Titulação: Mestre em Engenharia Química
Banca examinadora: Luiz Otávio Saraiva Ferreira, Izaque Alves Maia
Data da defesa: 29/07/2010
Programa de Pós Graduação: Engenharia Química

Dissertação de Mestrado defendida por Edgar Leonardo Martínez Arias e aprovada em 29 de Julho de 2010 pela banca examinadora constituída pelos doutores:

Prof. Dr. Rubens Maciel Filho – Orientador

Prof. Dr. Luiz Otávio Saraiva Ferreira – FEM/UNICAMP

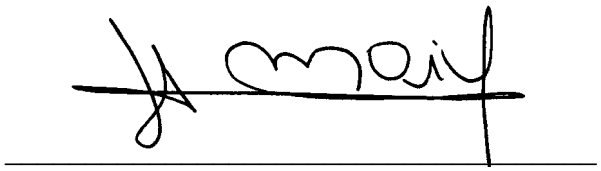

Dr. Izaque Alves Maia – CTI Renato Archer

Este exemplar corresponde à versão final da Dissertação de Mestrado em Engenharia Química

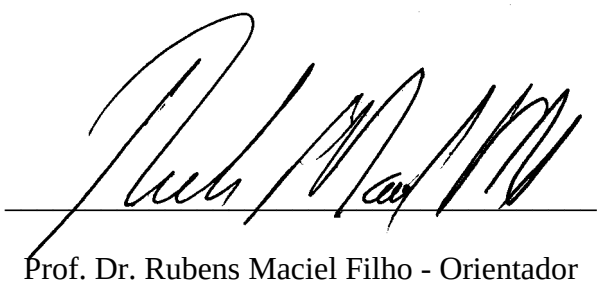

Prof. Dr. Rubens Maciel Filho - Orientador

Dedicada a minha família:

Rosa Ines Arias

Luis Daniel Martínez Lopez

Ronald Ricardo Martínez Arias

Agradecimentos

É um grande prazer para mim, reconhecer todas as pessoas que me ajudaram direta ou indiretamente na realização desta dissertação. Em primeiro lugar, gostaria de expressar minha profunda gratidão à minha família, Luis Daniel Martínez Lopez, Rosa Ines Arias e Ronald Ricardo Martínez Arias, por me apoiar na busca da minha superação pessoal. Apesar da distância, seus conselhos, motivação e amor sempre foram minha força para seguir adiante sem importar com todas as dificuldades.

Estou também grato ao meu orientador Dr. Prof. Rubens Maciel Filho, por me dar a oportunidade de trabalhar no seu grupo de investigação LOPCA. Estou muito grato por suas idéias, conselhos, incentivo e liberdade para o trabalho, o que me permitiu explorar novas idéias e finalizar este trabalho a tempo. Gostaria também de agradecer ao Dr. André Luiz Jardini Munhoz, de grande ajuda, estímulo e orientação durante o desenvolvimento da investigação. Sou grato a ambos pelo compartilhamento de idéias em várias questões, tais como elaboração de relatórios, planejamento de experimentos, etc., todas estas experiências me ajudaram a desenvolver minhas habilidades pessoais.

Agradeço também aos membros da comissão julgadora, Prof. Dr. Luiz Otávio Saraiva Ferreira, Dr. Izaque Alves Maia e o Dr. José Alberto Fracassi da Silva, por avaliar meu trabalho, suas considerações finais foram muito apreciadas.

Agradeço aos meus colegas do grupo de investigação LOPCA pela amizade e o suporte em questões acadêmicas e pessoais. Meu agradecimento especial a Arturo González Quiroga, Melvin Duran, Laura Plazas, Jeffrey Leon Pulido, Sergio Andres Villalva e Pablo Andres Alvarez, pela fundamental assistência na conclusão do meu trabalho. Eu sempre olhei para eles como uma espécie de critério para avaliar o meu próprio desempenho, minha motivação em muitos momentos foi inspirada pelo exemplo de trabalho duro e dedicação que me transmitiram. Obrigado pela agradável companhia, não me esquecerei das enriquecedoras conversas, especialmente na hora do café da manhã.

Desejo expressar meus mais queridos sentimentos a Patrícia Fazzio Martins, por sua orientação, paciência, ajuda, inestimável apoio e inspiração no final do meu projeto, sempre foi e será uma parte muito importante do meu sucesso e da minha vida.

Eu estou profundamente grato por ter tido excelentes colegas de quarto durante minha estadia na moradia Luis Enrique de Lima, Welington de Souza Filho, Kassio de Lima, Wellinton e Eduardo, pela amizade e confiança

Meus sinceros agradecimentos à Prof. Dr. Lucila e Dr. Luiz Gutierrez do Laboratório de Ótica da UNICAMP pela ajuda na fase inicial da construção dos microreatores. Também ao Sr. Angelo Bobbi e Maria Elena do Laboratório de Microfabricação do Laboratório Nacional de Luz Síncrotron (LNLS) pela assistência experimental e discussões frutíferas, além da experiência na construção de microdispositivos, sem a qual não teria sido possível concluir o trabalho.

Finalmente, eu gostaria de deixar meu profundo agradecimento à Fundação de Amparo à Pesquisa do Estado de São Paulo (FAPESP) pelo apoio financeiro.

Isto não é o fim.

Não é sequer o princípio do fim.

Mas é, talvez, o fim do princípio.

……. Winston Churchill

Resumo

A tecnologia da microreação é um importante método de intensificação de processos que oferece numerosos benefícios para a indústria de processos químicos. A elevada razão área superficial-volume aumenta as taxas de transferência de massa e energia, melhorando a eficiência e o desempenho dos reatores, e permitindo um aumento na segurança resultante do baixo *hold-up* em comparação com o reator convencional. O fluxo de líquidos imiscíveis nos microreatores tem mostrado uma intensificação da transferência de massa através da aplicação de estruturas internas que servem como misturadores passivos, o que aumenta a difusão e, conseqüentemente, aumenta a taxa de reação observada.

Nesta dissertação, destaca-se o estudo da hidrodinâmica e da influência dos parâmetros de reação na intensificação da produção contínua de biodiesel em três microreatores com configurações diferentes, através de técnicas experimentais e computacionais. Experimentos foram realizados para caracterizar o óleo de mamona como potencial matéria prima para a produção de biodiesel. Testes reológicos, calorimetria diferencial de varredura (DSC), termogravimetria (TG/DTG) e cromatografia gasosa foram utilizados para determinar as propriedades físicas e químicas do óleo vegetal.

Cromatografia de exclusão de tamanho (HPLC/SEC) foi utilizada para avaliar as diferentes variáveis que afetam a reação de transesterificação de óleo de mamona com etanol anidro tendo o hidróxido de sódio como catalisador em um reator em batelada. O efeito da temperatura, razão molar álcool/óleo, concentração de catalisador e tempo de reação foram analisados, observando a variação da composição do meio de reação. Um modelo matemático foi aplicado para descrever a cinética química de transesterificação.

Tecnologias de microfabricação convencionais, tais como fotolitografia e litografia macia foram aplicadas na fabricação de microreatores utilizando fotorresiste SU-8 e polidimetilsiloxano (PDMS). Várias dificuldades no processamento do fotorresiste SU-8 para obter estruturas complexas através do processo de fotolitografia foram discutidas. No processo de litografia macia o molde foi fabricado com base em técnicas de fotolitografia, onde o fotorresiste SU-8 foi usado para construir a estrutura dos moldes dos microreatores.

Experimentos foram realizados para a análise da influência da geometria do microreator. Três diferentes estruturas foram construídas: T, Omega e Tesla. A mistura

dentro dos microreatores para baixos números de Reynolds foi avaliada mediante procedimentos experimentais e simulações de dinâmica de fluidos (CFD). A caracterização qualitativa da mistura foi realizada através da observação da evolução da mistura do óleo de mamona/etanol para diferentes razões de fluxo com base na taxa de transferência de um corante solvatocrômico entre os dois líquidos imiscíveis. Além disso, mediante simulações CFD foi possível caracterizar as circulações internas e capturar o mecanismo de geração de mistura, melhorando a compreensão dos resultados obtidos experimentalmente.

Finalmente, a produção contínua de biodiesel foi estudada nos microreatores, a fim de avaliar a influência de parâmetros tais como: geometria, massa de catalisador, temperatura de reação, razão molar etanol/óleo e tempo de residência no rendimento da reação. Os resultados obtidos mostraram que o microreator Tesla exibiu maior mistura e alta conversão para baixos números de Reynolds em comparação com os microreatores T e Omega. Uma conversão de etil ésteres de aproximadamente 98,9% foi obtida no microreator Tesla, enquanto, para os microreatores T e Omega a conversão foi ao redor de 79,1% e 96,2%, respectivamente. Além disso, uma fibra óptica conectada ao espectrômetro portátil no infravermelho próximo foi utilizada para avaliar a possibilidade do monitoramento *on-line* da reação de transesterificação.

Palavras chave: Intensificação de Processos, Microreator, Biodiesel, Fluidodinâmica Computacional, Espectroscopia no Infravermelho Próximo.

Abstract

Microreactor technology is an important method of process intensification which offers potential benefits to the chemical process industries due to the well-defined high specific interfacial area available for heat and mass transfer, which increases transfer rates, improves efficiency and reactor performance, and enhances safety resulting from low hold-ups when compared to the conventional reactors. The immiscible liquid-liquid two-phase flow has shown a better intensifying of mass transfer through application of internal structures that serve as passive mixers in microreactors, which enhances diffusive penetration and consequently increases the reaction rates observed.

The present work highlights the hydrodynamics and the influence of process parameters in the intensification of the continuous biodiesel production using an alkaline catalyst in three different microreactors through complementary experimental and computational techniques. Initially, experiments were carried out to characterize the castor oil as potential feedstock for biodiesel production. Rheological test, differential scanning calorimetry (DSC), thermogravimetric analysis (TG/DTG) and gas chromatography were performed.

Size-exclusion chromatography (SEC) was used to evaluate the different variables that affect the transesterification reaction of castor oil with anhydrous ethanol and sodium hydroxide as catalyst in a jacketed glass batch reactor. The effects of temperature, ethanol/castor oil molar ratio, catalyst concentration, and reaction time were analyzed by observing the variation of the reaction medium composition. A mathematical model was applied to describe chemical kinetic of transesterification based on the reversible mechanism of the reactions.

Traditional micromanufacturing technology such as photolithography and soft lithography using SU-8 photoresist and polydimethylsiloxane (PDMS) respectively were employed for fabrication of microreactors. Several difficulties of SU-8 processing to obtain complex structures through the photolithography process have been discussed. In the soft lithography process the mold was fabricated based on photolithography techniques, and SU-8 photoresist was used to construct microreactor structure templates.

Experiments were carried out to allow an examination of the influence of reactor path geometry. Three different templates were applied for evaluation: T-, Omega, and

Tesla-shaped microreactors. The mixing inside of microreactors at low Reynolds number was evaluated with experimental procedures and computational fluid dynamics simulations (CFD). A qualitative characterization of the mixing was firstly carried out by observing the mixture evolution of castor oil/ethanol at different rate flow ratios on basis of the transfer of a solvatochromatic dye between the two immiscible fluids. In addition, CFD methodologies were developed to characterize internal circulations and to capture the generation mixing mechanism without chemical reaction, improved the understanding of immiscible ethanol/castor oil system.

Finally, continuous biodiesel production was studied in the microreactors in order to evaluate the influence of the geometrical parameters, catalyst amount, reaction temperature, molar ratio ethanol to oil, and residence time on performance of the reaction. The Tesla-Shaped microreactor exhibited higher conversions at low Reynolds number when compared with T- and Omega-shaped microreactors. Ethyl ester conversion was about 98.9% in Tesla-shaped microreactor, whereas for T- and Omega-shaped microreactor it was only about 79.1% and 96.2% respectively. On the other hand, fiber-optic near infrared spectroscopy was used to evaluate the possibility of monitoring quantitatively the transesterification reaction on-line.

Keywords: Process Intensification, Microreactors, Biodiesel, Computational Fluid Dynamics, Near Infrared Spectroscopy.

Sumário

Nomenclatura

Grupos Adimensionais

Re Número de Reynolds

We Número de Weber

Ca Número de Capilaridade

Latinas

c_p Capacidade calorífica

d_H Diâmetro hidráulico

D Coeficiente de difusão

Ea Energia de ativação

k_i Taxa de reação *i*

n Razão molar triglicerídeos/álcool

p Razão molar catalisador/álcool

R Constante universal dos gases

S_i Seletividade do componente *i*

T Temperatura

t Tempo

t_R Tempo de residência

u Velocidade media

x_i Conversão do componente *i*

Gregas

ρ Densidade

γ Taxa de cisalhamento

μ Viscosidade dinâmica

τ Tensão de cisalhamento

τ_d Tempo de difusão

σ Tensão de superficial, Tensão interfacial

Acrônimos

A	Sabão
DG	Diglicerídeos
E	Etil Ésteres
G	Glicerol
MG	Monoglicerídeos
ROH	Álcool
TG	Triglicerídeos
W	Água

Abreviaturas

CAD	Desenho assistido por computador
CCD	Câmera Digital de Alta Velocidade
CFD	Fluidodinâmica Computacional
CG	Cromatografia Gasosa
DSC	Calorimetria Diferencial de Varredura
FAME	Ésteres Metílico de Ácidos Graxos
FAPESP	Fundação de Amparo à Pesquisa do Estado de São Paulo
FFA	Ácidos graxos livres
LMA	Lei de ação de massas
LNLS	Laboratório Nacional de Luz Síncrotron
MEMS	Sistemas Micro-Eletro-Mecânicos
MEV	Microscopia Eletrônica de Varredura
NIR	Espectroscopia no infravermelho próximo
PDF	Função de distribuição de probabilidade
PDMS	Polidimetilsiloxano
SEC	Cromatografia de Exclusão de Tamanho
SEE	Erro Padrão
SU-8	Fotorresiste
TG	Termogravimetria

Capítulo 1.

Síntese da Investigação

1.1. Introdução

Na atualidade, os métodos para a obtenção de diversos produtos na indústria química e farmacêutica, como na engenharia de processos estão sendo direcionados ao desenvolvimento de processos químicos capazes de responder às variáveis necessidades dos processos relacionados, satisfazendo as crescentes exigências do mercado, as propriedades do produto requerido, diminuindo o impacto ambiental e custos de produção, procurando manter desta forma um equilíbrio sustentável. Entre os contextos de sustentabilidade, vêm ganhando espaço o conceito da intensificação de processos, sendo este um caminho promissório para o futuro das substâncias químicas e engenharia de processos. A intensificação de processo é caracterizada pelo uso de equipamentos modernos baseados em princípios científicos e métodos de produção novos, empregando, entre outros, equipamentos de tamanho reduzido que vão desde os milímetros aos micrometros os quais são construídos mediante métodos de microengenharia ou engenharia de precisão. Isto permite a substituição de grandes equipamentos com uso excessivo de energia, por plantas de menor tamanho e custo, mais eficientes, minimizando o impacto ambiental, promovendo segurança e controle, melhorando a automatização e ainda promovendo o acoplamento de varias operações em um único dispositivo, reduzindo o número de unidades requeridas. Porém, a intensificação de processo oferece oportunidade de tornar o sector mais ágil, acelerando a resposta às mudanças do mercado, facilitando o escalamento e fornecendo a base para um rápido desenvolvimento de novos produtos e processos.

Contudo, no desenvolvimento destes novos processos é importante obter uma compreensão suficiente dos fenômenos físicos e químicos, e sua interação ocorrendo na microescala. Com isto, sua quantificação leva à identificação das limitantes na intensificação do processo. Entre estes fenômenos encontram-se:

- O mecanismo químico da reação, o qual inclui a determinação dos produtos intermediários e o passo limitante da reação.

- A resistência à transferência de massa no local onde ocorre a reação, o qual pode influenciar significativamente a taxa de reação.
- Adequada descrição dos efeitos fluidodinâmicos, o qual muitas vezes é desprezado na modelagem de reatores. Pressupostos de "fluxo pistão" ou "perfeitamente misturado" são comuns e simplificam tremendamente os cálculos. Atualmente, o calculo dos perfis de fluxo esta começando a se tomar mais comuns na literatura devido ao avanço da tecnologia computacional, mas ainda é dificultada por o excessivo tempo requerido.
- O comportamento das fases em reações multifásicas. Vários sistemas de reação ocorrem em ambientes de múltiplas fases ou forma produtos que existem em diferentes fases e o entendimento de como as espécies se distribuem entre as fases é um elemento chave e com freqüência uma das mais difíceis de obter no desenvolvimento de novos processos.

A abordagem hierárquica, muitas vezes referida como "Modelagem Multiescala", é utilizada para estruturar a interação entre os diversos fenômenos do processo, como apresentado na figura 1.1.

Figura 1.1. Representação esquemática da Modelagem Multiescala

Considerando o processo de produção de biodiesel, de atual importância econômica no Brasil, a transesterificação de óleo vegetal ou gordura animal com álcool usando catalisador alcalino é o método convencional para obtenção do biodiesel. Devido que o álcool e o óleo vegetal são imiscíveis, considerável agitação é requerida para promover a transferência de massa entre as fases. Durante a transesterificação, a mistura reacionante passa de um sistema de duas fases (álcool/óleo) a uma emulsão e finalmente a um sistema de duas fases (alkil-éteres/glicerol). Estas transições de fase afetam a cinética e o equilíbrio das reações e resultam críticas para a produção do biodiesel dentro dos padrões para seu uso como combustível.

É por isto que muitas tecnologias novas estão sendo desenvolvidas na indústria, motivadas pela melhora no processo, aumento na segurança, reduções no consumo de energia, maior preocupação ambiental e até mesmo redução de custos de produção. Embora a comercialização do biodiesel esteja bem sedimentada, o processo ainda apresenta vários problemas, tais como reações incompletas, formação de emulsões, isolamento e purificação de produtos, além da especificação de rigorosos padrões de qualidade que força à indústria do biodiesel na busca de novos processos físicos e químicos que melhore a tecnologia existente. Assim, a intensificação de processos apresenta-se como um caminho promissor para o estudo e otimização da síntese de biocombustíveis como o biodiesel, em especial com o uso de microreatores os quais permitem uma eficiente transferência de massa e energia o que leva a uma redução nos tempos de reação, controle de processos mais precisos, alta reprodutibilidade e melhoramento na seletividade da reação.

1.2. Objetivos

O objetivo principal desta dissertação é estudar a síntese de biodiesel do óleo de mamona usando microreatores com diferentes geometrias. A fim de avaliar os efeitos da transferência de massa, a influência das variáveis de operação e a influencia da geometria no rendimento da reação, uma serie de técnicas experimentais e computacionais foram usadas dentro de uma seqüência lógica de procedimentos. As etapas e subetapas no desenvolvimento do trabalho são:

Caracterização do Óleo de Mamona

- Estudo da variação das propriedades físico-químicas do óleo de mamona com a temperatura.
- Comportamento reológico do óleo de mamona a diferentes taxas de cisalhamento e temperaturas.
- Determinação da composição de ácidos graxos, teor de umidade e acidez do óleo vegetal.

Construção do Microreator

- Aplicação das técnicas de microfabricação na construção de microreatores com diferentes geometrias.

- Estudo das variáveis do processo que influenciam na elaboração dos dispositivos microfluídicos.
- Comparação das vantagens e desvantagens entre as diferentes técnicas de microfabricação.

Fluidodinâmica

- Entendimento do comportamento fluidodinâmico da mistura etanol/óleo de mamona dentro dos microcanais.
- Avaliação da influencia da geometria na mistura mediante técnicas experimentais e computacionais.

Síntese de Biodiesel do Óleo de Mamona

- Estudo das condições ótimas na reação de transesterificação via catálise básica, em um reator batelada na escala laboratorial.
- Determinação do modelo cinético da reação de transesterificação que permita a análise das variáveis que afetam o rendimento da reação.
- Avaliação da reação de transesterificação do óleo de mamona em um microreator com diferentes geometrias em função das principais variáveis de reação.
- Comparação do rendimento da reação entre o reator batelada e o microreator a fim de avaliar os efeitos da transferência de massa.
- Examinar a possibilidade do monitoramento em tempo real da reação de transesterificação dentro dos microreatores mediante o uso de espectroscopia no infravermelho próximo usando fibra ótica.

1.3. Metodologia

A metodologia utilizada neste trabalho (Figura 1.2) consta de uma parte experimental e outra parte de modelagem computacional. Além disso, esta pode ser dividida em quatro seções: caracterização do óleo vegetal, construção do microreator, microfluidodinâmica e síntese de biodiesel. Portanto, as metodologias aplicadas e suas contribuições na dissertação são como segue:

Na caracterização do óleo de mamona, análises térmicas e reológicas foram realizadas para investigar o efeito da temperatura sobre as propriedades físico-químicas do óleo. Os estudos reológicos foram realizados para determinar o comportamento mecânico

do óleo vegetal mediante o monitoramento da variação da tensão de cisalhamento a diferentes taxas de cisalhamento. Uma correlação empírica foi usada para descrever a variação da viscosidade dinâmica com a temperatura, onde as constantes foram ajustadas com os dados experimentais. As análises térmicas no calorímetro diferencial de varredura (DSC) e no analisador termogravimétrico (TG/DTG) permitiram avaliar a capacidade calorífica (Cp), temperatura de decomposição e entalpia do óleo vegetal. A composição do óleo foi obtida mediante a análise dos ácidos graxos no cromatógrafo gasoso (CG).

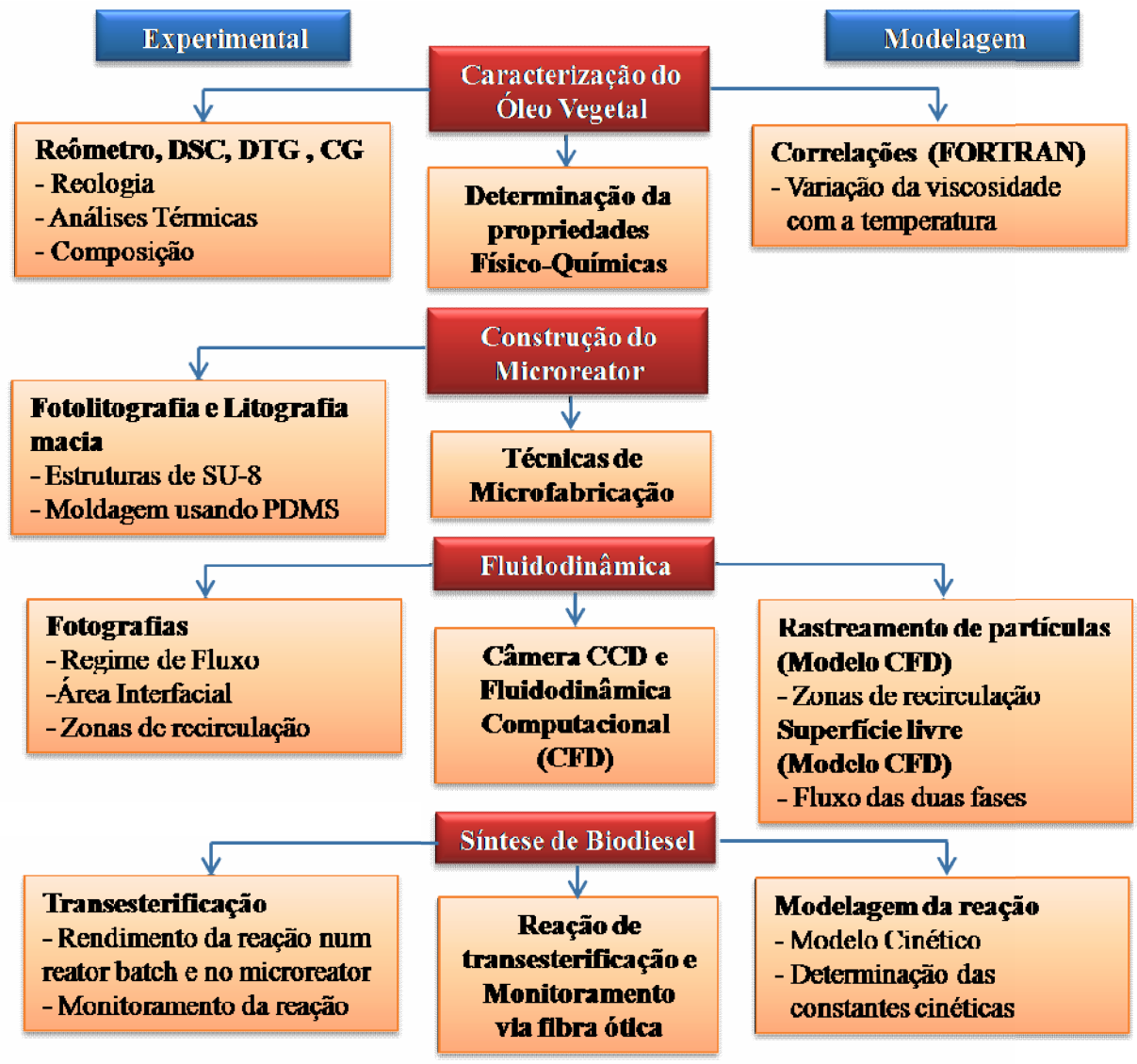

Figura 1.2. Metodologia e contribuições da dissertação

Na construção dos microreatores, técnicas de microfabricação como Fotolitografia e Litografia macia, "*Soft Lithography*" em inglês, foram usadas para a elaboração dos

microreatores. As variáveis do processo fotolitográfico como velocidade e tempo de rotação do *spinner*, tempos de aquecimento, exposição e revelação foram ajustadas para as dimensões desejadas. As dimensões dos microcanais feitos em sua totalidade da resina SU-8 ou PDMS foram caracterizados mediante microscopia eletrônica de varredura (MEV). Os inconvenientes na obtenção das microestruturas são brevemente discutidos, assim com as vantagens e desvantagens no uso do SU-8 e PDMS.

Para o estudo fluidodinâmico dentro dos microreatores, fotografias foram tomadas com uma câmera CCD de alta velocidade com o objetivo de investigar o regime de fluxo nos microcanais e identificar as zonas de recirculação do sistema bifásico óleo de mamona-etanol sem reação química. Os experimentos foram realizados nos microreatores com diferentes geometrias e diferentes razões de fluxo. Além disso, as fotografias foram usadas para investigar a área interfacial e o contato entre as fases. O tratamento das imagens foi realizado mediante métodos computacionais para obter uma estimativa da concentração ao longo do microreator. As zonas de recirculação interna que surgem devido ao cisalhamento entre as paredes do microcanal e a fase contínua foram caracterizadas usando simulações de fluidodinâmica computacional (*Computational Fluid Dynamic* - CFD).

Por ultimo, a síntese de biodiesel de mamona foi realizada de modo convencional (reator de batelada) e em um microreator. O monitoramento dos produtos da reação foi feita mediante cromatografia de permeação em gel (*Gel Permeation Chromatography* - GPC) e o rendimento da reação foi determinada. Uma comparação entre o processo convencional e o microreator foi realizada. Os efeitos da geometria do canal, o tempo de residência, razão óleo-etanol, massa de catalisador e temperatura foram estudados. Finalmente, a possibilidade do monitoramento da reação "*on-line*" foi avaliada mediante espectrometria no infravermelho próximo usando fibra ótica.

1.4. Organização da Dissertação

As contribuições da dissertação estão estruturadas em dez capítulos como se apresenta na Figura 1.3. Em alguns casos, os resultados obtidos em um capítulo são apresentados num outro capítulo e vise versa, em especial entre a parte experimental e modelagem, para sua direta comparação. Finalmente, a síntese de todas as contribuições da dissertação é resumida no Capítulo 10. Cada capítulo é subdividido em quatro partes: a introdução contendo uma breve descrição do tópico em particular e uma curta revisão da

literatura, a metodologia, os resultados e discussões, e finalmente as conclusões do capítulo. Detalha-se a seguir o conteúdo de cada capítulo.

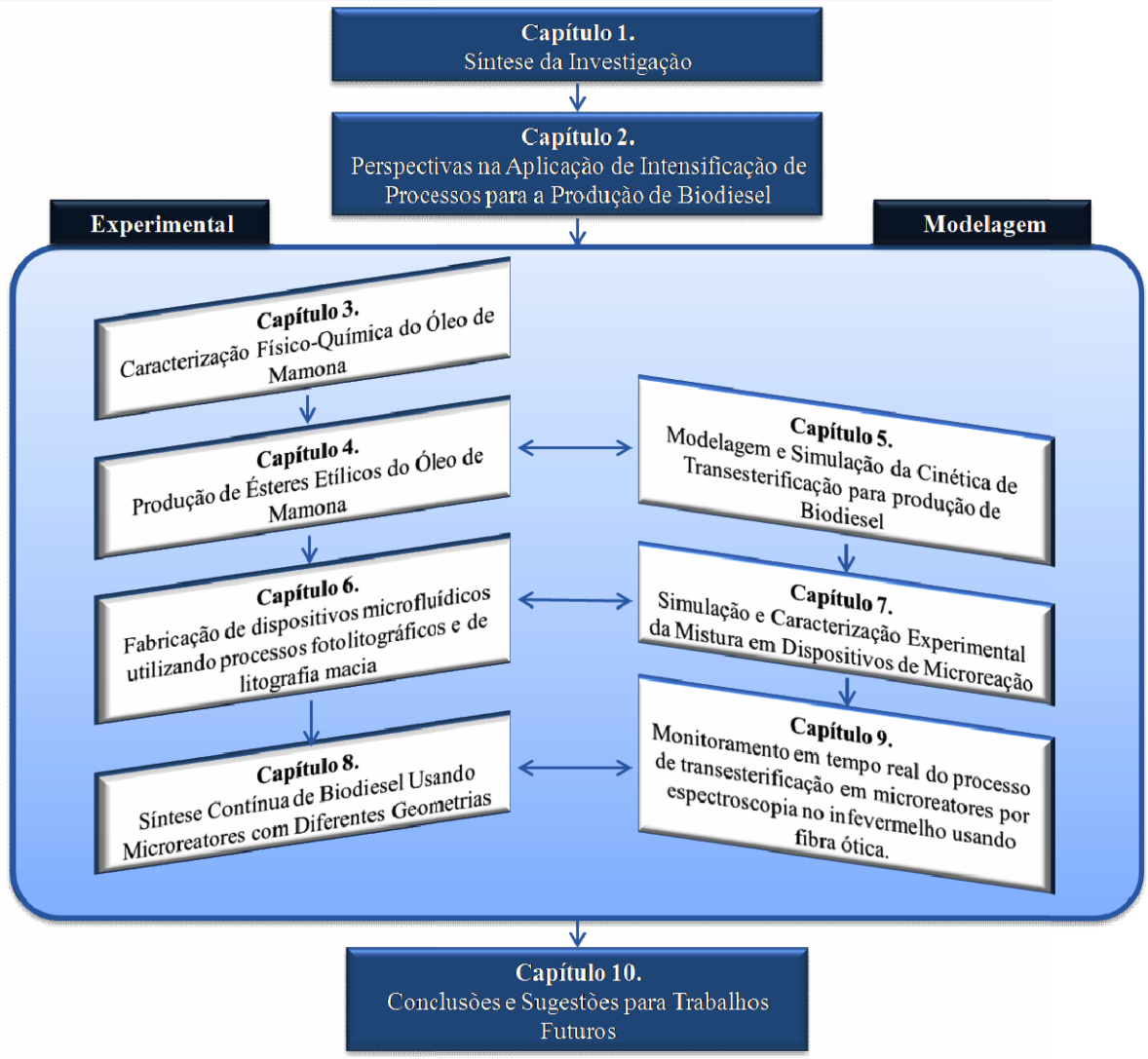

Figura 1.3. Organização da Dissertação

Capítulo 2: Apresenta-se uma revisão bibliográfica dos principais tópicos a serem tratados nesta dissertação. Discutem-se os conceitos da intensificação de processos, em particular no campo da tecnologia de microreação e as fundamentais vantagens dos microreatores, assim como seus benefícios no desenvolvimento de novos processos e dispositivos de análise. Uma breve discussão dos micromisturadores e seus mecanismos de mistura são também apresentados. Faz parte ainda do capítulo o estado atual da arte do biodiesel como a química do processo, matérias primas, tipos de catalisador e métodos de produção.

Capítulo 3: A caracterização físico-química do óleo de mamona é apresentada. Análises térmicas mediante o uso de calorimetria diferencial de varredura (DSC) e termogravimétria (TG/DTG), análise da composição do óleo usando cromatografia gasosa (CG) e testes reológicos foram realizadas. Uma correlação empírica que descreve a variação da viscosidade do óleo com a temperatura foi obtida mediante o ajuste de dados experimentais.

Capítulo 4: Este capítulo contém os estudos experimentais da reação de transesterificação do óleo de mamona com etanol em presença de hidróxido de sódio como catalisador. Os efeitos de várias condições de operação tais como tempo, temperatura, massa de catalisador, razão molar etanol/óleo de mamona são discutidos. Os resultados obtidos são apresentados em termos da seletividade de diglicerídeos, monoglicerídeos e glicerina assim como a conversão dos triglicerídeos (óleo vegetal) para etil ésteres (Biodiesel).

Capítulo 5: A modelagem e o ajuste dos parâmetros cinéticos para a reação de transesterificação via catálise básica são apresentados. Um algoritmo genético escrito na linguagem de programação FORTRAN é utilizado para gerar o valor inicial dos parâmetros cinéticos que servem como estimativa inicial para o algoritmo Levenberg-Maquard que finaliza o procedimento de ajuste. Os alcances e limitações do modelo cinético são discutidos em detalhe.

Capítulo 6: As técnicas de microfabricação utilizadas para a construção de dispositivos de microfluídica são apresentadas, a saber, o processo de fotolitografia de filmes usando a resina SU-8 e a técnica de Litografia macia ou "*soft lithography*" para obtenção de microestruturas em polidimetilsiloxano (PDMS). Os parâmetros dos processos foram ajustados para a obtenção de microcanais com geometrias internas que variam entre 120 – 500 μm. As vantagens e desvantagens dos processos utilizados são discutidas visando à reprodutibilidade e produção em série dos microdispositivos.

Capítulo 7: Este capítulo contém procedimentos experimentais para a análise da mistura do óleo de mamona e etanol sem reação química. A montagem experimental, metodologia e condições de operação usadas no estudo são informadas. Os efeitos de vários parâmetros de operação sobre o regime de fluxo e área interfacial são discutidos. Além disso, caracterização de zonas de estagnação e recirculações internas dentro dos

microcanais foi realizada mediante o uso de fluidodinâmica computacional (CFD). Finalmente, os resultados das simulações são comparados com os dados experimentais.

Capítulo 8: O capítulo apresenta a reação de transesterificação nos microreatores cujo desenvolvimento é mostrado no Capítulo 6. A síntese de biodiesel é analisada a diferentes condições de reação como temperatura, massa de catalisador, tempo de residência e razão de fluxo etanol/óleo. Diferentes geometrias foram construídas com o objetivo de estudar a influencia da geometria interna na mistura das fases e também a transferência de massa entre os reagentes. Uma comparação é feita com os dados experimentais obtidos no reator batelada (Capítulo 4) com o objetivo de por em evidência o ganho na aplicação da intensificação de processos.

Capítulo 9: Neste capítulo é apresentado o desenvolvimento de um novo método para o monitoramento "*on-line*" da reação de transesterificação em microreatores mediante a utilização de fibra ótica na região do infravermelho próximo. São descritos em detalhe os componentes do dispositivo de análise assim como a avaliação de seu potencial uso.

Capítulo 10: Finalmente, neste capítulo se apresenta as conclusões deste trabalho e sugestões para trabalhos futuros.

Capítulo 2.

Perspectivas na Aplicação de Intensificação de Processos para a Produção de Biodiesel

2.1. Introdução

A intensificação de processos abrange novas e complexas tecnologias que substituem equipamentos grandes, caros e com grande consumo energético por plantas de menor custo, mais eficiente e de menor tamanho, contribuindo para um menor impacto ambiental. Na intensificação de processos podem ser utilizadas unidades de operação híbridas, denominadas "multifuncionais", as quais juntam processos elementares tais como mistura, reação, separação, etc., aumentando a produtividade e seletividade, além de facilitar a separação de subprodutos indesejáveis. A redução do número de etapas leva a um investimento reduzido e à redução significativa do gasto de energia. Além disso, a seletividade do produto conduz a uma diminuição do consumo de matéria-prima e conseqüentemente dos custos de operação.

Uma das aplicações com boa perspectiva nesta década é o desenvolvimento de microreatores, micromisturadores, microseparadores e microtrocadores de calor aplicados na engenharia química. Estes dispositivos têm a capacidade de incrementar a velocidade de produção dos processos, permitindo condições de operação (temperatura, concentração e pressão) difíceis ou impossíveis de conseguir nos equipamentos convencionais. Uma maior quantidade de massa e energia pode ser transferida entre as faces devido ao incremento na relação área superficial-volume, aos maiores gradientes de concentração e temperatura, assim como à diminuição das dimensões características que conduzem a um menor percurso livre médio das moléculas. Isto faz os microdispositivos potencialmente atraentes na engenharia química devido a que estas características eventualmente resultam em mais altas conversões e seletividades, e assim em processos mais eficazes e ambientalmente amigáveis.

Todos estes benefícios estão sendo aproveitados na criação de novos processos químicos que permitam a produção de combustíveis alternativos para a geração de energia. No Brasil é de particular interesse o biodiesel, um combustível alternativo obtido a partir de fontes biológicas renováveis tais como óleos vegetais e gordura animal, sendo este biodegradável e não tóxico. Conseqüentemente a integração das vantagens na aplicação dos microreatores e as características do biodiesel conduzem a um processo totalmente eficiente, limpo e amigável com o meio ambiente.

No Brasil, o óleo de soja é a principal fonte utilizada para a produção do biodiesel na indústria. No entanto, outras fontes vegetais tais como óleos de girassol, amendoim, algodão, palma, coco e especialmente óleo de mamona podem ser também usadas. Por outro lado, o etanol obtido do bagaço de cana apresenta-se como uma potencial fonte de álcool, permitindo que o biodiesel seja obtido exclusivamente de materiais renováveis. Contudo, o processo para a obtenção do biodiesel ainda apresenta vários problemas, tais como reações incompletas, formação de emulsões, isolamento e purificação de produtos, além dos rigorosos padrões de qualidade dos combustíveis. Deste modo, a intensificação de processos mediante o desenvolvimento de micro-sistemas, apresenta um caminho promissor para a síntese de biodiesel, devido às eficientes taxas de transferência de massa e energia, o que leva a uma redução nos tempos de reação, controle mais preciso e melhoramento na seletividade da reação.

Portanto, neste capítulo se apresenta uma revisão dos principais avanços na área dos microreatores e na produção de biodiesel visando o desenvolvimento de um novo método para a produção contínua de biodiesel a partir do óleo de mamona e etanol mediante a aplicação de microreactores.

2.2. Desenvolvimento

O desenvolvimento deste capítulo é apresentado a seguir, no manuscrito intitulado: *Perspectives on Application of Process Intensification for Biodiesel Production.*

Research Review

Perspectives on Application of Process Intensification for Biodiesel Production

Abstract

The advances in microreactor technology in the last years have enabled an increase in the number of microreactor applications in the process engineering field. A considerable number of scientific papers have been published using microreactors, and reporting high throughput in the synthesis of chemicals, catalytic reactions, high-temperature reactions, reactions with unstable intermediates, as well as reactions involving hazardous chemicals. These performances are attributed to equivalent hydraulic diameter up to a few hundreds of micrometers in the microreactors enabling high mass and heat transfer and, therefore, increasing the reactor yields drastically compared to the conventional one. Such considerations have generated great interest in the chemical industry for the development of new alternatives for continuous production of alternative fuel as the biodiesel. This work provides a comprehensive review of the state of the art of the process intensification and microreactor technology applied in development of new process. In addition, a review of biodiesel technology is also done, as well as prospects in the application of the microreactor technology in the biodiesel production.

Keywords: Microreactors; Micromixers; Microfluidic systems; Microprocess; Biodiesel

Contents

1. Introduction

Over the last years a substantial research effort have been devoted to reduce greenhouse gas emissions to the environment aiming to decrease global warming and halt the climate change. Therefore, it is important to develop a chemical industry based in renewable energy sources, process environmentally friendly and sustainable technology. In this context, is desirable treat the chemicals being used in the processes of such way as to provide every molecule the same processing experience, yielding increased selectivity (Kashid, 2007). This can be done by improvement of existing processes, alternative routes of synthesis or developing new processing ways. A promissory alternative to this issue is to enhance the mass and energy transfer rates through microdevices application, which have the potential to increase the specific interfacial area, reducing the diffusional path lengths, contributing to the performance and process safety owing to the lower hold-up and suitable temperature control. In this aspect, the combination of process engineering and microsystem engineering together with the design, fabrication, and integration of functional microstructures is one of the most promising research and development areas of the last decade. This overall development is often referred in the scientific literature under the concept of “Process Intensification”.

Process intensification provides innovative challenges and opportunities to the chemical, pharmaceutical and bio-based industries to satisfy the need of sustainable production methods in order to increase the productivity, flexibility, safety, and, to decrease of energy consumption, waste generation, and operational cost without sacrificing product quality. It is being achieved by enhancing of phenomena such as fluids dynamics, heat and mass transfer through the integration of operations and functions in the process. The concept of process intensification was first considered as the miniaturization of the unit operations (Cross and Ramshaw, 1986). However, besides the size reduction, different hardware and methodologies are being exploited for process intensification. Examples of

new hardware developments are spinning disc reactor, oscillating flow reactor, heat exchange reactor, microchannel reactor, among others. The methodologies which are available are reactive distillation, reactive extraction, membrane separation and use of ultrasound, microwave and centrifugal fields, etc (Figure 1). In particular it can lead to the manufacture of new products which could not be produced by conventional process technology.

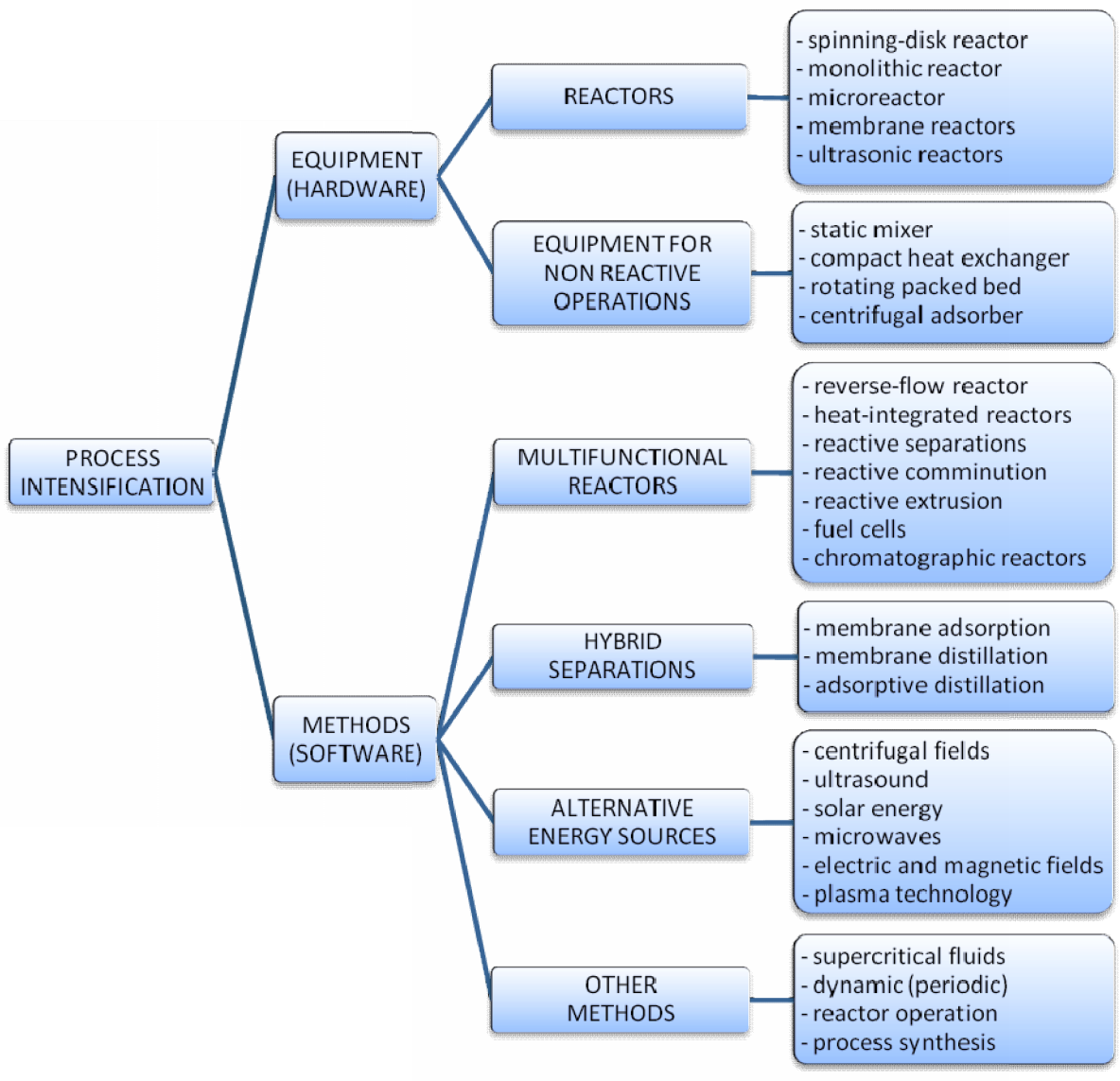

Figure 1. Tools of Process Intensification. *Source:* Keil, 2007.

In other words process intensification consist of the development of novel chemical engineering equipment and techniques, as compared to the present state-of-art, to bring dramatic improvements in manufacturing and processing (particularly in terms of land usage due higher production and/or number of products per unit manufacturing area), substantially decreasing equipment size/production-capacity ratio (reduction in investment and raw materials costs), energy consumption (lower costs of utilities), or waste production (less costs of waste processing). Therefore, the advantages that process intensification offers to process engineering can be summarized in six main areas: costs, safety, compactness, controlled well-defined conditions and time to the market (Stankiewicz and Moulijn, 2002) lead to a substantially smaller, cleaner, and more energy-efficient technology. Keil (2007) present an overview of equipment and methods employed in process intensification (Figure 1) which leads to higher process flexibility improved inherent safety and energy efficient, distributed manufacturing capability, and ability to use reactants at higher concentrations.

2. Microreaction technology

Among different methods for process intensification shown above, microreaction technology offers great benefits to the process industry. Since the heart of the chemical process industries are the reactors, considerable effort is consumed in its design and optimization. In recent years, a new concept of reactors - the microreactors - opens up new ways of performing chemical transformations with the potential to be promissory change in chemical reactor technology (Lerou *et al.*, 1996). Microreaction technology is characterized by a continuous flow through well-defined structures with characteristic dimensions between 0.1 to 1000 μm, which allow a strongly intensified transfer of mass and heat in the small dimensions of the microdevices being responsible for drastically enhanced heat and mass transfer. It results in specific advantage over conventional process technology. Hessel *et al.* (2004) present a comprehensive introduction thereon.

Microreactors are reaction systems fabricated by the use of methods of microtechnology and precision engineering (Ehrfeld *et al.*, 2000). Different materials such as metals, glass, polymers and ceramic are used to fabricate the microreactors and various techniques such as etching, lithography, electroplating, molding, polymer microinjection molding, and embossing techniques are applied to make the microchannels with different

cross-sectional geometries (*e.g.* circular, rectangular, square, etc.). Microfabrication techniques initially were used in microelectronics to construct sensors and actuators, emerging a new research field called microelectromechanical system (MEMS). An overview of the historical development of chemical handling in microscale is provided by Kothare (2006). Currently many research institute and academia are becoming involved with this subject, which is evidenced by increasing activity in the scientific literature. The Table 1 summarizes the recent literature reviews in the field of microreactor and microprocess engineering. In addition Hessel *et al.* (2008) gives a review on patent publications that have been granted for microprocess devices and their applications.

On the other hand, microreactors can be constructed either as single components or as part of integrated systems. It is well known that in a process each component mainly performs a single operation as a unit of mixing, heat exchange, or separation. Therefore, more than one unit of operation is generally necessary to give the desired effect. In the microscale, many applications require more complex systems know as integrated microreaction systems, where the components are assembled to form a complete and complex unit. Ehrfeld *et al.* (2002) and Hessel *et al.* (2005b) present some components developed of interest for microreaction in chemical engineering such as micropumps, micromixers, micro heat exchangers, catalyst supports and miniaturized analytical systems.

2.1. Fundamentals advantages of microreactors

The advantages of miniaturized reaction systems can be attributed to two principal characteristics: physical size and number of units. Namely, with decreasing linear dimensions, the gradients of properties such as temperature, concentration, density, or pressure, the driving forces for heat transfer, mass transport, or diffusional flux per unit volume or unit area, increase. Therefore, the volume of the system and its material holdup decrease resulting in shorter response times and simpler process control. In addition, miniaturization allows measurements to be performed with a device that needs less space, materials, and energy allowing an improvement of performance by integration of a variety of miniaturized functional elements.

Table 1. Recent literature review published in the field of microreactor technology and microprocess engineering.

Authors	Subject	Year
Benz *et al.*	The extraction performance for miniplant technology using static micromixers was evaluated. The micromixers proved to be highly efficient for extraction which was completed within a hundred milliseconds.	2001
Giordano and Cheng	The application of microfabrication techniques to problems involving fluids was reviewed. Representative work along with the ingenious fabrication methods was described.	2001
Jensen	Examples of the many designs for microreactors by different research groups were shown. These advantages and news reaction pathways are discussed as well as the integration of microreactors with sensor in µTAS for chemical synthesis.	2001
Löwe *et al.*	Here are presented scientific advances achieved very applications of microsystems in chemical production and their potential use in military or terrorist application.	2002
Obot	A critical review of the published about of microchannel transport phenomena was presented and transfer coefficients for smooth channels with different hydraulic channels was presented.	2002
Charpentier	Market demand, technological development and future of chemical engineering focused in process intensification by novel equipment based on scientific principles and new production operating methods was discussed.	2003
Hessel and Löwe	The three parts of this paper deals with developments of the various microcomponents and possible plants concepts for microreactors for applications in the big industry.	2003a,b,c
Doku *et al.*	In this paper was presented an overview of the critical issues in the development of on-chip multiphase chemistry systems, the microreactor design and the methods of phase contacting.	2005a
Gokhale *et al.*	Microchannel reactors were reviewed with particular reference to their applications and use as a cost effective tool during process development tasks.	2005
Hessel *et al.*	A review on microstructured mixer devices, their mixing principles concerning miscible liquids, typical elements design and application fields were presented.	2005a
De Jong *et al.*	This review provides an overview of the developments of mass transport control be means of membranes functionality into microfluidic devices and his field application.	2006
Günther and Jensen	A review of transport characteristic of pressure-driven, multiphase flows though microchannel networks and enhanced mixing represented with dimensionless scaling parameters was presented.	2006
Mae	In this paper, studies dealing with reactions and unit and unit operations conducted in microspace were surveyed and distinguished achievements were summarized.	2007
Mills *et al.*	Advances in microreactors development and introduces the combination of microreactors and micro-process devices to produce an integrated system was discussed.	2007
Hessel *et al.*	A review on recent patent publications in the field of microreactors technology and microprocess engineering was given.	2008
Mansur *et al.*	This review was focused on the recent developments in microfluidic mixers and mixing characteristic in active and passive micromixers.	2008
Kjeang *et al.*	This review article were summarizes the development of microfluidic fuel cell technology from the invention in 2002 until present.	2009
Kashid and Kiwi-Minsker	This paper provides a comprehensive overview of the state of the art of the microstructured reactor applied for multiphase reactions.	2009

The transport properties intensification and the decreased hold-up and response time allow several process conditions that can be applied in microreactor which cannot be realized in conventional macroscopic devices, for instance, the realization of nearly isothermal boundary conditions in a highly exothermic reaction by using the extreme heat-transfer rates of microreaction systems. In addition, unwanted and decomposition reactions occasioned by hot spots can be suppressed in microreactors. The use of microreactors greatly reduces the hazardous potential associated with reactions that are highly exothermic or potentially explosive and enhance safety with toxic substances or high operating pressures. These can be used in application of chemical reaction involving mixing, where the diffusional path of molecules is shortened, allowing set the conditions over a wide operating range and under favorably uniform conditions not achievable with standard equipment. Therefore, the microreactors allow the development of efficient processes through to find optimum conditions for a production plant with regard to yield and selectivity.

Another advantage is easily scale up because the production scale can be realized in principle by parallelization or "numbering up" the elements through the multiple repetitions of the microstructure. In addition, a large number of systems results in a higher flexibility in adapting production rate to varying demand, since a certain number of systems may be switched off or further systems may be added to the production plant. A plant design based on a large number of small reaction systems could be modified to perform different reactions by changing the manner in which the microreactor modules are interconnected (Jähnisch *et al.*, 2004). Some of the challenges in the design process when the microreactors operating in parallel are presented by Rebrov *et al.* (2007).

Current targets in the microreactor field include explosive reactions, handling flammable or toxic components, and processes with unwanted reactions by suppress side reactions and give products of higher purity. These activities widen the range of chemical reactions and processes for sustainable development and cost-effective production. Some of the systems that have been commercially used for production of various intermediates chemicals products and a variety of emerging process can be found in Goppi and Tronconi (2005) and Kreutzer *et al.* (2005).

3. Mixing in microfluidic devices

Mixing is a physical process that causes a uniform distribution of different components within a short period of time. Since flow regime inside micromixers is basically laminar due to the small channel dimension and the low Reynolds number, the majority of these are based on diffusional mixing. It is well known that among the mechanisms for mixing liquid or gaseous phases, molecular diffusion is the final step in all mixing processes. Thus, diffusion generally is a rather slow process and has to be assisted by the formation of thin layers, which is achieved simply by division of main stream into many small substreams or reduction of the channel width along the flow axis. Thereby, large contact surfaces and small diffusional paths are generated. In addition, a diverse number of mechanisms assisting diffusion may principally be applied. The Figure 2 depicts some arrangements based on different mixing concepts.

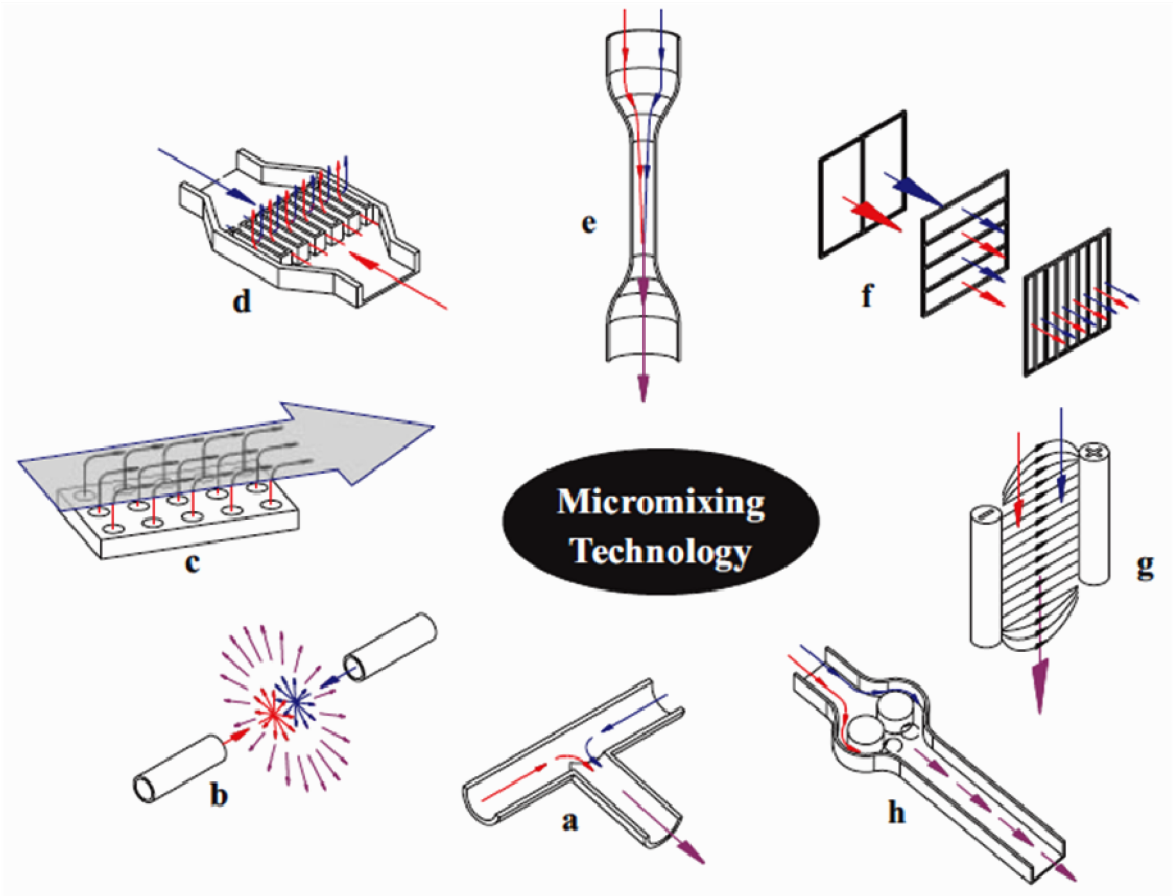

Figure 2. Schematic flow arrangements based on different mixing concepts. (a) Contacting of two substreams (b) Collision of two substreams (c) Injection of many substreams in a main stream (d) Injection of many substreams (e) Decrease of diffusion path (f) Manifold splitting and recombination (g) Externally forced mass transport (h) Periodic injection of small fluid segments. *Source*: Ehrfeld et al., 2000.

The field of micromixers has made rapid advances during the last decades and a large variety of different micromixers have been reported in literature. Comprehensives reviews of micromixers are given by Nguyen and Wu, 2005; Hessel *et al.*, 2005a; Jayaraj *et al.*, 2007; and Mansur *et al.*, 2008. Two basic principles are followed to introduce mixing at the microscale. Firstly, energy input from the exterior is used, termed *active mixing*. These external energy sources are ultrasound, acoustic, bubble-induced vibrations, electrokinetic instabilities, periodic variation of flow rate, electrowetting-induced merging of droplets, piezoelectric vibrating membranes, magneto-hydrodynamic action, small impellers, integrated microvalves/pumps, and others. Secondly, the flow energy, e.g. due to pumping action or hydrostatic potential, is used to restructure a flow in a way which results in faster mixing (Nguyen and Wereley, 2006). This is known as *passive mixing*. Thin lamellae are created in special feed arrangements, termed interdigital. A series of way to create multi-lamellae can be realized by Split-and-Recombine flow. Chaotic mixing creates eddy flow patterns which provide high specific interfaces though often these are spatially heterogeneous. In addition, the mixing can be achieved by the injection of many substreams, e.g. via nozzles, into one main stream. Collision of jets provides another means for turbulent mixing. Finally, a number of specialty flow guidance has been described as e.g. the Coanda effect (Hessel et al., 2005b), relying on a microstrucutre for redirecting the flow. The overview of different micromixers types is depicted in Figure 3.

4. Biodiesel technology

Actually, biofuels have become in valuable sources of sustainable energy. Interest in them rise in the recent years due to the depletion and scarcity of conventional fossil fuels, along with accelerated worldwide demand of fuel. The current alternative is the biodiesel which is obtained from biological sources. Biodiesel is attracting great attention due following advantages: it is an alternative to petroleum-based fuel, which implies lower dependence on crude oil foreign imports, is renewable fuel, helping to achieve renewable energy requirement, present a favorable energy balance, reducing greenhouse gas emissions in line with the Kyoto Protocol agreement, produce lower harmful emissions, which is very advantageous in environmentally sensitive areas, it is biodegradable and non-toxic fuel, and use agriculture surplus, which can also help to improve rural economies. The growing interest in biodiesel can be reflected by the number of scientific article, review and patents

published in the last decade (Schuchardt *et al.*, 1998; Ma and Hanna, 1999; Fukuda *et al.*, 2001; Pinto et al., 2005; Meher *et al.*, 2006; Al-Zuhair, 2007; Vasudevan and Briggs, 2008; Sarma *et al.*, 2008; Demirbas, 2009).

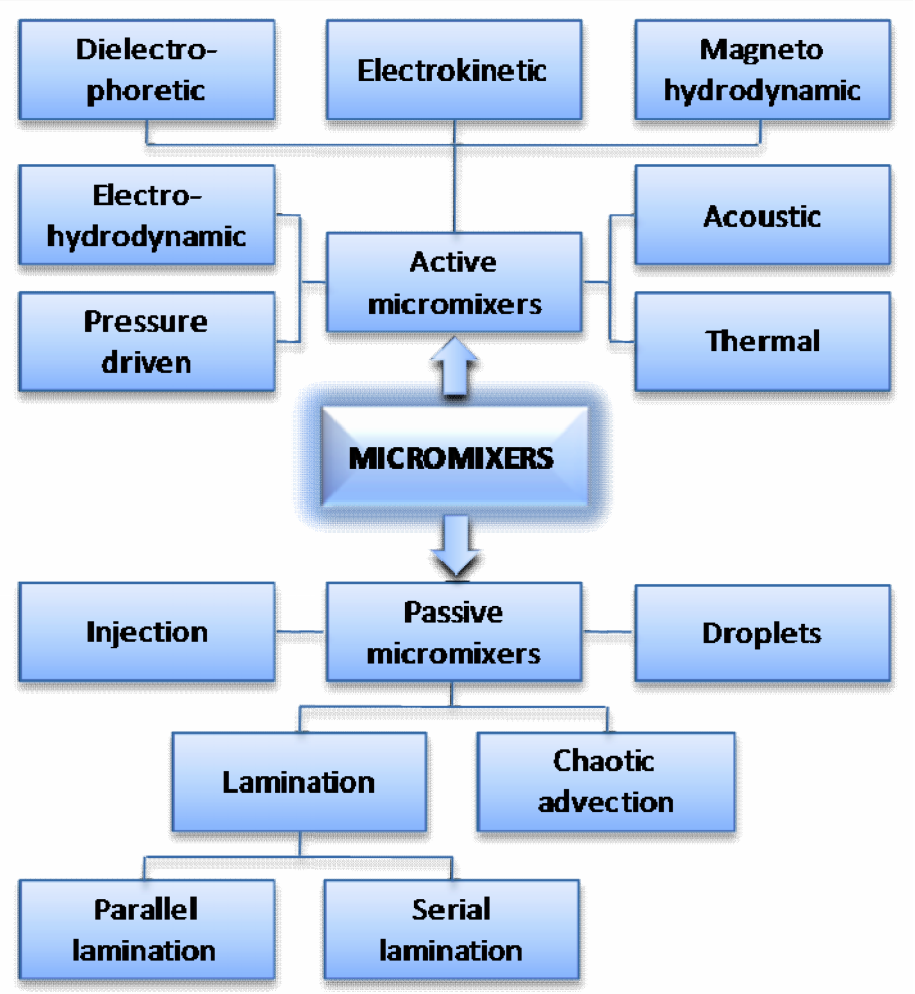

Figure 3. Overview of different micromixer types. *Source:* Nguyen and Wereley, 2006.

Biodiesel is defined as a mixture of monoalkyl esters of long chain fatty acids derived from a renewable lipid feedstock, such as vegetable oil or animal fat. It typically comprises alkyl fatty acid (chain length C_{14}-C_{22}) esters of short-chain alcohols. There are several choices for vegetable oils sources. In Brazil, soybean oil is a source that is already scaled up for biodiesel production (Pinto *et al.*, 2005). Nevertheless, other sources, such as sunflower, peanut, cotton, palm oil, babassu and, especially, castor oil, may be used. The alcohol source in general is methanol, but, in Brazil the ethanol from sugar cane has a great potential as alcohol source.

Esters from vegetable oils are the best substitutes for diesel because they do not demand any modification in the diesel engine and have a high energetic yield. The higher heating values (HHVs) of biodiesels (39-41 MJ/kg) are slightly lower than those of gasoline (46 MJ/kg), petrodiesel (43 MJ/kg), or petroleum (42 MJ/kg), but higher than coal (32-37 MJ/kg) (Demirbas, 2008a). Pure biodiesel fuel (100% esters of fatty acids) is referred as B100 and when it is blended with diesel fuel is referred as *e.g.* B20, 20% B100 and 80% diesel. Biodiesel is characterized by their physical and fuel properties including density, viscosity, iodine value, acid value, cloud point, pure point, gross heat of combustion, and volatility. In Brazil, the *Agência Nacional do Petróleo, Gás Natural e Biocombustíveis* (ANP) specified standard for biodiesel (B100) pursuant to resolution ANP Nº7, 19.3.2008 – DOU 20.3.2008 (2008). The premier standard setting organization in the world, American Standard for Testing and Materials (ASTM), has also specified standard for biodiesel (B100) D 6751 07 and blend stock.

4.1. Fundamentals of biodiesel manufacturing

4.1.1. Chemistry

Transesterification, also called alcoholysis, is a chemical reaction between a vegetable oil or animal fat with an alcohol to form esters and glycerol, the global reaction is show in Figure 4. The alcohols that may be used in the transesterification process are methanol, ethanol, propanol, butanol and amyl alcohol, but among all these alcohols methanol and ethanol are frequently used. Ethanol is preferred alcohol in the transesterification process compared to methanol because it is derived from agriculture products and is renewable and biologically less objectionable in the environment (Silva *et al.*, 2007). However, methanol is also preferable because of its low cost and its physical and chemical advantages (polar and shortest chain alcohol). Several aspects, including the reaction temperature, pressure, mixing intensity, alcohol-to-vegetable oil molar ratio, water content, type of catalyst and free fatty acid content have an influence on the course of transesterification (Freedman *et al.*, 1984). It was observed that increasing both reaction temperature and oil-to-alcohol molar ratio have a favorable influence on the yield of ester conversion, for the other hand, free fatty acids and water always produce negative effects (Bikou *et al.*, 1999; Kusdiana and Saka, 2004).

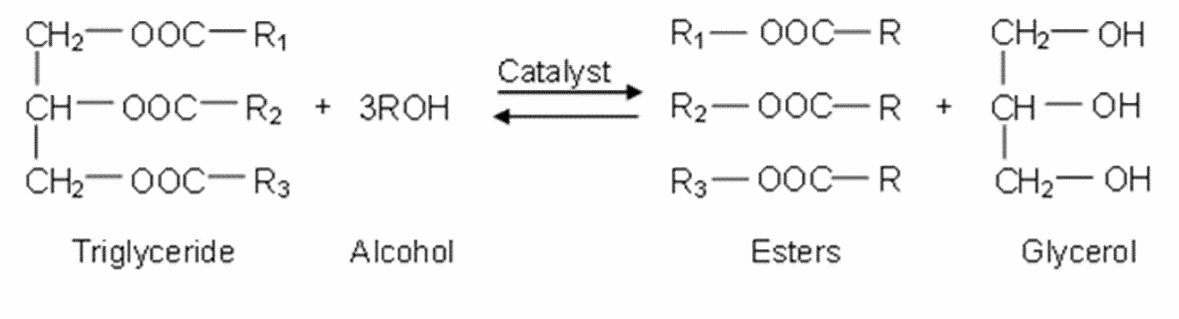

Figure 4. Transesterification of triglycerides with alcohol (R_i *is a hydrocarbon*)

Transesterification of triglyceride oils with alcohol represented by the general equation shown in Figure 4, consist of a number of consecutive reversible reactions (Freedman *et al.*, 1986) as shown in Figure 5, where the triglyceride is converted stepwise into diglyceride, monoglyceride, and finally, glycerol. In each step an ester is produced and thus three ester molecules are produced from one molecule of triglyceride. Therefore, the stoichiometric reaction requires 1 mol of a triglyceride and 3 mol of the alcohol, however, an excess of the alcohol is used to increase the yields of the alkyl ester but makes the recovery of the glycerol difficult.

$$Triglyceride + ROH \Leftrightarrow Diglyceride + RCOOR_1$$

$$Diglyceride + ROH \Leftrightarrow Monoglyceride + RCOOR_2$$

$$Monoglyceride + ROH \Leftrightarrow Glycerol + RCOOR_3$$

Figure 5. Consecutive reversible reactions of triglycerides with alcohol to produce esters and glycerol.

4.1.2. Raw materials

The source for biodiesel production is chosen according to the availability in each region or country. From a chemical point of view, vegetable oils from different sources have different fatty acid composition. The fatty acids are different in relation to the chain length, degree of unsaturation or presence of other chemical functions (Table 2). Esters prepared with long chain fatty acid or saturated fatty acid show higher cetane number, higher cloud point and cause nozzle clogging. Esters prepared with unsaturated fatty acid show low cetane number and suffer oxidation easily. Generally, cetane number, heat of combustion, melting point and viscosity of neat fatty compounds increase with increasing chain length and decrease with increasing unsaturation.

Table 2. Fatty acid composition of some vegetable oils (%). *Source:* Pinto *et al.*, 2005

Vegetable Oil	Palmitic 16:0	Stearic 18:0	Palmitoleic 16:1	Oleic 18:1	Linoleic 18:2	Recinic 12-OH-oleic	Other acids
Tallow	29.0	24.5	-	44.5	-	-	-
Coconut oil	5.0	3.0	-	6.0	-	-	65.0
Olive oil	14.6	-	-	75.4	10.0	-	-
Groundnut oil	8.5	6.0	-	51.6	26.0	-	-
Cotton oil	28.6	0.9	0.1	13.0	57.2	-	0.2
Corn oil	6.0	2.0	-	44.0	48.0	-	-
Soybean oil	11.0	2.0	-	20.0	64.0	-	3.0
Hazelnut Kernel	4.9	2.6	0.2	81.4	10.5	-	0.3
Poppy seed	12.6	4.0	0.1	22.3	60.2	-	0.8
Rapeseed	3.5	0.9	0.1	54.1	22.3	-	9.1
Safflower seed	7.3	1.9	0.1	13.5	77.0	-	0.2
Sunflower seed	6.4	2.9	0.1	17.7	72.8	-	0.1
Castor oil	-	3.0	3.0	3.0	1.2	89.5	0.3

Therefore, biodiesel properties are strongly influenced by the properties of each constituent fatty ester and appear attractive to enrich it with certain fatty esters with desirable properties in the fuel in order to improve the properties of whole fuel. Moreover, the biodiesel source should accomplish two requirements: low production costs and large production scale. In Brazil, biodiesel production has been adjusted to available crop in each region. In the North, palm kernel and soybean are the most used sources; in the Northeast, castor bean, palm oil, palm kernel, babassu, soybean and cotton seed; in the Central-West, soybean, cotton seed, castor bean and sunflower seed; in the Southeast, soybean, castor bean, cotton seed and sunflower seed; in the South, sunflower seed, soybean, rapeseed and cotton seed (Pinto *et al.*, 2005). Soybean because of the large agricultures areas, palm because of the high level of oil and castor seed which can be cultivated in all states, has provided considerable expansion of vegetable oil production in Brazil.

4.1.3. Catalysts type

Nowadays, the chemical catalysts are the most studied and used in biodiesel production because to the availability and low cost. Chemical catalysts permit proceed at a faster reaction rate than other forms of catalysis. In biodiesel production, usually there are two classes of chemical compounds used, alkali catalysts and acid catalysts (Homogeneous catalysts), but biocatalyst have been becoming increasingly important in the discussion of biodiesel production lately. In addition, another relatively new area of study is in the area of heterogeneous catalysts.

4.1.3.1. Homogeneous catalysts

Homogeneous catalysts are widely used today because ensuring simple and robust technology, as well as high reactions rates, despite some important economical and environment disadvantages (Demirbas and Balat, 2006). For the production of biodiesel by transesterification both acid and alkali catalyst can be applied, but the latter is much more efficient. The difference can be explained by the reaction mechanism, as shown by Figures 6 and 7 (Dimian and Bildea, 2008). As reported by Dimian and Bildea (2008), methanolysis with homogeneous acid catalysts (Figure 6) the first step consist of triglyceride activation by protonation (1) at the CO group where the oxygen is more active, followed by the formation of a carbocation complex (2). By nucleophilic attack with methanol (3) a tetrahedral carbon complex forms, which by losing the proton decomposes further (4) in a new methyl fatty ester and diglycerides. The methanolysis proceeds similarly with diglyceride and monoglyceride. It can be seen that if water is present it will produce fatty acid by hydrolysis in the step (3) and as a consequence it will decrease the yield of fatty ester. For this reason the water amount in the triglycerides should be reduced below 0.5%. Main acid-catalyzed transesterification methods are methanolic sulfuric acid, ferric sulfate, sulfonic acid, methanolic hydrogen chloride, and methanolic baron trifluoride. Among these, hydrochloric and Sulfuric acid are most commonly used as acid catalysts in the transesterification of biodiesel.

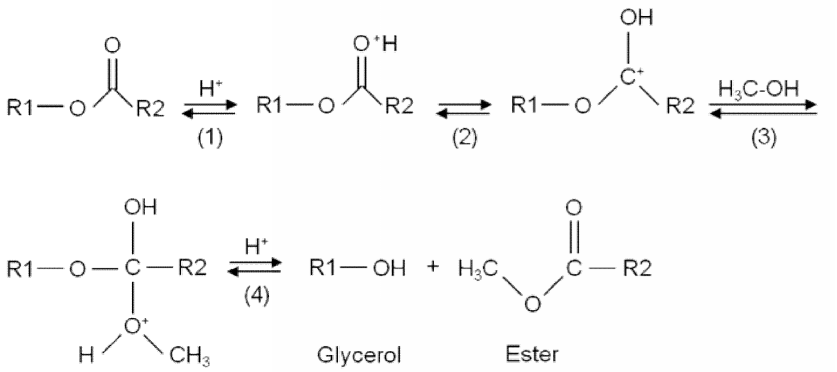

Figure 6. Mechanism of acid-catalyzed transesterification: R1-glyceride fragment, R2-fatty acid carbon chain

The advantage of acid-catalyzed esterification process is attributed to its low price and the ability of acids to minimize the amount of water and free fatty acid involved in the reaction. The use of an acid catalyst is observed to be more effective than alkali catalyst when the concentration of free fatty acids is high, greater than 1%. However, these reactions require post reaction clean-up though, because the acids involved produce a large

amount of salt during the reaction which can be corrosive. Besides with the presence of these salts, equipment maintenance also plays a crucial role in this process. Another drawback of this reaction is that it is much slower than others catalysts (Cao *et al.*, 2008).

On the other hand, base catalyst involves a completely different mechanism, as explained by Figure 7. The active species is an alkoxide, namely the methoxide ($^{-}O\text{-}CH_3$). This can be produced in-situ by the reaction of methanol with hydroxide liberating water:

$$NaOH + CH_3 - OH \Leftrightarrow Na^{+-}OCH_3 + H_2O$$

Generally, the methoxide is introduced to the reaction as pre-prepared from alcohol and an alkali metal (generally, KOH or NaOH). In this case, the absence of water favors the reaction rate, as well as easier post-processing. In base-catalyzed production the first step consists of the nucleofilic attack of the methoxide to the carbonyl group, which leads to the formation of a tetrahedral carboanionic complex (1). Next, the transition complex decomposes into a fatty ester and a diglycerol anion (2), which reacts with an alcohol molecule, reforming the catalytic species (3). The other transesterification stages take place similarly.

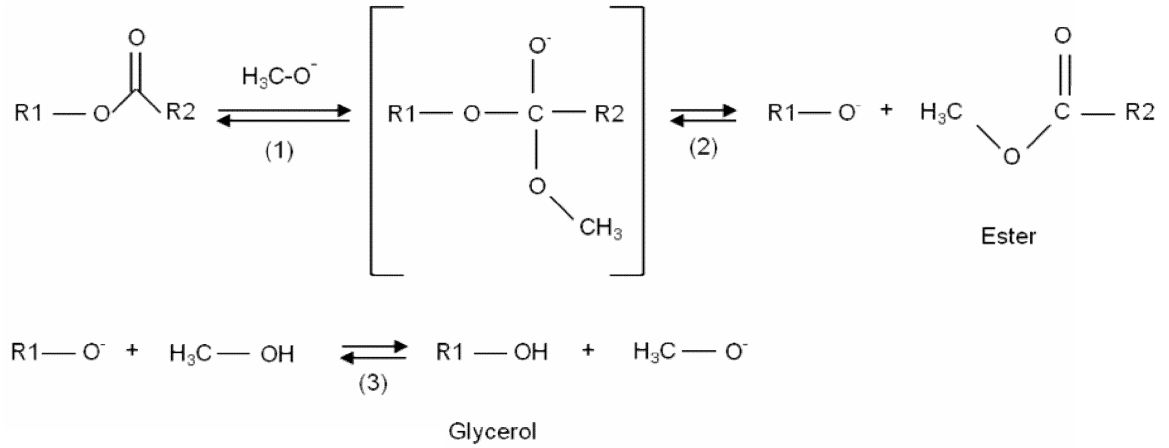

Figure 7. Mechanism of base-catalyzed transesterification of triglycerides: R1-glyceride fragment, R2-fatty acid carbon chain

The majority of researches have been centered on the use of alkali catalyst to carry out the transesterification of fatty acids (Liu and Zhao, 2007). This process has been shown to be faster that acid catalysis. Based in the reaction mechanisms depicted above, may be deduced an explanation: the formation of carboanionic tetrahedral intermediate results directly by the nucleophilic attack of the substitution species, while the carbocationic

complex needs an intramolecular arrangement. However, base-catalyst produces soap more commonly than acid-catalyst when the content of free fatty acids in the oil is high. This occurs because the free fatty acids and water are neutralized more readily by bases than by acids, which in turn, consume the catalyst. Therefore, alkali catalysts are inefficient in operations where the levels of water and free fatty acids are difficult to regulate (Vasudevan and Briggs, 2008).

The researches using these two methods together have been found to increase yield and decrease the reaction time, where an acid pretreatment on the oil is used, followed by the addition of an alkali catalyst. This increases the yield because the acid can efficiently lower the amount of free fatty acids in the oil and once the free fatty acids content has been decreased, alkali catalyst may be added, resulting in a faster reaction time as well as an increased yield (Berchmans and Hirata, 2008).

4.1.3.2. Heterogeneous catalysts

Despite that homogeneous catalysis offers a series of advantages, the fact that catalysts cannot be reused, catalyst residues have to be removed using several washing steps which increases production costs, makes the heterogeneous catalysts an attractive substitute. The heterogeneous catalysts permit to simplify product purification because it can be recovered by decantation or filtration or alternatively can be used in a fixed-bed catalyst arrangement. These include ZrO_2, ZnO, SO_4, 2-/SnO_2, 2-/ZrO_2, KNO_3/KL zeolite, and KNO_3/ZrO_2. The main advantages of these catalysts are that they are less corrosive and are more environmentally friendly. Because of this, they have the possibility of lowering the cost of biodiesel formation. Heterogeneous catalysts have also shown a reduction in the formation of soap, even in low quality oils, for this reason, a considerable research effort is being devoted in this area.

For the esterification reaction, solid catalysts with acidic character can be used, such as zeolites, ion-exchange resins, sulfated metal oxides, sulfated carbon fibers, etc. Ion-exchange resins achieve high reaction rate at temperatures below 130°C, but their chemical stability fall down at extended operations. On the contrary, sulfated zirconia and tin oxides can be used at higher temperatures and ensure high reaction rates, but are sensitive to deactivation by sulfur-group leaching if free water is present. On the other hand, in the transesterification reaction, some solid metal oxides, such as those of tin, magnesium, and

zinc could be used directly, but they actually act by a homogeneous mechanism producing a significant amount of soap. A variety of synthetic catalysts based on alkaline-earth metal oxides (Ca, Mg, Sn, Zn), as well as alkali metals (Na, K) hydroxides or salts impregnated on alumina have been studied to date, but their activity and robustness remains insufficient (Dembiras, 2008b).

4.1.3.3. Enzymatic catalysts

Biocatalysts are naturally occurring lipases which have been identified as having the ability to perform the transesterification reactions that are essential to biodiesel production which catalyze both the hydrolytic cleavage and the synthesis of ester bonds in glycerol esters. These lipases have been isolated from a number of bacterial species: *Pseudomonas fluorescens*, *Pseudomonas cepacia*, *Rhizomucor miehei*, *Rhizopus oryzae*, *Candida rugosa*, *Thermomyces lanuginosus*, and *Candida Antarctica* (Vasudevan and Briggs, 2008). According to a recent study, the *Pseudomonas cepacia* bacterium is the most promising organism for producing a lipase that can be used in transesterification (Shah and Gupta, 2007). Many of these lipases have since become commercially available; one of the most popular is Novozym 435 (Vasudevan and Briggs, 2008).

Biocatalysts have several advantages as enable conversion under mild temperature, pressure, and pH conditions. Neither the ester product nor the glycerol phase has to be purified from basic catalyst reduces or soaps. The phase separation is easier, high quality glycerol is obtained, and environmental problems due to alkaline wastewater are eliminated (Wu *et al.*, 1999). Moreover, both the transesterification of triglycerides and the esterification of free fatty acids occur in one process step. As consequence, oils with high acidic fatty content can be used without pre-treatment (Fukuda *et al.*, 2001). On the other hand, lipases show considerable activity in catalyzing transesterification with long or branched-chain alcohols, which can hardly be converted to fatty acid esters in the presence of conventional alkaline catalysts.

However, lipase-catalyzed transesterification also present a series of drawbacks (Al-Zuhair *et al.*, 2007). As compared to conventional alkaline catalysis, reaction efficiency tends to be poor, so that biocatalyst usually necessitates far longer reaction times and higher catalyst concentrations. Another difficulty in the industrial application of lipases is their high price, especially if they are used in the form of highly-purified, which cannot be

recovered from the reaction products. One strategy to overcome this difficulty is the immobilization of lipases on a carrier, enabling the removal of the enzymes from the reaction mixture and their reuse for subsequent transesterifications. Immobilization could furthermore be advantageous inasmuch fixed lipases tend to be more active and stable than free enzymes (Shah and Gupta, 2007).

4.2. Biodiesel production methods

The current technologies still remains not appropriate to solve all problems associated with use of vegetable oils and their derivates in alternative diesel fuel formulations. The high viscosity, acid composition, and free fatty acid content of such oils, as well as gum formation due to oxidation and polymerization during storage and combustion, carbon deposits, and lubricating oil thickening are some of the more obvious problems. Consequently, challenges remain in the production of biodiesel fuels that meet oxidative stability, performance and emissions requirements specified in the quality standards. Among the well-known processes of conversion of triglycerides onto usable fuel, mainly, microemulsion, pyrolysis, and transesterification (Srivastava and Prasad, 2000), the world community has widely accepted the transesterification process for industrial applications (Ma and Hanna, 1999; Sarma *et al.*, 2008). A large volume of patents have been disclosed in the recent years, some of which follow transesterification protocols that may be highly influential on the existing systems of biodiesel production and processing. Sarma *et al.* (2008) present a review showing the more important patents from the application point of view for a reliable-efficient technology to gradation of biodiesel production and processing.

4.2.1. Microemulsions

The use of microemulsions with solvents such as methanol, ethanol and 1-butanol has been studied in order to solve the problem of the high viscosity of vegetable oils (Fukuda *et al.*, 2001). Microemulsion is the formation of thermodynamically stable dispersions of two usually immiscible liquids, brought about by one or more surfactants. These are characterized by their isotropic, clear or translucent dispersion and a droplet size with dimensions usually in the range of 1-150 nm. It has been reported previously that short term performances of microemulsions of aqueous ethanol in soybean oil were nearly as good as that B20 diesel fuel (Ma and Hanna, 1999). However, recent studies in

microemulsions of vegetable oils and alcohols have shown cannot be recommended for long-term use in engines as they are prone to incomplete combustion and formation of carbon deposits.

4.2.2. Pyrolysis (thermal cracking)

Vegetable oils, animal fats and natural fatty acids can be pyrolyzed to produce many smaller chain compounds. Pyrolysis converts one substance into another by means of heat or by heat with the aid of a catalyst, typically in the absence of air or oxygen. SiO_2 and Al_2O_3 are typical pyrolysis catalyst. Pyrolytic chemistry is difficult to characterize because of the variety of reactions paths and the variety of reactions products that may be obtained from the reactions that occurs. Different types of vegetable oils reveal large differences in composition when they are thermally decomposed. Thermal decomposition of triglycerides produces compounds of several classes, including alkanes, alkenes, alkadienes, carboxylic acids, aromatics, sulphur, water and sediment, as well as giving acceptable copper corrosion values. This makes pyrolyzed oils unacceptable in terms of ash content, carbon residues, and pour point.

4.2.3. Supercritical fluids

The esterification in supercritical condition was studied initially as a method to solve the problem of miscibility of oil and methanol that obstruct the kinetics in normal conditions. Biodiesel has been produced using supercritical methanol (350°C and 45 MPa) to produce methyl esters by transesterification without using any catalyst. Studies of rapeseed oil transesterification in supercritical methanol found that transesterification proceeds very effectively and throughput similar as those obtained in the conventional method using an alkaline catalyst (Demirbas, 2006). Furthermore, the methyl ester yield in the supercritical methanol reaction using oils with elevated acids value is higher because the free fatty acids contained in the crude oil and fat also are effectively converted to methyl esters. According to kinetic analyses of the reaction in supercritical methanol, a reaction temperature of 350°C and methanol-to-rapeseed oil molar ratio of 42:1 produced the best reactions conditions (Kusdiana and Saka, 2001). Increasing the reaction temperature increases ester conversion, but recent research showed the real yield can be reduced by thermal degradation of biodiesel, namely of unsaturated fatty esters occurred at temperature above 400°C (He *et al.*, 2007).

5. Prospects of microreactor technology in the biodiesel production

In recent years, continuous synthesis of biodiesel fuel using microreactor system has been considered a promising process (Canter *et al.*, 2004). The advantage in the implementation of microreactor to obtained biodiesel is based on the small volumes of microreaction system that greatly intensifies heat and mass transfer due to a significant decrease in diffusion path length between reacting molecules and large increase of the surface area-to-volume ratio (Ehrfeld *et al.*, 2000). The conventional process the transesterification reaction typically takes place in conventional batch system and delay one or more hours to reach high levels of conversion. It is a typical two-phase reaction due to the immiscibility of oil and alcohol, therefore, the rate of transesterification is primarily controlled by the rate of mass transfer between the alcohol and oil phases (Zhou and Boocock, 2006). In the microreaction system the time that takes a reactant molecule to diffuse through the interface and react with another species is decreased drastically, which is highly improbable in even the most vigorously agitated batch reactor. Therefore, the residence time needed to achieve high conversion is reduced down to the order of few minutes and precise temperature control of the reaction can be achieved, hence the diffusion becomes a less significant resistance to the reaction. In addition, with decreased linear dimensions comes the ability convert a batch reaction to a continuous flow system.

Recently, the continuous synthesis of biodiesel fuel using a microreactor system has been reported. Canter (2006) reported biodiesel yields greater than 90% and 96% with a residence time of 4 and 10 min respectively, in a microreactor with channels of 100 μm thick. Sun *et al.* (2008) designed a microreaction system for the continuous production of biodiesel where the yield of methyl esters of 99.4% was obtained at the residence time of 5.89 min with KOH concentration of 1% and methanol/oil molar ratio of 6:1 at 60°C in a microtube reactor of 250 μm of diameter. Guan *et al.* (2008) reported biodiesel yield of about 100% at a residence time of 112 s and reaction temperature of 60°C in a microtube reactor of 1 mm of diameter and 160 mm of length. Jachuck *et al.* (2009) employed both slug and stratified flow behaviors in a narrow channel reactor and conversions greater 98% were achieved in a residence time of 3 min using a catalyst loading of 1% and reaction temperature of 60°C. In addition, these results were compared with conventional processes as shown by Kashid and Kiwi-Minsker (2009). Transesterification of sunflower oil with

methanol using KOH as catalyst in a microtube reactor was investigated by Guan *et al.* (2009a,b). It was observed that sunflower oil conversion reached 100% in the microtube with an inner diameter of 0.8 mm with a residence time of 100 s, methanol/oil molar ratio of 23.9 and temperature of 60°C. Wen *et al.* (2009) used stainless steel zigzag microchannel reactors with hydraulic diameter of 240-900 μm for continuous alkali-catalyzed biodiesel synthesis from soybean oil and methanol. A methyl ester yield of 99.5% was reached in a reactor with a hydraulic diameter of 240 μm, at a residence time of 28 s, a methanol/oil molar ratio of 9:1, a KOH concentration of 1.2 wt.% and temperature of 56°C. Transesterification of cottonsed oil and methanol with KOH as the catalyst for biodiesel production was carried out by Sun *et al.* (2010) in microstructured reactors. The reaction system included a micromixer that was connected to either a stainless steel capillary of diameter 0.6 mm or a poly(tetrafluoroethylene) (PTFE) tube with diameter of 3 mm and packed with Dixon rings. By using the stainless steel capillary the yield of biodiesel reached 94.8% under the conditions of a methanol /oil molar ratio of 8:1, a residence time of 44 s, and a reaction temperature of 70°C whereas using the PTFE tube the yield of biodiesel reached 99.5% at a residence time of 17 s. Lately, Martínez (2010) has made microreactors with different geometries, called Tesla-, Omega-, and T-shaped for continuous production of biodiesel from castor oil and ethanol with NaOH as catalyst. The influences of the main geometric parameters on the performance of the microchannel reactors were experimentally studied. It was found that the oil conversion was influenced by catalyst loading, ethanol/castor oil molar ratio, residence time and temperature. High ethyl esters yield of 93.5%, 95.3%, and 96.7 % for Tesla-, Omega-, and T-shaped microreactors respectively was reported using a catalyst loading of 1.0 wt.% NaOH, a reaction temperature of 50°C and a residence time of only 10 min. The Table 3 summarizes the main papers published using microreactors for the biodiesel production.

Although a single microreactor can only handle a very small capacity, it can be numbered-up, rather than scale-up to any required capacity. The numbering-up approach guarantees that desired features of a basic unit remain unchanged when increasing the total system capacity (Ehrfeld *et al.*, 2000). On the other hand, this technology makes distributive energy production possible, which reduces the need to distribute fuel via truck, tanker or pipeline (When *et al.*, 2009). These reports evidence the microreaction devices as

a promissory technology for the high-efficiency industrial production of biodiesel using microreactor technology.

Table 3. Comparison of different processes for the production of biodiesel

Reference	Process type	Reactants	Cat. Conc.	Residence time	Temp.	Conv.	Volume / Flow rate
Noureddini *et al.* (1997)	Batch	Soybean Oil + Methanol	0.2% NaOH	1 h	60°C	90%	217 mL
Noureddini *et al.* (1998)	Continuous	Soybean Oil + Methanol	0.4% NaOH	6.6 min	80°C	98%	300 mL/min
Darnoko *et al.* (2000a)	Batch	Palm Oil + Methanol	0.5% KOH	1 h	60°C	98%	544 mL
Darnoko *et al.* (2000b)	Continuous	Palm Oil + Methanol	1% KOH	40 min	60°C	90%	9.0 mL/min
Xu *et al.* (2003)	Batch	Soybean Oil + Methanol	30% Lipase	10 h	40°C	92%	250 mL
Dorado *et al.* (2004)	Batch	Brassica Oil + Methanol.	1.4% KOH	30 min	45°C	91.9%	250 mL
Hsu *et al.* (2004)	Continuous	oil + methanol	Lipase	48 h	50°C	96%	30 mL/min
Canter (2006)	Microreactor	Soybean Oil + Methanol.	NaOH	10 min	Room Temp.	96%	0.5 mL/min
Sun *et al.* (2008)	Microreactor	Cottonseed Oil + Meth.	1.0% KOH	5.89 min	60°C	99.4%	0.25 mL/min
Guan *et al.* (2008)	Microreactor	Sunflower Oil + Meth.	1.0% KOH	112 s	60°C	100%	4.1 mL/h
Jachuck et al. (2009)	Microreactor	Canola oil + Methanol	1.0% NaOH	3 min	60°C	99.8%	3.85 mL/min
Guan *et al.* (2009a)	Microreactor	Sunflower Oil + Meth.	1.0% KOH	93 s	25°C	92.8%	10 cm^3/h
Guan *et al.* (2009b)	Microreactor	Sunflower Oil + Meth.	4.5% KOH	100 s	60°C	100%	8.2 cm^3/h
Wen *et al.* (2009)	Microreactor	Soybean Oil + Methanol	1.2% KOH	28 s	56°C	99.5%	0.14 mL/min
Sun *et al.* (2010)	Microreactor	Cottonseed Oil + Meth.	1.0% KOH	44 s	70°C	94.8%	2.5 mL/min
Martínez (2010)	Batch	Castor Oil + Ethanol	0.5% NaOH	30 min	30°C	98.7%	1.0 L
Martínez (2010)	Microreactor	Castor Oil + Ethanol	1.5% NaOH	10 min	50°C	98.9%	1.5 mL/h

6. Conclusions and outlook

Microreactors and micromixers devices have shown considerable benefits in areas as diverse as catalysis, bioscience, polymers, advanced material synthesis, which is clearly evident by the numerous applications published in the scientific literature, some of these presented in Table 1. It is known that microreactors are suitable for reactions with intrinsic kinetics, requiring better transport and inherent safety, or performed under extreme operating conditions, for instance high temperature and pressure which permit develop specialized analytical tools. From the fluid dynamic point view, microreactor provides

well-defined flow regimes, such as slug and parallel/annular flow patterns, where the main parameters controlling the flow pattern are the geometry, fluid viscosity, surface roughness and interfacial tension.

Effective utilization of small amount of chemicals due to the high rate of heat and mass transfer provides a good environment for finding new routes for synthesis economical and environmentally friendly. The high interfacial area available can guarantee the absence of mass-transfer limitation in the reaction environment and facilitate homogeneous temperature along the cross section which helps to dissipate the heat released during the reaction. On the other hand, considerable study in the scaling up needs to be realized, in order to achieve throughput in the industrially required range, otherwise, many of the advantages of microreactors will be forfeited.

Micromixers are essential components in integrated microfluidic systems, where the mixed of a sample with other substances is necessary prior to certain chemical or biological reactions. The mixing principles in the microscale can be divided basically into two classes relying either on the pumping energy or provision of other external energy to achieve mixing, termed passive and active mixing, respectively.

Biodiesel has similar properties to petroleum diesel but with lower sulfur, CO_2 and particulate emissions. In conventional chemical processing, synthesis of fatty acid esters (biodiesel) is achieved by alkaline- or acidic-catalyzed transesterification of triglycerides (oil). The acid-catalyzed production of biodiesel has received less attention because it is slower than production using alkali catalyst. Nevertheless, the acid-catalyzed approach is less sensitive to free fatty acids in the feedstock oil than the alkali-catalyzed process.

Transesterification by either chemical catalyst has several drawbacks, which include being energy intensive, difficult to recover glycerol and requires wastewater treatment. In addition, free fatty acids present in the oil interfere with the reaction, especially for the alkaline catalyst case, leading to undesirable side products. A less energy intensive and environmental friendly procedure would be to use enzymes for oil transesterification. Enzymatic transesterification can overcome the problems facing conventional chemical methods because glycerol can be easily recovered without any complex process, free fatty acids contained in the oils can be completely converted to esters and subsequent wastewater treatment is not required.

Production of biodiesel from waste oil reduces the cost of biodiesel and is considered an important step in reducing and recycling waste oil. Methanol is the most commonly used alcohol in biodiesel production due to its low cost and high reactivity. However, ethanol shows promissory because it can be easily formed from renewable sources by fermentation, which makes the process of biodiesel production environmentally responsible.

With the inevitable depletion of the non-renewable resources of fossil fuels, and due to its favorable environmental features, the biodiesel shows to be fuel promissory. Nevertheless, still there are many obstacles that need resolved in order to effective production of biodiesel on an industrial scale and these include implementation of low-cost material (as waste oil and grease, animal fats, and nonedible sources), development of better and cheaper catalyst, improvements in current technology for producing high quality biodiesel, use of solvents that are nonfossil-based and conversion of the byproducts such as glycerol to useful products such as synthesis gas or hydrogen.

Microreactor technology has been revealed as promissory method for the high-efficient industrial production of biodiesel as shown by recent researches (see Table 3), where highest conversion can be achieved with significantly reduced residence time which decentralized plants could be developed.

Acknowledgements

The author gratefully acknowledges the financial support provided by The Scientific Research Foundation for the State of São Paulo (FAPESP).

References

Al-Zuhair, S. Review: Production of biodiesel: possibilities and challenges. *Biofuels, Bioproducts and Biorefining*, 1 (2007), 57-66.

Al-Zuhair, S.; Ling, F. W.; Jun, L. S. Proposed kinetic mechanism of the production of biodiesel from palm oil using lipase. *Process Biochemistry*, 42 (2007), 951-960.

Benz, K.; Jäckel, K.-P.; Regenauer, K.-J.; Schiewe, J.; Drese, K.; Ehrfeld, W.; Hessel, V.; Löwe, H. Review – Utilization of Micromixers for Extraction Process. *Chemical Engineering and Technology,* 24 (2001), 11-17.

Berchmans, H. J.; Hirata, S. Biodiesel production from crude Jatropha curcas L. seed oil with a high content of free fatty acid. *Bioresource Technology*, 99 (2008), 1716-1721.

Bikou, E.; Louloudi, A.; Papayannakos, N. The effect of water on transesterification kinetics of cotton seed oil with ethanol. *Chemical Engineering and Technology*, 22 (1999), 70-75.

Canter, N. A New Approach to Chemical Synthesis and Analysis. *Tribology and Lubrication Technology*, 60 (2004), 12-13.

Canter, N. Making biodiesel in a microreactor. *Tribology and Lubrication Technology*, 62 (2006), 15-17.

Cao, F.; Chen, Y.; Zhai, F.; Li, J.; Wang, J.; Wang, X.; Wang, S.; Zhu, W. Biodiesel Production From High Acid Value Waste Frying Oil Catalyzed by Superacid Heteropolyacid. *Biotechnology and Bioengineering*, 101 (2008), 93-100.

Charpentier, J.-C. Market Demand versus Technological Development: the Future of Chemical Engineering. *International Journal of Chemical Reactor Engineering*, 1 (2003), Article A14.

Cross, W. T.; Ramshaw, C. Process intensification: laminar flow heat transfer. *Chemical Engineering Research and Design*, 64 (1986), 293-301.

Darnoko, D.; Cheryan, M. Kinetics of palm oil transesterification in a batch reactor. *Journal of the American Oil Chemists Society*, 77 (2000a), 1263-1267.

Darnoko, D.; Cheryan, M. Continuous production of palm methyl esters. *Journal of the American Oil Chemists Society*, 77 (2000b), 1269-1272.

De Jong, J.; Lammertink, R. G. H.; Wessling, M. Membranes and microfluidics: a review. *Lab on a Chip*, 6 (2006), 1125-1139.

Demirbas, M. F.; Balat, M. Recent advances on the production and utilization trends of bio-fuels: A global perspective. *Energy Conversion and Management*, 47 (2006), 2371-2381.

Demirbas, A. Biodiesel production via non-catalytic SCF method and biodiesel fuel characteristic. *Energy Conversion and Management*, 47 (2006), 2271-2282.

Demirbas, A. *Biodiesel: A Realistic Fuel Alternative for Diesel Engines*. Springer, London (2008a).

Demirbas, A. Comparison of transesterification methods for production of biodiesel from vegetable oils and fats. *Energy Conversion and Management*, 49 (2008b), 125-130.

Demirbas, A. Progress and recent trends in biodiesel fuels. *Energy Conversion and Management*, 50 (2009), 14-34.

Dimian, A. C.; Bildea, C. S. *Chemical Process Design: Computer-Aided Case Studies*. Wiley-VCH Verlag GmbH & Co. KGaA, Weinheim (2008).

Dorado, M. P.; Ballesteros, E.; Lopez, F. J.; Mittelbach, M. Optimization of alkali-catalyzed transesterification of Brassica Carinata oil for biodiesel production. *Energy and Fuels*, 18 (2004), 77-83.

Doku, G. N.; Verboom, W.; Reinhoudt, D. N.; Van Den Berg, A. On-microchip multiphase chemistry – a review of microreactor design principles and reagent contacting modes. *Tetrahedron*, 61 (2005), 2733-2742.

Ehrfeld, W.; Hessel, V.; Löwe, H. *Microreactors: New Technology for Modern Chemistry*, Wiley-VCH Verlag GmbH & Co. KGaA, Weinheim (2000).

Ehrfeld, W.; Hessel, V.; Haverkamp, V. Microreactors. *Ullmann's Encyclopedia of Industrial Chemistry*, Wiley-VCH Verlag GmbH & Co. KGaA, Weinheim (2002).

Freedman, B.; Pryde, E. H.; Mounts, T. L. Variables affecting the yields of fatty esters from transesterified vegetable oils. *Journal of the American Oil Chemists Society*, 61 (1984), 1638-1643.

Freedman, B.; Butterfield, R. O.; Pryde, E. H. Transesterification kinetics of soybean oil. *Journal of the American Oil Chemists Society*, 63 (1986), 1375-1380.

Fukuda, H.; Kondo, A.; Noda, H. Biodiesel Fuel Production by Transesterification of Oils. *Journal of Bioscience and Bioengineering*, 92 (2001), 405-416.

Giordanno, N. and Cheng, J.-T. Microfluid mechanics: progress and opportunities. *Journal of Physics: Condensed Matter*, 13 (2001), R271-R295.

Gokhale, S. V.; Tayal, R. K.; Jayaraman, V. K.; Kulkarni, B. D. Microchannel Reactors: Applications and Use in Process Development. *International Journal of Chemical Reactor Engineering*, 3 (2005), Review R2.

Groppi, G.; Tronconi, E. Honeycomb supports with high thermal conductivity for gas/solid chemical process. *Catalysis Toda, 2nd International Conference on structured Catalysis and Reactors ICOSCAR-2*, 105 (2005), 297-304.

Guan, G.; Kusakabe, K.; Moriyama, K; Sakurai, N. Continuous Production of Biodiesel Using a Microtube Reactor, Chemical Engineering Transactions, 14 (2008), 237-244.

Guan, G.; Sakurai, N.; Kusakabe, K. Synthesis of biodiesel from sunflower oil at room temperature in the presence of various cosolvents, Chemical Engineering Journal, 146 (2009a), 302-306.

Guan, G.; Kusakabe, K.; Moriyama, K.; Sakurai, N. Transesterification of Sunflower Oil with Methanol in a Microtube Reactor. *Industrial and Engineering Chemistry Research*, 48 (2009b), 1357-1363.

Günther, A. and Jensen, K. F. Multiphase microfluidics: from flow characteristics to chemical and materials synthesis. *Lab on a Chip*, 6 (2006), 1487-1503.

He, H.; Wang, T.; Zhu, S. Continuous production biodiesel fuel from vegetable oil using supercritical methanol process. *Fuel*, 86 (2007), 442-447.

Hessel, V.; Löwe, H. Microchemical Engineering: Components, Plants Concepts, User Acceptance – Part 1. *Chemical Engineering and Technology*, 26 (2003a), 13-24.

Hessel, V.; Löwe, H. Microchemical Engineering: Components, Plants Concepts, User Acceptance – Part 2. *Chemical Engineering and Technology*, 26 (2003b), 391-408.

Hessel, V.; Löwe, H. Microchemical Engineering: Components, Plants Concepts, User Acceptance – Part 3. *Chemical Engineering and Technology*, 26 (2003c), 531-544.

Hessel, V.; Hardt, S.; Löwe, H. *Chemical Microprocess Engineering: Fundamentals, Modeling and Reactions*, Wiley-VCH Verlag GmbH & Co. KGaA, Weinheim (2004).

Hessel, V.; Löwe, H.; Schönfeld, F. Micromixers – a review on passive and active mixing principles. *Chemical Engineering Science*, 60 (2005a), 2479-2501.

Hessel, V.; Löwe, H.; Müler, A.; Kolb, G. *Chemical Micro Process Engineering – Processing and Plants*, Wiley-VCH Verlag GmbH & Co. KGaA, Weinheim (2005b).

Hessel, V.; Knobloch, C.; Löwe, H. Review on Patents in Microreactor and Micro Process Engineering. *Recent Patent on Chemical Engineering*, 1 (2008), 1-16.

Hsu, A. F.; Jones, K. C.; Foglia, T. A.; Marmer, W. N. Continuous production of ethyl esters of grease using an immobilized lipase. *Journal of the American Oil Chemists' Society*, 81 (2004), 749-752.

Jachuck, R.; Pherwani, G.; Gorton, S. M. Green engineering: continuous production of biodiesel using an alkaline catalyst in an intensified narrow channel reactor. *Journal of Environmental Monitoring*, 11 (2009), 642-647.

Jähnisch, K.; Hessel, V.; Löwe, H.; Baerns, M. Chemistry in Microstructured Reactors. *Angewandte Chemie International Edition*, 43 (2004), 406-446.

Jensen, K. F. Microreaction engineering – is mall better?. *Chemical Engineering Science*, 56 (2001), 293-303.

Kashid, M. N. *Experimental and Modelling Studies on Liquid-Liquid Slug Flow Capillary Microreactors*, Dr.-Ing. Dissertation, Dortmund University (2007).

Kashid M. N. and Kiwi-Minsker L. Microstructured reactors for multiphase reactions: state of the art. Industrial and Engineering Chemistry Research, 48 (2009), 6465-6485.

Keil, F. J. *Modeling of Process Intensification*, Wiley-VCH Verlag GmbH & Co. KGaA, Weinheim (2007).

Kjeang, E.; Djilali, N.; Sinton, D. Microfluidic fuel cells: A review. *Journal of Power Sources*, 186 (2009), 353-369.

Kockmann, N. *Transport Phenomena in Micro Process Engineering*, Springer – Verlag Berlin Heidelberg (2008).

Kothare, M. V. Dynamic and control if integrated microchemical systems with application to micro-scale fuel processing. *Computers & Chemical Engineering*, 30 (2006), 1725-1734.

Kreutzer, M.; Kapteijn, F.; Moulijn, J.; Heiszwolf, J. Multiphase monolith reactor: Chemical reaction engineering of segmented flow in microchannels. *Chemical*

Engineering Science, 7th International Conference on Gas-Liquid and Gas-Liquid-Solid Reactor Engineering, 60 (2005), 5895-5916.

Kusdiana, D.; Saka, S. Kinetics of transesterification in rapeseed oil to biodiesel fuel as treated in supercritical methanol. *Fuel*, 80 (2001), 693-698.

Kusdiana, D.; Saka, S. Effect of water on biodiesel fuel production by supercritical methanol treatment. *Bioresource Technology*, 91 (2004), 289-295.

Lerou, J.; Harold, M.; Ryley, J.; Ashmead, J.; O´Brien, T.; Johnson, M.; Perrotto, J.; Blaisdell, C.; Rensi, T.; Nyquist, J. *Microfabricated minichemical systems: Technical feasibility*. Microsystem Technology for Chemical and Biological Microreactors, DECHEMA , Mainz, Germany (1996).

Liu, B.; Zhao, Z. Biodiesel production by direct methanolysis of oleaginous microbial biomass. *Journal of Chemical Technology and Biotechnology*, 82 (2007), 775-780.

Löwe, H.; Hessel, V.; Mueller, A. Microreactors. Prospects already achieved and possible misuse. *Pure and Applied Chemistry*, 74 (2002), 2271-2276.

Ma, F.; Hanna, M. A. Biodiesel production: a review. *Bioresource Technology*, 70 (1999), 1-15.

Mae, K. Advance chemical processing using microspace. *Chemical Engineering Science*, 62 (2007), 4842-4851.

Mansur, E. A.; Mingxing, Y.; Yundong, W.; Youyuan, D. A State-of-Art Review of Mixing in Microfluidic Mixers. *Chinese Journal of Chemical Engineering*, 16 (2008), 503-516.

Martínez, E. L. Development and Assessment of Microreactors Applied to Biodiesel Production, University of Campinas, M.Sc. Thesis, Campinas, São Paulo, Brazil, 2010.

Meher, L. C.; Vidya Sagar, D.; Naik, S. N. Technical aspects of biodiesel production by transesterification – a review. *Renewable and Sustainable Energy Reviews*, 10 (2006), 248-268.

Mills, P. L.; Quiram, D. J.; Ryley, J. F. Microreactor technology and process miniaturization for catalytic reactions – A perspective on recent developments and emerging technologies. *Chemical Engineering Science*, 62 (2007), 6992-7010.

Noureddini, H.; Zhu, D. Kinetics of Transesterification of Soybean Oil. *Journal of the American Oil Chemists Society*, 74 (1997), 1457-1463.

Noureddini, H.; Harkey, D.; Medikonduru, V. A continuous process for the conversion of vegetable oils into methyl esters of fatty acids. *Journal of the American Oil Chemists Society*, 75 (1998), 1775-1783.

Nguyen, N.-T.; Wu, Z. Micromixers – a review. *Journal of Micromechanics and Microengineering*, 15 (2005), R1-R16.

Obot, N. T. Toward a better understanding of friction and hear/mass transfer in microchannels – A literature review. *Microscale Thermophysical Engineering*, 6 (2002), 155-173.

Pinto, A. C.; Guarieiro, L. L. N.; Rezende, M. J. C.; Ribeiro, N. M.; Torres, E. A.; Lopes, W. A.; Pereira, P. A.; Andrade, J. B. Biodiesel: An Overview. *Journal of the Brazilian Chemical Society*, 16 (2005), 1313-1330.

Radisic, M.; Iyer, R. K.; Murthy, S. K. Micro- and nanotechnology in cell separation. *International Journal of Nanomedicine*, 1 (2006), 3-14.

Rebrov, E.; Ismagilov, I.; Ekatpure, R.; Croon, M.; Shouten, J. Header design for flow equalization in microstructured reactors. *AIChE Journal*, 53 (2007), 28-38.

Sarma, A. K.; Sarmah, J. K.; Barbora, L.; Kalita, P.; Chatterjee, S.; Mahanta, P.; Goswami, P. Recent Inventions in Biodiesel Production and Processing – A Review. *Recent Patents on Engineering*, 2 (2008), 47-58.

Schuchardt, U.; Sercheli, R.; Vargas, R. M. Transesterification of Vegetable Oils: A Review. *Journal of the Brazilian Chemical Society*, 9 (1998), 199-210.

Shah, S.; Gupta, M. N. Lipase catalyzed preparation of biodiesel from Jatropha oil in a solvent free system. *Process Biochemistry*, 42 (2007), 409-414.

Silva, C.; Weschenfelder, T. A.; Rovani, S.; Corazza, F. C.; Corazza, M. L.; Dariva, C; Oliveira, J. V. Continuous Production of Fatty Acid Ethyl Esters from Soybean Oil in Compressed Ethanol. *Industrial and Engineering Chemistry Research*, 46 (2007), 5304-5309.

Srivastava, A.; Prasad, R. Triglycerides-based diesel fuels. *Renewable and Sustainable Energy Reviews*, 4 (2000), 111-133.

Stankiewicz, A.; Moulijn, J. A. Process intensification. *Industrial and Engineering Chemistry Research*, 41 (2002), 1920-1924.

Sun, J.; Ju, J.; Ji, L.; Zhang, L.; Xu, N. Synthesis of Biodiesel in Capillary Microreactors. *Industrial and Engineering Chemistry Research*, 47 (2008), 1398-1403.

Sun, P.; Wang, B.; Yao, J.; Zhang, L.; Xu, N. Fast Synthesis of Biodiesel at High Throughput in Microstructured Reactors. *Industrial and Engineering Chemistry Research*, 49 (2010), 1259-1264.

Vasudevan, P. T.; Briggs, M. Review: Biodiesel production – current state of the art and challenges. *Journal of Industrial Microbiology and Biotechnology*, 35 (2008), 421-430.

Wen, Z.; Yu, X.; Tu, S.-T.; Yan, J.; Dahlquist, E. Intensification of biodiesel synthesis using zigzag micro-channel reactors. *Bioresource Technology*, 100 (2009), 3054-3060.

Wu, W. H.; Foglia, T. A.; Marmer, W. N.; Phillips, J. G. Optimizing Production of Ethyl Esters of Grease Using 95% Ethanol by Response Surface Methodology. *Journal of the American Oil Chemists' Society*, 76 (1999), 517-521.

Xu, Y.; Du, W.; Liu, D.; Zeng, J. A novel enzymatic route for biodiesel production from renewable oils in a solvent-free medium. *Biotechnology Letters*, 25 (2003), 1239-1241.

Zhou, W.; Boocock, D. Phase behavior of the base-catalyzed transesterification of soybean oil. *Journal of the American Oil Chemists Society*, 83 (2006), 1041-1045.

2.3. Conclusões

Neste capítulo foi apresentada uma breve revisão dos principais conceitos envolvidos na intensificação de processos, tecnologia de microreação e produção de biodiesel. Como pode ser visto na atualidade muitas tecnologias novas estão sendo desenvolvidas na indústria química, motivadas pela melhora no processo, aumento na segurança, melhora na utilização da energia, uma maior preocupação ambiental e até mesmo redução de custos de produção.

É evidente que a miniaturização tem fundamentais vantagens nos dispositivos de reação e análise. Com a diminuição das dimensões lineares, os gradientes e, portanto, as forças condutoras de transferência de massa e energia aumentam por unidade de volume, o que conduz a curtos tempos de resposta e mais simples processos de controle. Devido à intensificação das propriedades de transporte e a diminuição do "*hold up*", uma variedade de condições podem ser aplicadas nos microreatores os quais não podem ser realizadas nos reatores convencionais. Por exemplo, a realização de reações altamente exotérmica em condições aproximadamente isotérmicas pode ser atingida devido às elevadas taxas de transferência de energia dos sistemas de microreação. Além disso, a aplicação de micromisturadores favorece a mistura em sistemas multifásicos já que é diminuído o caminho difusional das moléculas permitindo uma interação maior entre as fases. Como resultado, as condições de reação podem ser manipuladas numa ampla faixa de operação, dificilmente conseguidas com equipamentos de laboratório ou plantas de produção convencionais. O uso da intensificação de processos é de fato um caminho promissor para as demandas de engenharia química no processo de globalização e sustentabilidade.

Por outra parte, com o inevitável esgotamento dos recursos não renováveis de combustíveis fósseis, e devido às suas características ambientais favoráveis, o biodiesel promete ser o combustível do futuro. Neste contexto, o biodiesel apresenta as seguintes vantagens: (1) uma alternativa aos combustíveis derivados do petróleo, o qual implica menor dependência das importações do petróleo bruto estrangeiro; (2) é um combustível renovável, ajudando atingir o objetivo de produzir energia renovável; (3) um balanço energético favorável; (4) redução de emissões de gases, efeito estufa, em concordância com o acordo do protocolo de Kyoto; (5) baixas emissões nocivas, o qual é muito vantajoso em áreas ambientalmente sensíveis tais como as grandes cidades e minas de extração; (6)

combustível biodegradável e não tóxico, sendo benéfico para áreas ambientalmente sensíveis; (7) a utilização dos recursos agrícolas excedentes, a qual pode também ajudar a melhorar a economia rural. Levando em consideração as vantagens acima, existe um crescente interesse na expansão da indústria do biodiesel. Neste contexto, a investigação está focada no melhoramento da qualidade e produção do biodiesel e o incremento do número de matérias primas disponíveis.

A reação de transesterificação pode ser catalisada por catalisadores homogêneos e heterogêneos. Por sua vez, os catalisadores homogêneos incluem ácidos e álcalis. Os mais comumente usados catalisadores alcalinos são hidróxido de sódio, metóxido de sódio e hidróxido de potássio. Os ácidos sulfúrico, clorídrico e sulfônico são usualmente preferidos como catalisadores ácidos. Já no caso dos catalisadores heterogêneos incluem-se silicatos de titânio, compostos metálicos alcalinotérreos e resinas de intercâmbio iônico.

Os catalisadores básicos são os mais comuns, já que o processo é mais rápido e as condições de reação são moderadas. No entanto, sua utilização na transesterificação de óleos vegetais produz sabão pela neutralização dos ácidos graxos livres presentes no óleo e a saponificação dos triglicerídeos. A formação de sabão é uma reação indesejável, devido a que consume parte do catalisador, diminui a produção de biodiesel e complica os passos de separação e purificação. A formação de sabão pode ser evitada utilizando um catalisador ácido. Além disso, os catalisadores ácidos esterificam os ácidos graxos livres para produzir alquilésteres de ácidos graxos, aumentando a produção de biodiesel. No entanto, a transesterificação de catálise ácida é muito mais lenta que a reação de catálise básica e precisa de condições extremas de temperatura e pressão.

Recentemente, tem havido um aumento no desenvolvimento de catalisadores heterogêneos para a produção de metilésteres de ácidos graxos, devido que sua utilização na reação de transesterificação economiza e simplifica muito o pós-tratamento dos produtos. Além disso, a utilização de catalisadores heterogêneos não produz sabão através da neutralização dos ácidos graxos livres e a saponificação dos triglicerídeos. Embora, a reação catalítica heterogênea também exige condições de reação extremas, enquanto à produção de ésteres metílicos e o tempo de reação ainda são desfavoráveis em comparação com os catalisadores alcalinos.

Recentemente, uma crescente atenção vem sendo dada ao desenvolvimento de microreatores para a produção de biodiesel (Tabela 3) e os resultados mostram estes como um promissor método devido à grande intensificação da transferência de massa e energia e maior relação área superficial–volume. A lentidão da reação de transesterificação no processo convencional tem sido atribuída à grande resistência difusiva entre as fases. Portanto, altas conversões são atingidas no microreator onde a resistência à difusão se converte menos significante.

Capítulo 3.

Caracterização Físico-Química do Óleo de Mamona

3.1. Introdução

Atualmente, a mamona é uma oleaginosa de relevante importância econômica e social no Brasil, onde de suas sementes se extraem um óleo de excelentes propriedades, de largo uso como insumo industrial. A quantidade de óleo extraída da semente está compreendida entre 40-60% em peso. Como componente principal, destaca-se o ácido ricinoléico (12-hidróxi-9-octadecenóico), que representa aproximadamente 90% da constituição total do óleo. O ácido ricinoléico tem ligação insaturada e se caracteriza por sua alta massa molar (298) e baixo ponto de fusão (5^{o}C). A presença de um maior teor de hidroxiácidos no óleo de mamona se reflete nas suas propriedades coligativas.

O óleo da mamona tem inúmeras aplicações. Ele pode ser usado na fabricação de tintas e isolantes, serve como lubrificante na aeronáutica, e é a base na manufatura de cosméticos, drogas farmacêuticas e em vários processos industriais. É um óleo bastante estável em variadas condições de pressão e temperatura, possuindo também estabilidade à oxidação. Não muda as suas características em variações bruscas de temperatura, razão do seu imprescindível emprego na aviação. O óleo de mamona produz biolubrificantes altamente resistentes, com melhores características do que os derivados do petróleo. Embora, nos óleos vegetais, o aquecimento pode ocasionar reações complementares de decomposição térmica, cujos resultados podem inclusive levar à formação de compostos poliméricos e alteração na viscosidade, demonstrando a importância de se estudar o comportamento térmico e reológico. Neste capítulo é feita uma análise térmica e reológica com o objetivo de determinar a viscosidade e estabilidade térmica de óleo de mamona bruto a diferentes temperaturas.

3.2. Desenvolvimento

O desenvolvimento deste capítulo é apresentado a seguir, no manuscrito intitulado: *Physicochemical Characterization of the Castor Oil.*

Physicochemical Characterization of the Castor Oil

Abstract

Castor oil has been shown to be an alternative raw material for biodiesel production. Currently, although the most of oils used for biodiesel production are derived from edible oils such as soybean and palm, castor oil is not edible, being constituted mainly by ricinoleic acid which represents 90% of its total composition. Because of this and other unique properties in relation to other vegetable oils, castor oil is considered like a potential renewable source for fuels production. Therefore, the characterization of this vegetable oil is important for further processing into biodiesel. This study presents the analysis of fatty acid composition, as well as thermal and rheological properties of a Brazilian castor oil. A Newtonian behavior and a linear temperature dependence of the density were observed in the temperature range studied. An empirical correlation was used for modeling the viscosity changes with temperature and good concordance with experimental data was obtained. The thermal decomposition of castor oil presented three consecutive events, due to polyunsaturated, monounsaturated and saturated fatty acid decomposition, respectively. In addition, moisture content value and free fatty acids percentage in the oil were also analyzed.

Keywords: Castor oil; Differential Scanning Calorimetry; Thermogravimetry; Rheology

1. Introduction

In industry, raw material properties are important input parameters required for unit operations design and new technological processes development. For instance, it is important for heat transfer equipment design, transport processes, pressure drop calculation and reactor design. On the basis of published data concerning to flow properties of oils (Fasina *et al*., 2006; Duntt e Prasad, 1989), the oil viscosity and thermal properties have a direct relationship with some chemical characteristic of lipids, such as the degree of unsaturation and the chain length of the fatty acids that constitute the triacylglycerols. For instance, the oil viscosity slightly decreases with increment the degree of unsaturation and rapidly increases with polymerization degree. Furthermore, studies carry out about the effects of temperature on vegetable oils show that the oil viscosity usually decreases with temperature increasing (Noureddini ET al., 1992; Coupland e McClements, 1997; Vazquez e Guerrero, 1993).

In biodiesel industry, the raw material sources are chosen according to the availability in each region or country. Any fatty acid source may be used to prepare biodiesel, but most industrial processes use soybean as raw material. Since the prices of edible vegetable oils, as soybean oil, are higher than the price of diesel fuel, waste vegetable oils and non-edible vegetable oils are preferred as potential inexpensive raw material sources. The biodiesel obtained from these raw materials is comparable in composition and in engine performance to diesel fuel obtained from crude oil, and furthermore, it is predicted to be more cost effective for biodiesel production than soybean oil.

In recent years, castor oil has showed to have high potential for being an alternative in biodiesel production. Ricinoleic acid, the major component of castor oil, constitutes roughly 85% of the total fatty acids, allowing to castor oil be miscible with methanol and ethanol (Osava, 2003; Conceição *et al.*, 2007), representing an advantage in transesterification to biodiesel. In Brazil, the use of castor oil has demonstrated to have technical and ecological benefits and stands as an opportunity for agricultural development in arid and impoverished areas like the northeast zone of the country. Therefore, in order to incorporate castor oil in biodiesel market, it is necessary to use analytical methods to evaluate its processing and storing conditions. Currently, the thermal analyses methods as differential scanning calorimetry (DSC) and thermogravimetry (TG) have received considerable attention due to its advantages such as higher precision and sensitivity, as well as, use of smaller amount of sample and faster results obtainment in comparison to the conventional methods (Conceição *et al.*, 2002). In addition, the rheological analyses are key tool to study the solution, suspension and mixing behavior of the fluids (Santos *et al.*, 2004).

In this study, it was made a physicochemical characterization of castor oil by determining thermal properties such as specific heat, decomposition temperature and enthalpy, as well as, rheological behavior at different temperatures in order to evaluate its potential use as feedstock for biodiesel production. The techniques used for the mentioned analyses were differential scanning calorimetry (DSC), thermogravimetry (TG), and rheological analyses. The Andrade's empirical correlation was used to predict the viscosity dependence with temperature and the model constants were fitted to the experimental data

obtained. Finally, gas chromatography was used to determinate the acid fatty composition of the vegetable oil.

2. Experimentation

2.1 Materials

The Castor oil used in this study was obtained of the Campestre Ind. & Com. De Óleos Vegetais Ltda., Brazil. The vegetable oil was used as purchased without any pretreatment and all chemicals and solvents utilized in the analyses were of high grade of purity.

2.2 Viscosity and Rheological test

The experimental procedures to viscosity determination and rheological behavior were performed with a Stabinger Viscometer - Anton Paar model SVM3000 and a HAAKE RheoStress model 6000, respectively. The concentric plate-plate measuring system was used to evaluate the rheological properties of the sample. This measured system consisted of two plates of 60 mm diameter, one stationary (bottom plate) and the other movable (Top plate). The top plate was used to shear oil samples contained a linear gap of 1 mm between the stationary and the movable plate. Shear rates were ramped from 0.1 to 200 s^{-1} at temperatures of 25 to 100°C.

2.3 Thermal Analyze

TG/DTG curve of castor oil was obtained in a thermobalance TGA-50 Shimadzu, in nitrogen atmosphere with a flow of 50mL/min, using alumina crucibles with a dynamic method of analysis, at heating rate of 10°C/min and interval of temperature of 25-900°C. DSC experiments were done on a DSC-823e Mettler Toledo, with a computer-based controller. Before of experiments, the DSC cell was purged with low-pressure nitrogen gas and calibrate with high purity indium. Typically 5-10 mg of oil sample was weighted in an open aluminum pan, hermetically sealed and placed in the DSC module with a similar empty pan as reference. Nitrogen was used as purge gas at a 50mL/min flow rate. Sample was subjected to the following temperature program: sample was cooled to 10°C using liquid nitrogen as the cooling medium and held for 5 min to homogenize the initial temperature. Then the sample was heated at 260°C at a rate of 10°C/min. Conceição *et al.* found that the heating rate that reproduces better results in the thermoanalytical analyses is 10°C/min because increasing the heating rate the distribution of the heat in the sample will

be lower leading to a displacement of the TG and calorimetric curves to higher temperatures. From obtained data, heat flow (W/g) versus temperature, the oil properties as specific heat, enthalpy and degradation temperature was determined.

2.4 Fatty Acid Composition

The fatty acid composition of the oil was analyzed with gas chromatography after transesterifiaction. FAMEs were prepared by transesterification of oil (70 mg) with sodium methoxide (0.5 N, 0.5 mL), heptane (5 mL) and sodium chloride saturated (10 mL). The methyl esters were analyzed on a Varian Star 3600 CX, equipped with a flame-ionization detector (FID). A polar capillary column D23 (50% cyanopropyl-phenyl and 50% dimethyl polysiloxane) with 0.25 mm internal diameter, 30 m length and 0.25 µm film thickness was used at a column head pressure of 10 psi. Hydrogen (99.995%) at approximately 23 mL/min was used as the carrier gas, and nitrogen (99.999%) at 20 mL/min was used as the makeup gas. The FID and injection temperatures were both maintained at 300 and 250°C, respectively. The injection mode was splitless, and sample of about 1 µL was injected with a 10 µL loop. The initial column oven temperature was 50°C, temperature was programmed to 180°C at 10°C/min and held at this temperature by 5 min before heated until 240°C at a rate of 5°C/min. FAME peaks were identified by comparison of retention times to a standard mixture (SUPELCO). The peaks areas were computed and percentages of FAME were obtained as area percentages by direct normalization.

2.5 Free Fatty acid and moisture content

The measurement was made in the titration Karl Fisher of Mettler Toledo, model DL31. The determination of moisture content present in the castor oil was made with titration of the conventional Karl Fisher reagent (iodine solution, Sulfur dioxide and imidazol) in the solvent anhydride methanol P.A. in presence of vegetable oil. For determination of free fatty acid content in the vegetable oil, the procedure based by method Ca 5a-40 AOCS by titration was made.

3. Results and Discussion

3.1 Rheology

As can be seen in the Figure 1 and 2, the castor oil exhibits a linear relation between shear stress and shear rate within the temperature range studied of 25 to 100°C. Consequently, the linear relation indicated a Newtonian behavior of castor oil and therefore

the viscosities at each temperature can be obtained from the slope of the fit of experimental shear stress-shear rates data to Newton's law of viscosity equation:

$$\sigma = \mu\dot{\gamma} \quad (1)$$

where σ is shear stress (mPa), γ is the shear rate (s^{-1}), and μ is viscosity (mPa·s). The values of the viscosities estimated at different temperatures are given in Table 1. In each case, the regression coefficient (R^2) obtained by fitting Equation 1 to the experimentally obtained shear stress-shear rate data was greater than 0.999. Densities of the castor oil were also obtained which shown a decreased linear with temperature. Equation of the linear fit is presented in Figure 2.

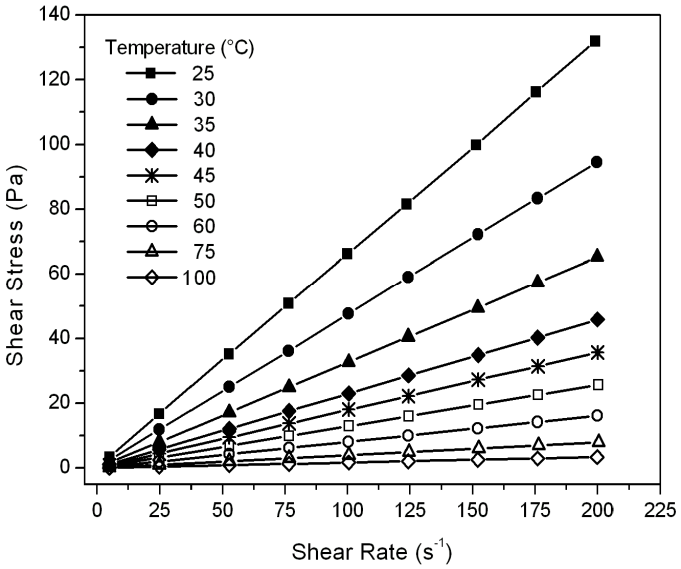

Figure 1. Shear Stress vs. Shear rate of castor oil

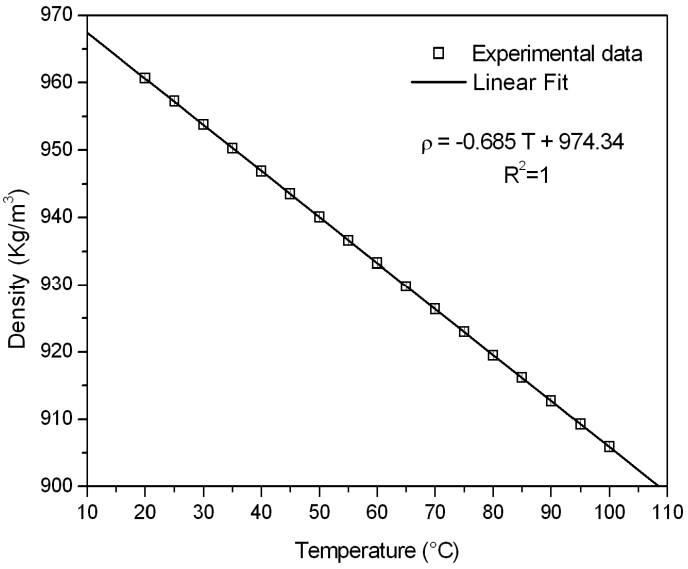

Figure 2. Density vs. temperature of castor oil

Table 1. Viscosity (mPa·s) and density (Kg m^{-3}) of castor oil at different temperatures

Temperature (°C)	Dynamic Viscosities (mPa·s)	Density (Kg/m^3)	Temperature (°C)	Dynamic Viscosities (mPa·s)	Density (Kg/m^3)
25	689.72	957.3	65	62.629	929.8
30	473.70	953.8	70	50.242	926.4
35	333.83	950.3	75	40.943	923.0
40	240.69	946.9	80	33.809	919.5
45	177.14	943.5	85	28.278	916.2
50	132.95	940.1	90	23.869	912.7
55	101.70	936.6	95	20.376	909.3
60	79.065	933.3	100	17.564	905.9

As expected, the viscosities of the oil decreased exponentially with increased temperature (Table 1). The viscosities at 25°C were about 39 fold greater than those at 100°C. This rheological behavior is similar to the results obtained by Santos *et al.* (2004) and Geller *et al.* (2000) to some vegetable oils and triglycerides. As can be seen, this will have significant effects on the energy required to pump the oil at elevated temperatures compared with refrigerated temperatures.

The viscosity variations are primarily caused by temperature and composition changes. This is due to the thermal movement among molecules and the reduction of intermolecular bond force, making flux between them easier and reducing viscosity. The correlations for the viscosity dependent temperature of fatty acids, triglycerides, and vegetable oils follow a general Andrade form, which can be represented as

$$\ln \mu = A + \frac{B}{T+C} + D \cdot T + \frac{E}{T^2} \quad (2)$$

where T is temperature and the terms A, B, C, D, and E are empirical coefficients that are determined based on regression analysis of the measured viscosity data or some basic considerations of the chemical structure (Anand *et al.*, 2009). For most liquids at temperatures below the normal boiling point, the plot of ln μ *vs.* 1/T or ln μ *vs.* ln T is approximately linear. Therefore, most correlations are presented in this form.

In this study, the dependence of castor oil viscosities on temperature was modeled using equations 2. Several researches have used this equation to describe the viscosity-temperature relationship of several systems (Valeri *et al.*, 1997; Abramovic and Klofutar, 1998; Azian *et. al.*, 2001; Fasina *et al.*, 2006). In this case, the empirical coefficients A, B, C, D, and E were estimated by using the function optimization FORTRAN-77 subroutine based on a genetic algorithm (PIKAIA) (Charbonneau, 2002). PIKAIA is public domain

software available electronically by the High Altitude Observatory (http://www.hao.ucar.edu/modeling/pikaia/pikaia.php). The standard error of estimate (SEE, Equation 3) was computed and used to compare the goodness of fit (an equation with lower SEE value gives a better fit to experimental data compared with an equation with higher SEE value) of the equations to the experimental data.

$$SEE = \sqrt{\frac{\sum_{i=l}^{n}\left(Y_i - Y_i'\right)^2}{n-p}} \qquad (3)$$

where Y is the oil viscosity at a particular temperature, Y_i' is the predicted viscosity from Equation 2, n is the number of data points, and p is the number of parameter. The values estimated of the empirical coefficients A, B, C, D, and E using the PIKAIA algorithm were: -11.158, 3038.875, 151.521, 0.019 and -3.806, respectively. The estimative of viscosity for the castor oil in temperature range of 25 to 100°C present a standard error (SEE) of 0.099, which indicate a good estimation. Figure 3 show the experimental data and predicted viscosities from the correlation for castor oil.

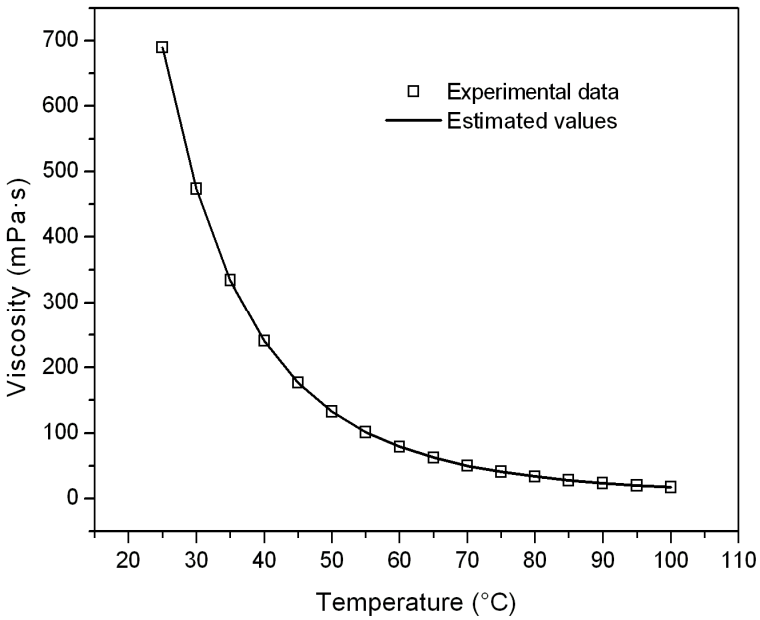

Figure 3. Viscosity *vs.* temperature for castor oil

3.2 Thermal Analysis

Thermal decomposition of castor oil was analyzed by TG and DSC methods and profiles are shown in Figure 4 and 5. The TG/DTG and DSC dynamic curve presented three events of thermal decomposition, between 300 and 500°C, with no residues after thermal treatment up to 900°C.

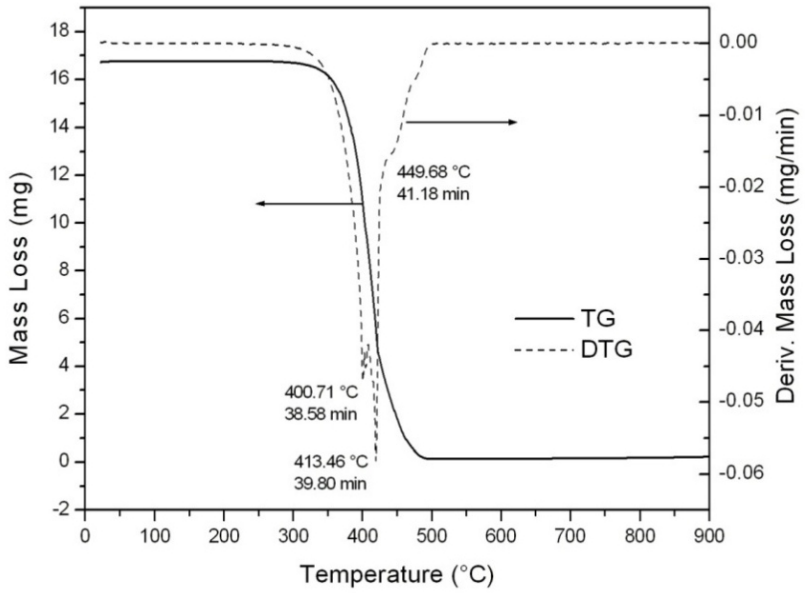

Figure 4. TG/DTG curves of castor oil

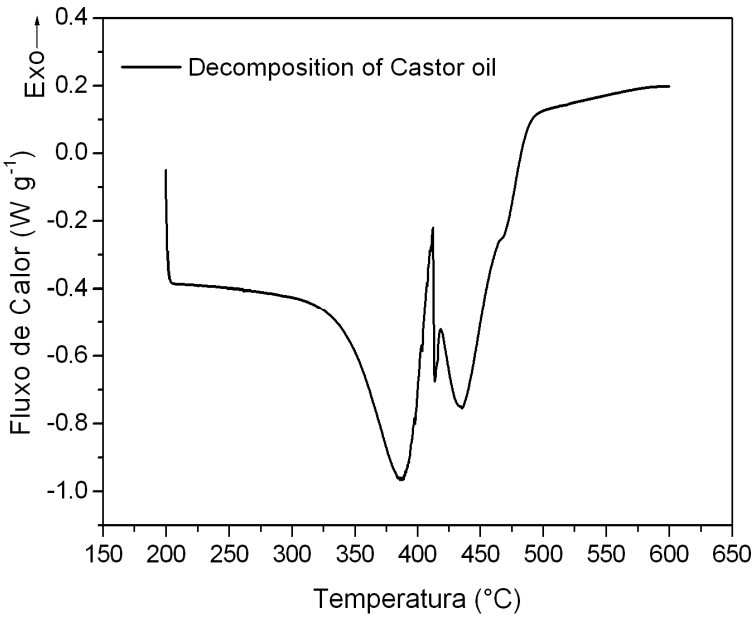

Figure 5. DSC curve of castor oil

The same results were obtained by Santos *et al.* (2004), which carried out thermogravimetric analyses for some edible oils. According to TG/DTG data (Figure 4), the first event (300-405°C) was attributed to the polyunsaturated fatty acid decomposition, which is the most important step to determine the thermal stability. Triglycerides comprise 96-98% of vegetable oil. During their heating, volatile compounds are produced and constantly removed by the vapor formed. These products are mainly formed by thermal reactions of unsaturated fatty acids (Felsner and Matos, 1998).

The second thermal decomposition event (405-420°C) is due to monounsaturated fatty acids decomposition. In this event, double bonds are broken leading to saturation in triglyceride molecules that constitute vegetable oil. The third thermal decomposition event, in the temperature range of 420-500°C, it is due to saturated fatty acids thermal decomposition.

The DSC curve (Figure 5) presents the same three events observed in the TG/DTG analyze where the endothermic transitions are due to thermal decomposition of saturated and unsaturated fatty acids, validating the thermoanalytical analyzes for the castor oil. Curve of specific heat capacity of castor oil obtained through standard procedures ASTM E 1269 and DIM 51007 is shown in Figure 6. The Cp and enthalpies calculated from DSC curves for castor oil are presented in Table 2. These values are in agreement with literature data for vegetable oils published by other researches (Conceição *et al.*, 2007; Santos *et al.*, 2004; Osmont *et al.*, 2007).

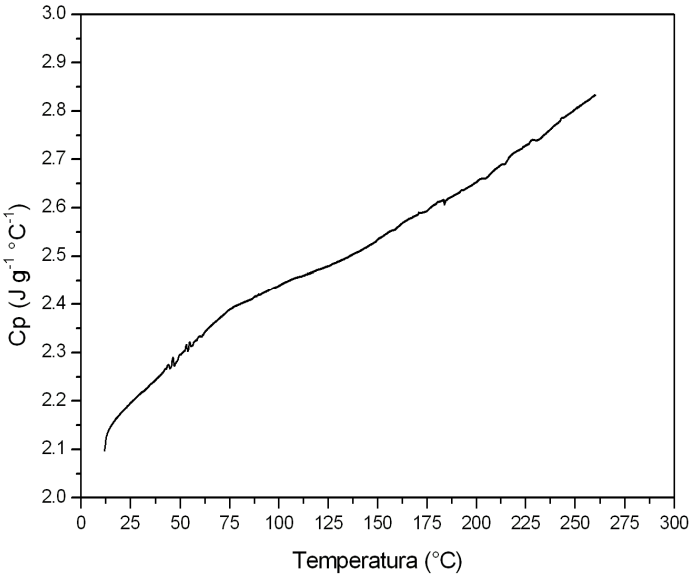

Figure 6. Specific heat capacity of castor oil

3.3 Fatty Acid Composition

The corresponding gas chromatogram for castor oil is shown in Figure 7 and the composition in fatty acid is illustrated on Table 3, which is in agreement with data published in elsewhere (Antoniosi, 1995; Conceição *et al.*, 2007). The castor oil possesses comparative atypical chemical characteristics to the majority of vegetable oils, presenting the ricinoleic acid trygliceride (12-hydroxy-9-octadecenoic), which is a less frequent hydroxylated fatty acid in vegetable oils, as its main constituent.

Table 2. Specific heat capacities and enthalpies of castor oil

Temp. (°C)	Cp (J g^{-1} °C^{-1})	Enthalpy (J g^{-1})	Temp. (°C)	Cp (J g^{-1} °C^{-1})	Enthalpy (J g^{-1})	Temp. (°C)	Cp (J g^{-1} °C^{-1})	Enthalpy (J g^{-1})
15	2.147	7.953	95	2.429	174.5	175	2.593	358.5
20	2.174	17.64	100	2.439	185.5	180	2.610	370.6
25	2.195	27.48	105	2.450	196.6	185	2.617	382.7
30	2.215	37.44	110	2.457	207.8	190	2.628	394.9
35	2.234	47.50	115	2.464	219.0	195	2.640	407.2
40	2.253	57.65	120	2.472	230.3	200	2.653	419.5
45	2.268	67.88	125	2.479	241.6	205	2.662	431.9
50	2.295	78.17	130	2.488	253.0	210	2.681	444.4
55	2.320	88.57	135	2.498	264.5	215	2.693	457.0
60	2.334	99.03	140	2.509	276.0	220	2.716	469.7
65	2.353	109.6	145	2.520	287.5	225	2.729	482.4
70	2.371	120.3	150	2.534	299.2	230	2.739	495.2
75	2.389	131.0	155	2.548	310.9	235	2.753	508.1
80	2.399	141.8	160	2.559	322.7	240	2.771	521.0
85	2.408	152.6	165	2.575	334.6	245	2.788	534.0
90	2.420	163.5	170	2.585	346.5	250	2.803	547.1

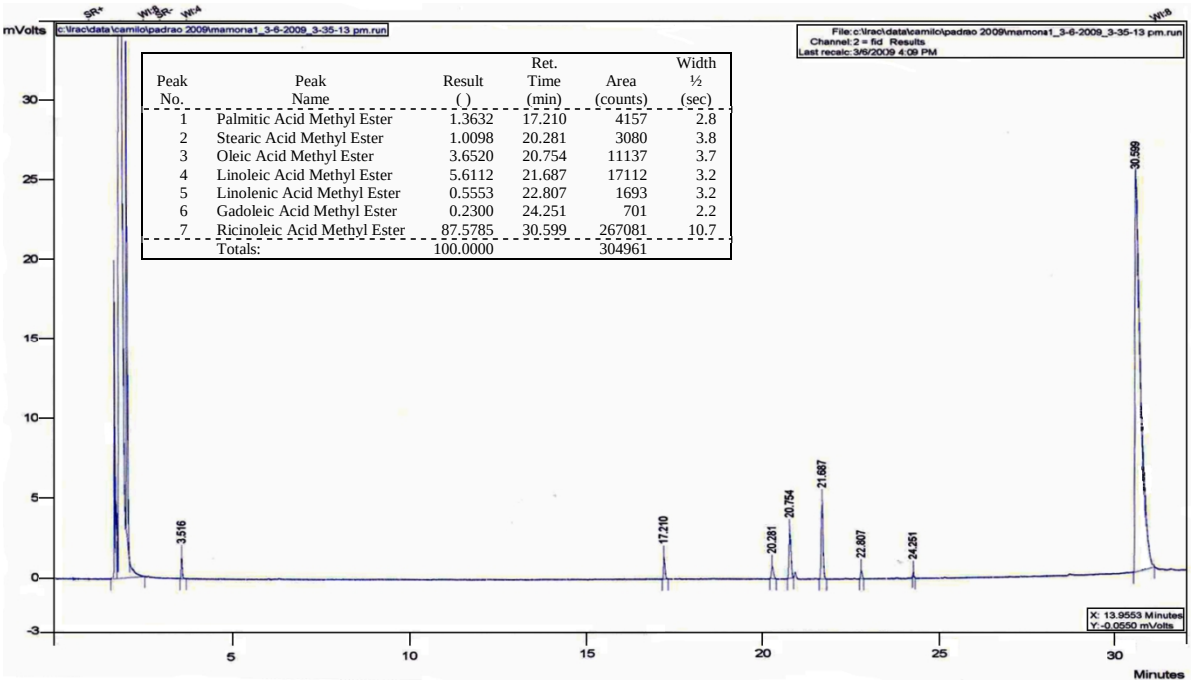

Figure 7. Gas chromatogram of castor oil

The accented presence of a unique type of fatty acid in the composition of the triglycerides is an outstanding characteristic of the castor oil. Ricinoleic acid which possesses 18 carbons, presents the peculiarity of being one of the few natural fatty acids whose chemical structure possesses three highly reactive functional groups: the carbonyl group in 1st carbon, the double linking or insaturation in 9th carbon and the hydroxyl group in 12th carbon. The functional groups present in the ricinoleic acid make possible for the

castor oil to be submitted to diverse chemical processes in which different products can be obtained, thence its vast industrial application.

Table 3. Composition in fatty acid of castor oil

Fatty acid	Structure (xx:y)	Composition (%)
Palmitic acid	16:0	1.4
Stearic acid	18:0	1.0
Oleic acid	18:1	3.7
Linoleic acid	18:2	5.6
Linolenic acid	18:3	0.6
Gadoleic acid	22:1	0.2
Ricinoleic acid	18:1-OH	87.5

3.4 Free Fatty acid and moisture content

The free fatty acid and moisture content are the key parameter for determining the viability of vegetable oils to be used in transesterification process. The free fatty acid content obtained for castor oil was 0.66%, calculated as oleic acid. Vegetable oils should have low content of free fatty acid because these may react with the alkaline catalyst during the transesterification process to form saponified products (Ferrari *et al.*, 2005; Dorado *et al.*, 2002) which reduces the conversion efficiency (Kusdiana e Saka, 2001). Commercial vegetable oils usually have a level of acidity of 0.5-3% (Kusdiana e Saka, 2001) but Dorado *et al.* (2002) indicated that for a complete reaction in the biodiesel production the content of free fatty acids should be less than 3%.

Moisture content for castor oil was of 0.10%. This value is consistent with the literature data (Fagundes *et al.*, 2004) which is indicative of a possible satisfactory conversion in transesterification reaction. High moisture values lead to catalyst deactivation and formation of free fatty acids, consequently, transforming fatty acids into soap and water which affects the reaction performance (Ferrari *et al.*, 2005).

4. Conclusions

Rheological data showed a linear relationship of shear stress to shear rate, indicating that vegetable oil has Newtonian behavior. The data adjustment to Newton's law of viscosity showed a regression coefficient greater than 0.999 for all temperatures analyzed. The Andrade's correlation used to model the dependence of the oil viscosity with temperature presented a standard error of 0.099 showed good concordances with experimental data in the temperature range analyzed.

Thermal decomposition profile of castor oil by both methods TG/DTG and DSC presented three consecutive events corresponding to polyunsaturated fatty acid decomposition, monounsaturated fatty acids decomposition and saturated fatty acids thermal decomposition, respectively. The specific heat, free fatty acid and moisture content of the vegetable oil showed to castor oil as promissory alternative for the production of biodiesel.

Acknowledgements

The author gratefully acknowledges the financial support provided by The Scientific Research Foundation for the State of São Paulo (FAPESP).

Bibliography

Abramovic, H.; Klofutar, C. The Temperature Dependence of Dynamic Viscosity for Some Vegetable Oils, Acta Chimica Slovenica, 1998, 45, 69-77.

American Oil Chemists Association Official Method Ca 5a-40, Free Fatty Acids, 1997, 1-2.

Anand, K.; Ranjan, A.; Mehta, P. S. Estimating the viscosity of vegetable oil and biodiesel fuels, Energy and Fuels, 2009, DOI:10.1021/ef900818s.

Antoniosi, N. R. Análise de óleos e gorduras vegetais utilizando métodos cromatográficos de alta resolução e métodos computacionais, Doctoral Thesis, Universidade de São Paulo, São Carlos, 1995.

ASTM E 1269-01, Standard Test Method for Determining Specific Heat Capacity by Differential Scanning Calorimetry, American Society for Testing and Materials, West Conshohocken, 2001.

Azian, M. N.; Mustafa, A. A.; Panau, F.; Ten, W. K. Viscosity estimation of triacylglycerols and of some vegetable oils, based on their triacylglycerol composition, Journal of the American Oil Chemists Society, 2001, 78, 1001-1005.

Charbonneau, P. Release notes for PIKAIA 1.2 NCAR Technical Note 451+IA (Boulder: National Center for Atmospheric Research), 2002.

Conceição, M. M.; Melo, A. M. L.; Narain, N.; Santos, I. M. G.; Souza, A. G. Isothermal Kinetic Study of Corn and Its Derivates, Journal of Thermal Analysis and Calorimetry, 2002, 67, 373-379.

Conceição, M. M.; Candeia, R. A.; Silva, F. C.; Bezerra, A. F.; Fernandes, V. J.; Souza, A. G. Thermoanalytical Characterization of Castor Oil Biodiesel, Renewable and Sustainable Energy Reviews, 2007, 11, 964-975.

Coupland, J. N.; McClements, D. J. Physical Properties of Liquid Edible Oils, Ibid, 1992, 69, 1189-1191.

DIN 51007, General Principles of Differential Thermal Analysis, German National Standard, Deutsches Institut Fur Normung, 1994.

Dorado, M. P.; Ballesteros, E.; Almeida, J. A.; Schellert, C.; Lohrlein, H. P.; Krause, R. An Alkali-Catalyzed Transesterification Process for High Free Fatty Acid Waste Oils, Transaction of the ASAE, 2002, 45, 525-529.

Dutt, N. V. K.; Prasad, D. H. L. Inter-relationships among the properties of fatty oils, Journal of the American Oil Chemists Society, 1989, 66, 701-705.

Fagundes, F. P.; Bezerra, J. P.; Garcia, M. A.; Medeiros, A. C. R.; Borges, M. R.; Garcia, R. B.; Costa, M. Avaliação das Propriedades do Óleo de Mamona na Produção de Biocombustível, 3º Congresso Brasileiro de P&D em Petróleo e Gás, 2005.

Fasina, O. O.; Hallman, H.; Craig-Schmidt, M.; Clements, C. Predicting Temperature-Dependence Viscosity of vegetable Oils from Fatty Acid Composition, Journal of the American Oil Chemists Society, 2006, 83, 899-903.

Felsner, M. L.; Matos, J. R. An. Assoc. Bras. Quím., 47 (1998) 308.

Ferrari, R. A.; Oliveira, V.; Scabio, A. Biodiesel de Soja – Taxa de Conversão em Ésteres Etílicos, Caracterização Físico-Química e Consumo em Gerador de Energia, Química Nova, 2005, 28, 19-23.

Geller, D. P.; Goodrum, J. W. Rheology of Vegetable Oil Analogs and Triglycerides, Journal of the American Oil Chemists Society, 2000, 77, 111-114.

Kusdiana, D.; Saka, S. Methyl Esterification of Free Fatty Acids of Rapeseed Oil as Treated in Supercritical Methanol, Journal of Chemical Engineering of Japan, 2001, 34, 383-387.

Noureddini, H.; Teoh, B. C.; Clements, D. Viscosities of Vegetable Oils and Fatty Acids, Journal of the American Oil Chemists Society, 1992, 69, 1189-1191.

Osava, M. Energy in a castor bean (online), 2003. <http://www.tierramerica.net/english/2003/0526/ianalisis.shtml> (accessed 18.06.2010).

Osmont, A.; Catoire, L.; Gökalp, I. Thermochemistry of Methyl and Ethyl Esters from Vegetable Oils, International Journal of Chemical Kinetics, 2007, 39, 481-491.

Santos, J. C. O.; Santos, I. M. G.; Conceição, M. M.; Porto, S. L.; Trindade, M. F. S.; Souza, A. G.; Prasad, S.; Fernandes, V. J.; Araújo, A. S. Thermoanalytical, Kinetic and Rheological Parameters of Commercial Edible Vegetable Oils, Journal of Thermal Analysis and Calorimetry, 2004, 75, 419-428.

Tan, C. P.; Che Man, Y. B. Differential Scanning Calorimetric Analysis of Edible Oils: Comparison of Thermal Properties and Chermical Composition, Journal of the American Oil Chemists Society, 2000, 77, 143-155.

Valeri, D.; Meirelles, A. J. Viscosities of fatty acids, triglycerides, and their binary mixtures, Journal of the American Oil Chemists Society, 1997, 74, 1221-1226.

Vazquez, J. F.; Guerrero, R. Regression Models that Describe Oil Absolute Viscosity, Ibid, 1993, 70, 1115-1119.

3.3. Conclusões

A viscosidade e densidade do óleo de mamona foram analisadas numa faixa de temperatura de 25 a 100°C. Observouse a diminuição exponencial da viscosidade do óleo com o incremento da temperatura. Este mostra o significativo ganho na energia requerida no bombeamento do óleo a elevadas temperaturas já que com um aumento da temperatura de 20 a 100°C, a viscosidade do óleo de mamona cai entorno de 39 vezes. A correlação de Andrade para descrever a variação da viscosidade dinâmica com a temperatura foi ajustada com os dados experimentais mediante o uso de um algoritmo genético PIKAIA escrito na linguagem de programação FORTRAN. Observouse que o modelo descrever a variação da viscosidade com a temperatura com um erro padrão (SEE) de 0.1%.

O perfil de decomposição térmica do óleo de mamona apresentou três eventos de decomposição, entre 300 e 500°C, sim resíduo depois do tratamento térmico até 900°C. O primeiro evento ocorreu na faixa de temperatura entre (300-405°C) atribuído à decomposição dos ácidos graxos poliinsaturados, sendo este o mais importante passo para a determinação da estabilidade térmica. O segundo evento de decomposição térmica ocorreu entre 405-420°C sendo atribuído à decomposição dos ácidos graxos monoinsaturados. O terceiro evento de decomposição térmica, na faixa de 420-500°C foi atribuído à decomposição térmica dos ácidos graxos saturados. Observou-se também que os resultados obtidos no DSC estiveram em concordância com os resultados obtidos no TG.

Através da análise da composição de ácidos graxos do óleo de mamona foi verificado que o ácido ricinoléico (12-hidroxi-9-octadecenóico) é o seu principal constituinte. O ácido ricinoléico é um ácido pouco freqüente nos óleos vegetais, e é constituído por um grupo hidroxila no décimo segundo carbono de sua cadeia carbônica. Isto o torna altamente reativo e confere propriedades coligativas diferenciadas ao óleo de mamona com relação aos demais óleos vegetais, tais como: viscosidade, densidade e solubilidade em álcool. Estas características tornam possível submeter o óleo de mamona a processos químicos diversos, em que diferentes produtos podem ser obtidos.

Além disto, o óleo de mamona apresentou uma composição de ácidos graxos livres de 0,66%, expresso em porcentagem de ácido oléico, e um teor de umidade de 0,10%. Estes valores encontrados são indicativos de uma possível conversão satisfatória no processo de transesterificação.

Capítulo 4.

Produção de Ésteres Etílicos do Óleo de Mamona

4.1. Introdução

Combustíveis alternativos para motores diesel têm-se tornado muito importantes devido a dois principais fatores: a) Diminuição das reservas de petróleo, b) Conseqüências ambientais causadas pelos gases de exaustão de máquinas movidas a combustíveis do petróleo. Dentre estes combustíveis alternativos o biodiesel é um candidato bastante promissor. As vantagens do uso do biodiesel são várias; na combustão emite baixas quantidades de CO, materiais particulados e hidrocarbonetos não queimados; o CO_2 produzido na combustão pode ser reciclado pela fotossíntese, minimizando assim o impacto do efeito estufa; ponto de fulgor alto e menos volátil o que o torna mais seguro para o transporte e manipulação; melhora a lubricidade do motor reduzindo o desgaste e aumentando a vida útil da máquina; não é tóxico; biodegradável e é um combustível renovável. O Biodiesel pode ser obtido através da reação de transesterificação de triglicerídeos, oriundos de óleos e gorduras vegetais ou animais, com um álcool de cadeia curta, resultando em alquil ésteres e glicerol. Dos álcoois de cadeia curta o metanol é o mais utilizado, entretanto este reagente é oriundo do petróleo e também é bastante tóxico. O uso de etanol é uma boa opção já que além de ser obtido da biomassa, o Brasil produz grandes quantidades desta matéria-prima. A reação de transesterificação é realizada na presença de catalisadores ácidos, básicos ou enzimáticos. Uma das matérias-primas bastante promissoras para a produção de biodiesel é o óleo de mamona. A mamona (*Ricinus comunnis*) desperta grande interesse para a produção de biodiesel, por ser uma oleaginosa que possui uma boa concentração de óleo em sua semente e também por ser uma planta de fácil cultivo e resistente ao clima árido. Tais características tornam a mamona uma boa alternativa como matéria prima na produção de biodiesel.

4.2. Desenvolvimento

O desenvolvimento deste capítulo é apresentado a seguir, no manuscrito intitulado: *Fatty Acid Ethyl Esters Production from Castor Oil.*

Fatty Acid Ethyl Esters Production from Castor Oil

Abstract

Actually, there exist several processes for converting vegetable oils (mainly triglycerides) into fatty acid ethyl esters (biodiesel). Transesterification of vegetable oils using alcohol in a basic catalytic environment is the most commonly used method for biodiesel production. The triglycerides conversion is affected by various factors, namely, type of alcohol used, molar ratio of alcohol/oil, type and amount of catalyst, reaction temperature, reaction time and feedstock quality (*e.g.,* free fatty acid content and moisture content). In this work, transesterification of castor oil by using ethanol and NaOH as catalyst has been studied under different conditions of temperature (between 30-70°C), catalyst concentrations (0.5-1.5 wt.% referred to the oil mass), and molar ratio ethanol/oil (from 6 to 12 mol alcohol per mol oil). The reaction products were analyzed for their residual content of triglycerides, diglycerides, monodiglycerires, glycerol, and esters by size-exclusion chromatography (SEC). The equilibrium conversions of triglycerides were observed to be in the range of 96-99% and were attained between 30-45 min. It was also observed an increment of equilibrium conversion with the increasing of the temperature and the molar ratio, while increasing the catalyst concentration had no significant effect on reaction time. The optimal operating parameters for laboratory-scale reactions were obtained at 30°C with a 12:1 molar ratio of ethanol/castor oil and 1.0% of NaOH by weight of castor oil for 99.1% yield of ethyl esters obtained.

Keywords: Ethanolysis; Size-exclusion chromatography; Transesterification; Castor oil

1. Introduction

In the last years, the world has been confronting with an energy crisis caused by the energetic resources depletion and the environmental problems increasing. This situation has led to looking for an alternative fuel, which should be not only sustainable but also environment friendly. Vegetable oils, and particularly their fatty acid alkyl esters, have showed to be a good diesel fuel alternative that does not require engine modifications. Chemical transformation of vegetable oil to fatty acid alkyl esters provides many advantages, such as viscosity reduction and minimization of carbon deposits on injector nozzles. As an initiative of the Brazilian government to stimulate the biodiesel production in the northeast region of the country (Lima, 2004), the castor oil plant (*Ricinus communis*)

has been recognized as a potential source for its production. Castor oil, obtained from seeds of *Ricinus communis* by pressing and/or solvent extraction, is constituted almost entirely (*ca.* 90%) by triglycerides containing the unusual ricinoleic acid (12-hydroxy-*cis*-octadec-9-enoic acid). Owing to the presence of a hydroxyl group at C_{12} of ricinoleic acid, castor oil presents several unique chemical and physical properties that are exploited in various industrial applications, including the production of coatings, plastics, and cosmetics.

Triglycerides present in vegetable oils can be converted by means of a transesterification (alcoholysis) reaction with an excess of ethanol (ethanolysis) into a fuel known as biodiesel (fatty acid ethyl esters), with chemical and physical properties close to those of diesel fuel, and that can be used either as pure biodiesel or as a mixture with conventional diesel (Meher *et al.*, 2006; Al-Zuhair, 2007; Vasudevan and Briggs, 2008). Transesterification of triglycerides to biodiesel and glycerol can be catalyzed by bases, acids and enzymes (lipases). The kinetic reaction depends on the type of alcohol used (methanol, ethanol, propanol or butanol), oil composition (including free fatty acid and water), type and amount of catalyst, temperature, and alcohol-oil molar ratio. Homogeneous base catalysts (mainly sodium and potassium hydroxides) are the most commonly used due to their high activity and other advantages that make them economically superior than mineral acids and immobilized lipases (Gerpen, 2005). Nevertheless, washing process to separate the biodiesel produced of the catalyst generates a considerable amount of waste-water. Therefore, because of both environmental and economical reasons, there exists an increasing interest in the possibility of replacing the homogeneous bases by heterogeneous solid catalyst (Dossin *et al.*, 2006).

Transesterification kinetic of vegetable oils has been studied extensively during the last two decades. An understanding of transesterification kinetic is critical for determining the optimum reaction conditions for the conversion of vegetable oils into esters. Moreover, transesterification reaction variables, such as alcohol/triglyceride molar ratio, type of catalyst, and alcohol polarity, have an important effect on the following stages of the process, thereby affecting the yield and purity of the esters produced. The aim of this work was to evaluate the influence of variables such as time, temperature, ethanol/castor oil molar ratio, and catalyst concentration, on the alkaline ethanolysis of castor oil. To carry out the corresponding reactions for this study, the stirrer speed was kept constant and sodium hydroxide was used as catalyst because of its high efficiency. The effect of

temperature, molar ratio alcohol to vegetable oil and mass of catalyst (sodium hydroxide) was investigated by observing the variation of the reacting medium composition i.e., ethyl esters produced, freed glycerol, unreacted triglycerides, and intermediate monoglycerides and diglycerides content, all this through gel permeation chromatography.

2. Experimentation

The experiments were carried out at atmospheric pressure and temperatures of 30, 50, and 70°C in a jacketed glass batch reactor with a drain cock at the bottom. This reactor was fitted with a sampling device and mechanical stirrer comprising a stainless steel turbine. The reaction temperature was controlled by means of a heated circulating water bath. In the experimental set up (Figure 1), 200 g of castor oil (Campestre Ind. & Com. De Óleos Vegetais Ltda., Brazil; acid value of 1.3 mg KOH/g measured according to AOCS Ca 5a-40 method), was initially charged into the reactor and preheated to the reaction temperature. The stirrer speed was set at 600 rpm, which provided satisfactory mixing. Then catalyst was rapidly added into the reactor dissolved in the amount of ethanol necessary to give desired alcohol/oil molar ratio. NaOH (Aldrich, 99.99%) was used as catalyst in amounts ranging from 0.5 to 1.5 wt.% referred to the oil mass. Ethanol/oil molar ratios considered were with ethanol in excess, 6:1, 9:1 and 12:1, due to the reversible character of the chemical reactions involved; a molecular weight of 926 was assumed for castor oil based in the fatty acid composition estimated according to AOCS Ce 1f-96 method (Fillières *et al.*, 1995). Samples (0.1 ml) were withdrawn during the experiments at various intervals and diluted in 10 ml of tetrahydrofuran (HPLC grade) to quench immediately the reaction and immediately cooling.

Figure 1. Experimental set-up for transesterification of castor oil

The size-exclusion chromatography (SEC) was used for the analysis of triglycerides, diglycerides, monoglycerides, ethyl esters and glycerol according to Shoenfelder method (Schoenfelder, 2003). For this purpose a VISCOTECK GPC/SEC TDA max^{TM} chromatograph with triple detector array: refractive index (RI), viscometer and light scattering detectors was utilized. Data collection and area analysis was performed with GPC/SEC software. The mobile phase was tetrahydrofuran (THF) grade HPLC (JT Baker, USA) at flow rate of 0.8 ml/min. Three GPC/SEC Phenogel analytical columns (Phenomenex, Torrance, CA) with different pore size, dimension of 300 mm x 7.8 mm and packed with spherical styrene divinylbenzene copolymer beads with an average particle size of 5 µm were used. It was first placed a column with a pore size of 100 Å, corresponding to a molar mass range of 100 - 6x10^3 and this was connected in series to two columns with a pore size of 50 Å, corresponding to a molar mass range of 50 - 3x10^3. Sample injection volume was 20 µl, and all analyses were carried out at 40°C.

The main difficulty was obtaining pure standards to calculate the correlation factors of mono-, di-, and triglycerides of castor oil. It was not possible to have a whole mixture of individual standards to reconstitute the lipid composition of castor oil, in particular the unusual ricinoleic acid. Therefore, standard mixture of 1,2,4-butanetriol, diolein, glycerol, monoolein, tricaprin, and triolein was used for calibration. In addition, tripalmitin, trilinolein, ethyl palmitate, ethyl stearate, ethyl oleate and ethyl ricinoleate was used as reference standard as well. Identification and calibration of the GPC/SEC peaks were performed analyzing the above mentioned standard mixture prepared gravimetrically within a range of concentrations obtained in the transesterification reaction samples. Standard calibration curves were obtained for each substance (triglycerides, diglycerides, monoglycerides, and fatty acid ethyl esters) and used to convert the integrated GPC/SEC areas to mass concentrations.

The relative percentage of each component is given by the following equation:

$$x_i = \frac{c_i \cdot 100}{c_{TG}+c_{DG}+c_{MG}+c_G+c_E} \quad (1)$$

The rate of conversion of castor oil to ethyl esters has been defined as:

$$R = \frac{c_E \cdot 100}{c_{TG}+c_{DG}+c_{MG}+c_E} \quad (2)$$

3. Results and Discussions

3.1 Method of analysis

Separation of each lipid category present in the reaction products of transesterification by Size-exclusion chromatography (SEC) is not possible. SEC is a method mainly used for separating and characterizing substances of high molar mass, wherein column packing with controlled pores sizes are used. Therefore, the degree of retention depends on the size and shape of the solute molecules dissolved in the mobile phase relative to the size and geometry of the column packing pores. Small molecules will permeate the smaller pores, intermediate-sized molecules will permeate only part of the pores and be excluded by the remaining ones, and very large molecules will be completely excluded. As a result, the solute molecules leave the column in the order of decreasing hydrodynamic size (related to the molar mass). Owing that column packing do not have a narrow pore size distribution, this is not sufficient to separate all molecular species, resulting in a poor discrimination of species of close molecular weight, leaving the column at very close retention times, and being detected together in a single peak (Arzamendi *et al.*, 2006).

The transesterification process involves three consecutive reversible reactions, which are accompanied by a significant variation in molar mass among the several types of substances produced. The first step is the conversion of triglycerides (molar mass of 970-807) to diglycerides (molar mass of 677-569), which is followed by the conversion of diglycerides to monoglycerides (molar mass of 385-331) and finally of monoglycerides to glycerol (molar mass of 92), yielding one molecule of ethyl ester (molar mass of 339-284) from each acylglycerol at each step. For this reason, the order in which these substances are detected by SEC are; triglycerides, diglycerides, monoglycerides, ethyl esters, and glycerol. The set column used, a combination of Phenogel column with a pore size of 100 Å and two Phenogel columns with a pore size of 50 Å, showed a good separation and reproducibility (Figure 2), which allowed suitable monitoring and evaluation of the transesterification reaction. In addition, after this period the chromatographic instrument is ready for starting a new analysis since the columns temperature and the flow rate of the mobile phase were not changed, unlike with gas chromatographic methods customarily used for this application, where sophisticated column temperature programs are applied (Freedman *et al.*, 1986a).

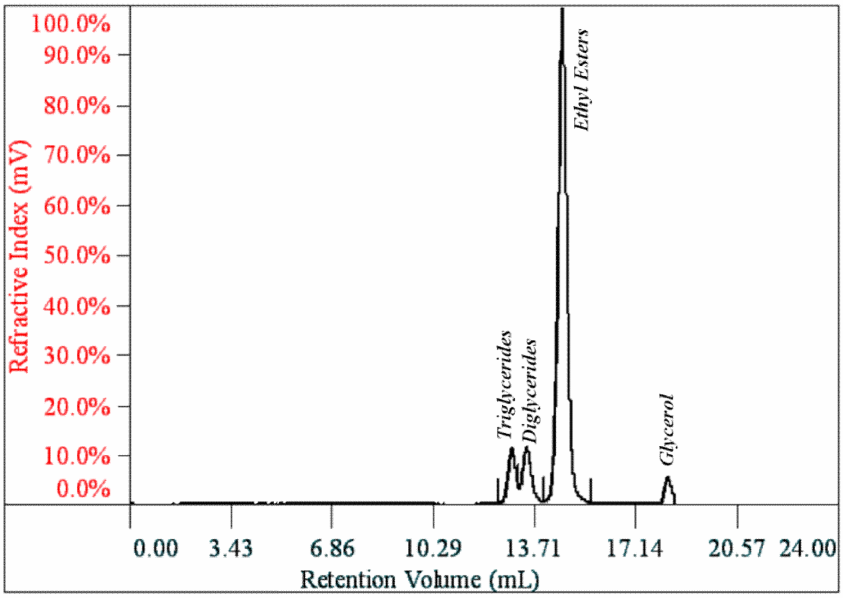

Figure 2. SEC Chromatogram typical of transesterificaton reaction of the castor oil.

Amongst the several variables affecting the synthesis of biodiesel, temperature reaction, catalysts concentration, and alcohol/oil molar ratio are recognized to be of the greatest relevance (Freedman *et al.*, 1984; Boocock *et al.*, 1998, Vicente *et al.*, 2004). Other important variables affecting also the transesterification reaction but not considered in this study are the water and free fatty acids contents of the oil and the use of organic solvents with the aim of improving the ethanol-oil miscibility. In following sections, results about the influence of time, temperature, ethanol/castor oil molar ratio and catalyst mass on the transesterification reaction of castor oil will be presented.

3.2 Effect of the time on the transesterification reaction

The concentration changes of the ethanolysis reaction medium at a molar ratio of 6:1, catalyzed by 0.5% NaOH by weight of castor oil, and 30°C is shown in Figure 3. As can be seen the reaction proceeded quickly during the first 15 min, obtaining an ethyl ester composition (Equation 1) of 73.6% and reaching the equilibrium after 30 min with ethyl ester composition at around 74%. On the other hand, the concentration of the di- and monoglycerides stabilized around of 3% and 1.3% at the end of the reaction, respectively (Figure 4). These results are consistent with behavior presented by other oils used. For instance, Ma *et al.* (1999) studied the effect of the reaction time on transesterification of beef tallow with methanol. It was reported that during the first 5 min the reaction proceeded very fast and the production of beef tallow methyl esters reached the maximum value at about 15 min.

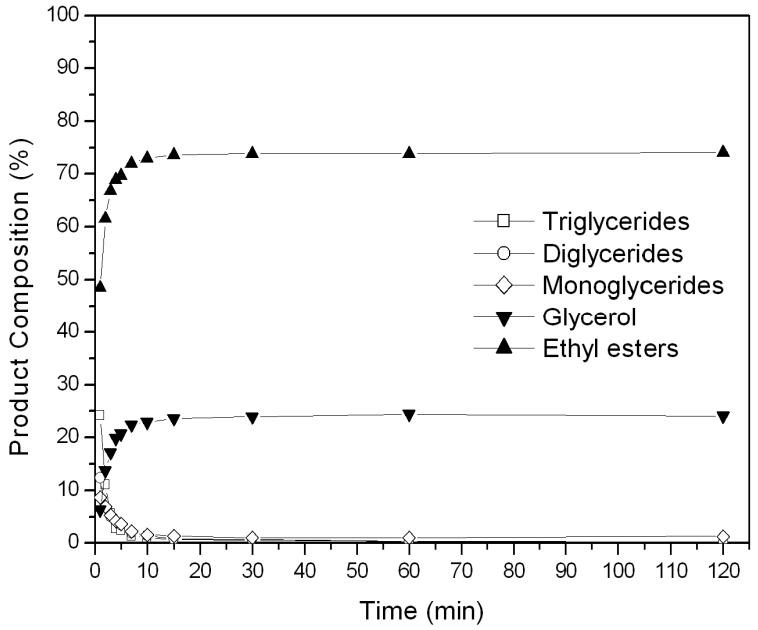

Figure 3. Effect of time on the transesterificaton reaction carried out at 30°C, ethanol/oil molar ratio of 6:1 using 0.5 wt.% NaOH based on the oil mass.

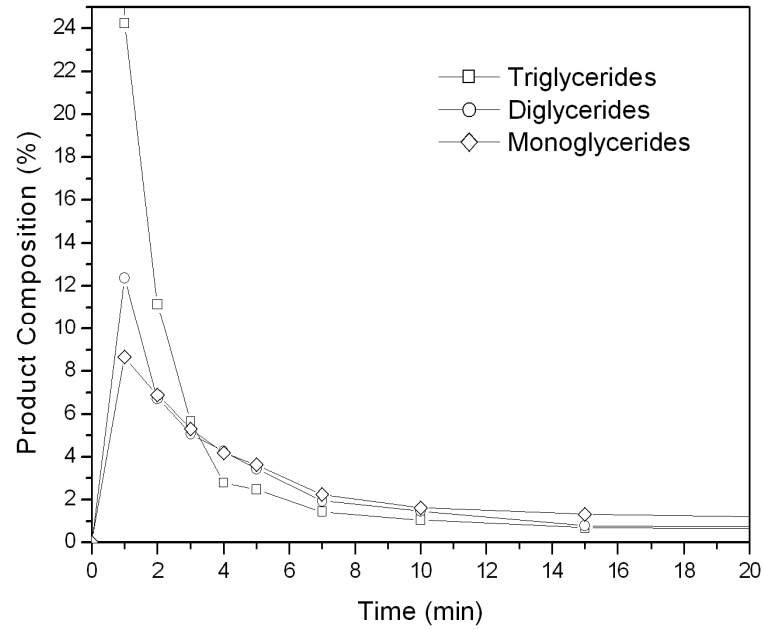

Figure 4. Effect of time on the transesterificaton reaction carried out at 30°C, ethanol/oil molar ratio of 6:1 using 0.5 wt.% NaOH based on the oil mass for tri-,di-,and monoglyceride through first 20 min.

3.3 Influence of the catalyst concentration on the ethyl ester yield

In most industrial chemical processes, the catalyst turns out be expensive compared to the reagents. The catalyst also generates additional costs because it is necessary to remove it from reaction medium at the end. As concerns the catalyst used in

the biodiesel production, there is a general agreement that basic compounds are the most active ones. In this regard, sodium hydroxide is the most commonly used due to their relatively low cost and high solubility in ethanol where the hydroxide ions react to form ethoxide anions, which are considered the active species (Dimian and Bildea, 2008). The amount of catalyst charged into the reactor is customary expressed as a percentage of the mass of oil to be transesterified; catalyst concentrations in the 0.5-1.5 wt.% range are the typical in ethanolysis reactions, although low concentrations (0.3-0.5wt.%) have been found to be optimal in some instances (Meher et al., 2006). In this work, three catalyst concentration were examined: 0.5, 1.0, and 1.5 wt.% based on the oil mass at the 30°C and an ethanol/castor oil molar ratio of 6:1 (Figure 5).

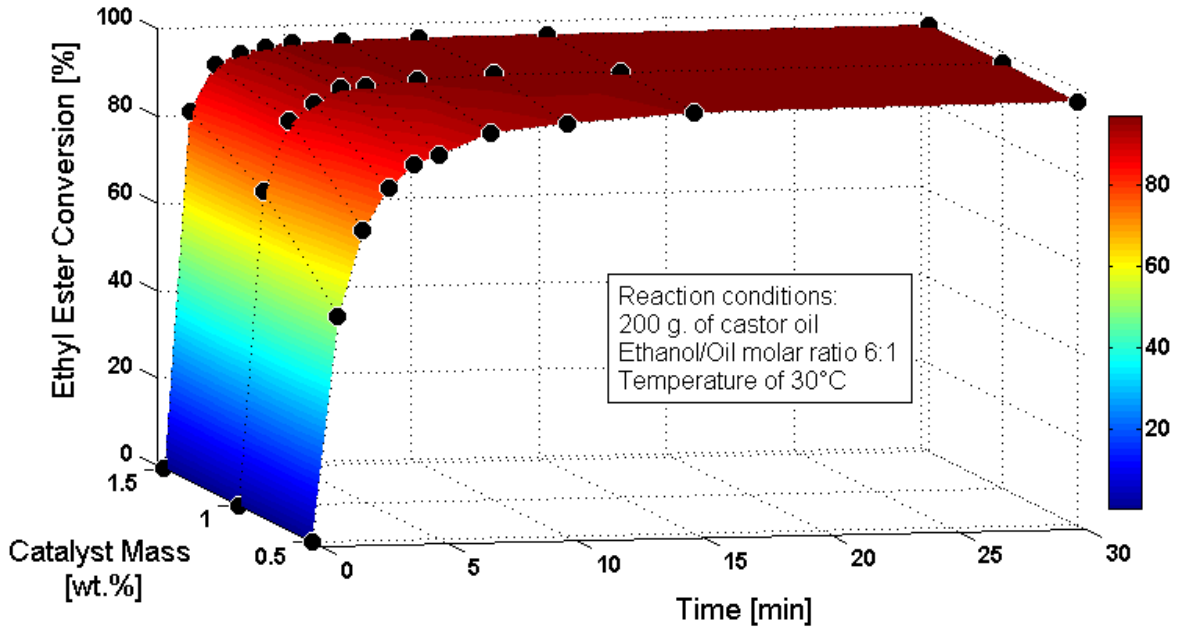

Figure 5. Effect of catalyst concentration on ester conversion (wt.% based on the castor oil mass).

As can be seen in the Figure 5, a catalyst concentration higher than 1.0% does not significantly increase the rate of conversion of ethyl esters and has no significant effect on the equilibrium, except for the speed of the reaction during the first 30 min. It was observed in all experiments that equilibrium conversions were achieved between 30-45 min and were in the range of 96-99%. It is well known that the minimum concentration of catalyst required is hard to evaluate because a compromise must be made between duration of the reaction and catalyst concentration. In the case of the castor oil transesterification, a time of 15, 7, and 4 min are needed to reach a conversion at around of 96% with catalyst mass of 0.5, 1.0, and 1.5 wt.%, respectively.

The selectivities to diglycerides, monoglycerides and glycerol for a series of transesterification reactions carried out at the condition described above are depicted in Figure 6. Oil conversion and products selectivities were calculated as Arzamendi *et. al.* (2006):

$$X_{oil} = \frac{N_{TG0} - N_{TG}}{N_{TG0}} \quad (3)$$

where X_{oil} is the oil conversion at time t, and N_{TG0} and N_{TG} are the moles of oil initially charged into reactor and remaining at time t, respectively. It was assumed that the oil consist exclusively of triglycerides.

$$S_i = \frac{N_i}{N_{TG0} - N_{TG}}, \qquad \text{i=DG, MG} \quad (4)$$

where S_i is the selectivity to diglycerides (DG) or monoglycerides (MG) at time t, and N_i are the moles of the product for which the selectivity is being calculated contained in the reaction time t. The glycerol selectivity was calculated from:

$$S_{GLY} = 1 - S_{MG} - S_{DG} \quad (5)$$

From Equations 4 and 5 was seen that in the transesterification reaction after 3 min the castor oil conversions were about 0.83, 0.93 and 0.96 for NaOH concentrations of 0.5, 1.0 and 1.5 wt.%, respectively. On the other hand, Meneghetti *et al.* (2006) studied the effect of the amount and nature of the catalyst on the yields of fatty acids ethyl esters from castor oil. It was found more efficient transesterification of castor oil using methoxide and acid catalyst that basic catalyst, but it was found also that high acid value exhibit by castor oil may lead to the neutralization of part of catalyst present, thus reducing the formation of ethoxides and producing soaps within the reaction medium.

Base-catalyzed ethanolysis is an addition-elimination reaction involving the nucleophilic attack of the ethoxide anion on a carbon atom of the carbonyl groups of acylglycerols resulting in the displacement of the oxygen atom of glycerol and the formation of an ethyl ester. As the ethoxide anion results from the reaction of ethanol with the hydroxide ions, the concentration of ethoxide ions increases as the amount of NaOH charged into the reactor, but the use of high concentrations can lead to a reduction in the yield as a result of an increase the side reactions like soap formation, thus explaining the results shown in Figure 5.

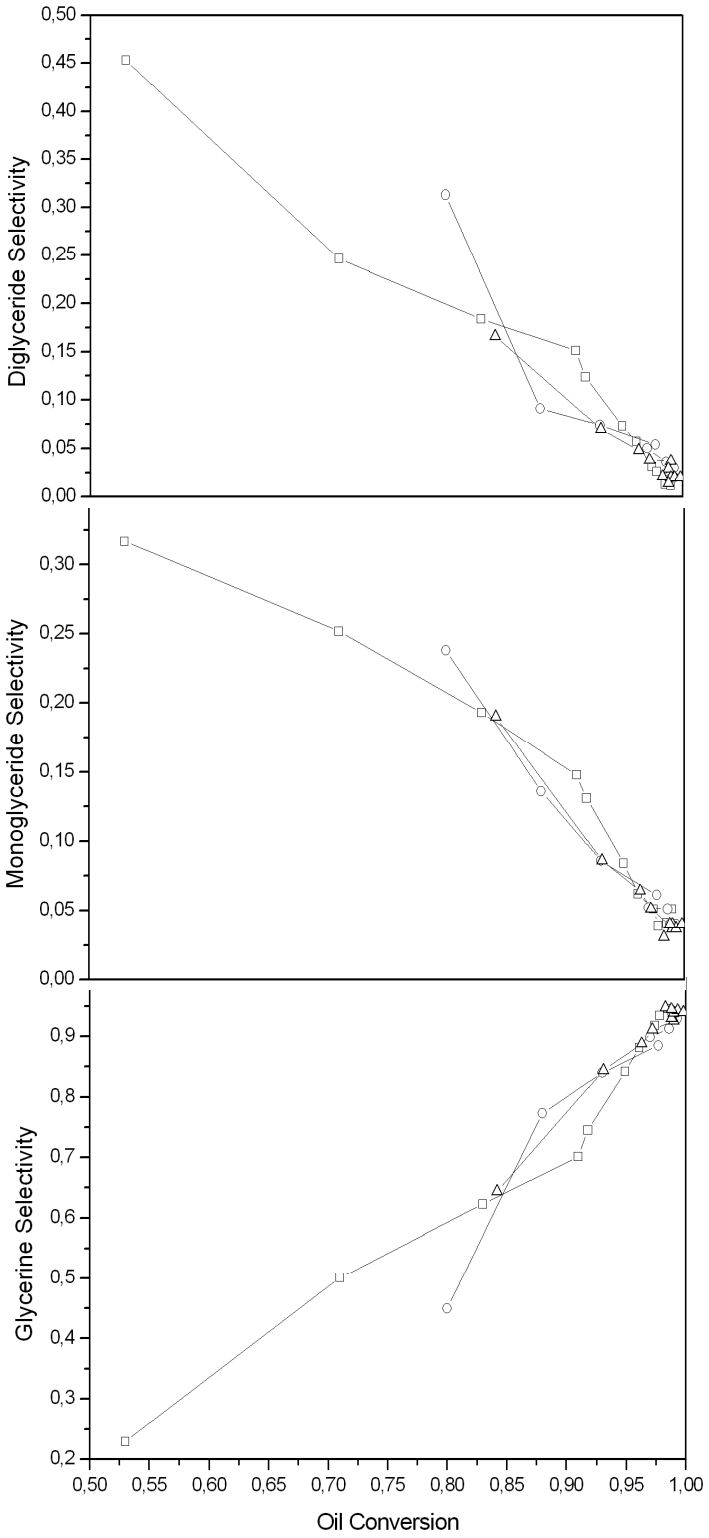

Figure 6. Selectivities evaluated to diglycerides, monoglycerides and glycerol as a function of castor oil conversion for a series of transesterification reactions carried out at 30°C with 200 g of oil, ethanol/oil molar ratio of 6:1 and concentration of NaOH: 0.5 wt.% (□), 1 wt.% (○) and 1.5 wt.% (Δ).

Regarding the reactions selectivity, it can be seen from Figure 6 that the results are consistent with a reaction scheme of three consecutive reactions with diglycerides and monoglycerides acting as intermediates and glycerol as end product (Freedman *et al.*, 1986b; Boocock *et al.*, 1996). Indeed, for very low oil conversions the diglycerides and monoglycerides selectivity tends to 1 whereas for glycerol is close to 0. As the reaction advances the diglycerides and monoglycerides selectivity continuously decreases and the glycerol selectivity increases to reach a value close to 1 by the end of the reaction.

3.5 Effect of ethanol/castor oil molar ratio on the ethyl ester conversion

The effect of the ethanol/oil molar ratio in the transestetification reaction of castor oil at 30°C with 0.5 wt.% NaOH is presented in Figure 7. There is a positive effect of the alcohol excess on the oil conversion for reaction times where the oil conversion and the equilibrium reaction increase with the ethanol/oil molar ratio. For instance, after 5 min the rate of conversion of castor oil to ethyl esters is 87.92% for an ethanol/oil ratio of 6:1, 95.39% for a ratio of 9:1 and increases up to 98.13% for a 12:1 ratio. As was expected, the alcohol in excess helps to shift the forward reactions leading to improve the conversion of triglycerides (Figure 8). It was observed a significant increase in equilibrium conversion with an enhance in molar ratio of 6:1 to 9:1, but a increase in molar ratio of 9:1 to 12:1 has a negligible effect on the rate of conversion of ethyl esters. This behavior can be attributed to a high increasing in the molar ratio of ethanol/oil can results in the excessive dilution of catalyst decreasing of yield reaction.

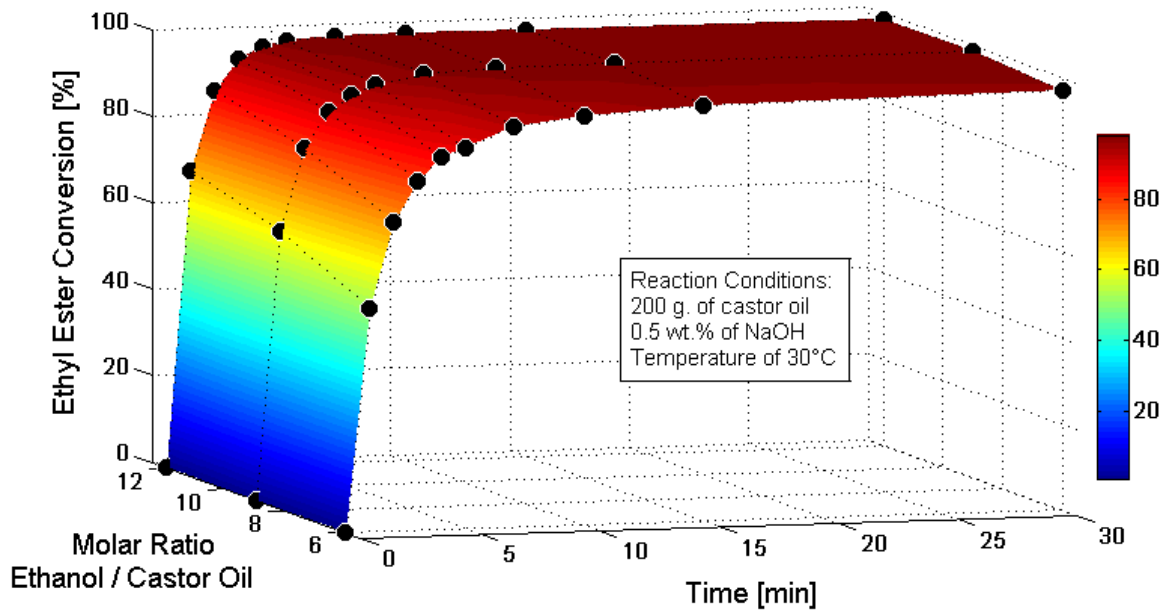

Figure 7. Effect of Ethanol/Castor oil molar ratio on the ethyl ester conversion

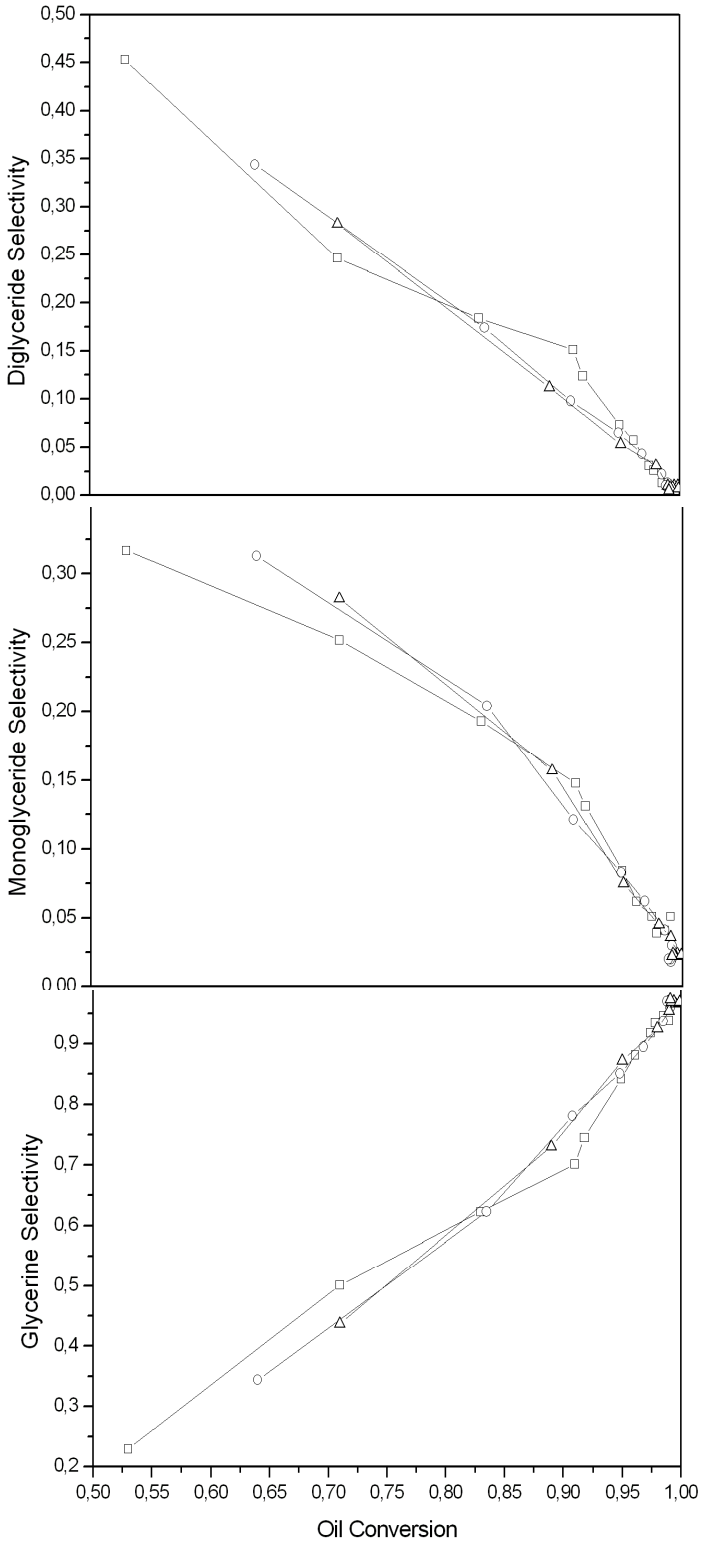

Figure 8. Selectivities evaluated to diglycerides, monoglycerides and glycerol as a function of castor oil conversion for a series of transesterification reactions carried out at 30°C with 200 g of oil, 0.5 wt.% NaOH and ethanol/oil molar ratios: 6:1 (□), 9:1 (○) and 12:1 (Δ).

Indeed, the selectivities to diglycerides and monoglycerides decrease much faster in the reaction performed with highest ethanol/oil ratio. This is a consequence of the two-phase nature of the reaction and the fact that the NaOH catalyst is located in the ethanol phase where the mono- and diacylglycerols are formed and further easily react to ethyl esters. Nivea *et al.* (2006) found castor oil conversions higher than 93.78% for reactions conducted at 30°C with large catalyst content, up to 1.3 wt.% and lower ethanol:castor oil molar ratio or with catalyst content from 0.8 to 1.2 wt.% with large ethanol:castor oil molar ratio, up to 19:1.

3.3. Effect of temperature on ethyl ester conversion

The rate of ethyl ester conversion was studied for temperatures of 30, 50 and 70°C (Figure 8) to an ethanol/castor oil molar ratio of 6:1 and 0.5% of NaOH by weight of castor oil. It could be observed a decrease in the time needed to achieve equilibrium conversion with an increase in temperature. The reaction equilibrium was achieved between 20-30 min in all experiments. The ethyl ester conversions at 30, 50 and 70°C were observed to be at about of 94.6%, 96.6% and 97.1%, respectively, at 10 min of reaction time. In addition, there was an increase insignificant of the ethyl ester conversion between a reaction conducted at the near ethanol's boiling point and a reaction at 50°C. After 30 min the conversions were almost the same for all temperatures analyzed, approximately of 97.1%.

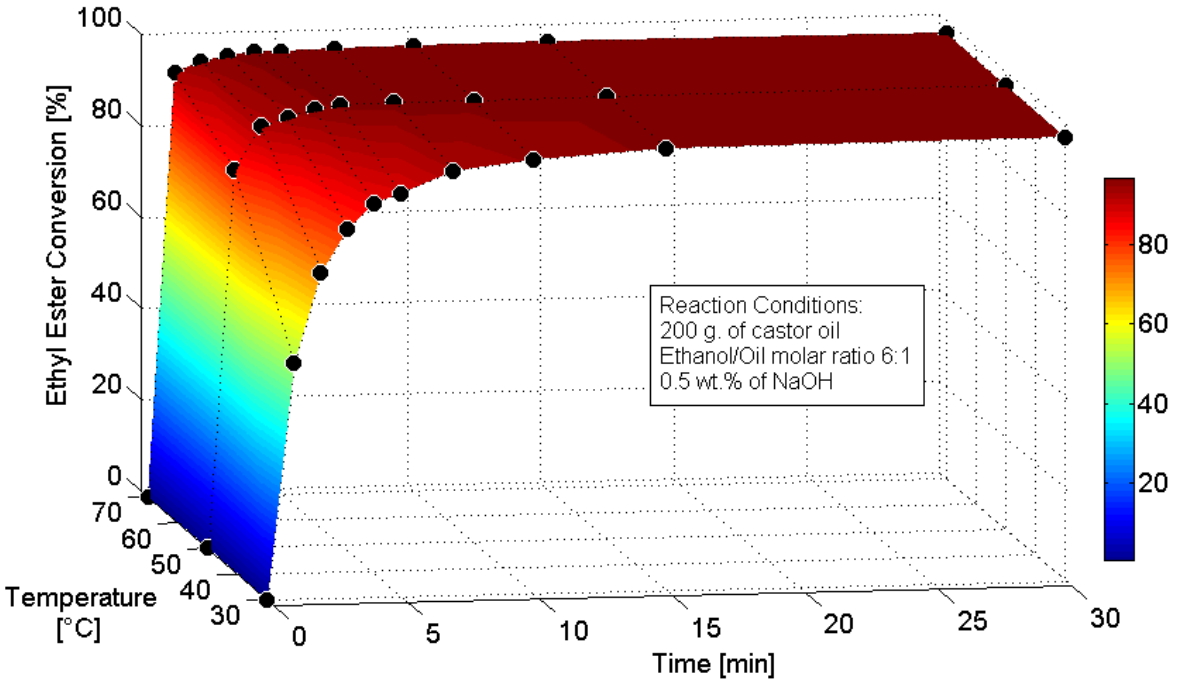

Figure 8. Effect of temperature on the transesterificaton reaction using sodium hydroxide as catalyst.

3.6 Optimal conditions for ethanolysis of castor oil

The study of the different variables affecting the reaction yield of castor oil with ethanol was conducted under laboratory-scale conditions and, therefore, it is hard to determine the choice of optimum conditions of the process for industrial-scale. However, can be seen that an ethanol/castor oil molar ratio of 12:1, 1.0% of NaOH by weight of castor oil and 30°C gives best results (Figure 8), considering the high yield and relative short reaction time observed (30 min). Nevertheless, this need not be the same for large scale. Indeed, economic compromises, must be adapted among the four parameter examined. Consequently, the reaction carried out at 30°C, molar ratio ethanol/castor oil of 9:1, and 0.5% of NaOH seems a good choice, keeping the economic compromise between variables studied, with an ethyl ester conversion of 98.7% in 30 min. These results are in concordance with work made by Smith (1949), where methanolysis of castor oil to methyl ricinoleate proceeded most satisfactorily at 25-35°C with a molar ratio of 6:1-12:1 and 0.005-0.35% (by weight of oil) of NaOH catalyst.

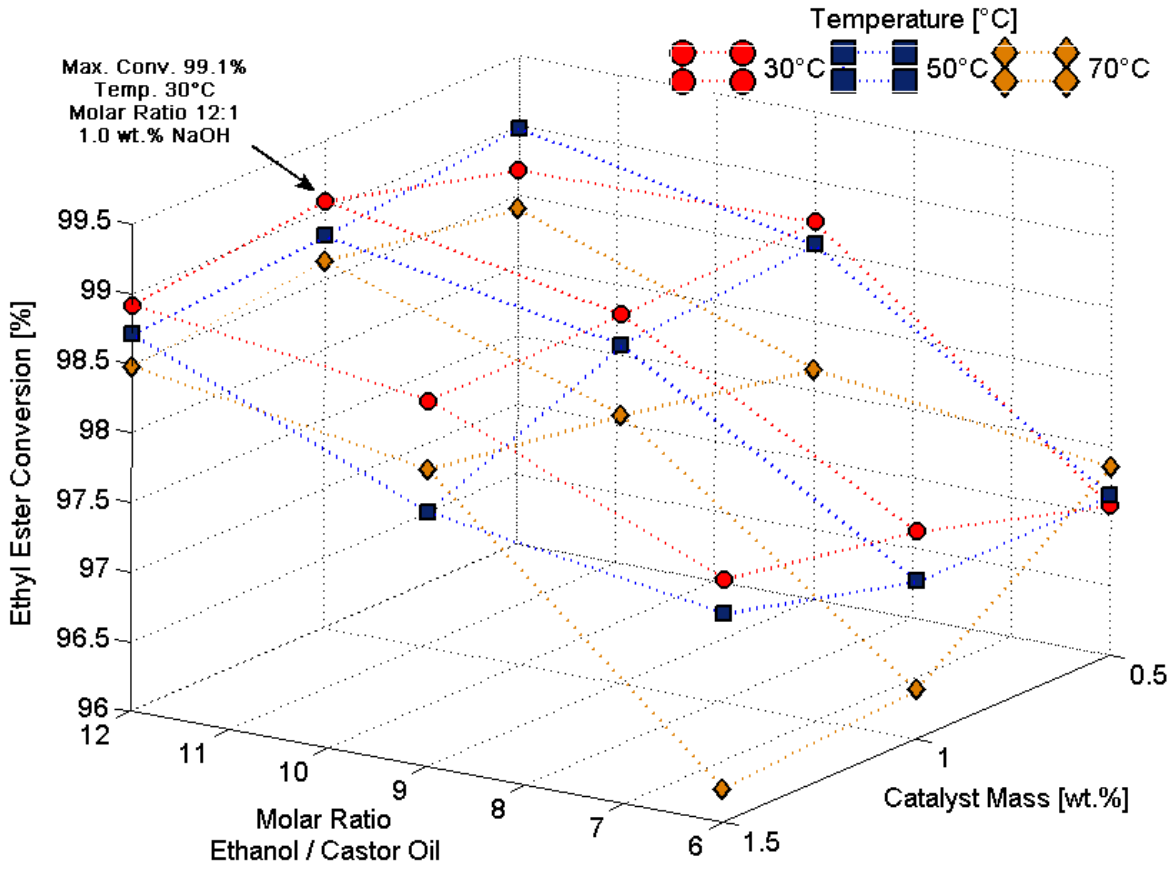

Figure 8. Ethyl ester conversions at different experimental conditions for a reaction time of 30 min.

4. Conclusions

Production of biodiesel from castor oil was carried out by homogeneous basic catalysis. The study indicated that given enough time, the transesterification reaction advanced satisfactorily at mild temperatures with alkali catalyst, attaining high equilibrium conversions. In addition, the rate of reaction was observed to be strongly influenced by reaction temperature, ethanol/castor oil molar ratio, and catalyst concentration. However, has been seen that the end products of the reaction present difficulties with respect to the separation and purification of the biodiesel produced.

The analytical method based on size exclusion chromatography allowed the simultaneous determination of the several compounds involved in the ethanolysis reaction and the evaluation the effects of the reaction. It was observed that increasing temperature resulted in increased rate of reaction and smaller time to achieve the equilibrium conversions. It was observed in all experiments that equilibrium conversions were achieved between 30-45 min and were in the range of 96-99%. No significant effects on the reaction rate were observed after 30 min, for increments of catalyst concentration from 1.0 to 1.5 wt.% NaOH, molar ratio from 9:1 to 12:1, and reactions conducted near at boiling point of ethanol.

On the other hand, conversion rates of castor oil to ethyl esters were 87.92% for an ethanol/oil ratio of 6:1, 95.39% for a ratio of 9:1 and 98.13% for a 12:1 ratio, after 5 min. In addition, the ethyl ester conversions at 30, 50 and 70°C were observed to be about of 94.6%, 96.6% and 97.1%, respectively, at 10 min of reaction time. From the results obtained, it could be seen that an ethanol/castor oil molar ratio of 12:1, 1.0% of NaOH by weight of castor oil and 30°C gave the best results, considering the high yield and relative short reaction time. Nevertheless, the reaction carried out at 30°C, molar ratio ethanol/castor oil of 9:1, and 0.5% of NaOH seems a good choice, keeping the economic compromise between variables studied, with an ethyl ester conversion of 98.7%.

Acknowledgements

The author gratefully acknowledges the financial support provided by The Scientific Research Foundation for the State of São Paulo (FAPESP).

Bibliography

Al-Zuhair, S. Production of biodiesel: possibilities and challenges, Biofuels, Bioproducts and Biorefining, 1 (2007), 57-66.

American Oil Chemists Association Official Method Ca 5a-40, Free Fatty Acids, 1997, 1-2.

American Oil Chemists Association Official Method Ca 5a-40, Free Fatty Acids, 1997, 1-2.

Arzamendi, G.; Arguiñarena, E.; Campo, I., Gandía, L. M. Monitoring of biodiesel production: Simultaneous analysis of the transesterification products using size-exclusion chromatography, Chemical Engineering Journal, 122 (2006), 31-40.

Boocock, D. G. B.; Konar, S. K.; Mao, V. Fast one-phase oil-rich processes for the preparation of vegetable oil methyl esters, Biomass and Bioenergy, 11 (1996), 43-50.

Boocock, D. G. B.; Konar, S. K.; Mao, V.; Lee, C.; Buligan, S. Fast Formation of High-Purity Methyl Esters from Vegetable Oils, Journal of the American Oil Chemists' Society, 75 (1998), 1167-1172.

Dimian, A. C.; Bildea, C. S. *Chemical Process Design: Computer-Aided Case Studies*. Wiley-VCH Verlag GmbH & Co. KGaA, Weinheim (2008).

Dossin, T. F.; Reyniers, M. F.; Marin, G. B. Kinetics of heterogeneously MgO-catalyzed transesterification, Applied Catalysis B: Environmental, 61 (2006), 35-45.

Freedman, B.; Pryde, E. H.; Mounts, T. L. Variables affecting the yields of fatty esters from transesterified vegetable oils, Journal of the American Oil Chemists' Society, 61 (1984), 1638-1643.

Freedman, B.; Kwolek, W. F.; Pryde, E. H. Quantitation in the analysis of transesterified soybean oil by capillary gas chromatography, Journal of the American Oil Chemists' Society, 63 (1986a), 1370-1375.

Freedman, B.; Butterfield, R. O.; Pryde, E. H. Transesterification kinetics of soybean oil, Journal of the American Oil Chemists' Society, 63 (1986b), 1375-1380.

Fillières, R.; Benjelloun-Mlayah, B.; Delmas, M. Ethanolysis of rapessed oil: Quantification of ethyl esters, mono-, di-, and triglycerides and glycerol by high-performance size-exclusion chromatography, Journal of the American Oil Chemists' Society, 72 (1995), 427-432.

Gerpen, J. V. Biodiesel processing and production, Fuel Processing Technology, 86 (2005), 1097-1107.

Lima, P.C.R. O Biodiesel e a Inclusão Social, Estudo sobre recursosMinerais, Hídricos e Energéticos, Consultoria Legislativa, Câmara dos Deputados, Governo do Brasil, Brasília, Distrito Federal (2004).

Ma, F.; Hanna, M. A. Biodiesel production: a review, Bioresource Technology, 70 (1999), 1-15.

Ma, F.; Clements, L. D.; Hanna, M. A. The Effect of Mixing on Transesterification of Beef Tallow, Bioresource Technology, 69 (1999), 289-293.

Meher, L. C.; Sagar, D. V.; Naik, S. N. Technical aspects of biodiesel production by transesterification - a review, Renewable and Sustainable Energy Reviews, 10 (2006), 248-268.

Meneghetti, S.; Meneghetti, M.; Wolf, C.; Silva, E.; Lima, G.; Coimbra, M.; Soletti, J.; Carvalho, S. Ethanolysis of Castor and Cottonseed Oil: A Systematic Study Using Classical Catalysts, Journal of the American Oil Chemists' Society, 83 (2006), 819-822.

Peña, R.; Romero, R.; Martínez, S. L.; Ramos, M. J.; Martínez, A.; Natividad, R. Transesterification of Castor Oil: Effect of Catalyst and Co-Solvent, Industrial and Engineering Chemistry Research, 48 (2009), 1186-1189.

Schoenfelder, W. Determination of monoglycerides, diglycerides, triglycerides and glycerol in fats by means of gel permeation chromatography, European Journal of Lipid Science and Technology, 105 (2003), 45-48.

Smith, M. K. Process of Producing Esters. US Patent 2,486,444 (1949).

Vicente, G.; Martínez, M.; Aracil, J. Integrated biodiesel production: a comparison of different homogeneous catalysts systems, Bioresource Technology, 92 (2004), 297-305.

Vasudevan, P. T.; Briggs, M. Biodiesel production – current state of the art and challenges, Journal of Industrial Microbiology and Biotechnology, 35 (2008), 421-430.

4.3. Conclusões

Neste capítulo foi estudado o efeito das principais variáveis que afetam a produção de biodiesel a partir do óleo de mamona, tais como: concentração de catalisador, razão molar etanol/óleo e a temperatura. O método analítico, baseado na cromatografia de exclusão por tamanho permitiu a determinação simultânea das concentrações dos diversos compostos envolvidos na reação de transesterificação do óleo de mamona. O método se mostrou ser simples, robusto, relativamente rápido e com resultados precisos e reprodutíveis.

O aumento da concentração de catalisador de 0,5% para 1,0% provocou um considerável aumento na conversão. Por outro lado, um aumento da concentração de catalisador de 1,0% para 1,5% não ocasionou um considerável efeito sobre conversão do óleo, conforme verificado no gráfico 5. Além disso, a evolução da seletividade dos produtos da reação com o tempo foi afetada pela concentração de catalisador. Uma maior seletividade foi observada para os diglicerideos e monoglicerideos durante os primeiros minutos da reação com uma menor concentração de catalisador. Conforme avança a reação, a seletividade dos diglicerideos e monoglicerideos cai, sendo favorecida então a seletividade da glicerina.

Nos ensaios em que foram utilizados uma razão molar etanol:óleo de mamona de 6:1, 9:1 e 12:1, verificou-se um aumento da conversão com o tempo de reação. Esse comportamento demonstra que a reação atinge a estabilidade em conversões inferiores às obtidas em 30 minutos de reação. Além disso, observou-se um aumento da conversão com o aumento da razão molar álcool etílico:óleo de mamona para a mesma concentração de catalisador e temperatura. Isto foi verificado ao se observar o gráfico 7, onde uma conversão de 87,92, 95,39 e 98,13% foi obtida para uma razão molar álcool:óleo de 6:1, 9:1 e 12:1, respectivamente, e um tempo de reação de 5 min.

Observou-se também que o aumento da temperatura resulta em um aumento na taxa de reação e um menor tempo para atingir a conversão de equilíbrio. Um efeito menos significativo foi observado a temperaturas maiores de 50°C o que produz só um pequeno aumento da conversão. A variação de temperatura de 50°C para 70°C provocou um aumento na conversão de 0,6% em 10 minutos de reação e de 0,2% em 60 minutos de reação. Este comportamento é devido à maior solubilidade do óleo de mamona em álcool a

temperatura ambiente em comparação com outros óleos vegetais. Portanto, o aumento de temperatura não contribui no aumento da solubilidade entre o óleo de mamona e o etanol.

No entanto, tem sido visto que os produtos finais da reação apresentam dificuldades no que diz respeito à separação e purificação do biodiesel produzido. O biodiesel produzido a partir de óleo de mamona apresenta uma alta viscosidade e só poderia ser usado como uma mistura com o diesel mineral ou com biodiesel obtido de óleos menos viscosos em diferentes proporções.

Capítulo 5.

Modelagem e simulação da cinética de transesterificação para a produção de biodiesel

5.1. Introdução

O biodiesel é uma alternativa na tentativa de substituição do óleo diesel por biomassa, iniciada pelo aproveitamento de óleos vegetais *in natura*. Uma das grandes vantagens do biodiesel é sua adaptabilidade aos motores do ciclo diesel, diferindo, de outros combustíveis limpos como o gás natural ou biogás, que requerem adaptação dos motores. Sua viabilidade, do ponto de vista econômico, está relacionada à substituição das importações e às vantagens ambientais inerentes tais como a redução de emissão de materiais particulados e de enxofre, que evitará custos com saúde pública, e de gases responsáveis pelo efeito estufa.

No momento, a obtenção de biodiesel por transesterificação é o processo mais utilizado nas plantas industriais. A reação de transesterificação apresenta uma cinética bastante diferenciada em função do tipo de catalisador utilizado, sendo a catálise básica homogênea aquela que fornece maior velocidade de reação e a mais utilizada industrialmente. O conhecimento sistemático da cinética de transesterificação de óleos vegetais é de fundamental importância no projeto de processos de produção de biodiesel via rota básica. Na literatura são apresentados diferentes modelos para a cinética da transesterificação (Diasakou *et al*., 1999; Darnoko *et al*., 2000; Freedman *et al*. 1986; Noureddini e Zhu, 1997; Meher *et al*., 2006). No entanto, um pequeno número destes trabalhos trata com a transesterificação de óleo de mamona e etanol.

Sabe-se que os óleos vegetais são basicamente compostos por vários triglicerídeos, os quais são transformados ao longo da reação em diglicerídeos, monoglicerídieos e finalmente ésteres, o que torna a quantificação química dos produtos formados nas etapas intermediarias complicada. Por outra parte, a descrição matemática dos modelos cinéticos da transesterificação leva a um conjunto de equações diferenciais ordinárias que

representam o balanço de massa das espécies reagentes. Estas equações formam um sistema de variáveis acopladas e altamente não linear que não apresenta solução analítica. Assim, a simulação numérica torna-se uma importante ferramenta para obter a solução deste sistema de equações e avaliar condições apropriadas de reação ou mesmo condições de otimização de processo.

Desta forma, neste capítulo teve-se como objetivo desenvolver a modelagem da cinética de transesterificação do óleo de mamona com etanol via catálise básica, com o intuito de obter uma ferramenta de simulação numérica que possibilite a predição do rendimento da reação para condições de operação estabelecidas.

5.2. Desenvolvimento

O desenvolvimento deste capítulo é apresentado a seguir, no manuscrito intitulado: *Modeling and Simulation of Transesterification Kinetics for Biodiesel Production.*

Modeling and Simulation of Transesterification Kinetics for Biodiesel Production

Abstract

A mathematical model describing chemical kinetics of transesterification of castor oil for biodiesel production has been represented. The model is based on the reverse mechanism of transesterification reactions and describes dynamics concentration changes of triglycerides, diglycerides, monoglycerides, biodiesel, and glycerol production. The chemical model is described (after rational simplifications) by a system of differential kinetic equations which are solved numerically by computing methods. Reaction rate constants, k_i, were written in the Arrhenius form and were determined for all the forward and reverse reactions. An analysis of key process variables such as temperature and molar ratio ethanol/castor oil was performed to achieve the maximum castor oil conversion rate to biodiesel. The predictive power of the model was checked for the very wide range of operational conditions and parameters values by fitting different experimental results for homogeneous catalytic process. The theoretical data obtained with kinetic model were compared numerically and/or graphically with experimental parameters not used in the previous fit. A very good correlation between model simulation and experimental data was observed. The results showed that at temperatures of 30 and 50°C the $k_{DG\text{-}MG}$ (k_4) and $k_{MG\text{-}G}$ (k_6) were higher than $k_{TG\text{-}DG}$ (k_2), which indicated that the first step reaction was the limit step for the overall reaction, whereas that at temperatures higher of 70°C the rate constant $k_{MG\text{-}G}$ (k_6) showed lower value. In addition, the reaction rate constant forward showed be higher that reversible rate constant for all temperatures.

Keywords: Biodiesel; Modeling; Transesterification kinetics; Castor oil.

1. Introduction

Humanity's dependence on petroleum for produce transportation fuel increases every year due the present pattern of consumption, thereby increasing the demand and the cost of diesel fuel. Global production of petroleum arguably already peaked, while demand appears enhance in the future with the continuous growing of new economies as case of Brazil. On the other hand, the environmental impact of fossil fuels is well known. It contributes to global warming by transferring previously sequestered carbon molecules into the atmosphere as carbon dioxide, a greenhouse gas. It also is a major source of air

pollution through other combustion products found in exhaust. Finally, the nations that cannot supply their own petroleum needs are forced into an unfavorable balance of payments with petroleum exporters. Therefore, alternative fuels technically feasible, economically competitive, and environmental acceptable and readily available are being explored (Meher *et al.*, 2006).

Biofuels offer a partial solution to many of these problems and has emerged as a viable substitute for petroleum diesel. It can be produced from a number of natural, renewable sources, being vegetable oils the main feedstocks. Outstanding benefits of biodiesel are the high cetane numbers that it naturally achieves and the lack of polluting heteroatoms like sulfur or nitrogen, having high flash point and being biodegradable and non-toxic. It has been claimed that biofuels do not contribute to global warming. Like petroleum, exhaust from biofuels contains carbon dioxide. Since plants remove carbon dioxide from the atmosphere during photosynthesis, the net production of CO_2 is arguably zero. Furthermore, production of biodiesel is easily done and requires low energy inputs.

The common means for biodiesel production is base-catalyzed transesterification, where diglycerides and monoglycerides are the intermediates in this process, and the glycerol as byproduct of reaction. These reactions are affected by alcohol/oil feed ratio, free fatty acids, moisture, catalyst concentration, temperature, and mixing. Although the relevance of biodiesel production is self-evident, a better understanding of process operation and optimization based on kinetic models that account for all of the above parameters is still needed. During the last years, several studies about mathematical modeling of the transesterification process involving various types of vegetable oils have been carried out (Noureddini and Zhu, 1997; Narváes *et al.*, 2007; Bambase *et al.*, 2007). However, the description of the kinetics of transesterification for biodiesel remains controversial. Most efforts in the literature have focused on finding the best fit of empirical data to simple models of reaction order but there are conflicting findings as to the order of reaction, and estimates of reaction rate constants vary widely. Owing that the difficulty in modeling of transesterification process is essentially on the precise description of the kinetic, a robust modeling with incorporating reliable computer-aided procedures is necessary.

After analyzing the prior work on kinetics, this work present a kinetic model based on careful examination of chemical mechanisms and of competing reactions. It then

describes the extensions to the model that are needed in order to build a predictive model for biodiesel reactions. A computer simulation of the rate equations, with extensions for the effect of temperature, amount of catalyst, and alcohol-oil molar ratio are used to analyze the implications of the model. In addition, a systematic method for estimation of reaction rate constant is described.

2. Theoretical background

To our knowledge, the work on chemical kinetics specific to biodiesel production began with Freeman and colleagues in the early 1980's (Freedman *et al.*, 1984; Freedman *et al.*, 1986). In Freedman's model, the overall reaction,

$$TG + 3ROH \xrightarrow{NaOH} G + 3E \quad (1)$$

occurs as a sequence of three steps:

$$TG + ROH \Leftrightarrow DG + E$$

$$DG + ROH \Leftrightarrow MG + E \quad (2)$$

$$MG + ROH \Leftrightarrow G + E$$

where TG means triglycerides, DG means diglycerides, MG means monoglycerides, ROH means alkyl alcohol, G means glycerol, and E means alkyl esters or biodiesel.

The forward reactions are said to be second order, referring to the overall order of the proposed forward reaction step. When the molar ratio of alcohol to triglyceride is very high, then the concentration of alcohol can be assumed constant. The rate of reaction is then dependent solely on the concentration of triglyceride, a condition which Freedman calls "pseudo-first-order". On the other hand, where the data not fit the sequential model, Freedman proposes a "shunt reaction" in which three alcohols simultaneously attack a triglyceride.

Freedman investigated transesterification of soybean oil using butanol and methanol, with molar ratios of alcohol to oil of 30:1 and 6:1, at temperatures ranging from 20 to 60 °C. With butanol, he found forward reactions to be second order at 6:1 and pseudo-first order at 30:1. With methanol, he found the forward reactions to be fourth order at 6:1, implying the shunt reaction, and pseudo-first order at 30:1. All reverse reactions

were found to be second order. He found the rate constants as a function of temperature, and derived the activation energies by taking the slope of the plot of ln(k) vs. 1/T. This method is derived from the Arrhenius equation, which relates reaction coefficients to temperature:

$$k = A \cdot exp\left(-\frac{Ea}{RT}\right) \tag{3}$$

were A is the Arrhenius pre-factor, and Ea is the activation energy of the reaction. Taking the *ln(x)* of both sides of equation,

$$\ln(k) = -\frac{Ea}{RT} + \ln(a) \tag{4}$$

This equation is linear with respect to 1/T. If k is determined for varying temperatures, the plot of ln(k) vs. 1/T should produce a straight line of slope –Ea/R.

Mittelbach and Trathnigg (1990) discussed the kinetics of methanolysis of sunflower oil. Although they no proposed any rate equations or derived any rates constants, they studied the parameters affecting the transesterification reaction. Although Freedman had considered the reaction to be single phase, Mittelbach found that a two-phase system could be observed for the first 2 minutes, followed by a period of about 5 to 10 minutes, where almost complete solution occurred. As soon as a considerable amount of glycerin had formed a two phase system was established again. Moreover, Mittelbach found that the conversion of triglycerides did not follow second-order kinetics as indicated by Freedman. He found that the reaction rate is temperature dependent, but the percent conversion is not a strong function of temperature provided that the reaction proceeds at least ten minutes.

Noureddini and Zhu (1997) again studied the kinetics of transesterification of soybean oil. They used the same reaction model proposed by Freedman. However, they took measurements at differing mixing intensities, measured by the Reynolds number of the stirrer. They also computed Arrhenius parameters for both the standard Arrhenius equation (Equation 3), and the modified equation

$$k = AT^n \exp(-Ea/RT) \tag{5}$$

where n is an experimentally derived parameter.

They found no correlation of the data to the shunt reaction, that is, the reaction constants for the shunt reaction were negligibly small. They also found that the activation

energies varied with Reynolds number and their rate constant for the reverse direction of the first two reactions are larger than the rate constants in the forward direction.

Boocock *et al.* (1998) commented on anomalies in Freedman's results. Their study suggests that the reaction rate drops off over time, due both to inadequate mixing and to reduced effectiveness of the catalyst because of reduced polarity. Bikou *et al.* (1999) investigated the effect of water on the kinetics of ethanolysis of cotton seed oil, their data fitting suggested that each of the three reaction steps should be third order with respect to ethanol. However, the remainder of the paper does not depend on the kinetic model. Instead, they investigated the effect of water on the equilibrium constants of the three steps in the overall reaction. They found that presence of water shifted the direction of the reaction to the left for all three steps.

Darnoko and Cheryan (2002) studied the kinetics of palm oil transesterification. They found that the best fit to their data was a pseudo-second-order model for the initial stages of the reaction, followed by first-order or zero-order kinetics. In the same year, Komers *et al.* (2002) derived a kinetic model from proposed mechanisms for all the competing reactions that take place during transesterification. These include formation of methoxide, methanolysis, and saponification. After simplifying assumptions, they derived a system of six rate equations involving eight reaction species and ten rate constants. The resulting model explicitly treats the amount of water and catalyst present. The model supports Bikou's research on the negative effect of water on the equilibrium reactions. Komer claims to be able to predict the reactions with 78% probability, considering only kinetic factors.

2. Mathematical model formulation

In this work, a kinetic model derived by Turner (2005) was used. This model is basically an extension of the Komer's model. The kinetic model was generalized for any alkyl alcohol, designated ROH, and any base catalyst. In addition, Turner normalized all species by the total concentration of bound and unbound glycerol in the reaction mixture. The kinetic model begins with simplifying assumptions:

- The concentration of free fatty acids is negligible.

- Of all the theoretically possible reactions only two proceed to from products: the alcoholysis of glycerides (TG, DG, MG) and the saponification of TG, DG, MG, or alkyl esters (E).
- All of the isomers of TG, DG, MG, and E proceed at the same rate, with the same mechanism.
- Alcoholysis is catalyzed by OH- or RO- (alkoxide) ions. Concentrations of OH- and RO- ions are much smaller than those of TG and ROH.

The possible reactions are then

Formation of alkoxide:

$$ROH + OH^- \underset{k1r}{\overset{k1}{\Longleftrightarrow}} RO^- + H_2O \tag{6}$$

Alcoholysis:

$$TG + RO^- \underset{k2r}{\overset{k2}{\Longleftrightarrow}} DG^- + E$$

$$DG^- + ROH \underset{k3r}{\overset{k3}{\Longleftrightarrow}} DG + RO^-$$

$$DG + RO^- \underset{k4r}{\overset{k4}{\Longleftrightarrow}} MG^- + E$$

$$MG^- + ROH \underset{k5r}{\overset{k5}{\Longleftrightarrow}} MG + RO^-$$

$$MG + RO^- \underset{k6r}{\overset{k6}{\Longleftrightarrow}} G^- + E$$

$$G^- + ROH \underset{k7r}{\overset{k7}{\Longleftrightarrow}} G + RO^- \tag{7}$$

Saponification:

$$E + OH^- \xrightarrow{k8} ROH + A$$

$$TG + OH^- \xrightarrow{k9} DG + A$$

$$DG + OH^- \xrightarrow{k10} MG + A$$

$$MG + OH^- \xrightarrow{k11} G + A \tag{8}$$

where A is the soap of the corresponding fatty acid chain.

The above reactions are assumed to be elementary, thus obeying the law of mass action (LMA). Straightforward application of LMA produces thirteen differential equations

describing the thirteen species present in the reactions. The number of differential equations and their complexity were reduced through simplifying assumptions. The steady state assumption, which holds that certain species react so much faster than others that their rate of change is essentially zero, was taken. Its application results in an algebraic equation which contains the rate constants for every reaction in which the species in question participates.

Reactions (2), (4), and (6) in Equation 7, which are simple exchange of hydrogen atoms, proceed much faster than others, that is

$$k2, k2r \gg k3, k3r$$
$$k4, k4r \gg k5, k5r$$
$$k6, k6r \gg k7, k7r$$
$$k3, k3r, k5, k5r, k7, k7r > k8, k9, k10, k11 \quad (9)$$

It therefore follows that

$$\frac{d[H_2O]}{dt} = \frac{d[RO^-]}{dt} = \frac{d[DG^-]}{dt} = \frac{d[MG^-]}{dt} = \frac{d[G^-]}{dt} = 0 \quad (10)$$

The species present in the reaction mixture were normalized by Turner as follows:

$$TG = [TG]/a$$
$$DG = [DG]/a$$
$$MG = [MG]/a$$
$$G = [G]/a$$
$$A = [A]/a$$
$$OH = [OH^-]/a$$
$$W = [H_2O]/a$$
$$ROH = [ROH]/a$$
$$E = [E]/b$$
$$a = [TG]_0 + [DG]_0 + [MG]_0 + [G]_0 \quad (11)$$

Eliminating small terms and substituting the equilibrium relations into the rate equations for the corresponding species, the resulting differential equations are

$$-\frac{dTG}{dt} = a \cdot OH \cdot (k2' \cdot TG \cdot ROH - k2r' \cdot DG \cdot E + k9 \cdot TG)$$

$$-\frac{dDG}{dt} = a \cdot OH\,(-k2' \cdot TG \cdot ROH + k2r' \cdot DG \cdot E + k4' \cdot DG \cdot ROH - k4r' \cdot MG \cdot E - k9 \cdot TG + k10 \cdot DG)$$

$$-\frac{dMG}{dt} = a \cdot OH\,(-k4' \cdot DG \cdot ROH + k4r' \cdot MG \cdot E + k6' \cdot MG \cdot ROH - k6r' \cdot G \cdot E - k10 \cdot DG + k11 \cdot MG)$$

$$\frac{dG}{dt} = a \cdot OH \cdot (k6' \cdot MG \cdot ROH - k6r' \cdot G \cdot E + k11 \cdot MG)$$

$$-\frac{dROH}{dt} = a \cdot OH\,(k2' \cdot TG \cdot ROH - k2r' \cdot DG \cdot E + k4' \cdot DG \cdot ROH - k4r' \cdot MG \cdot E + k6' \cdot MG \cdot ROH - k6r' \cdot G \cdot E - k8 \cdot E)$$

$$\frac{dE}{dt} = -\frac{dROH}{dt}$$

$$-\frac{dOH}{dt} = a \cdot OH\,(k8 \cdot E + k9 \cdot TG + k10 \cdot DG + k11 \cdot MG)$$

$$\frac{dA}{dt} = -\frac{dOH}{dt} \tag{12}$$

where

$$k2' = \frac{k2 \cdot K1}{W}$$

$$k2r' = \frac{k2r \cdot K1}{K3 \cdot W}$$

$$k4' = \frac{k4 \cdot K1}{W}$$

$$k4r' = \frac{k4r \cdot K1}{K5 \cdot W}$$

$$k6' = \frac{k6 \cdot K1}{W}$$

$$k6r' = \frac{k6r \cdot K1}{K7 \cdot W} \tag{13}$$

and

$$K1 = \frac{k1}{k1r} = \frac{[RO^-][H_2O]}{[ROH][OH^-]}$$

$$K3 = \frac{k3}{k3r} = \frac{[DG][RO^-]}{[DG^-][ROH]}$$

$$K5 = \frac{k5}{k5r} = \frac{[MG][RO^-]}{[MG^-][ROH]}$$

$$K7 = \frac{k7}{k7r} = \frac{[G][RO^-]}{[G^-][ROH]} \quad (14)$$

The initial conditions for the differential equations system are as follow:

$$TG_0 = \frac{[TG]_0}{a}$$

$$a = [TG]_0 + [DG]_0 + [MG]_0 + [G]_0$$

$$ROH_0 = \frac{[ROH]_0}{a} = n$$

$$OH_0 = \frac{[OH^-]_0}{a} = p$$

$$DG_0 = \frac{[DG]_0}{a};\ MG_0 = \frac{[MG]_0}{a}; G_0 = \frac{[G]_0}{a}; E_0 = \frac{[E]_0}{a}; A_0 = \frac{[A]_0}{a} \quad (15)$$

It can be seen that the initial value of ROH is simply the molar ratio of alcohol to triglycerides (*n*) and the initial value of OH is the molar ratio of catalyst to triglycerides (*p*). The following balance equations are also applied:

$$TG + DG + MG + G = 1$$

$$ROH + E = n$$

$$OH + A = p$$

$$E + 3TG + 2DG + MG + A = d$$

$$d = E_0 + 3TG_0 + 2DG_0 + MG_0 + A_0 \quad (16)$$

There are four balance equations in Equation (19). The first keeps track of the glycerol backbone common to all the glycerides: TG, DG, MG, and G. Since this backbone is never destroyed, the sum of these chains must equal the initial amount, which in Turner's model (Turner, 2005) is represented by the variable "*a*". In the overall reaction, the alcohol molecules are only consumed to make alkyl esters. Thus, the second balance equation states

that the sum of the alcohol molecules and the ester molecules must equal the original quantity of alcohol molecules "*n*". Similarly, the hydroxide ions are only consumed in the production of soap. Therefore, the number of hydroxide ions plus the number of soap molecules must equal the original amount of hydroxide ions, as indicated in the third balance equation. Finally, since fatty acid chains are not destroyed either, their total number is also constant, equal the original quantity of fatty acid chains present in the reaction mixture. The fourth balance equation enforces this condition.

3. Experimental data

3.1. Materials

The castor oil was obtained from Campestre Ind. & Com. De Óleos Vegetais Ltda. (São Paulo, Brazil). The castor oil had 0.66% of free fatty acid (determined according to the AOCS official method Ca 5a-40 as oleic acid). The sodium hydroxide, anhydrous ethanol, and all the analytical standards were supplied by Sigma-Aldrish Chemical Company, Inc. (St. Louis, Mo).

3.2. Equipment

The experiments were carried out in a batch stirred tank reaction of a 1 liter reactor with a drain cock at the bottom, equipped with in a jacketed glass, reflux condenser, a mechanical stirred, and a stopper to withdrawn sample during the experiments.

3.3. Analytical methods

The size-exclusion chromatography (SEC) was used for the triglycerides, diglycerides, monoglycerides, ethyl esters and glycerol analysis according to Shoenfelder method (Schoenfelder, 2003). The system consisted of a VISCOTECK GPC/SEC TDA max^{TM} chromatograph with triple detector array: refractive index (RI), viscometer and light scattering detectors. Data collection and analysis was performed with GPC software. The mobile phase was HPLC grade THF (JT Baker, USA) and three GPC/SEC Phenogel analytical columns connected in series were used (Phenomenex, Torrance, CA), 300 mm x 7.8 mm, packed with spherical styrene divinylbenzene copolymer beads with an average particle size of 5 µm. The first column with a pore size of 100 Å and the next two columns with a pore size of 50 Å. Identification and calibration of the GPC/SEC peaks were performed analyzing standards prepared gravimetrically within a range of concentrations the transesterification reactions as mentioned elsewhere (Martínez, 2010).

3.4. Solving of kinetic equations of the reaction model

As can been see above, the kinetic model proposed for the ethanolysis of castor oil is described quantitatively by a system of 8 kinetic differential equations where concentration is function time (Equation 12) and 4 algebraic equations of concentration balance (Equation 16) resulting from appropriate stoichiometric equations of species envolved in the reaction (Equations 6-8). All these equations are expressed in nondimensional relative concentrations of the reaction components. The differential kinetic equations cannot be integrated analytically and therefore their solving was done numerically using the methodology presented below.

3.4.1. Parameter estimation using optimization methods

The procedure utilized in this work is based on solving the reaction scheme given, by means of numerical method *Runge-Kutta-Felhberg* and optimizing of the kinetic parameters with respect to set of concentration-time experimental data for reaction components analyzed by SEC (González Quiroga, 2009). The kinetic parameters for modeling the biodiesel production (*k2'*, *k2r'*, *k4'*, *k4r'*, *k6'*, *k6r'*, *k8*, *k9*, *k10*, and *k11*) were estimated by minimizing an objective function. Let θ specify a kinetic parameters vector which contains all kinetic rate constants, the optimal kinetic parameter vector was found out by minimizing the objective function $F_c(\theta)$:

$$F_C(\theta) = \sum_{K}^{np} \sum_{l}^{ns} \left(\frac{C_{l,k}^{p} - C_{l,k}^{e}}{C_k^{inf}} \right)^2 \tag{17}$$

where *np*, *ns*, $C^{p}_{l,k}$, $C^{e}_{l,k}$, and C^{inf}_{k} are the number of experimental profiles, the number of experimental sampling points, the predicted component concentration for the profile *k* at the sampling point *l*, the experimental component concentration for the profile *k* at the sampling point *l*, and the ultimate component concentration for the profile *k*, respectively.

The determination of the feasible region of the total search space in the multiparameter optimization of the model is complex. For that reason, the optimization procedure to minimize the Equation (17) is based on the combination of two optimization techniques. Initially, the potential of the global searching of a genetic algorithm (Charbonneau, 2002) available electronically from the anonymous.ftp archive of the High Altitude Observatory (http://www.download.hao.ucar.edu/archive/pikaia) was used to obtain an appropriate initial guess of the kinetic parameters of the model. Subsequently, the

Levenberg-Maquard algorithm (routine DRNLIN of the IMSL MATH LIBRARY FORTRAN-90), which converges much more quickly than genetic algorithm to the optimal, was used to continue the optimization of the kinetic parameters near to the global optimum region, as the initial values were already determined by the genetic algorithm.

4. Results and Discussion

4.1. Initial conditions

As was reported earlier, castor oil and solution of NaOH in ethanol were used as initial components of the reaction. Initial conditions of single experiments vary in the ratio of the initial molar concentration of TG (*a*) and ROH (*b*), $n=b/a$ in interval n (6 to 12) and in the molar ratio of the initial concentration of catalyst NaOH (*c*) and TG, $p=c/a$ in interval p (0.116 to 0.347), which corresponds with 0.5 to 1.5 wt.% of NaOH regarding the weight of castor oil (TG) as 100%. The rate of ethyl ester conversion was studied for temperatures of 30, 50 and 70°C. The Table 1 contains the values of n, p and temperatures for all experiments realized.

Table 1. Initial ratios of reactants $n=[ROH]_0/[TG]_0$ and $p=[NaOH]_0/[TG]_0$ as well as temperatures for experiments realized.

Temp. [°C]	n	p	Experiment	Temp. [°C]	n	p	Experiment	Temp. [°C]	n	p	Experiment
30	6	0.116	1	50	6	0.116	10	70	6	0.116	19
		0.232	2			0.232	11			0.232	20
		0.347	3			0.347	12			0.347	21
	9	0.116	4		9	0.116	13		9	0.116	22
		0.232	5			0.232	14			0.232	23
		0.347	6			0.347	15			0.347	24
	12	0.116	7		12	0.116	16		12	0.116	25
		0.232	8			0.232	17			0.232	26
		0.347	9			0.347	18			0.347	27

4.2. Dependences actual concentrations vs. time

The dependences of relative molar concentrations TG, DG, MG, G, E, A and OH vs. time t were determined for all experiments by means of the method *Runge-Kutta-Felhberg* (section 3.4.1) and based on the experimental dependences concentration vs. time of the measured reaction components. The theoretical relations of concentration vs. time for

these components were computed for experiments 1-10 and 19 from Table 1 using the calculated optimal combinations of the rate constants for the above assumed reaction scheme in the time period 0 to120 min applying the optimization procedure presented in the section 3.4.1 based on the combination of two optimization techniques, algorithm genetic and Levenberg-Maquard. These computed and experimental dependences were compared tabular and graphically. An example of these graphic comparisons for experiments 1, 10 and 19 are depicted in Figures 1-6 using the optimal combination of the rate constants given in Table 2.

Table 2. Values of rate constants ki' [$m^3 \cdot mol^{-1} \cdot min^{-1}$] of the experiments No. 1-10 and 19 calculated by the method *Runge-Kutta Felberg* with optimization.

	30°C	50°C	70°C
k2'	10.662	37.226	135.658
k2r'	4.685	12.763	33.548
k4'	22.134	154.068	1032.751
k4r'	13.771	54.528	222.057
k6'	20.695	36.216	71.691
k6r'	1.083	2.623	6.922
k8	0.188	0.200	0.230
k9	0.613	2.120	7.654
k10	1.752	12.077	80.222
k11	0.633	1.095	2.147

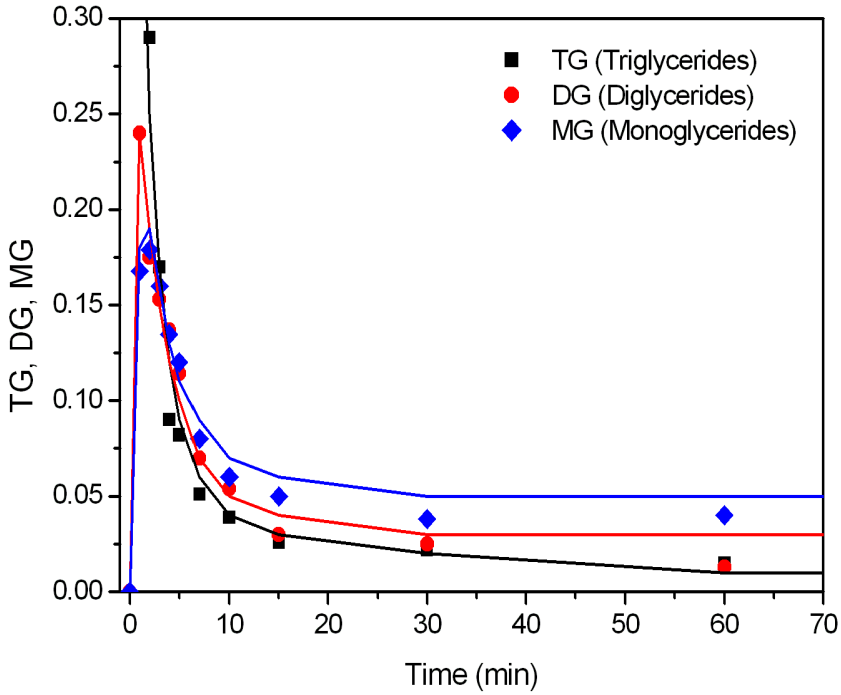

Figure 1. Experiment No. 1 (n=6, p=0.116 and T=30°C). Comparison of the theoretical dependences of actual relative concentrations TG, DG, MG vs. time, computed with the optimal combination of the rate constants (full curves), with the experimental data (points).

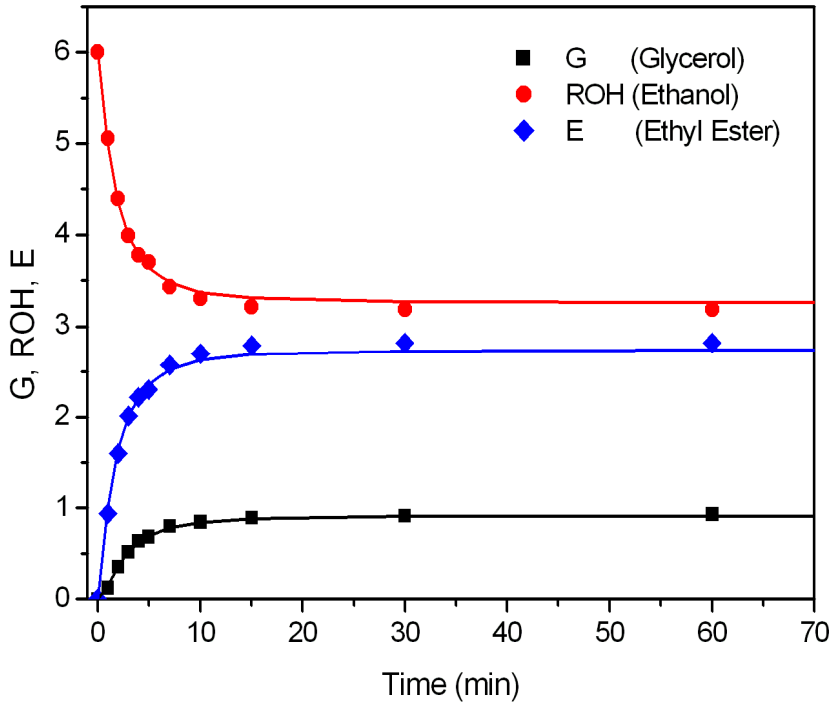

Figure 2. Experiment No. 1 (n=6, p=0.116 and T=30°C). Comparison of the theoretical dependences of actual relative concentrations G, ROH, E vs. time, computed with the optimal combination of the rate constants (full curves), with the experimental data (points).

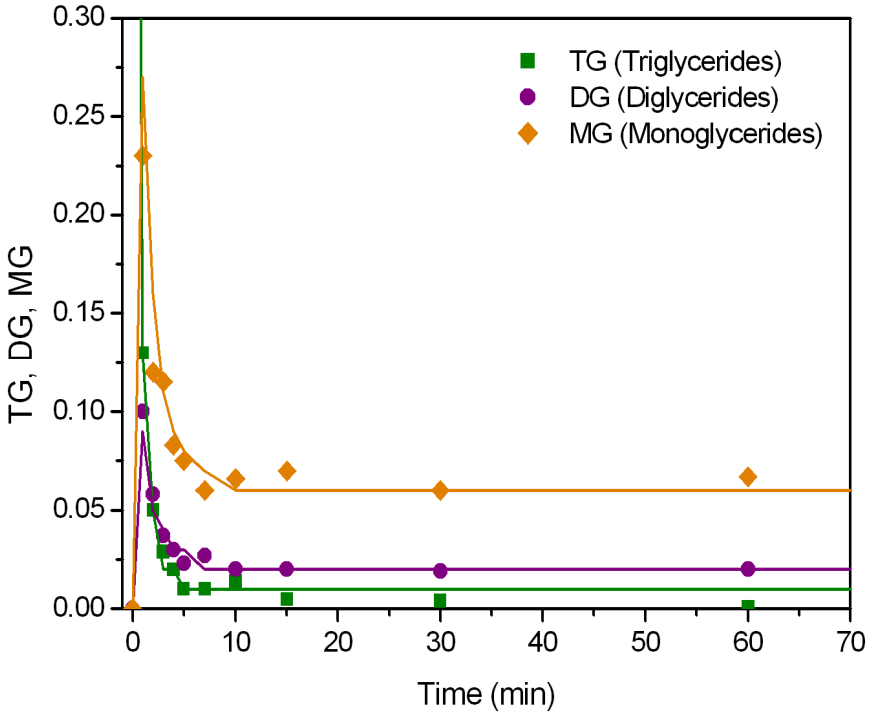

Figure 3. Experiment No. 10 (n=6, p=0.116 and T=50°C). Comparison of the theoretical dependences of actual relative concentrations TG, DG, MG vs. time, computed with the optimal combination of the rate constants (full curves), with the experimental data (points).

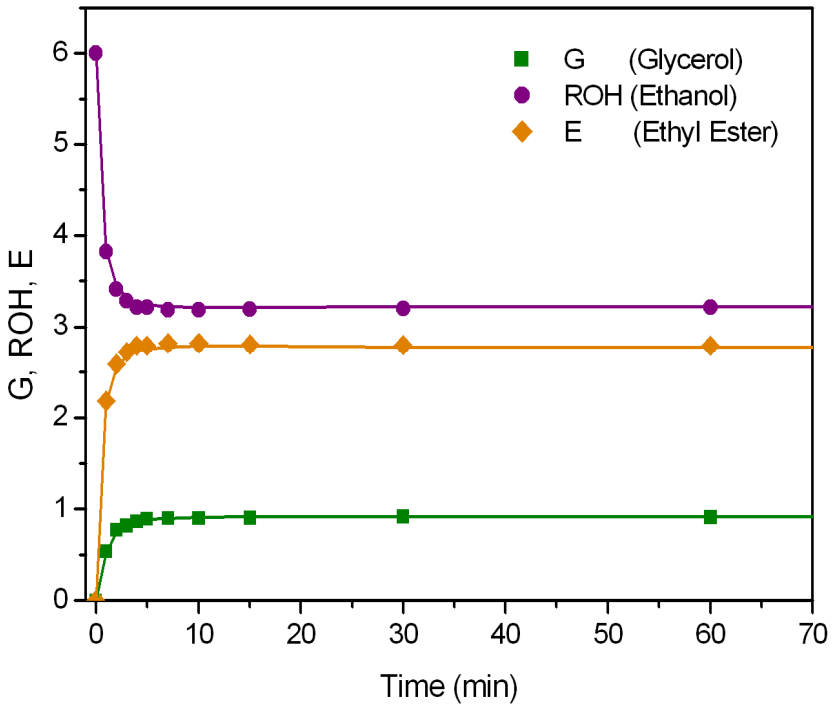

Figure 4. Experiment No. 10 (n=6, p=0.116 and T=50°C). Comparison of the theoretical dependences of actual relative concentrations G, ROH, E vs. time, computed with the optimal combination of the rate constants (full curves), with the experimental data (points).

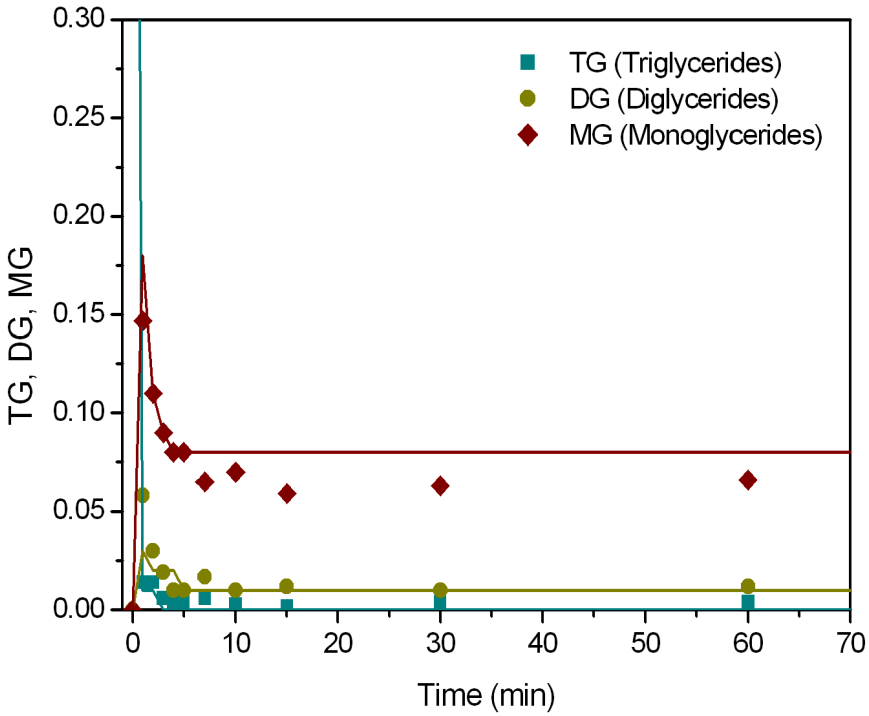

Figure 5. Experiment No. 19 (n=6, p=0.116 and T=70°C). Comparison of the theoretical dependences of actual relative concentrations TG, DG, MG vs. time, computed with the optimal combination of the rate constants (full curves), with the experimental data (points).

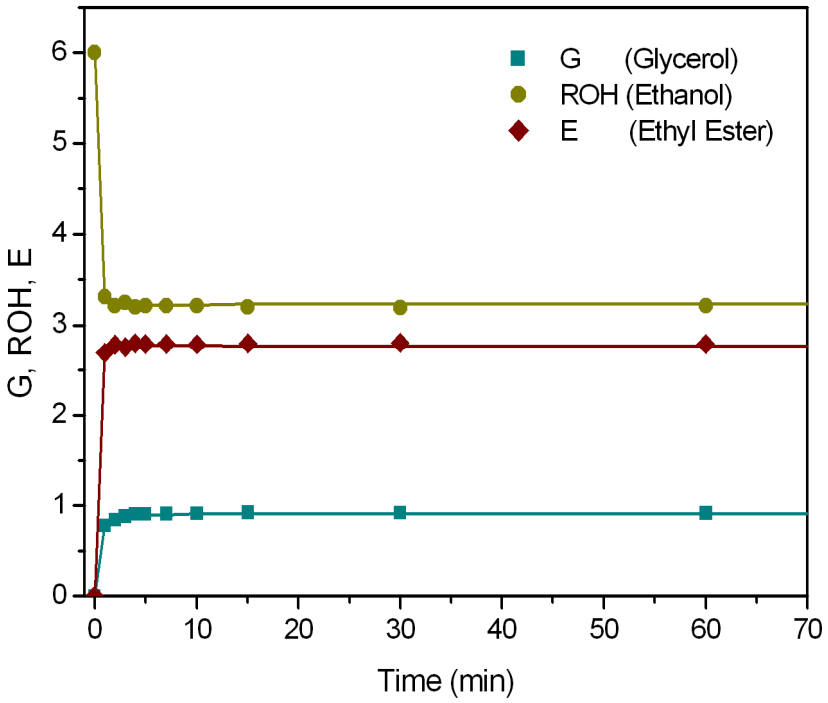

Figure 6. Experiment No. 19 (n=6, p=0.116 and T=70°C). Comparison of the theoretical dependences of actual relative concentrations G, ROH, E vs. time, computed with the optimal combination of the rate constants (full curves), with the experimental data (points).

The castor oil transesterification was very rapid because the ethyl ester concentration was 2.05 mol/L (94.6%), 2.11 mol/L (96.6%), 2.14 mol/L (97.1%) after 10 minutes for an ethanol/oil ratio of 6:1, 0.5% of NaOH by weight of castor oil and temperatures of 30, 50 and 70°C, respectively. In the transesterification reaction, the reactants initially form a two-phase liquid system, because the TG and alcohol phases are not miscible (Noureddini and Zhu, 1997). This fact decreases the contact between the reactants and consequently, the reaction conversion. However, the castor oil and its derivates present higher solubility in alcohol than other vegetable oils (Kulkarni and Sawant, 2003) and it leads to increase the mass transfer in the first stage of the reaction, and hence the ester conversion. In addition, as can be seen in the Table 2, at temperatures of 30 and 50°C the $k_{DG\text{-}MG}$ (k_4) and $k_{MG\text{-}G}$ (k_6) were higher than $k_{TG\text{-}DG}$ (k_2), which indicated that the first step reaction was the limit step for the overall reaction, whereas that at temperatures higher of 70°C the rate constant $k_{MG\text{-}G}$ (k_6) showed lower value than $k_{DG\text{-}MG}$ (k_4) and $k_{MG\text{-}G}$ (k_6) due to increase vegetable oil solubility in alcohol with increase of temperature. Furthermore, the reaction rate constant forward showed be higher that reversible rate constant for all temperatures.

On the other hand, the procedure for parameter estimation showed to have good performance with relative lower computer burden. The results showed good agreement between experimental and calculated data therefore the second order model described adequately the reaction conditions.

4.3. Energy of Activation

The relationship between reaction rate constant, k_i, and temperature is given by the integrated form of the Arrhenius equation: $\ln(k) = (-E_a/RT) + \ln(a)$ where E_a is the energy of activation ($J \cdot mol^{-1}$), R is the universal gas constant R=8.314 $J \cdot mol^{-1} \cdot K^{-1}$, T is the temperature (K) and ln(a) is the log of Arrhenius pre-factor. From a plot of ln(k) vs. 1/T, the slope (E_a) can be determined for the k_i-values obtained at different temperatures. Figures 7 and 8 show the dependence of ln (k) on –(1/R·T), confirming that the Arrhenius equation can be applied for determining the activation energies for the ethanolysis reactions. The values obtained are summarized in Table 3. Linear regression analysis data showed a correlation coefficient higher 0.99 for all reaction rate constants. Energies of activation ranged from 4319-83005 J/mol which are consistent with published data in literature (Lima da Silva *et al.*, 2008).

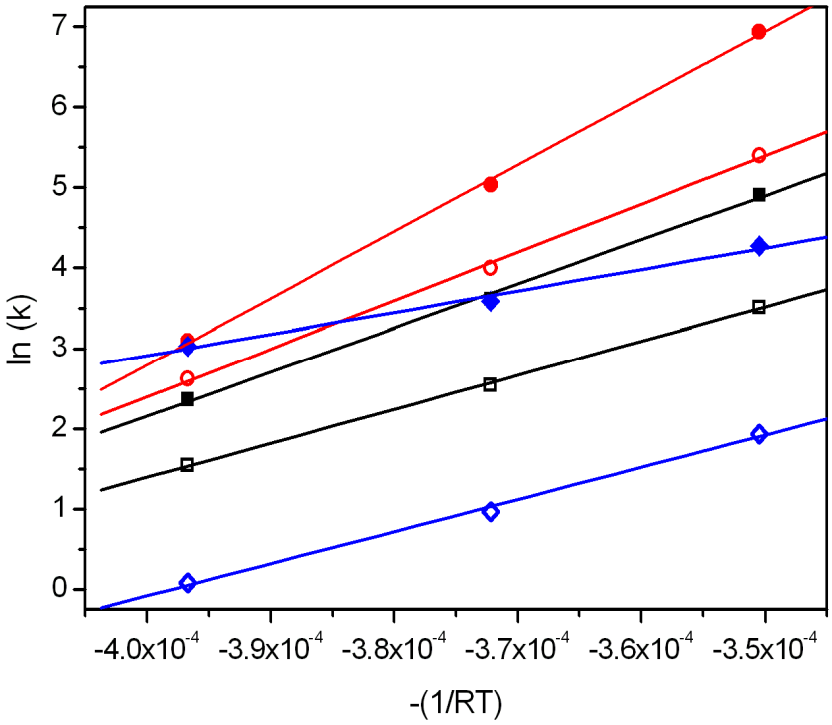

Figure 7. Arrhenius plot of ln(k) vs. –(1/R·T) for the ethanolysis of castor oil (■, k2'; □, k2r'; ●, k4'; ○, k4r'; ♦, k6'; ◊, k6r').

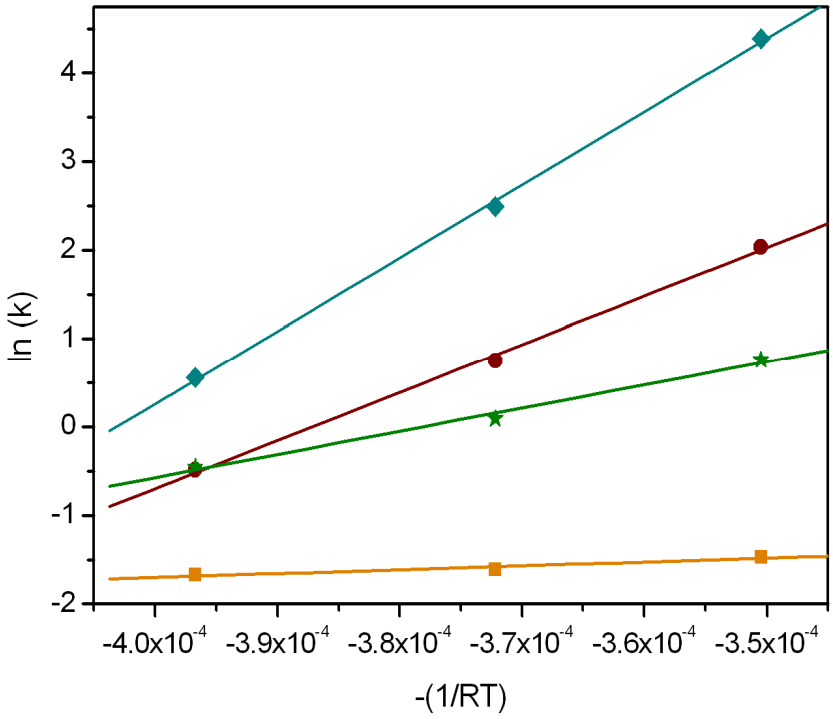

Figure 8. Arrhenius plot of ln(k) vs. –(1/R·T) for the ethanolysis of castor oil (■, k8; ●, k9; ♦, k10; ж, k11).

Table 3. Energy of activation for ethanolysis of castor oil.

Rate		Ea (J/mol)	A
TG → DG	(k2')	54908	2.99E+10
DG → TG	(k2r')	42529	9.80E+07
DG → MG	(k4')	83005	4.27E+15
MG → DG	(k4r')	60031	2.92E+11
MG → G	(k6')	26777	8.22E+05
G → MG	(k6r')	40021	8.20E+06
E → A	(k8)	4319	1.03E+00
TG → A	(k9)	54501	1.46E+09
DG → A	(k10)	82598	2.90E+14
MG → A	(k11)	26320	2.10E+04

4.4. Criteria of validation of the kinetic model

The validity of the transesterification kinetic model for biodiesel production of castor oil (Equation 15) was verified by comparison of:

- Experimental dependences of relative concentrations of a set of reaction components vs. time with corresponding theoretical dependences calculated for this reaction scheme using the optimum values of the rate constants (see section 4.2).
- Experimental dependences of the relative concentrations of the main reaction components (TG, DG, MG, G, E, A and OH) vs. time t for n at given ratio p not used in

the parameter estimation with the corresponding theoretical dependences calculated for this reaction scheme.

4.5. Dependences concentrations vs. time

The graphical comparison of the theoretical and experimental dependences (Figures 1-6) shows a good agreement of this very complicated and polyphaseous reaction. The values of the rate constants presented in Table 2 obtained with use of the kinetic computing program (*Runge-Kutta Felberg* with optimization: *genetic* and *Levenberg-Maquard* algorithms) showed give good results. This result can be considered as satisfying with respect to the complicated reaction and the simplifying presumptions. Important conclusions can be expressed about the velocities of the single reaction steps: The esterification step in the proposed scheme is controlled by the rate constant k2'; it is about slower than constants k4' and k6' and the reverse esterification step is controlled by constants k2r', k6r' that are slower than k4r'. Saponification is slower than ethanolysis (under the used reaction conditions). The saponification of ethyl esters was evidently slower than glycerides. This means that the main part of soaps formed (*A*) in biodiesel production from castor oil and NaOH solution in ethanol is formed by hydrolysis of TG, DG and MG and not of E.

4.6. Dependences concentrations of the main reaction components not used in the parameter estimation with the presumed kinetic model

Dependences component concentrations not used in the parameter estimation with the presumed kinetic model are depicted in Figure 9 and 10 for experiment 15 (Table 1). It show that the kinetic model agrees with the experiments equally well with other conditions not used in the parameter estimation which demonstrate the predictive power of the kinetic model used. However, some differences for TG, DG, MG profiles can be seen, this should being due that the model used may not be adequate to account for all the variables involved, for instance transport, portioning, and polarization. In the initial two-phase system, the reaction is hampered by the inability of the reactant molecules to contact each other. This is a transport limitation. After products being to form, the catalyst is drawn disproportionately to the glycerol phase, but it is needed in the biodiesel phase, where the remaining reactants are found. At this stage, transport and partitioning effects are involved. In addition Booncock *et al.* (1998) has hypothesized a reduced effectiveness of the catalyst

due to reduced polarization. This might also explain why E_a for some reverse reactions are greater than those of corresponding forward reactions. Therefore, further research is needed to develop a model that might provide a narrower range of E_a values.

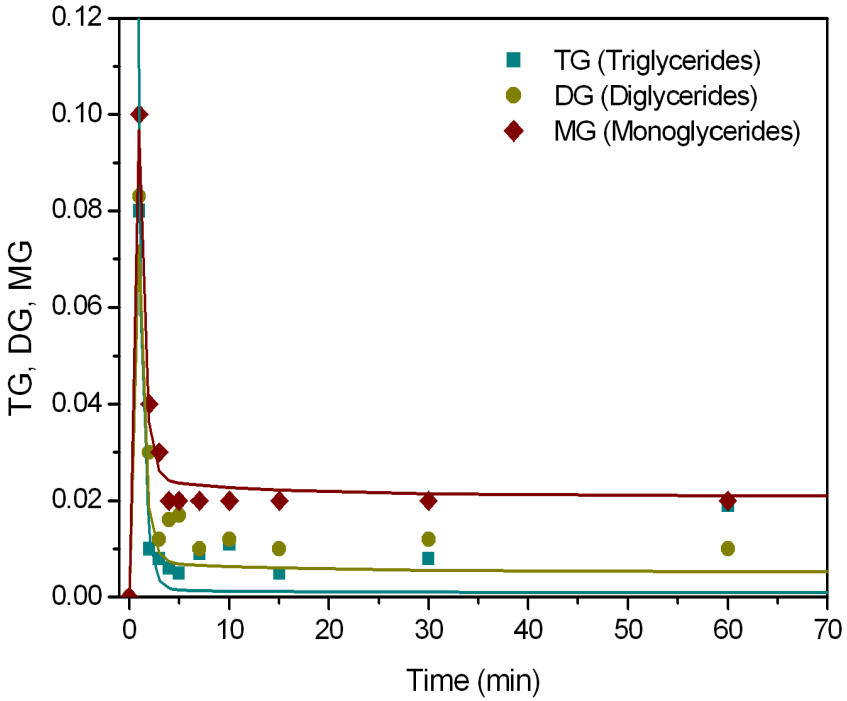

Figure 9. Experiment No. 15 (n=9, p=0.347 and T=50°C). Comparison of concentrations TG, DG, MG computed with the optimal combination of the rate constants (full curves), with the experimental data (points).

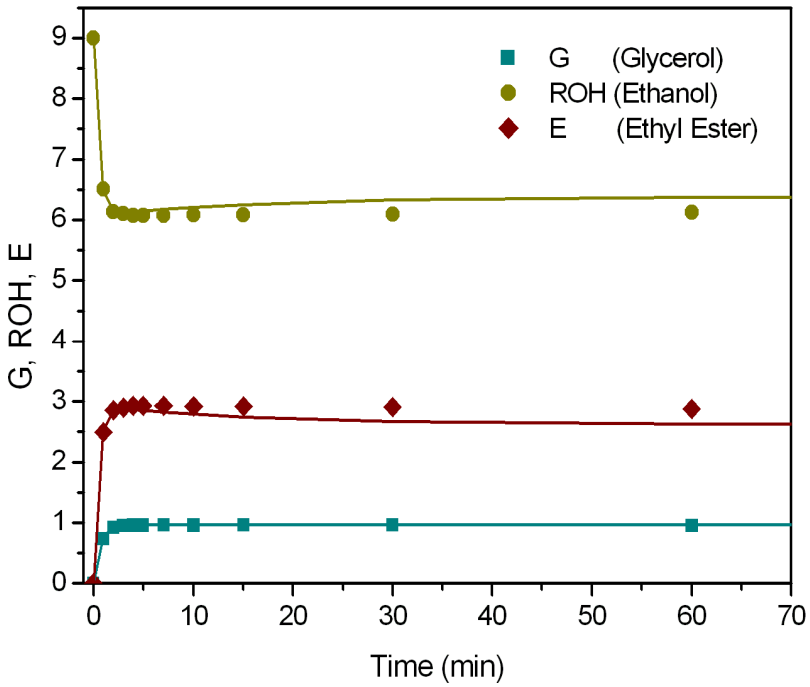

Figure 10. Experiment No. 19 (n=6, p=0.116 and T=70°C). Comparison of concentrations G, ROH, E computed with the optimal combination of the rate constants (full curves), with the experimental data (points).

5. Conclusions

The kinetic modeling and reaction mechanism between castor oil and a solution of NaOH in ethanol in a closed, mixed and thermostated batch reactor was studied at temperatures of 30-70°C and the performance of a reliable systematic procedure to describe the reaction kinetic of the transesterification process was assessed.

Experiments were realized with ethanol molar ratios ($n=[ROH]_0/[TG]_0$) in the interval of 6-12 and catalyst molar ratio ($p=[NaOH]_0/[TG]_0$) in the interval of 0.116-0.347 which correspond a concentrations of 0.5-1.5 wt.% NaOH by weight of castor oil. From reaction mixture, samples were taken in suitable time periods, the stopped reaction and the concentrations of TG, DG, MG, G and E in the samples were determined by analytical methods. These experimentally data of concentrations vs. time were numerically and/or graphically compared with the corresponding theoretical data obtained by solution of the system of kinetic and balance equations (Equations 12 and 16) for the presumed reaction scheme. This scheme resulted by application the law of mass action considering that the process is controlled only by its chemical and not by physical and interphase steps. This scheme can be expressed by the set of stoichiometric equations (Equations 6-8) with optimum rate constants *ki'*, *kir'*, and *ki* presented in the Table 2.

The validity if this scheme is supported also by a prediction of component concentrations outside of the conditions used in the parameter estimation. The kinetic model presented acceptable fits, in comparison to experimental observation, using the proposed methodology. Based on the kinetic model, the reaction rate constants for consecutive reactions were calculated and the results indicated that at temperatures of 30 and 50 °C the first step reaction ($TG \rightarrow DG$) was limited step for the overall reaction whereas that a 70°C the three step reaction ($MG \rightarrow E$) was limited step for the reaction. Values of activation energy for ethanolysis reaction indicated that higher temperatures favor the consumption of TG e DG (for the reaction $TG \leftrightarrow DG$ and $DG \leftrightarrow MG$ values of Ea for the forward reaction has a magnitude higher than the corresponding backward step), but also favor the formation of MG (for $MG \leftrightarrow G$ values of Ea for the forward reaction has a magnitude lower than the Ea of the inverse reaction.

However, the tested chemical scheme does not describe the experiments perfectly. The main reason is probably the neglect of the permanent heterogeneity of the reaction

mixture. Nevertheless, the kinetic model described could help to optimized the actual technology of biodiesel production, for instance in the option of the optimal reaction time at chosen temperature as well as to define process operating strategies in order to have high performance operation.

Acknowledgements

The author gratefully acknowledges the financial support provided by The Scientific Research Foundation for the State of São Paulo (FAPESP).

Bibliography

Bambase, M. E.; Nakamura, N.; Tanaka, J.; Matsumura, M. Kinetics of Hydroxide-catalyzed methanolysis of crude sunflower oil for the production of fuel-grade methyl esters, Journal of Chemical Technology & Biotechnology, 2007, 82, 273-280.

Bikou, E.; Louloudi, A.; Papayannakos, N. The effect of water on transesterification kinetics of cotton seed oil with ethanol, Chemical Engineering and Technology, 1999, 22, 70-75.

Boocock, D. G. B.; Konar, S. K.; Mao, V.; Lee, C.; Buligan, S. Fast formation of high-purity methyl esters from vegetable oils, Journal of the American Oil Chemists Society, 1998, 75, 1167-1172.

Charbonneau, P. Release notes for PIKAIA 1.2 NCAR Technical Note 451+IA (Boulder: National Center for Atmospheric Research), 2002.

Darnoko, D.; Cheryan, M. Kinetics of palm oil transesterification in a batch reactor, Journal of the American Oil Chemists Society, 2000, 77, 1263-1267.

Freedman, B.; Pryde, E. H.; Mounts, T. L. Variables affecting the yields of fatty esters from transesterified vegetable oils, Journal of the American Oil Chemists Society, 1984, 61, 1638-1643.

Freedman, B.; Butterfield, R. O.; Pryde, E. H. Transesterification kinetics of soybean oil, Journal of the American Oil Chemists Society, 1986, 63, 1375-1380.

González Quiroga, A. Modelagem, Simulação e Análise de Reatores Contínuos para a Hidrólise Enzimática de Bagaço de Cana, University of Campinas, M.Sc. Thesis, Campinas, São Paulo, 2009.

Komers, K.; Skopal, F.; Stloukal, R.; Machek, J. Kinetics and mechanism of the KOH – catalyzed methanolysis of rapeseed oil for biodiesel production, European Journal of Lipid Science and Technology, 2002, 104, 728-737.

Lima da Silva, N.; Rivera, E. C.; Batistella, C. B.; Ribeiro de Lima, D.; Maciel Filho, R.; Wolf Maciel, M. R. Biodiesel Production from Vegetable Oils: Operational Strategies for Large Scale Systems, 18th European Symposium on Computer Aided Process Engineering – ESCAPE18, 2008, 1101-1106.

Martínez, E. L. Development and Assessment of Microreactors Applied to Biodiesel Production, University of Campinas, M.Sc. Thesis, Campinas, São Paulo, Brazil, 2010.

Meher, L. C.; Sagar, D. V.; Naik, S. N. Technical Aspect of Biodiesel Production by Transesterification – A review. Renewal and Sustainable Energy Reviews, 2006, 10, 248-268.

Mittelbach, M.; Trathnigg, B. Kinetics of alkaline catalyzed methanolysis of sunflower oil, Fat Science and Technology, 1990, 92, 145-148.

Narváes, P. C.; Rincón, S. M.; Sánchez, F. J. Kinetic of Palm Oil Methanolysis, Journal of the American Oil Chemists' Society, 2007, 84, 971-977.

Noureddini, H.; Zhu, D. Kinetics of transesterification of soybean oil, Journal of the American Oil Chemists Society, 1997, 74, 1457-1463.

Peterson, C. L.; Cook, J. L.; Thompson, J. C.; Taberski, J. S. Continuous flow biodiesel production, Applied Engineering in Agriculture, 2002, 18, 5-11.

Schoenfelder, W. Determination of monoglycerides, diglycerides, triglycerides and glycerol in fats by means of gel permeation chromatography, European Journal of Lipid Science and Technology, 105 (2003), 45-48.

Turner, T. L. Modeling and simulation of reaction kinetics for biodiesel production, North Carolina State University, M.Sc. Thesis, Raleigh, NC, 2005.

5.3. Conclusões

A modelagem cinética e o análise do mecanismo de reação do óleo de mamona e etanol em presença de NaOH como catalisador em um reator batelada foi realizado a temperaturas entre 30-70°C. Por outra parte, um procedimento sistemático confiável para a obtenção dos parâmetros cinéticos da reação foi proposto.

A transesterificação do óleo de mamona ocorreu a uma taxa de reação alta onde a concentração de ésteres etílicos foram de 2,05 mol/L (94,6%), 2,11 mol/L (96,6%) e 2,14 mol/L (97,1%) a temperaturas de 30, 50 e 70°C, respectivamente, após 10 minutos de reação com uma razão etanol/óleo de 6:1, 0,5% de NaOH em peso de óleo. Estes resultados foram atribuídos a que na reação de transesterificação, os reagentes inicialmente formam um sistema bifásico, já que o álcool e o óleo vegetal não são miscíveis, porém diminuindo o contato entre os reagentes e, conseqüentemente, a conversão da reação. No entanto, o óleo de mamona e seus derivados apresentam maior solubilidade em álcool do que outros óleos vegetais o que leva a um aumento da transferência de massa na reação e, portanto, na conversão de éster.

O processo para a estimação das constantes cinéticas da reação, mediante a integração de dois algoritmos de otimização, a saber, o algoritmo genético para a estimação do chute inicial que é usado pelo método do Levenberg-Maquard para otimização final, mostrou um bom desempenho na otimização da função multivariável com um custo computacional relativamente baixo. Os resultados mostraram boa concordância entre os dados experimentais e os calculados, indicando que o modelo de segunda ordem apresentado neste trabalho descreve adequadamente o avanço da reação.

Além disso, como pode ser visto na Tabela 2, nas temperaturas de 30 e 50°C as constantes de taxa $k_{DG\text{-}MG}$ *(k4)* e $k_{MG\text{-}G}$ (*k6*) foram superiores a $k_{TG\text{-}DG}$ (*k2*), o qual indica que o primeiro passo da reação foi o passo limitante na reação global, enquanto que a altas temperaturas como 70°C a constante da taxa de reação $k_{MG\text{-}G}$ (*k6*) apresentou um valor inferior a $k_{TG\text{-}DG}$ (*k2*) e $k_{DG\text{-}MG}$ (*k4*). Este comportamento pode ser atribuído ao aumento da solubilidade do óleo vegetal no álcool com o aumento da temperatura. Além disso, as constantes de taxa de reação direta mostraram serem maiores que as constantes de taxa reversíveis para todas as temperaturas estudadas. Pode ser visto também, que a saponificação dos ésteres etílicos é mais lenta do que os glicerídeos, ilustrado pelas

constantes de taxa de reação $k_{E\text{-}A}$ (*k8*), $k_{TG\text{-}A}$ (*k9*), $k_{DG\text{-}A}$ (*k10*) e $k_{MG\text{-}A}$ (*k11*). Isto significa que a maior parte do sabão formado (A) na produção de biodiesel a partir do óleo de mamona e etanol com NaOH como catalisador é causado pela hidrólise dos TG, DG e MG.

Os valores de energia de ativação para a reação de etanólise indicaram que a temperaturas elevadas é favorecido o consumo de TG e DG (para a reação DG↔TG e MG↔DG os valores da *Ea* para a reação direta são maiores que os valores correspondentes da reação reversa), mas também é favorecido a formação de MG (para MG ↔ G o valor da Ea para a reação direta é menor que a Ea da reação inversa).

No entanto, algumas diferenças nos valores preditos pelo modelo para os dados experimentais não usados na otimização dos parâmetros cinéticos, foram encontradas. Estas discrepâncias foram atribuídas ao fato que o modelo não toma em conta a heterogeneidade da mistura de reação. Contudo, o modelo poderia ajudar a otimizar a tecnologia atual de produção de biodiesel, por exemplo, na escolha do tempo de reação ideal para uma temperatura particular, ou bem, para definir estratégias operacionais a fim de se obter no processo alto rendimento.

Capítulo 6.

Fabricação de dispositivos microfluídicos utilizando processos fotolitográficos e de litografia macia

6.1. Introdução

A comunidade científica tem observado, nas últimas décadas, o surgimento, crescimento e consolidação de uma nova tendência mundial: a miniaturização. Em diferentes ramificações da ciência é comum, e cada vez mais necessário, o uso de dispositivos miniaturizados. O rápido desenvolvimento de sistemas miniaturizados, nos mais diferentes campos da pesquisa, tem dominado o progresso da tecnologia moderna.

Da mesma forma que os microchips eletrônicos revolucionaram o universo dos computadores e da eletrônica, os dispositivos microfluídicos tem revolucionado o campo da química analítica e engenharia química nos últimos anos. Inicialmente, a principal razão para a miniaturização era reduzir o tamanho dos dispositivos ao invés de aumentar seu desempenho, mas com a mudança da escala macro para micro, outras vantagens foram obtidas, como a redução do volume de reagentes e amostras, breves tempos de reação, seletividade, altas conversões, condições operacionais difíceis de atingir em processos convencionais, baixo custo de fabricação e análise em tempo reduzido (Tabelink, 2005). Além disso, com o desenvolvimento de dispositivos microfluídicos, tornou-se possível integrar várias etapas analíticas, como introdução da amostra, pré-tratamento da amostra, reações químicas, separação analítica e detecção em um único dispositivo. Devido à idéia de inserir várias etapas, normalmente desenvolvidas em um laboratório, em um chip, estes microdispositivos são também denominados "lab-on-a-chip". Todos estes fatores, aliados à portabilidade, impulsionaram o desenvolvimento explosivo e maciço de sistemas analíticos e de reação em micro-escala nos últimos anos.

Os microdispositivos podem ser fabricados através de tecnologias convencionais ou alternativas, usando diferentes substratos, sendo o fotorresiste SU-8 um dos mais utilizados para esta finalidade, devido à sua elevada resistência química, possibilidade de

deposição de filmes espessos e alta fotossensibilidade (menor tempo de exposição à radiação). Nas tecnologias convencionais, há a necessidade do uso de uma fonte energética para fazer a transferência da imagem dos microcanais para o substrato utilizado. Tipicamente, essa transferência é primeiramente feita para a superfície de um fotorresiste sensível à radiação utilizada. A exposição à radiação promove uma interação entre o feixe incidente e o substrato. Conseqüentemente, a absorção de luz ou o espalhamento inelástico das partículas pode afetar a estrutura química do fotorresiste, alterando sua solubilidade, promovendo uma reação de polimerização e permitindo a revelação da imagem fotogravada. Processos litográficos, como litografia por raios-X, litografia por feixe de elétrons ou litografia com radiação ultravioleta (UV), são os mais utilizados.

Por outro lado, existem técnicas alternativas como a microfabricação por moldagem, onde inicialmente um molde rígido é fabricado contendo a imagem negativa da estrutura microfluídica de interesse. Este molde é utilizado na etapa de replicação dos microdispositivos, a qual consiste em transferir a estrutura microfluídica do molde para o substrato, através de moldagem, onde o molde pode ser utilizado diversas vezes na etapa de replicação dos dispositivos microfluídicos. No processo de litografia macia um polímero líquido é misturado com um agente reticulador e colocado em contato com um molde. Após da reticulação, o polímero torna-se sólido e a estrutura microfluídica do molde é transferida para o polímero reticulado. O PDMS (polidimetilsiloxano) é o material mais utilizado neste processo, devido às excelentes propriedades ópticas, baixo custo, boa resistência química e alta flexibilidade.

Portanto, este capítulo descreve a utilização de técnicas de microfabricacão tais como fotolitografia e litografia macia na elaboração de dispositivos microfluídicos com diferentes designs. Os principais aspectos relacionados ao desenvolvimento dos processos, instrumentação e alguns aspectos relacionados com as suas vantagens e desvantagens são abordados.

6.2. Desenvolvimento

O desenvolvimento deste capítulo é apresentado a seguir, no manuscrito intitulado: *Fabrication of microfluidic devices using photolithography and soft lithography processes.*

Fabrication of microfluidic devices using photolithography and soft lithography processes

Abstract

There has been recently, a rapid development of microfluidic systems for use in micro total analysis systems and for microchemical synthesis applications. Miniaturization of analytical systems can reduce costs, increase portability, and provide faster analysis with lower consumption of reagents and sample. For microfluidic systems to become widespread in chemical, biochemical and biological fields it will be required manufacturable methods for the production of fluidic structures of low cost or even disposable devices. It is also required, systems that are compatible with organic solvents for synthesis or analysis of organic compounds and the integration of detection methods *on-chip* to maximize throughput and allow dynamic optimization of reaction conditions. In this work, methods are described for fabricating microfluidic devices by using SU-8 (a photodefinable epoxy with good chemical resistance) through photolithography. In addition, soft lithography, lift-off and O_2 plasma surface activation sealing techniques were also employed for rapid prototyping of cost effective PDMS microfluidic devices.

Keywords: Microfluidic devices; Microfabrication process; SU-8; PDMS

1 Introduction

The rapid progress in microfabrication technologies and utilizing microelectromechanical systems (MEMS) during the last three decades have attracted great interest in the development of microdevices for fluids manipulation due the number of fluid-based processes that could benefit from miniaturization. Research in integrated microfluidic devices (which are typically referred to as lab-on-a-chip devices or micro total analysis systems [μTAS]) has expanded to include sample preparation, fluidic handling, separation systems, cell handling, and cell culturing (Nguyen and Wereley, 2006). The incorporation of these techniques has led to microfluidic devices that have been used to perform capillary electrophoresis based separations, magnetic microparticle based separations, immunoassays, DNA analysis, and dangerous reactions along with the design of highly efficient microreactors.

Normally, microfluidic devices have microchannels whose dimensions are less than 1 mm and greater than 1 μm. Above 1 mm the flow exhibit behavior that is the same

as most macroscopic flow (Gad-el-Hak, 2002). Below 1 µm the flow is better characterized as nanoscopic. Flow in microscale devices differ from their macroscopic counterparts because small scale make molecular effects such as wall slip more important and it amplifies the magnitude of certain ordinary continuum effects to extreme levels, for instance, mass and heat transfer. Microchannels can be fabricated in many materials – glass, polymers, silicon, metals – using various processes including surface micromachining, molding, embossing, and conventional machining with microcutters (Gad Hak, 2002; Tabeling, 2005; Madou, 2002). In this work, fabrication techniques such as photolithography and soft lithography have been used to make microfluidic devices.

1. Photolithography

One principal process that has a central role in microscale structures fabrication is lithography. Depending on the energy beam, lithography techniques can be further divided into photolithography, electron lithography, X-ray lithography, and ion lithography (Gad-el-Hak, 2002). There seems to be an obvious advantage to using small wavelengths, to achieve higher micromachining precision. However, in practice photolithography and X-ray lithography are the most relevant techniques for the fabrication of microfluidic structures (Banks, 2006).

In photolithography, a pattern is transferred to a photosensitive polymer (a photoresist) by exposure to a light source through an optical mask. An optical mask usually consist of opaque patterns (usually chrome or iron oxide) on a transparent support (usually quartz) used to define features on a wafer. For microfluidic applications with relatively large structures, a mask printed on a plastic transparency film by high-resolution laser printer is an option for low-cost and fast prototyping. Photolithography and pattern transfer involve a set process steps as summarized in Figure 1. The mask is positioned on the top of a substrate, such as a glass wafer. The substrate is coated with a photoresist, which will carry the pattern after the subsequent exposure step. The exposure step transfers the pattern on the mask into the photoresist layer. Energy from the exposure source, such as ultraviolet (UV) light or X-rays, change the properties of exposed photoresist. In the development step, unexposed negative resist is dissolved, while the exposed area remains due to crosslinking. In contrast, exposed positive resist is etched away in the developer solution.

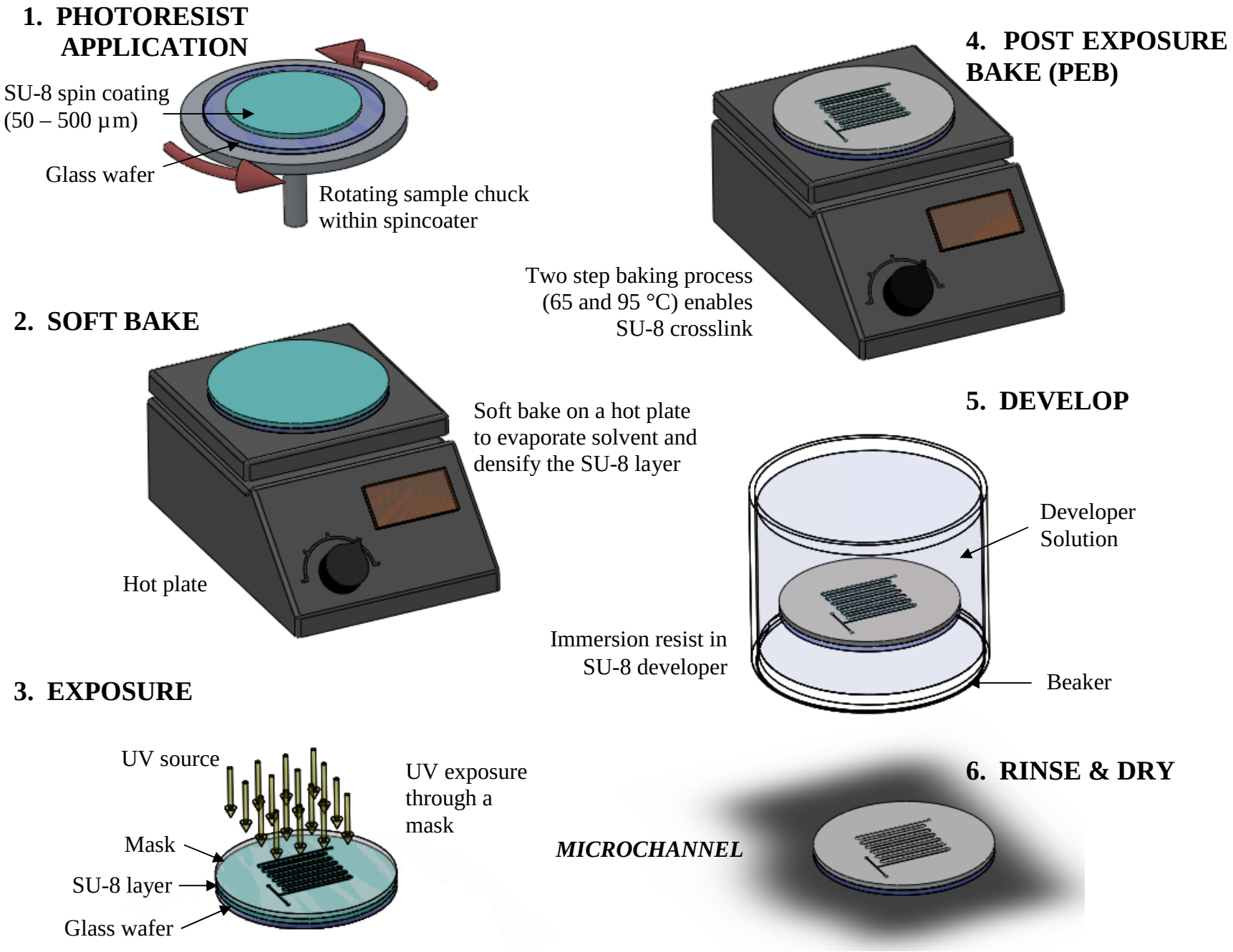

Figure 1. Process flow for creating SU-8 microfluidics structures using SU-8 resist.

Most photolithography systems use a mercury lamp as a light source. Mercury lamp wavelengths of the I-line, H-line, G-line, and E-line are 365 nm, 404.7 nm, 435.8 nm, and 546.1 nm, respectively. Because of its simplicity and fast prototyping capability, photolithography of thick resists is a favored technology for the fabrication of microfluidic devices. Thick resists structured by photolithography can be used as structure or template for molding polymeric devices. Therefore, the structured resist should have a high aspect ratio, which is suitable for making microchannels. The high aspect ratio requires special resist, such as SU-8, or a high-energy beam, such as X-rays.

In fabrication of the fluidic structures with lithography there are several important requirements for the materials used. Adequate mechanical strength, compatibility with chemicals, hydrophobicity, and surface charge are some microfluidic properties of the materials. These requirements are dependent on the application. Material strength requirements are best achieved by tight network of polymer achieved by polymerization of monomers or by cross-linking of oligomers in the case of negative photoresists. Positive photoresist normally lack the mechanical, thermal and chemical durability required in fluidic application.

1.1. Photoresist SU-8

SU-8 is a negative photoresist based on EPON SU-8 epoxy resin for the near-UV wavelengths from 365 to 436 nm. At these wavelengths the photoresist has very low optical absorption, which makes photolithography of thick films with high aspects ratios possible. Photoresist SU-8 is based on epoxies, which are referred to as oxygen bridges between two atoms. Epoxy resins are molecules with one or more epoxy groups, which during the curing process are converted to a thermoset form or a three-dimensional network structure.

SU-8 photoresist consist of three basic components: epoxy resin such as EPON SU-8, solvent called *gamma-Butyrolactone* (GBL) and Photoinitiator such as triarylium-sulfonium salts. Standard SU-8 processes consist in the procedure depicted above. Because of its simple process and the relatively good mechanical properties, SU-8 is used as structural material for many microfluidic applications.

SU-8 has been shown to be biocompatible (Voskerician *et al.*, 2003; Kotzar *et al.*, 2002). It is chemically stable; no background has been noticed from the material itself in analytical application and SU-8 has been shown to be compatible with most chemicals

applied in analytical applications. Transparency of the material enables optical detection. Drawbacks of the material are relatively high coefficient of thermal expansion (CTE) that may cause stresses to wafers if SU-8 is used with materials with widely different CTE values at elevated temperatures. SU-8 cross-links tightly making mechanically strong structures possible, but negative aspect of high cross-linking density is difficult removal of the material. However, good patternability of SU-8 enables wafer-level batch fabrication of accurately defined microfluidic components. Depending on the microchip area several microfluidic devices can be fabricated on one wafer and several wafers can be fabricated at the same time.

2. Soft Lithography

Soft lithography enables large-scale production of polymeric devices with high accuracy. The term “soft” refers to an elastomeric stamp with patterned relief structures on its surface. Polydimethylsiloxane (PDMS) has been used successfully as the elastomeric material. There are different techniques to transfer the pattern on this elastomeric stamp: microcontact printing and replica micromolding (Xia and Whitesides, 1998). In many applications, the elastomeric PDMS part can be used directly as a microfluidic device with microchannels on it.

2.1. Polydimethylsiloxane (PDMS)

Although all kinds of polymers can be used for the fabrication of an elastomeric stamp, PDMS exhibits unique properties suitable for this purpose. PDMS has an inorganic siloxane backbone with organic methyl groups attached to silicon (Figure 2). PDMS has high optical transparency above a wavelength of 230 nm and low self-fluorescence. PDMS has a low interfacial free energy, which avoids molecules of most polymers sticking on or reacting with its surface. The interfacial free energy of PDMS can be manipulated with plasma treatment. The modified surface properties of PDMS are needed for certain applications. PDMS is stable against humidity and temperature. This material is optically transparent and can be cured by UV light. PDMS is an elastomer and can therefore attach on nonplanar surfaces. PDMS is mechanically durable. These characteristic make PDMS an ideal material for soft lithography.

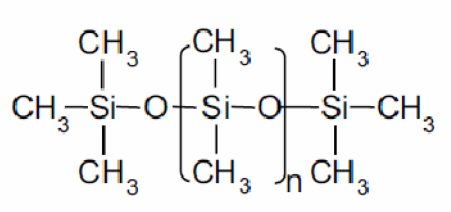

Figure 2. Chemical structure of PDMS

According to McDonald and Whitesides (2002), fabrication in PDMS is easy, and their uses as materials reduces the time, complexity, and cost of prototyping and manufacturing (Soper et al., 2000; Becker and Gartner, 2000). Poly(dimethysiloxane) (PDMS) has been one the most actively developed polymers for microfluidics (McDonald *et al.*, 2000). Fabrication of systems of channels in PDMS is particularly straightforward since it can be cast against a suitable mold with sub-0.1-µm fidelity. PDMS is also more than a structural material: its chemical and physical properties make possible fabrication of devices with useful functionality (Table 1).

Table 1. Physical and Chemical Properties of PDMS (McDonald and Whitesides, 2002)

Property	Characteristic	Consequence
Optical	Transparent; UV cutoff, 240nm	Optical detection from 240 to 1100 nm
Electrical	Insulating; breakdown voltage, $2x10^7$ V/m	Allows embedded circuits; international breakdown to open connections
Mechanical	Elastomeric; tunable Young's modulus, typical value of ~750 kPa	Conforms to surfaces; allows actuation by reversible deformation; facilitates release from molds
Thermal	Insulating; thermal conductivity, 0.2 W/(m·K); coefficient of thermal expansion, 310 µm/(m·°C)	Can be used to insulate heated solutions; does not allow dissipation of resistive heating from electrophoretic separation
Interfacial	Low surface free energy ~20 erg/cm^2	Replicas release easily from molds; can be reversibly sealed to materials
Permeability	Impermeable to liquid water; permeable to gases and nonpolar organic solvents	Contains aqueous solutions in channels; allows gas transport through the bulk material; incompatible with many organic solvents
Reactivity	Inert; can be oxidized by exposure to a plasma; $Bu_4N^+F^-$((TBA)F)	Unreactive toward most reagents; surface can be etched; can be modified to be hydrophilic and also reactive toward silanes; etching with (TBA)F can later topography of surfaces
Toxicity	Nontoxic	Can be implanted in vivo; supports mammalian cell growth

However, PDMS also presents a number of drawbacks, such as volume change and elastic deformation. The design of a PDMS part should consider the shrinking effect upon curing. A number of organic solvents can swell PDMS as well. Furthermore, elastic deformation can limit the aspect ratio of the designed structure. A too-high aspect ratio leads to a pairing effect, in which two parallel structures attach to each other. An aspect

ratio that is too low leads to a sagging of noncontact regions, which makes further steps of soft lithography impossible. The recommended aspects ratios for PDMS structures are between 0.2 and 2 mm (Xia and Whitesides, 1998).

3. Experimentation

The microreactors designs were based on internal geometries proposed by Hong *et al.* (2004) and Yu *et al.* (2008) in this work called like Tesla- and Omega-shaped, respectively. The microreactors manufacturing was carried out in the *Microfabrication Laboratory of the Brazilian Synchrotron Light Laboratory (LNLS).*

3.1. SU-8 Microreactor

Drawing and computer-aided design (CAD) program, Autodesk AutoCAD®, was used to design mask for the microfluidics devices. On quartz wafers was deposited chrome using electron beam to form a pattern design in the CAD program. Also, a transparency was tested as a mask for microdevices whose pattern was printed with a HP LaserJet 4250n printer.

Commercial glass wafers of 80 mm in diameter were used as substrates. SU-8 50 supplied from Microchem Corporation was applied in the experiments. SU-8 served both as a material for the channels and also as bonding adhesive. The process was done in cleanroom to avoid material particle contamination. Basic processing steps for fabrication of fully enclosed SU-8 microstructures between glass wafers are shown in Figure 3. Structures made fully of SU-8 are beneficial due of symmetry and mechanical stresses (Tuomikoski and Franssila, 2004) which is an advantage to fabrication of microchannels.

Process for fabrication of SU-8 microstructures begins with application of SU-8 on a clean glass wafer. Wafers were cleaned before application by immersing them for the short time (30 seconds) in hydrofluoric acid (HF) solution. After rising in DI-water and drying with nitrogen, wafers were dehydrated in a convection oven at the temperature of 120°C for at least one hour. Reason for this step was to refresh surface glass wafers to improve adhesion of SU-8.

After dehydration bake, SU-8 photoresist was spun onto glass wafer using the photoresist spinner. The set spinner parameter were: a ramp speed to 500 rpm at 100 rpm/second acceleration holding at this speed for 10 seconds to allow the resist to cover the

entire surface, then ramped to final spin speed of 2000 rpm at an acceleration of 300 rpm/second and holding in this speed for 30 seconds to achieve the final thickness of 50 µm (Micro-Chem). The wafer was soft bake on a hot plate in two-step baking process: for 10 min at 65°C and 30 min at 95°C. The two-step bake was done to allow the solvent evaporate out of the film at a more controlled rate, which results in better coating fidelity, edge bead reduced and better resist-to-substrate adhesion. The film was thus exposed in LOMO EM-5006 mask aligner with a dose of 1500 mJ/cm^2 measured at wavelength of 365 nm. Basically, the luminous flux initiates physic-chemical reactions in the polymer, which modify the solubility in certain solvents.

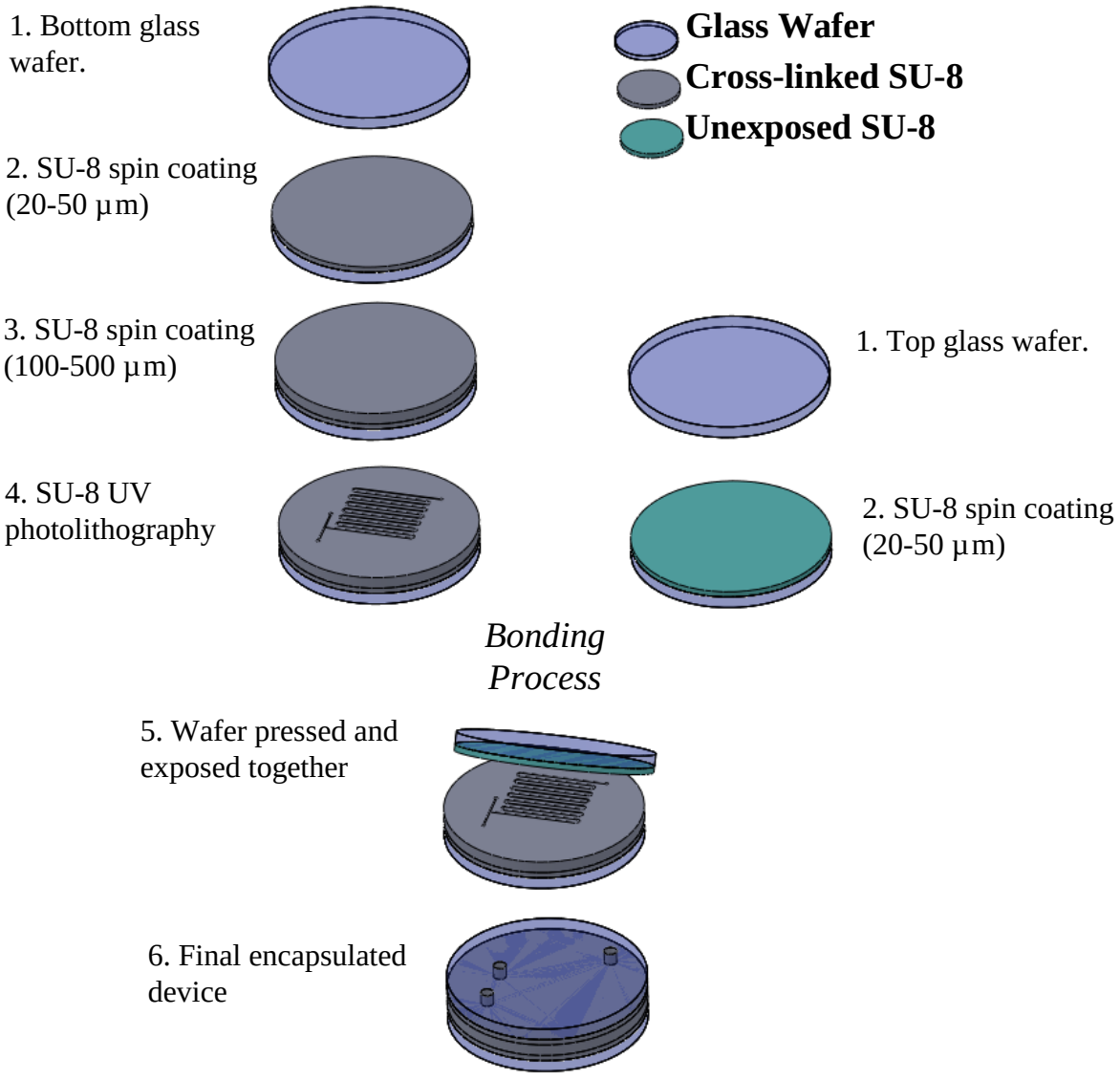

Figure 3. Fabrication process scheme

After exposure, a post exposure bake (PEB) was performed to crosslink the exposed photoresist. It was done on a hot plate holding the temperature for 1 minute at 65°C and followed by temperature ramped to 95°C and holding the temperature there for 5 more minutes. This two step bake minimize stress, wafer bowing and resist cracking. Slow cooling back to room temperature was done to reduce mismatch-effects caused by thermal expansion.

Similar steps mentioned above were done to fabricate the microchannels. A second SU-8 layer was applied on top of the first SU-8 layer. The spinning speed was adjusted to define layer thickness of 500 µm: ramp speed to 200 rpm at 100 rpm/second acceleration holding at this speed for 10 seconds then ramped to spin speed of 400 rpm at an acceleration of 300 rpm/second and holding in this speed for 30 seconds.

After application of SU-8, wafer was softbaked on a hot plate by ramping the temperature first to 65°C for 90 minutes and after to 95°C for 180 minutes. Wafer was kept for 60 minutes at the glass transition temperature of SU-8 (measured to be 64°C by Pfeifer *et al.*, 2001) to minimize the edge bead effect and other thickness irregularities. At the glass transition temperature or above, SU-8 exhibits self-planarization.

Here the photomask was clamped to the photoresist and its substrate. Exposure dose was of 5280 mJ/cm^2 measurement at wavelength of 365 nm. The light transfers the mask pattern onto the photoresis layer. After exposure, PEB was performed to crosslink selectively the exposed portions of the photoresist by ramping the temperature first to 65°C for 10 min and followed to 95°C by 30 min. Slow cooling back to room temperature was done to reduce deformation of the structures

Structure was developed by immersion in a beaker with SU-8 developer until all unexposed SU-8 were removed. To determine whether all the unexposed SU-8 was removed, the structure was removed from the beaker, rinsed with isopropyl alcohol, and then dried with nitrogen air. The SU-8 is a negative resist, so the unexposed negative resist is dissolved, while the exposed area remains due to crosslinking.

After wafer preparation steps, adhesive bonding layer of SU-8 was applied on a glass wafer as illustrated in Figure 3. Adhesive SU-8 layer from 50 µm thickness was applied. Similar to structural layer, also the bonding layer was soft bake on a hot plate keeping temperature at the beginning 15 minutes in 65°C to planarize the layer. After that

temperature was ramped up to 95°C and kept there for 10 minutes. Glass wafer with adhesive SU-8 was cooled down to 68°C and the wafer with SU-8 structure was heated up to 68°C, and the wafers were pressed together. This thermal equalization reduced structure deformation during bonding, in addition, at this temperature void formation is minimized and unintentional gap filling is controlled (Tuomikoski and Franssila, 2005). Pressure of 2 N ca. was applied to initiate contact between wafers.

After contact is achieved over the whole wafer, bonding layer was exposed through the glass wafer with a dose of 2640 mJ/cm^2. Post exposure bake was done to finish bonding by crosslinking across the structural and adhesive SU-8 layers heating to 65°C and holding for 1 minute followed temperature ramped to 95°C and holding there for 5 more minutes. Again slow cooling was required to reduce stresses in the bonded stack. In this procedure, no additional pressure was applied after initial contact was made, eliminating expensive vacuum bonding system that is often used in adhesive bonding (Niklaus *et al.*, 2001; Dziuban, 2006).

3.2. PDMS Microreactor

Soft lithography was used for rapid prototyping of microfluidic devices because it has a number of useful properties: low cost, low toxicity, transparency from the visible wavelengths into the near ultraviolet wavelengths, and chemical inertness. In addition, it is possible to go from design to production or replicated structures in less than 24 h and is applicable to almost all polymers that can be prepared from polymeric precursors.

First, PDMS was mixed from the two commercially available prepolymers consisting of a long chain polymer (base) such as Sylgard 184 and short chain polymer with initiator (curing agent) both purchased from Dow Corning. The weight ratio of the base and the curing agent was 10:1. The solid master was fabricated using SU-8 negative photoresist (Figure 4(a)) as was described above. The PDMS mixture was poured onto the replication master and degassed in a desiccator at 5-6 Pa for one hour to eliminate air bubbles. The whole set is then cured at relatively low temperature at 100°C for 1 hour.

After PDMS layer was peeled off and the external access to the microfluidic array was obtained by drilling holes in the PDMS layer (Fredrickson and Fan, 2004) (Figure 4(b)). The sealing process was carried out by oxidizing PDMS surface through RF (radio frequency) oxygen plasma using a PLAB SE80 plasma cleaner (Plasma Technology,

Wrintong, England). The plasma working parameters were obtained from Jo *et al.* (2000): 16 Pa of O_2, 70 W RF power and 20 s exposition. After plasma oxidation, the PDMS layer was brought into contact with another piece of surface-activated PDMS (Figure 4(c)), pressed against each other manually and allowed to stand for two hours. This process forms a watertight and irreversible seal.

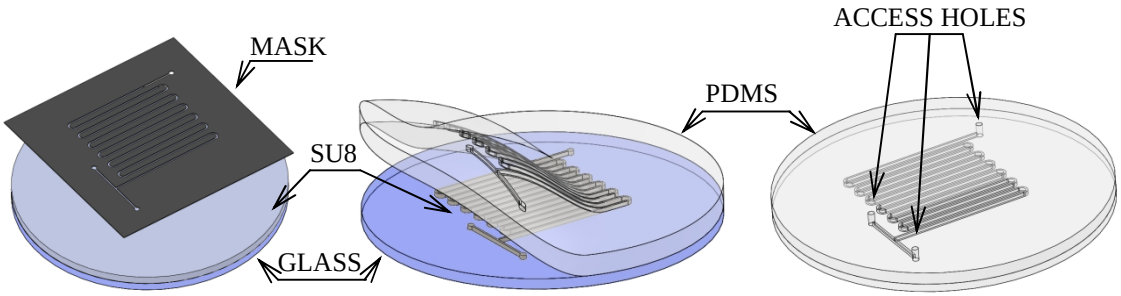

Figure 4. Fabrication of microchannels with soft lithography: (a) spin coating a glass wafer with SU-8, UV-exposure with a clear field mask, development of SU-8 master; (b) pouring PDMS on the mold, peeling off the PDMS part; and (c) surface treatment of PDMS in oxygen plasma and bonding to PDMS.

4. Results and Discussions

4.1. SU-8 Microreactor

4.1.1. Particularities of lithography with SU-8

The main difficulties found with lithographic patterning of thick SU-8 films have been described in more detail by Campo and Greiner (2007) and only a brief outline is given here in relation with the processing steps in the microreactors construction described above.

4.1.1.1. Mask Fabrication

The mask pattern for the photolithography process was drawn using computer-aided design (CAD) program, Autodesk AutoCAD®. The mask was drawn with an internal unit equivalent of 1 micrometer to ensure that the design the same dimensions as the actual mask. The design was then transferred to quartz wafers by means to electron beam writing system. In figure 5 the reactor designs and the characteristic dimensions are shown. Reaction fluid was fed to and removed from microreactor headers via 1/16 inch tubing and fittings. The features inside of the microchannel were designed to both increase the contacting area and enhance the reactant mixing in the microreactor.

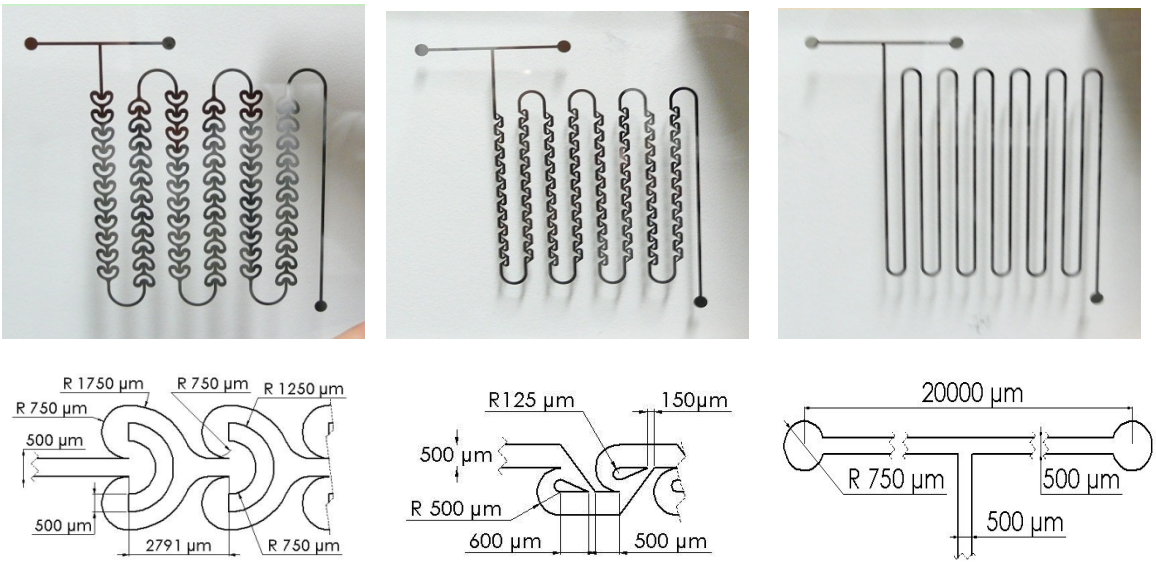

(a) (b) (c)

Figure 5. Masks made with electron beam printed: (a) Omega- , (b) Tesla- , (c) T- design.

Masks in UV-exposures are normally glass or quartz plates with about 100 nm layer of chromium to define non-exposed parts. Alternatively, a mask printed on a plastic transparency film by high-resolution laser printer is an option to reduce cost and to speed up the design cycle. In order to assessment performance of this method, one simple mask was printed on a plastic transparent film in a HP LaserJet 4250n printer as shown in Figure 6(a), which was used in the fabrication of microchannel T. The resulting microchannel T made of SU-8 resist, using the transparent mask is shown in the figure 6(c-d).

As shown in Figure 6(c-d), the disadvantage of using transparency masks are rougher channel walls and undefined structures as result of micropores in the mask (Figure 6(b)) where small areas are exposed, creating waste-structures in middle of the microchannels.

4.1.1.2. Preparation of Wafer

Careful cleaning of the substrate is important because physical contaminants such as particles can hinder the lithography process by preventing light from exposing the photoresist or by disturbing the surface uniformity of the coated photoresist, creating unwanted effects. In addition, the presence of water or water vapor compromises the adhesion between the photoresist and the substrate. These unwanted effects are shown in the Figure 7.

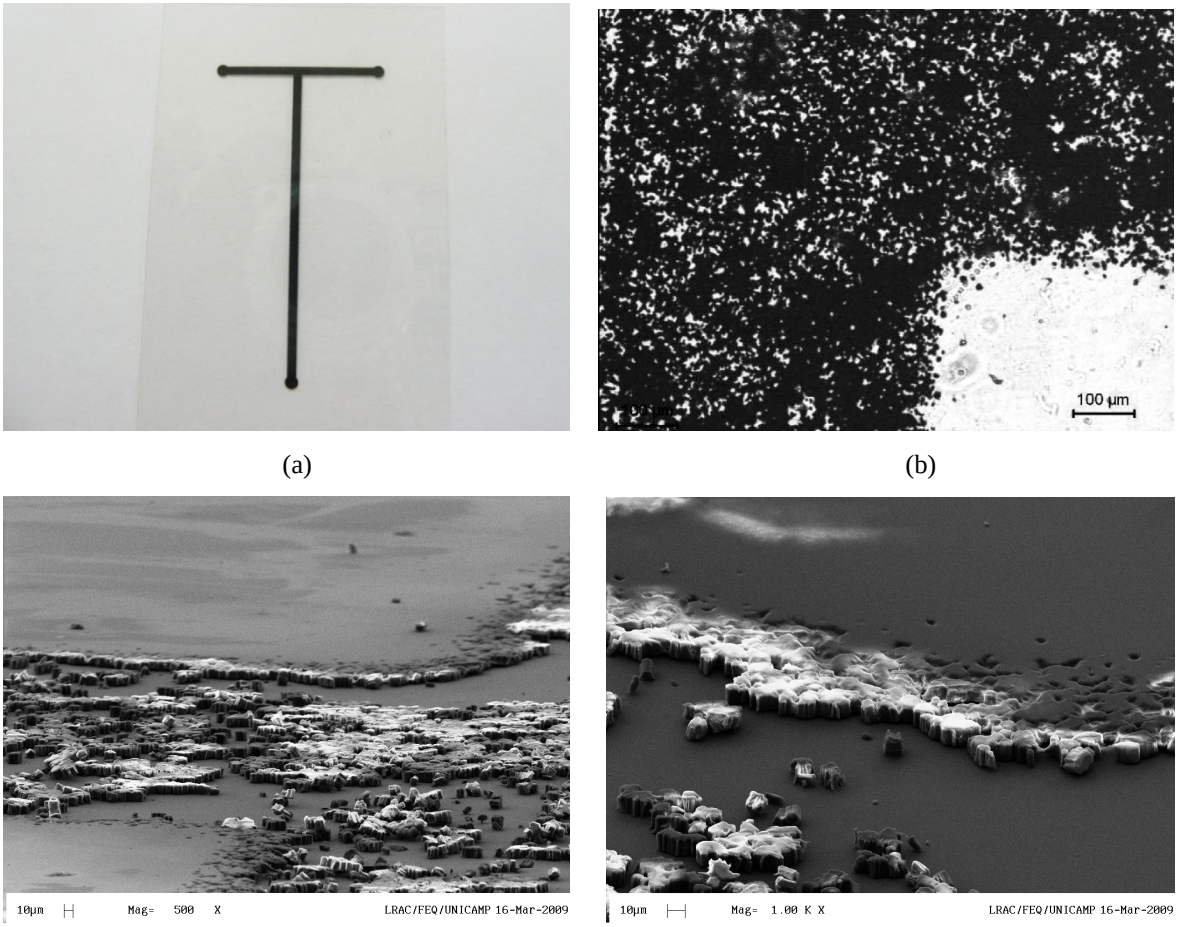

(a) (b)

(c) (d)

Figure 6. Microchannel made with a mask printed on a plastic transparent film by a HP LaserJet 4250n printer: (a) pattern of the transparency mask, (b) image of the mask 100 times larger by optical microscope, (c) waste-structures in the middle of the channel and (d) undefined channel walls.

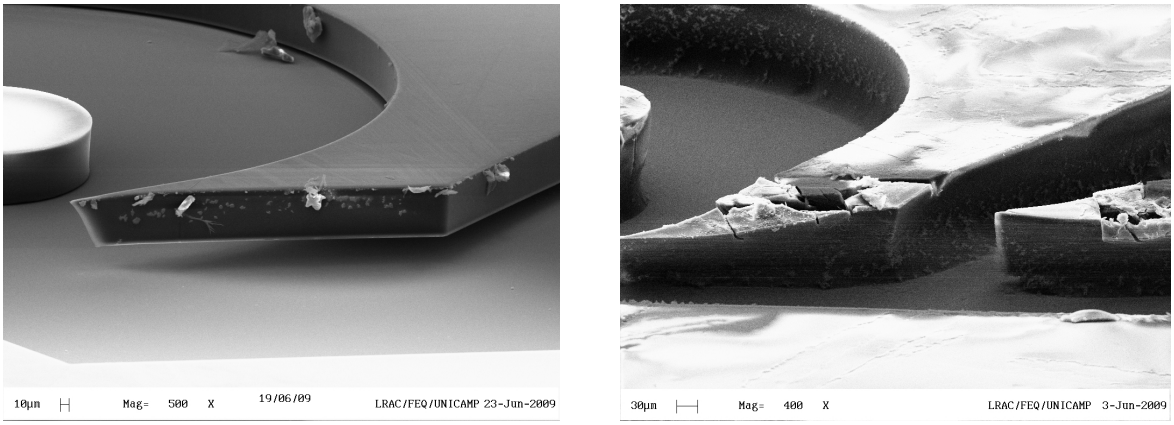

Figure 7. Unwanted effects caused by poor preparation of the substrate wafer.

In fabrication of fluidic structures with lithography there are several important requirements for the materials in comparison with normal lithography. Adequate mechanical strength, possibility to apply and expose uniformly thick layers of polymers are the basic requirements for the photoresist layer patterning.

Additionally, it has to consider microfluiditics properties of the materials: compatibility with chemicals, hydrophobicity, surface charge and so on. These requirements are dependent on the application. Material strength requirements are best achieved by tight network of polymers achieved by polymerization of monomers or by crosslinking of oligomers in the case of negative photoresists. Positive photoresist normally lack the mechanical, thermal and chemical durability required in fluidic applications.

4.1.1.3. Film Stress and Solvent Gradients

Solvent removal during soft baking is accompanied by volume shrinking and mechanical stress. The accumulated stress increases with increasing film thickness and feature lateral dimensions and may result in debonding of the resist layer from the substrate if adhesion is weak. Recent studies have demonstrated that the soft-baking time is the major factor contributing to the overall film internal stress during processing (up to 50%), followed by exposure dose, post-exposure bake time and development time with a 30, 15 and 5% contribution, respectively (Barber *et al.*, 2005). In Figure 8 are shown cracking problems due to internal stress of thick SU-8 films after of soft-baking, exposure dose, post-exposure bake and development processes.

The soft-baking time determines the final solvent content of the resist. Short soft-baking times leave a softer resist film which is less prone to internal stress during subsequent processing steps. However, high levels of solvent after soft baking may result in formation of bubbles during post-exposure baking, collapse of features due to lower mechanical stability at the bottom because of the higher solvent contend and increased lateral diffusion rates of the acid generator molecules outside of the masked areas during post-exposure baking and therefore lower contrast between cross-linked and un-cross-linked areas. If the resist is too hard, cross-linking in the irradiated areas will be hindered. Consequently, the optimum soft-baking time needs to be optimized for each particular thickness and application.

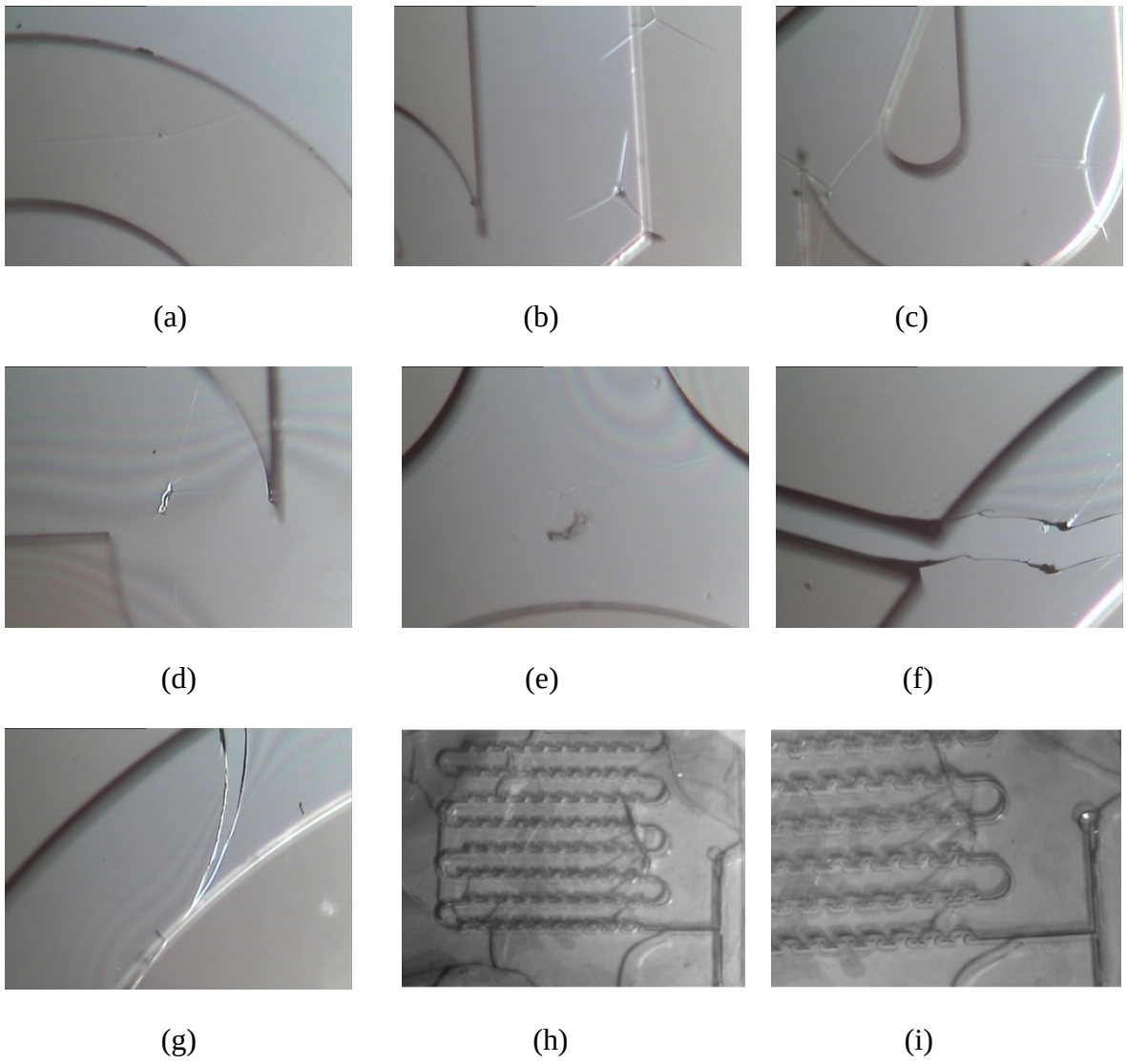

Figure 8. Cracking problems due to internal stress of thick SU-8 films after soft-baking, exposure dose, post-exposure bake and development: (a-c) micro-cracking (100 times larger by optical microscope), (d-e) debonding of the resist layer from the substrate (100 times larger by optical microscope), (f-g) macro-cracking (100 times larger by optical microscope), (h-i) total cracking (4 optical microscope magnification).

The distribution of the solvent across the film thickness is another crucial factor. Solvent evaporation during soft baking is diffused controlled. The evaporation rate is determined by the diffusion coefficient of the solvent in the resist, which increases exponentially with increasing temperature and free volume. The free volume is determined by the amount of the retained solvent, which acts as a plasticizer. At the beginning of the soft baking, the solvent evaporates quickly because of the very high solvent concentration. The diffusion coefficient is larger enough to evaporate solvent from the bottom of the film and, therefore, there is no significant solvent gradient across the film thickness. The

evaporation rate decreases gradually as the solvent gradient appears in the film. If the soft-baking temperature is high, the solvent near the surface is evaporated completely while the solvent level of interior is still high. A “skin” of dried, glassy polymer appears on the film and hinders diffusion of the solvent from the interior.

Solvent gradients become more pronounced as the thickness is increased. The length scale of diffusion of the solvent during the soft baking becomes so large that the solvent trapped below the surface cannot escape easily. Furthermore, the problem is not necessarily solved by extending the time of the soft bake indefinitely because, eventually, the level of the cross-linking that occurs during the soft bake, (albeit at a very low rate) will reach an unacceptable level whereby the SU-8 can no longer completely develop (Becnel *et al.*, 2005).

Solvent content and solvent gradients may also vary depending on the equipment used for soft baking (Kubenz *et al.*, 2003; Wang *et al.*, 2005). Two baking methods are commonly used: hot plates and ovens. In an oven, the resist is uniformly heated by convection from all sides. Skin formation on the resist surface is often observed, which reduces further solvent evaporation. This phenomenon can be avoided by hot plate baking. Here, the resist is heated from below by heat conduction, and a temperature gradient develops in the resist layer (higher temperature at the bottom of the resist). This has a favorable effect in thinner resist layers (convection, quicker solvent remove). However, for large thickness a uniform bake of the layer is not possible anymore.

4.1.1.4. Resist UV absorption

As a photosensitive organic material, SU-8 absorbs light in the UV range (Yang and Wang, 2005). Absorption increases progressively during exposure due to chemical changes induced during photoactivation (Gaudet *et al.*, 2006). Consequently, there is a gradual light intensity drop across the film thickness when an UV beam penetrates the resist layer from the top to the bottom, and this drop becomes more pronounced during exposure. This results in the top part of the resist being irradiated with higher dosage as the bottom part, and generates T-profiles instead of vertical profiles in photolithographic SU-8 structures (Figure 9).

The UV absorption spectrum of the unexposed SU-8 resist shows much higher absorbance at shorter wavelengths than at longer wavelengths. In addition, the absorbance

change during exposure is also more pronounced at short wavelengths. This means that the longer wavelength components of the irradiation source penetrate further down and expose the bottom part. For this reason, it is recommended to filter out the wavelengths below 365 nm during exposure.

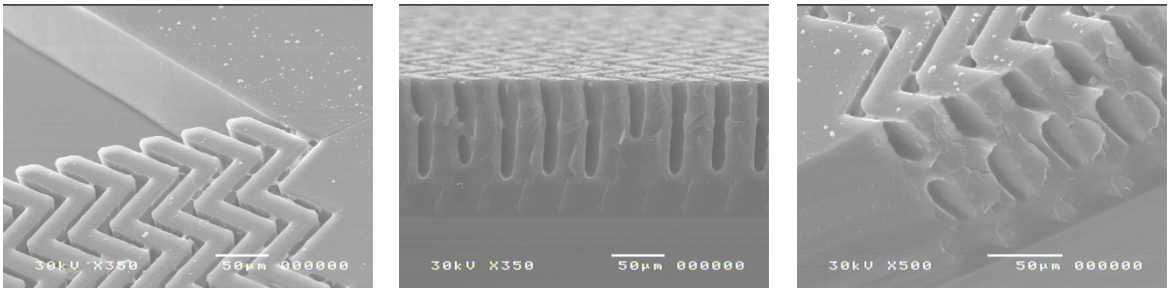

Figure 9. Unwanted effects caused by diffraction effects (Fresnel diffraction) resulting in pattern edges being irradiated with higher doses and consequently pattern enlargement of the features (T-profile).

4.1.1.5. Long Development Times

Pattern development involves diffusion of developer molecules onto the non-cross-linked SU-8 regions and diffusion of solvated polymer chains out of them to the developer solution. The time required for development is determined by the exposure dose, soft-baking time and temperature, the temperature and agitation during development and the geometry of the pattern. High aspect ratio features such as narrow and deep holes, tubes, or horizontally orientated long channels are more difficult to develop. This process, if possible at all, may take many hours and cause dramatic damage of fine features as a consequence of swelling of cross-linked regions or debonding of the resist layer from the wafer (Figure 10).

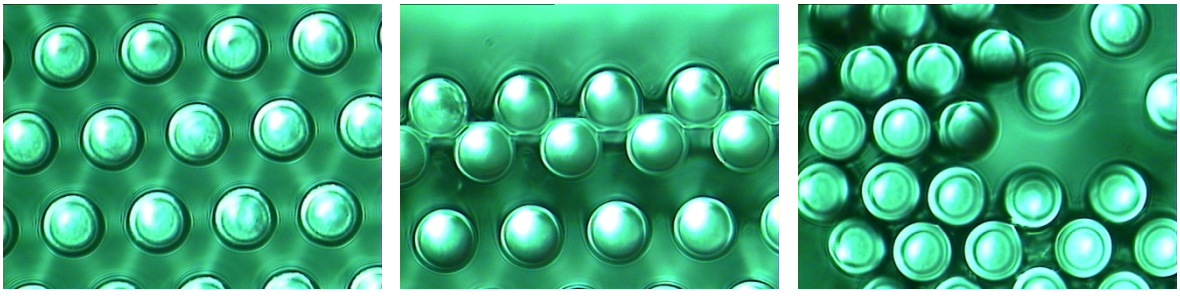

(a) (b) (c)

Figure 10. Debonding effect of the resist layer from the wafer as a consequence of long development times: (a) pattern of SU-8 micropillars with 20 µm diameter and 100 µm height (100 times larger by optical microscope), (b-c) undefined structure due to debonding of the resist layer (100 times larger by optical microscope).

Development has been accelerated by moderately increasing the temperature of the developing solution, by reducing the exposure time and consequently the cross-linking degree or by agitation (Chan-Park *et al.*, 2004). Stirring of the developer solution enhances diffusion, which increases the development rate. Downward orientation of the wafer during stirring has been demonstrated to improve development of high aspect ratio structures, as it allows gravitational forces to aid in the removal of resist (Cheng and Chen, 2004; Cheng and Chen, 2001).

Stirring during development is not always beneficial. Strong stirring may cause high aspect ratio structures to deflect in the pressure gradient and this may lead to pattern deformation, debonding, adhesion between nearby structures and finally pattern loss. Sonic development in its two categories, ultrasonic and megasonic, can be applied to solve this problem. Ultrasonic development uses frequencies in the Kilohertz range to agitate the developer. This increases the pressure at the resist surface and accelerates diffusion and development. However, ultrasonic waves also cause vibrations in the pattern structure which may result in cracking and debonding over time. For this reason, ultrasonic baths are not always beneficial in high aspect ratio processing.

Megasonic agitation, which uses frequencies well above the vibrational modes of the resist structures (typically 1 to 10 MHz), has been proved to be more effective. SU-8 structures ranking from 20 µm to 1.5 mm in height and with aspect ratios up to 50 by optical and well over 100 by x-ray lithography have been reported (Meyer *et al.*, 2002; Williams and Wang, 2004). Conventional development restricted the feature's aspect ratio to 30. Parameters such as damping capacity, agitation power density, orientation of the sonic wave relative to the features and substrate may also influence the process but have not yet been considered.

4.1.1.6. Collapse of Structures During Rising

As the high of the features increase and their lateral size decrease (higher aspect ratio), collapse of the SU-8 pattern becomes an important problem. Collapse occurs when the adhesive forces between the features in contact overcome the forces required for bending them. Simple mechanical calculations have established the dependence of pattern collapse on Young's modulus of the resist material, its surface energy and the pattern geometry (height, width and interfeature distance) (Hui *et al.*, 2002). The maximum aspect

ratio achievable increases with increasing SU-8 stiffness, decreasing SU-8 surface energy and increasing feature spacing. Increasing SU-8 stiffness may be performed by adding inorganic fillers to the resist formulation. However, composite SU-8 exhibits higher viscosity and this may worsen planarization properties. Alternatively, the cross-linking degree may also be increased, although this may result in higher volume shrinkage and increased film stress. Recently, collapse has been prevented by reinforcing the SU-8 high aspect ratio structures through 'bridges' which prevent them from lateral bending (Peele *et al.*, 2005).

In lithographic processing, there is a more dramatic reason for pattern collapse. It occurs during development and rinse, and is a consequence of the capillary forces acting on the resist walls during solvent evaporation and causing bending and stiction of neighboring features (Tanaka *et al.*, 1993a; Namatsu *et al.*, 1995) (Figure 11). Capillary forces increase with increasing surface tension of the rising liquid and decreasing contact angle between liquid and resist (i.e. increased wetting of the resist by the liquid) (Kondo *et al.*, 2006).

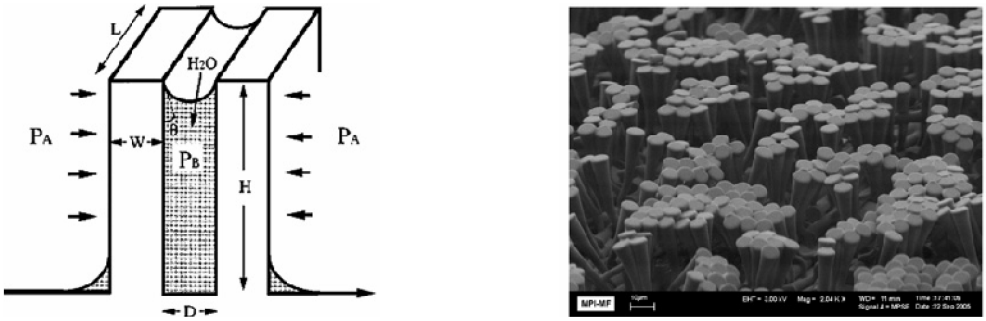

Figure 11. Pattern collapse due to capillary forces during drying. The acting forces are represented in (a) (Namatsu *et al.*, 1995), (b) Collapsed SU-8 micropillars with 5 µm diameter and aspect ratio > 8 (Campo and Greiner, 2007).

Substitution of the rinse water by water/alcohol mixtures with lower surface tension (72 mN m^{-1} for water and 21.8 mN m^{-1} for isopropanol) has been proposed as an alternative to avoid collapse during drying (Tanaka *et al.*, 1993b). However, this method has been rejected by other authors because of the strong wetting of SU-8 by isopropanol (contact angle, $\theta = 20°$ for isopropanol and 81° for water). Other low-surface-tension solvents such as perfluorohexane (10 mN m^{-1}) have also been suggested (Yamashita, 1996; Namatsu *et al.*, 2000). However, these solvents lack compatibility with SU-8 processing chemicals (perfluorocarbon solvents have poor miscibility with developer and rinse

solution). Furthermore, the finite value of its surface tension is still not sufficient to prevent pattern collapse in nanolithography, even though it is so small.

Freeze drying offers another alternative, but this process requires large processing times (Tanaka *et al.*, 1993c). Supercritical drying using CO_2 after replacement of rising water (insoluble in CO_2) by alcohols (soluble in CO_2) provides another route for preventing collapse. In a supercritical liquid, the surface tension becomes negligible and the capillary force is nonexistent. However, special equipment to withstand high pressures and elevated temperatures is required (Namatsu *et al.*, 2000). This factor renders this method not universally applicable for wet processing.

4.1.2. Bonding Process

The adhesive bonding method was used for sealing of the microreactor. In this technique an intermediate adhesive layer of SU-8 was applied to bond the substrate to structure. The main advantage of this procedure over other techniques such as anodic and fusion bonding is low cost, low bonding temperature, greater tolerance to surface roughness and topography, and is not required expensive vacuum bonding systems (Tuomikoski and Franssila, 2005). Nevertheless, bonding with SU-8 patterning is a tradeoff between two main problems: void formation and filling of the channels by the adhesive SU-8.

Temperature during bonding should be low to avoid filling of the channels by the flow of adhesive layer SU-8. Microchannels are filled during bonding because of thickness non-uniformities of SU-8 layers. Thus, when wafers are pressed into contact, any additional SU-8 flows and fills channels. Capillary forces increase this effect. Thickness non-uniformities can be caused, for instance, by edge beads, unintentional tilt, dirt particles, curvature of the substrate or mask, bubbles after spinning or by soft baking under non-ideal conditions on a hot plate.

However, by lowering the bonding temperature, bonding quality suffers and voided area increases significantly. This occurs because the amount of solvent that remain reduces cross-linking density and consequently bond strength. Solvent also reduces the viscosity of the adhesive SU-8 layer leading to more pronounced filling of the channels. Furthermore, solvent can later outgas, degrading bonding quality.

Therefore, glass transition temperature of SU-8 is an important parameter because viscosity changes rapidly around this temperature and blocking of the microchannels and

non-bonded area are defined by the viscosity. Glass transition temperature of non-cross-linked SU-8 has been measured to be 64°C (Pfeifer *et al.*, 2001). Bonding close to glass transition temperature of SU-8 allowed slight flow of the bonding layer, enabling sealing of large areas. Tuomikoski and Franssila (2004) found the bonding temperature of 68°C to be a good compromise for complete bonding of the wafer with minimized microchannel filling. Cross-sections of bonded three-layer SU-8 channels are shown in Figure 12.

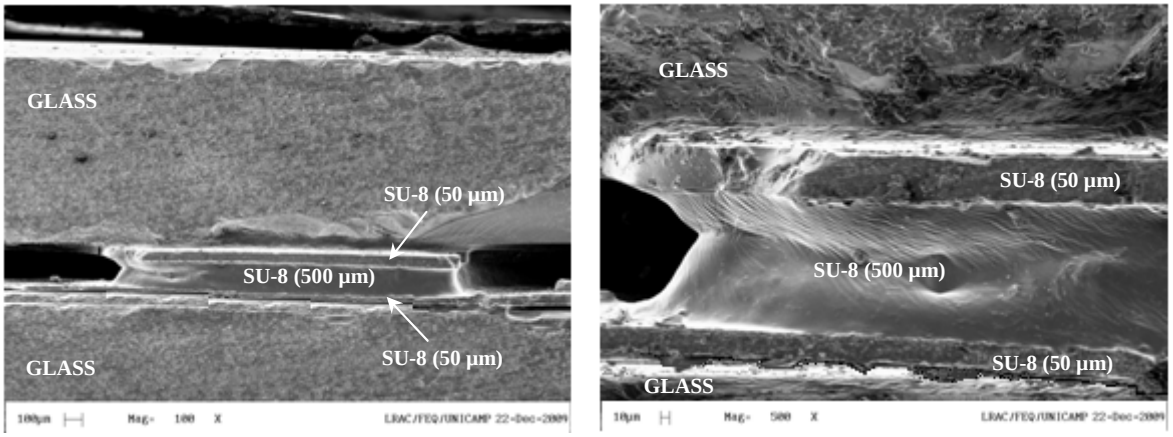

(a) (b)

Figure 12. Cross-sectional SEM images of the structure has glass wafer on the bottom followed by three layers of SU-8: insulating layer, structural layer and bonding layer and glass wafer in the top: (a) bonding after channel formation, (b) insulated SU-8 channel.

4.1.3. Final Microdevices

The final microreactors structures with microchannels of 500 µm of height obtained after follow the construction process and solve the difficult described above for Tesla-, Omega-, and T-shaped are shown in Figure 13.

4.2. PDMS Microreactor

4.2.1. SU-8 Mold Fabrication

The master structure of microchannels was photopatterned on glass wafer using SU-8 photolithography. The resist pattern was transferred into glass following the procedure described above. As shown in Figure 14, three different geometries were fabricated. The width and height of the channels was of 500 µm, and the length was of 10^6 µm approximately.

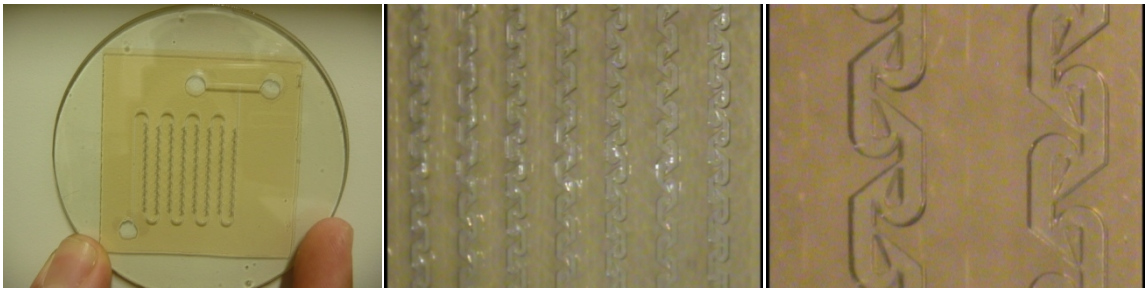

(a) (b) (c)

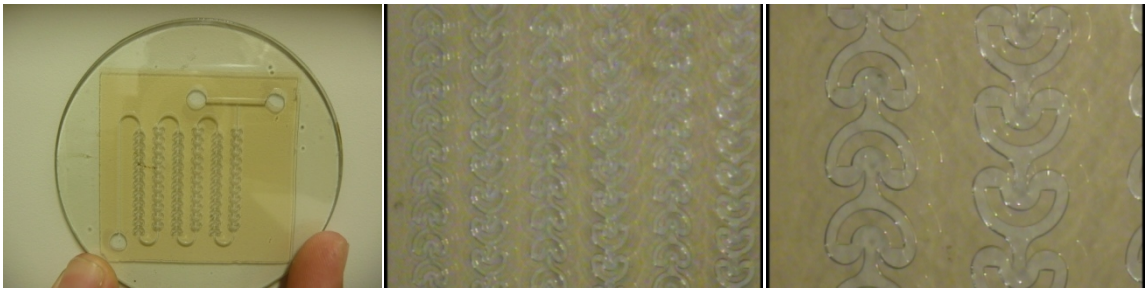

(d) (e) (f)

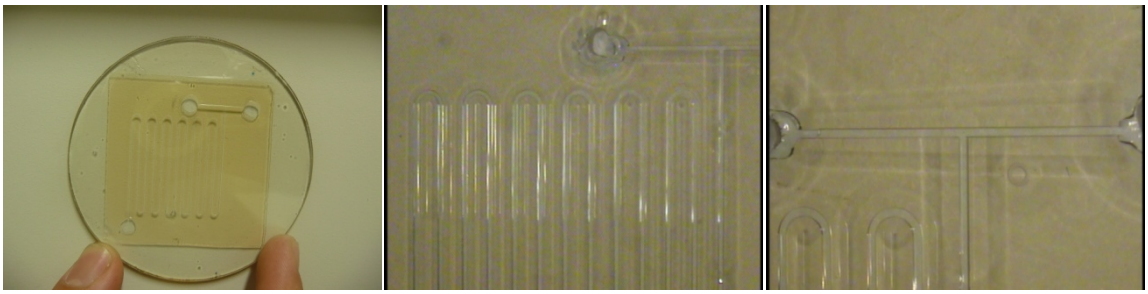

(g) (h) (i)

Figure 13. Seated microfluidic channel formed using the three-layer SU-8 process illustrated in figure 2 and 3. Tesla-shaped: (a) Photograph of the whole SU-8 microreactor formed, (b) Channel design 20 magnification by optical microscope, (c) Channel design 100 times larger by optical microscope. Omega-shaped: (d) Photograph of the whole SU-8 microreactor formed, (e) Channel design 20 times larger by optical microscope, (f) Channel design 100 times larger by optical microscope. T-shaped: (g) Photograph of the whole SU-8 microreactor formed, (h) Channel design 20 times larger by optical microscope, (i) Channel design 100 times larger by optical microscope.

The mold that is required for fabricating the microfluidic channels has high-aspect-ratio trenches. Creating high-aspect-ratio trenches in the mold can be more challenging than creating the corresponding of the structures. This is mainly due to the difficulty in completely developing the photoresist all the way from the bottom of the trenches. If the trenches are tall and narrow, it is difficult for the photoresist developer to reach the bottom of the trench, dissolve the unexposed resist and get exchange with fresh developer to

complete the process. Regular stirring methods are ineffective, aggressive methods can damage the structures and an optimal development process needs to be adopted.

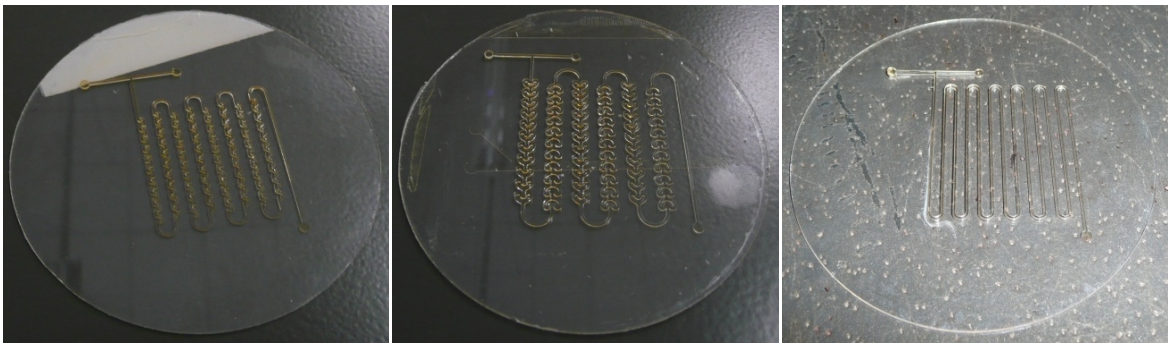

(a) (b) (c)

Figure 14. Pattern transferred into the substrate for replica molding. Tesla-, Omega-, and T-shaped respectively.

In addition, like in the SU-8 structures, diffraction and stray light can lead to sloping sidewalls and overexposed areas, and exposure in undesired location. If larger substrates are used, the resist thickness has to be uniform over the whole substrate or else the channel dimensions would vary in the microfluidic device creating non-uniform flow rates. Producing a uniformity thick photoresist later can be very challenging, because the SU-8 is very viscous and does not flow well. Therefore it can be seen that all current process using UV lithography for SU-8 mold fabrication has limitations in terms of mold size, SU-8 thickness or aspect ratios.

Additionally, the high-aspect-ratio also makes the casting and peeling of the PDMS elastomer a challenging process because the thin walled PDMS channel can collapse due to lack of the mechanical strength. The aspect-ratio challenge is compounded when you consider that the structures used in this mold extend over significant distances at a high-aspect-ratio.

4.2.2. Replica Molding to PDMS Structure

The use of PDMS structures is inexpensive, and multiple copies can be replicated from de original SU-8 master which can be reused many times without deformation, making this process attractive for various application. As seen in Figure 15, the PDMS microreactor replicated from SU-8 master maintain the integrity over large area.

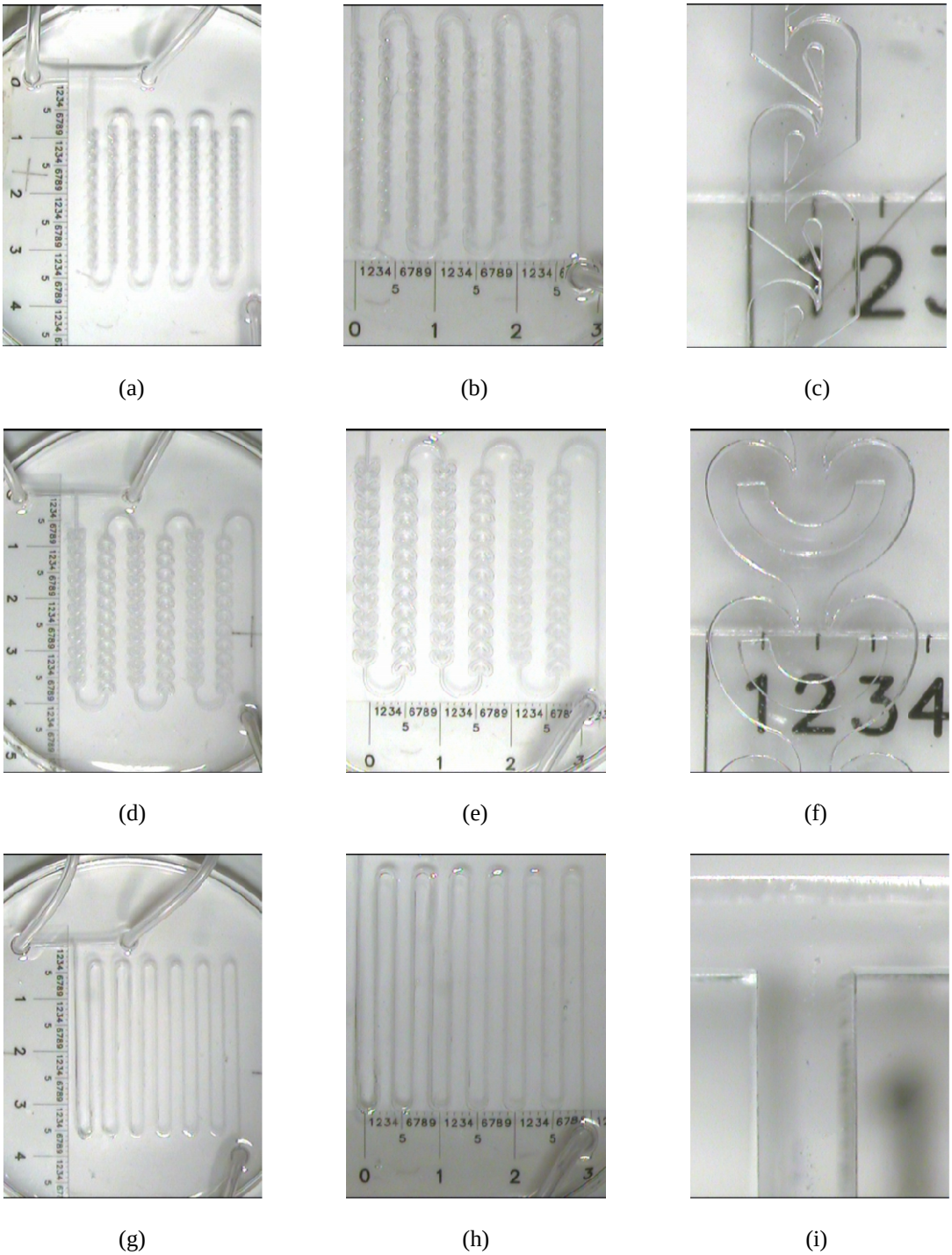

Figure 15. PDMS structures fabricated with SU-8 molds as illustrated in figure 4. Tesla-shaped: (a) Photograph of the whole SU-8 microreactor formed, (b) Channel design 20 times larger by optical microscope, (c) Channel design 100 times larger by optical microscope. Omega-shaped: (d) Photograph of the whole SU-8 microreactor formed, (e) Channel design 20 times larger by optical microscope, (f) Channel design 100 times larger by optical microscope. T-shaped: (g) Photograph of the whole SU-8 microreactor formed, (h) Channel design 20 times larger by optical microscope, (i) Channel design 100 times larger by optical microscope.

4.2.3 Bubble Problems

The PDMS was degassed at a vacuum before poured on the SU-8 mold. However, it was observed that bubbles remains inside PDMS structure after curing (Figure 16). Therefore, it was necessary to degas the PDMS after it was poured on SU-8 mold to remove bubbles trapped in both high and intricate shapes of the pattern. In addition, the PDMS have to peel very slowly from the SU-8 pattern to prevent tearing of the PDMS.

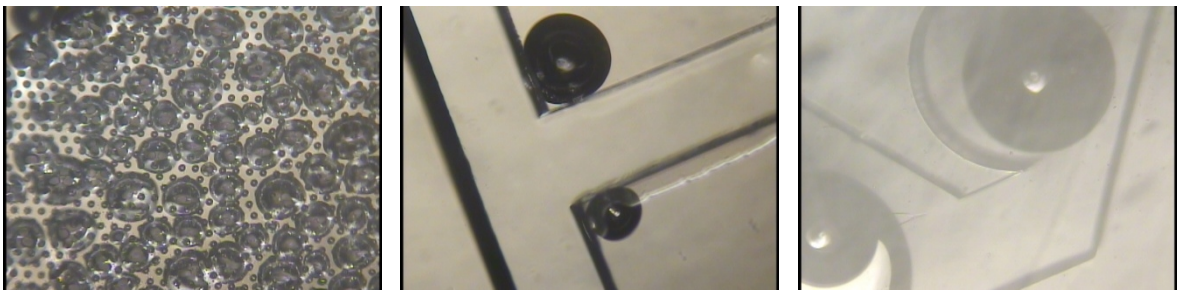

Figure 16. Air bubbles trapped in the shapes of the microchannels.

4.2.4 Bonding Process

As discussed by Duffy *et al.* (1998), enclosed channels are formed simply by oxidizing the PDMS replica containing the channels and a second, flat piece of PDMS in a plasma discharge (Figure 17). Bringing the two oxidized PDMS surfaces into conformal contact forms a tight, irreversible seal. The seal between the two pieces of PDMS was sufficiently strong that the two substrates could not be peeled apart without failure in cohesion of the bulk PDMS. In addition, this method retains the integrity of the channels, is carried out at room temperature and low pressures, and is completed in seconds to minutes.

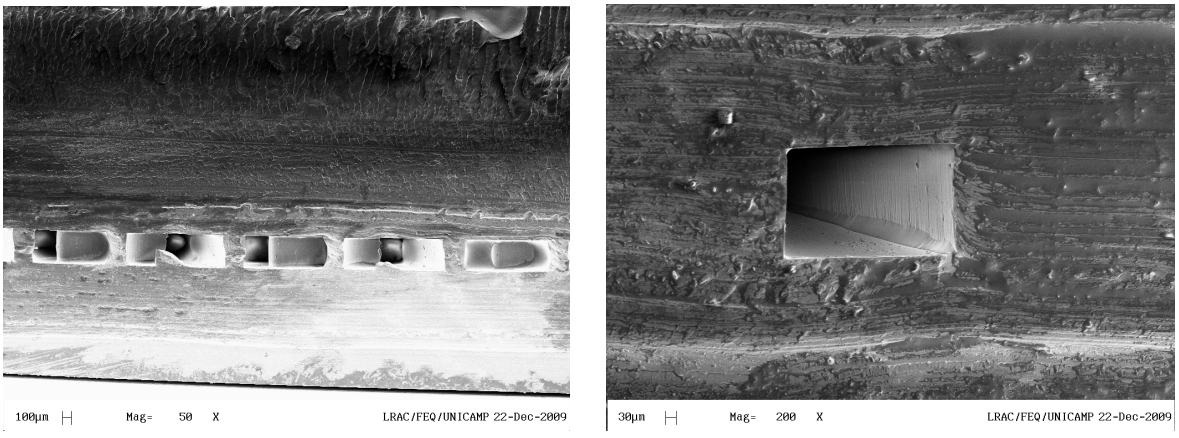

(a) (b)

Figure 17. SEM images of the bonded PDMS structure: (a) cross-sectional of structure, (b) insulated channel.

The nature of the strong bond between two pieces of oxidized PDMS is due to the fact that PDMS in a plasma discharge converts $-OSi(CH_3)_2O-$ groups at the surface to $-O_nSi(OH)_{4-n}$. Therefore, the formation of bridging, covalent siloxane (Si-O-Si) bonds by a condensation reaction between the two PDMS substrates is the most likely explanation for their reversible seal.

4. Conclusions

In this study it has been explored the use of SU-8 (an epoxy-based, negative resist) as a material for the construction of microreactors. A simple technique that uses SU-8 as a bonding layer enables the formation of sealed microchannels. The compatibility of this technique compared to conventional microfabrication methods as well as bonding at temperature less than 100°C enables application of various materials like metals or other polymers, enabling low cost MEMS structures with closed channels and cavities to be fabricated. Bonding process is easy and no special equipment was required. Mechanical strength of the bonds was good and gap filling during bonding was not found.

Some of the difficulties of SU-8 processing to obtain complex structures have been discussed. It can be see that planarization defects, film stress, UV absorption, development and rise time contribute to final result of the device. It is worth to mention that these difficulties make this process not suitable for industrial implementation due to high cost and low throughput; being sometimes SU-8 processing looks more like an art than science.

A simple and inexpensive fabrication method using soft lithography and molding microfluidic devices was also used. Uniform SU-8 molds of 500 µm tall with different features were fabricated. Vertical sidewalls and clean structures were obtained with this process. Continuous flow devices made from PDMS has been successfully replicated from the fabricated mold from SU-8 maintaining the integrity over large area.

In comparison to photolithography of SU-8 photoresist, the major advantage of the soft lithography process is that multiple devices can be produced rapidly from a single reusable master with only minimal use of clean room facilities, resulting in nearly identical reactors easily for repeating experiments. In addition, with different masks used, microreactor molds with different design parameters can be easily produced.

Acknowledgements

The author gratefully acknowledges the financial support provided by The Scientific Research Foundation for the State of São Paulo (FAPESP) and research support by The Brazilian Synchrotron Light Laboratory (LNLS).

Bibliography

Banks, D. Microengineering, MEMS, and Interfacing – A Practical Guide, Taylor & Francis Group, New York, 2006.

Barber, R. L.; Ghantasala, M. K.; Divan, R.; Vora, K. D.; Harvey, E. C.; Mancini, D. C. Optimisation of SU-8 processing parameters for deep X-ray lithography, Microsystem Technologies, 11 (2005), 303-310.

Becnel, C.; Desta, Y.; Kelly, K. Ultra-deep x-ray lithography of densely packed SU-8 features: II. Process performance as a function of dose, feature height and post exposure bake temperature, Journal of Micromechanics and Microengineering, 15 (2005), 1249-1259.

Becker, H.; Gartner, C. Polymer Microfabrication Methods for Microfluidic Analytical Applications, Electrophoresis, 21 (2000), 12-26.

Campo, A; Greiner, C. SU-8: a photoresist for high-aspect-ratio and 3D submicron lithography, Journal of Micromechanics and Microengineering, 17 (2007), R81-R95.

Chan-Park, M. B.; Zhang, J.; Yan, Y.; Yue, C. Y. Fabrication of large SU-8 mold with high aspect ratio microchannels by UV exposure dose reduction, Sensors and Actuators B, 101 (2004) 175-182.

Cheng, C.-M.; Chen, R.-H. Development behaviors and microstructure quality of downward-development in deep x-ray lithography, Journal of Micromechanics and Microengineering, 11 (2001), 692-696.

Cheng, C.-M.; Chen, R.-H. Key issues in fabricating microstructures with high aspect ratios by using deep x-ray lithography, Microelectronic Engineering, 71 (2004), 335-342.

Duffy, D. C.; McDonald, J. C.; Schueller, O. J. A.; Whitesides, G. M. Rapid Prototyping of Microfluidic Systems in Poly(dimethylsiloxane), Analytical Chemistry, 70 (1998), 4947-4984.

Dziuban, J. A. Bonding in microsystem technoilogy, Springer, 2006, Netherlands.

Fredrickson, C. K.; Fan, Z. H. Macro-to-micro interfaces for microfluidic devices, Lab on a Chip, 4 (2004), 526-533.

Gad-el-Hak, M. The MEMS Handbook, New York, CRC Press LLC, 2002.

Gaudet, M.; Camart, J.-C.; Buchaillot, L.; Arscott, S. Variation of absorption coefficient and determination of critical dose of SU-8 at 365 nm, Applied Physics Letters, 88 (2006), 024107.

Hong, C.-C.; Choi, J.-W.; Ahn, C. H. A novel in-plane passive microfluidic mixer with modified Tesla structures, Lab on Chip, 4 (2004), 109-113.

Hui, C. Y.; Jagota, A.; Lin, Y. Y.; Kramer, E. J. Constraints on microcontact printing imposed by stamp deformation, Langmuir, 18 (2002), 1394-1407.

Jo, B. H.; Van Leberghe, L. M.; Motsegood K. M.; Beebe, D. J. Three-Dimensional Micro-Channel Fabrication in Polydimethylsiloxane (PDMS) Elastomer, Journal of Microelectromechanical Systems, 9 (2000), 76-81.

Kondo, T.; Juodkazis, S.; Misawa, H. Reduction of capillary force for high-aspect ratio nanofabrication, Applied Physics A, 81 (2006), 1583-1586.

Kotzar, G.; Freas, M.; Abel, P.; Fleischman, A.; Roy, S.; Zorman, C.; Moran, J.; Melzak, J. Evaluation of MEMS materials of construction of implantable medical devices, Biomaterials, 23 (2002), 2737-2750.

Kubenz, M.; Ostrzinski, U.; Reuther, F.; Gruetzner, G. Effective baking of thick and ultra-thick photoresist layers by infrared radiation, Microelectronic Engineering, 67-68 (2003), 495-501.

Madou, M. J., Fundamentals of Microfabrication: The Science of Miniaturization, 2nd ed., Boca Raton, FL: CRC Press, 2002.

McDonald, J. C.; Duffy, D. C.; Andreson, J. R.; Chiu, D. T.; Wu, H.; Schueller, O. J. A.; Whitesides, G. M. Fabrication of Microfluidic Systems in Poly(dimethylsiloxane), Electrophoresis, 21 (2000), 27-40.

McDonald, J. C.; Whitesides, G. M. Poly(dimethylsiloxane) as a Material for Fabricating Microfluidic Devices, Accounts of Chemical Research, 35 (2002), 491-499.

Meyer, P.; El-Kholi, A.; Schulz, J. Investigations of the development rate of irradiated PMMA microstructures in deep x-ray lithography, Microelectronic Engineering, 63 (2002), 319-328.

Namatsu, H.; Kurihana, K.; Nagase, M.; Iwadate, K.; Murase, K. Dimensional limitations of silicon nanolines resulting from pattern distortion due to surface-tension of rinse water, Applied Physics Letters, 66 (1995), 2655-2657.

Namatsu, H.; Yamazaki, K.; Kurihara, K. Supercritical resist dryer, Journal of Vacuum Science and technology B, 18 (2000), 780-784.

NANO^{TM} SU-8, Negative Tone Photoresist Formulations 50-100, Micro-Chem.

Niklaus, F.; Enoksson, P.; Kälvesten, E.; Stemme, G. Low-temperature full wafer adhesive bonding, Journal of Micromechanics and Microengineering, 11 (2001), 100-107.

Nguyen, N.-T.; Wereley, S. T. Fundamentals and Applications of Microfluidics, Second Edition, Artech House, Inc., London, 2006.

Peele, A. G.; Shew, B. Y.; Vora, K. D.; Li, H. C. Overcoming SU-8 stiction in high aspect ratio structures, Microsystem Technologies, 11 (2005), 221-224.

Pfeifer, K.; Fink, M.; Gruetzner, G.; Bleidiessel, G.; Schulz, H.; Scheer, H. Multistep profiles by mix and match of nanoimprint and UV lithography, Microelectronic Engineering, 57-58 (2001), 381-387.

Soper, S. A.; Ford, S. M.; Qi, S.; McCarley, R. L.; Kelly, K.; Murphy, M. C. Polymeric Microelectromechanical Systems, Analytical Chemistry, 72 (2000), 642A-651A.

Tabeling, P. Introduction to microfluidics, New York, Oxford University Press, 2005.

Tanaka, T; Morigami, M.; Atoda, N. Mechanism of resist pattern collapse, Journal of the Electrochemical Society, 140 (1993a), L115-L116.

Tanaka, T; Morigami, M.; Atoda, N. Mechanism of resist pattern collapse during development process, Japanese Journal of Applied Physics, 32 (1993b), 6059-6064.

Tanaka, T; Morigami, M.; Oizumi, H.; Ogawa, T. Freeze-drying process to avoid resist pattern collapse, Japanese Journal of Applied Physics, 32 (1993c), 5813-5814.

Tuomikoski, S.; Franssila, S. Wafer-Level Bonding of MEMS Structures with SU-8 Epoxy Photoresist, Physica Scripta, T114 (2004), 223-226.

Tuomikoski, S.; Franssila S. Free-standing SU-8 microfluidic chips by adhesive bonding and release etching, Sensors and Actuators A, 120 (2005), 408-415.

Voskerician, G.; Shive, M.; Shawgo, R.; Recum, H.; Anderson, J.; Cima, M.; Langer, R. Biocompatibility and biofouling of MEMS drug delivery devices, Biomaterials, 24 (2003), 1959-1967.

Wang, C.; Jia, G.; Taherabadi, L. H.; Madou, M. J. A novel method for the fabrication of high-aspect ratio C-MEMS structures, Journal of Microelectromechanical Systems, 14 (2005), 348-358.

Williams, J. D.; Wang, W. Using megasonic development of SU-8 to yield ultra-high aspect ratio microstructures with UV lithography, Microsystem Technologies, 10 (2004), 694-698.

Xia, Y.; Whitesides, G. M. "Soft lithography", Annual Review of Materials Science, 28 (1998), 153-194.

Yang, R.; Wang, W. A numerical and experimental study on gap compensation and wavelength selection in UV-lithography of ultra-high aspect ratio SU-8 microstructures, Sensors and Actuators B, 110 (2005), 279-288.

Yamashita, Y. Sub-0.1 μm patterning with high aspect ratio of 5 achieved by preventing pattern collapse, Japanese Journal of Applied Physics, 35 (1996), 2385-2386.

Yu, L.; Nassar, R.; Fang, J.; Kuila, D.; Varahramyan, K. Investigation of a Novel Microreactor for Enhancing Mixing and Conversion, Chemical Engineering Communication, 195 (2008), 745-757.

6.3. Conclusões

Neste estudo, foi explorado o uso da resina SU-8, um fotorresiste negativo a base de epóxi, como material para a construção de microreatores mediante litografia UV. O SU-8 é especialmente desenvolvido para aplicações em MEMS (Sistemas Micro Electro Mecânicos) que demandam elevada razão de aspecto e grandes espessuras. Diferentes estruturas com dimensões até 500 µm foram obtidas. Aparecimento de trincas, baixa adesão, dilatação, inchação, delaminação e colapso das estruturas foram observados e atribuídas ao alto nível de stress do resiste induzido pelo processo. As possíveis causas e soluções foram discutidas em detalhe.

Uma técnica simples para a selagem dos microcanais foi utilizada a qual usa um delgado filme de SU-8 como adesivo. A compatibilidade desta técnica com métodos convencionais de microfabricação, assim como a selagem a uma temperatura inferior a 100 °C permite a aplicação de diversos materiais como metais ou outros polímeros, permitindo a obtenção de dispositivos MEMS de baixo custo. O processo é simples e rápido, sem a necessidade de equipamento especial. Além disso, a obstrução dos microcanais devido ao possível escoamento do fotorresiste SU-8 para dentro dos microcanais durante a selagem não foi observado.

Pode-se observar que esta tecnologia de microfabricação propicia a produção de microestruturas com excelente definição e resolução. No entanto, o custo na implementação de um laboratório de microfabricação contendo um ambiente completamente limpo, estação fotolitográfica, "spinner", chapas de aquecimento, perfilômetro, além a necessidade de material de consumo como fotorresistes, reveladores, máscaras metálicas, substratos de vidro, silício e quartzo, é extremamente alto. No Brasil, o Laboratório de Microfabricação (LMF) localizado no Laboratório Nacional de Luz Síncrotron (LNLS), vinculado ao Ministério de Ciência e Tecnologia/CNPq, conta com toda a infra-estrutura necessária para a fabricação de microestruturas.

Portanto, com as dificuldades encontradas no processo fotolitográfico percebe-se que este não é adequado para aplicação industrial devido ao alto custo e baixo volume de produção, sendo que o processo com SU-8 deve ser visto mais com uma arte do que como uma ciência exata. Assim, a pesquisa por métodos alternativos e economicamente viáveis, é um permanente objetivo da comunidade científica.

As técnicas de microfabricação por moldagem apresentam-se como uma alternativa para a construção de dispositivos microfluídicos em grande escala. Entre estes, a litografia macia foi usada para a obtenção dos microreatores. Neste processo, inicialmente um molde rígido é fabricado contendo a imagem negativa da estrutura microfluídica de interesse. Este molde é utilizado na etapa de replicação dos microdispositivos, a qual consiste em transferir a estrutura microfluídica do molde para o substrato, através de moldagem. Geralmente o substrato é um material polimérico, embora, metais e cerâmicas também podem ser utilizados.

Neste processo, moldes de SU-8 com dimensões de 500 µm de altura e diferentes geometrias foram obtidos. Os dispositivos finais feitos de PDMS foram replicados com êxito a partir do molde fabricado onde estruturas com paredes verticais e livres de bolhas de ar foram reportadas.

Em comparação com a fotolitografia do SU-8, a litografia macia apresenta uma grande vantagem já que vários dispositivos podem ser produzidos rapidamente a partir de um único molde, com o uso mínimo de equipamentos especializados de sala limpa, resultando em reatores com idêntica geometria e dimensões facilitando a reprodução dos experimentos. Além disso, mostrou-se que com diferentes máscaras, moldes de dispositivos microfluídicos com diferentes designs podem ser facilmente produzidos, possibilitando a integração de múltiplas etapas analíticas em um único e portátil substrato.

Capítulo 7.

Simulação e Caracterização Experimental da Mistura em Dispositivos de Microreação

7.1. Introdução

O interesse no desenvolvimento de sistemas microfluídicos tem atraído a atenção de pesquisadores em diversos campos do conhecimento tais como física, química, biologia, medicina e engenharia. Dentro destes microdispositivos se faz necessário um íntimo contato entre as substancias utilizadas para que se alcance uma boa homogeneidade da mistura e uma distribuição uniforme da temperatura. Para tal fim são necessários micromisturadores, onde diferentes aplicações além da mistura podem ser obtidas as quais incluem: emulsificação, suspensão, reações químicas e sistemas de troca térmica.

Os micromisturadores são operados em condições contínuas e devido às pequenas dimensões dos microcanais, o regime de escoamento resultante é predominantemente laminar, portanto, o processo de mistura entre os fluidos se dá principalmente pela difusão molecular. Conseqüentemente, para misturar efetivamente em um tempo razoável, os fluidos devem ser manipulados de tal maneira que a área interfacial entre eles aumente, e com isto, melhorando o processo de mistura pela redução da distância difusional entre as moléculas.

Diversos mecanismos de mistura existem para promover o contato íntimo entre os fluidos, incluindo: a multilaminação, divisão e recombinação, junções *"T"* e *"Y"*, convecção caótica, injeção periódica, injeção em uma corrente principal, transporte de massa forçada e a colisão de alta energia. Contudo, regras usuais para o projeto de micromisturadores ainda não foram desenvolvidas. Entretanto, à parte de seu tamanho diminuto, os micromisturadores são usados como reatores contínuos, o que sugere que a abordagem para o projeto com o objetivo de mistura em microcanais deve ser tratada de maneira similar àqueles de mistura laminar em escala macroscópica.

Em um escoamento laminar não perturbado, as linhas de corrente correm paralelas umas as outras e não há mistura convectiva nas direções radial e tangencial, o que resulta em um baixo grau de homogeneidade espacial. Além disso, o perfil parabólico de velocidade do escoamento laminar em dutos circulares gera uma falta de homogeneidade, a qual se traduz em larga distribuição de tempo de residência. Na atualidade, estudos numa variedade de esquemas para agitar o escoamento para mistura em sistemas microfluídicos vêm sendo desenvolvidos. Estes estudos incluem micromisturadores ativos e passivos. Em comparação com os misturadores ativos, os micromisturadores passivos não necessitam de partes móveis, e a mistura é obtida pelo movimento natural do fluido conforme ele atravessa os elementos de mistura do micromisturador. Entretanto, os micromisturadores ativos precisam ser providos de acessórios para fornecer forças externas, e não são facilmente integrados a outros sistemas microfluídicos.

Além disto, o material com o qual estes dispositivos são fabricados, e principalmente as técnicas utilizadas para sua fabricação podem inviabilizar o desenvolvimento dos mesmos. A realização de testes em laboratório das diferentes configurações pode ser uma tarefa dispendiosa elevando os custos de desenvolvimento dos microdispositivos. Tendo em vista estas restrições, a utilização de ferramentas computacionais como a dinâmica dos fluidos computacional apresenta-se como uma ferramenta valiosa, a qual permite uma série de simulações numéricas ao invés de testes em laboratório, as quais reduzem tempo e investimento no desenvolvimento de um novo equipamento, além de permitir uma melhor escolha no dimensionamento dos sistemas.

Por outro lado, a microscopia ótica é a ferramenta comumente utilizada para a caracterização dos micromisturadores, já que oferece um meio não invasivo de medição na microescala. Juntamente com câmeras digitais e processamento de imagens, uma série de medições em micromisturadores pode ser realizada. A imagem captada com o instrumento óptico é uma matriz de variação contínua de sombras e tons de cores. A intensidade dos pixels em uma imagem digital pode ser representada em um histograma de escala de cinza, que mapeia o número de pixels em cada nível de cinza presentes na imagem. Portanto, o histograma pode ser usado diretamente para a avaliação do grau de mistura onde o histograma de escala de cinza de um campo de concentração bem misturado mostra um único pico, entretanto, quando o histograma de um campo de concentração não misturado mostra dois picos de intensidade correspondentes aos dois líquidos.

Neste capítulo, a qualidade da mistura em microreatores com três diferentes geometrias constituídas basicamente por um canal com a forma Tesla, Omega e T foi estudada utilizando métodos experimentais assim como dinâmica de fluidos computacional (CFD). A caracterização qualitativa dos fenômenos de mistura nas geometrias propostas foi realizada através da observação da evolução mistura de óleo de mamona e etanol a diferentes razões de fluxo, usando uma tinta azul na fase etanol como traçador e uma câmera CCD acoplada ao microscópio ótico. Para otimizar o desempenho dos dispositivos microfluídicos, simulações CFD com o software ANSYS CFX 11.0 foram realizadas. O potencial de mistura de cada microreator foi avaliado comparando as imagens tomadas em diferentes regiões do sistema e identificando as zonas em que o fluxo apresenta maior mistura. Finalmente, as simulações foram comparadas com os resultados experimentais com o intuito de avaliar a metodologia usada na simulação.

7.2. Desenvolvimento

O desenvolvimento deste capítulo é apresentado a seguir, no manuscrito intitulado: *Simulation and Experimental Characterization of the Mixing in Microreaction Devices.*

Simulation and Experimental Characterization of the Mixing in Microreaction Devices

Abstract

The laminar flow pattern and mixing performance of three different microreactors has been investigated using experimental and numerical approaches. The microreactor geometries consist of a channel with either Tesla-, Omega- or T-shaped. The numerical results show that Tesla-shaped microreactor produced split of the lamination flow, whereas the Omega-shaped creates convective mixing, composed of large and small vortex. Particle tracking shows that very little convective mixing occurs in the T-shaped microreactor. Experimental analysis shows the variance of tracer dispersion and the stretching, and quantifying the mixing in the microreactors has been presented. The experimental findings are in excellent agreement with CFD results.

Keywords: Microreactors; Laminar flow; Mixing performance; Computational fluid dynamic.

1. Introduction

In recent years, microtechnology has been employed for the design of miniaturized devices, or so-called microreactors, with characteristic internal dimensions of the order of a few tens of microns for the development of microchemical processing (Ehrfeld *et al.*, 2000; Hessel and Löwe, 2003a-c, Aubin *et al.*, 2003). In addition, these microfluidic systems have attracted a great deal of attention in a range of fields as diverse as physics, chemistry, biology, medicine and engineering (Jeon and Shin, 2009). Amongst the various process engineering components that exist, micromixers play an important role. As discussed by Hessel and Löwe (2003a), micromixers have a large potential of application in tasks, such as mixing, blending, emulsification and suspension, as well as for use as reactors. The mixing efficiency in microprocesses is therefore very important for the definition of process performance and will affect various parameters including heat and mass transfer rates, process operating time and cost, as well as product quality (Aubin *et al.*, 2003).

Due to the small size of the internal structures in the micromixers, the flow is predominantly laminar and excludes the possibility of turbulent mixing. On the micro-scale, mixing can only be accomplished through molecular diffusion and it can take some

seconds. In order to effectively mix at this scale in a reasonable time, fluids must be manipulated so that the interfacial surface area between the fluids is increased massively and the diffusional path is decreased, thereby enhancing molecular diffusion to complete the mixing process (Ehrfeld *et al.*, 2000).

Several different types of mixers for microfluidic applications have been proposed (Nguyen and Wu, 2005; Hessel *et al.*, 2005; Hardt *et al.*, 2005). Mixing at the micro-scale can be classified into passive mixing and active mixing. In active mixing, external energy is used for the mixing process such as micropumps (Glasgow and Aubry, 2003), ultrasound (Yang *et al.*, 2001) and acoustically induced vibrations (Liu *et al.*, 2002) and electro-hydrodynamic (El Moctar *et al.*, 2003) and magneto-hydrodynamic actions (West *et al.*, 2002). In passive mixing, external energy is not required but diffusion and chaotic advection induces mixing. Parallel lamination (Soleymani *et al.*, 2008), serial lamination (Schwesinger et al., 1996) and interdigital multi-lamination (Hessel et al., 2003d; Hardt and Schönfeld, 2003) provide fast mixing by decreasing the mixing path and increasing the contact surface between the mixing phases. Chaotic advection can be generated by special geometries in the mixing channel (Stroock *et al.*, 2002).

Microreactors have brought a big impact in chemical technologies. Because of the small size, microreactor allows the control over a number of production process parameters. Reaction conditions that are unusual at the macroscale are technically possible in microreactors. The advantages of reactions in microreactors are the small thermal inertia, the uniform temperature, the high gradient of the different physical fields, the short residence time, and the high surface to volume ratio. The small thermal inertia allows fast and precise temperature control in microreactors. Miniaturization leads to higher rates of heat and mass transfer. Compared to their macroscale counterparts, micromixers can offer more aggressive reaction conditions. The large surface to volume ratio allows effective suppression of homogeneous side reactions in heterogeneously catalyzed gas phase reactions. The small size makes reaction in microreactors safe because of the suppression of flames and explosions (Löwe *et al.*, 2002).

However, in order to define the reaction conditions and to design a microstructured reactor for a specific chemical transformation, detailed knowledge of the hydrodynamic in the microchannels is necessary. Controlled hydrodynamics allows decreasing the pressure drop, improve the mass transfer and facilitate the product

separation from the reaction mixture. The common modes of interface in the case of liquid-liquid two-phase flow are “slug flow” and “parallel flow”. In the case of slug flow, two mechanisms are known to be responsible for the mass transfer between two fluids: (a) internal circulation (Kashid *et al.*, 2005) which takes place within each slug and (b) the concentration gradients between adjacent slugs lead to the diffusion between the phases. In the case of parallel pattern, the flow is laminar and the transfer of molecules between the two phases is supposed to occur only by diffusion.

No conventional technique has been fully established in the literature to evaluate directly or indirectly the flow behavior and/or quality of mixing in micromixers/reactors. Direct measures include flow visualization and mixing detection techniques such as mixing-sensitive chemical conversions like competing parallel or consecutive reactions where yields and/or selectivities that are achieved for specific reactions products are used as a measure to quantify the mixing performance (Ehrfeld *et al.*, 1999; Kockmann *et al.*, 2006), ionic conductivity, radioactive tracers, and various optical analytical techniques (Sinton, 2004; Kuswandi *et al.*, 2007). Indirect measures from which the degree of mixing can be quantified include Poincare section analysis (Beebe *et al.*, 2001), residence-time distribution (Nauman, 2004; Trachsel *et al.*, 2005) and numerical particle tracking method (Aubin *et al.*, 2003).

In this study, the mixing quality with low Reynolds number in three different geometries consisting of a channel with either Tesla-, Omega- or T-shaped has been investigated using both numerical and experimental approaches. A qualitative characterization of the mixing phenomena was firstly carried out by observing the mixture evolution of castor oil/ethanol a different rate flow ratios on basis of the transfer of a solvatochromatic dye between the two immiscible fluids (Panić *et al.*, 2004). To optimize the performance of the microfluidic devices, simulations CFD using the commercial finite volume-based software package, ANSYS CFX (of Ansys inc., EUROPE) were conducted based on three-dimensional meshes. The mixing potential of each reactor was also evaluated by identifying the zones in the flow that have the greatest potential for mixing. It should be noted that the importance of experimental procedures in the study of mixing behavior in microchannels for single- and multi-phase systems lies in its capability for validating the CFD results, which can be used as a powerful predictive tool for characterizing flow and mixing behavior in microchannels.

2. Experimental and methods

2.1 Microreactor design

The passive microfluidic systems were design based on internal geometries propose by Hong *et al.* (2004) and Yu *et al.* (2008). Figure 1 shows the schematic geometries of the proposed passive micro-mixers. In this study, the investigation was focused in mixing on the passive mixers without chemical reaction in order to evaluate the behavior of the immiscible fluids inside of microchannels and the overall performance of the system. These designs along of the channel were expected to induce more effective mixing performance than the basic T-shaped, which had no internal geometries. The Omega channel microreactor differs from conventional T-shaped in having back flow that lead to chaotic flow, which can rapidly increase the mixing efficiency (Yu *et al.*, 2008). On the other hand, Tesla structures showed excellent mixing performance over a wide range of flow conditions in the micro-scale of blue- and yellow-dyed DI water (Hong *et al.*, 2004). The mixing performance shows patterns similar to Taylor dispersion, with contribution from both diffusion and convection. Our work differs from the above mentioned works due to the fact that the immiscible liquid-liquid two-phase flow patterns rather than one phase flow one studied by means of both experimental and CFD tools. The velocity profiles, such as the velocity and direction, were expected to change near the obstructions, increasing the area contact and transverse dispersion of the immiscible fluids.

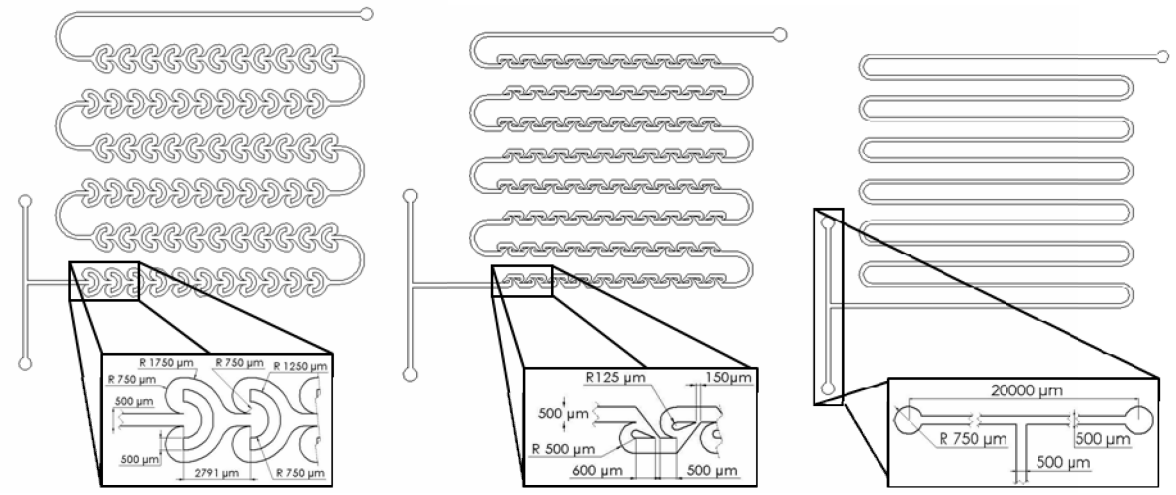

Figure 1. Schematic geometries of microreactors channels with characteristic dimension: (a) Omega-shaped, (b) Tesla-shaped and (c) T-shaped

2.2 Fabrication method

The fabrication processes were composed of mold fabrication by photolithography, replica molding and surface treatment. Drawing and computer-aided design (CAD) program, Autodesk AutoCAD®, was used to draw the mask for the microfluidics devices. Chrome was deposited on quartz wafers using electron beam to create the mask designed in the CAD program. In the mold fabrication process, a 3 in. glass wafer was used as the substrate.

SU-8 50 photoresist (MicroChem Inc.) was spun onto glass wafer using the photoresist spinner a ramp speed to 200 rpm at 100 rpm/second acceleration holding at this speed for 10 seconds to allow the resist to cover the entire surface, then ramped to final spin speed of 400 rpm at an acceleration of 300 rpm/second and holding in this speed for 30 seconds to achieve the final thickness of 500 µm. The wafer was soft bake on a hot plate in two-step baking process: for 90 min at 65°C and 180 min at 95°C and slow cooling back to room temperature was done. The film was thus exposed in LOMO EM-5006 mask aligner with a dose of 5280 mJ/cm^2 measured at wavelength of 365 nm. After exposure, PEB was performed to crosslink selectively the exposed portions of the photoresist by ramping the temperature first to 65°C for 10 min and followed to 95°C by 30 min. Slow cooling back to room temperature was done. Structure was developed by immersion in a beaker with SU-8 developer until all unexposed SU-8 were removed. To determine whether all the unexposed SU-8 was removed, the structure was removed from the beaker, rinsed with isopropyl alcohol, and then dried with nitrogen air. The SU-8 is a negative resist, so the unexposed negative resist is dissolved, while the exposed area remains due to crosslinking.

Micro patterns of PDMS were generated on the substrate by a replica molding method. In the fabrication processes, polydimethylsiloxane (PDMS) was the basic component of the microfluidic devices. A Sylgard 184 kit (Dow Corning Corporation) consisting of a long chain polymer (base) such as Sylgard 184 and short chain polymer with initiator (curing agent) was employed. PDMS based materials have many advantages such as low production cost, non-toxicity, reversible deformation and an optically clear surface. The weight ratio of the base and the curing agent was 10:1. The PDMS mixture was poured onto the mold and degassed in a desiccator at 5-6 Pa for one hour to eliminate air bubbles. The whole set is then cured at relatively low temperature at 100°C for 1 hour. After the PDMS based chips were fabricated, their surface was cleaned with acetone.

After PDMS layer was peeled off and the external access to the microfluidic array was obtained by drilling holes in the PDMS layer (Fredrickson and Fan, 2004). The sealing process was carried out by oxidizing PDMS surface through RF (radio frequency) oxygen plasma using a PLAB SE80 plasma cleaner (Plasma Technology, Wrintong, England). The plasma working parameters were obtained from Jo *et al.* (2000): 16 Pa of O_2, 70 W RF power and 20 s exposition. After plasma oxidation, the PDMS layer was brought into contact with another piece of surface-activated PDMS, pressed against each other manually and allowed to stand for two hours. This process forms a watertight and irreversible seal. As result, microfluidic devices made from PDMS were obtained with microchannels of 500 μm of height.

2.3 Experimental procedure

A schematic diagram of the experimental apparatus is shown in Figure 2. The working fluids are castor oil (Campestre Ind. & Com. De Óleos Vegetais Ltda., São Bernardo do Campo, Brazil) and anhydrous ethanol (Merck, São Paulo, Brazil) with minute amounts of solvatochromatic dye (Reichardt's dye, Sigma-Aldrich) dissolve in it for better visualization of the flow phenomena. Castor oil and ethanol dyed were introduced inside the microreactors by two syringe pumps (Samtronic Infusion Systems ST670, Brazil). The behavior of the fluids in the microreactors was followed under a light source with CCD camera (Panasonic 1/3" CCD Color CCTV Camera WV-CP484).

In each series of experiments, the molar ratios of ethanol dyed to castor oil were adjusted to 9, 12, 17, and 25 by changing the flow rates. Ethanol/oil molar ratios of 9, 12, 17, and 25 correspond to ethanol/oil volume ratios of 0.54, 0.72, 1.03, and 1.51 respectively. All experiments were performed at room temperature and pressure. In order to verify the reproducibility of the experiments, two camera–snapshots were taken for each flow and repeated twice.

The Reynolds number varied with flow rate, but the variation was not significant as all the values were in the laminar region. The values of Reynolds numbers were calculated based on castor oil and ethanol flow rates and it are displayed in Table 1. The residence times showed in the Table 1 were based on the oil since it generally have higher flow rate than ethanol.

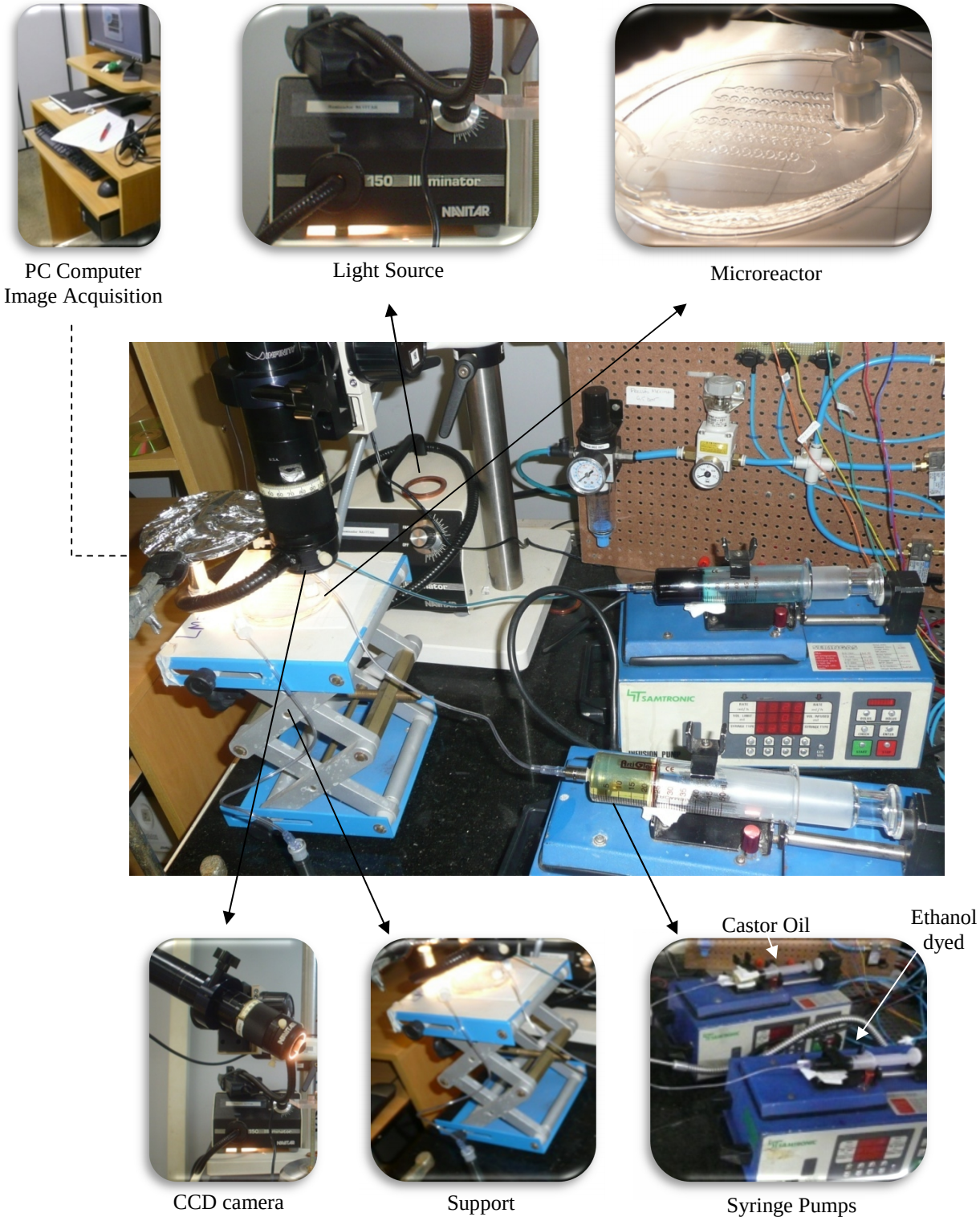

Figure 2. Experimental set-up for the monitoring the colorimetric variations. The digital camera was focused on the microstructure and recorded the microflow in the microchannel in real-time.

Table 1. Reynolds number and flow conditions for experimental tests

Volumetric rate castor oil (mL/h)	Molar Ratio	Volume ratio	Volumetric rate ethanol dyed (mL/h)	Residence time (s)	Reynolds number	
					Ethanol	Castor oil
1	9	0.54	0.5	900	0.183	7.71E-04
	12	0.72	0.7		0.256	
	17	1.03	1.0		0.365	
	25	1.51	1.5		0.548	
3	9	0.54	1.6	300	0.584	2.31E-03
	12	0.72	2.2		0.804	
	17	1.03	3.1		1.132	
	25	1.51	4.5		1.644	
7.5	9	0.54	4.1	120	1.498	5.78E-3
	12	0.72	5.4		1.973	
	17	1.03	7.7		2.813	
	25	1.51	11.3		4.128	

2.4 Numerical Simulation

The numerical three-dimensional simulation of the flow and mixing in the microreactors has been performed using ANSYS CFX 11.0 (of Ansys inc., EUROPE). This is a general purpose commercial CFD package that solves the Navier-Stokes equations using finite volume method via coupled solver which provides comprehensive modeling capabilities for a wide range of incompressible and compressible, laminar and turbulent fluid flow problems. In addition, it also provides reasonable solutions for the steady or transient states. The regime of microfluidic devices developed in this study was included in laminar region (Re<<2000), and fluids were considered incompressible liquids.

Mixture model involved in multiphase models of ANSYS CFX was used to obtain phase distribution and velocity profiles. The mixture model is suitable for simulating the transport of two liquids, and the phases are treated as interpenetrating continua. The mixture model solves the mixture momentum equation and sets relative velocities to describe the disperse phases. A mesh composed of tetrahedral, prismatic and pyramidal elements of 2,226,399 (428,607 nodes), 2,187,117 (423,302 nodes), and 2,006,539 (418,207 nodes) elements for Omega-, Tesla-, and T-shaped microreactors, respectively, were used. The meshs obtained for the different geometries of microreactors and used in the simulations are shown in Figure 3. The prismatic elements are located adjacent to the walls and ensure that the boundary layer is properly resolved. A preliminary grid convergence study was carried out in order to verify that the solution is grid-independent. Castor oil and ethanol at 25°C and 1 atm were used as the operating fluids. The boundary

condition at the system inlet was a uniform velocity profile with $v_x = 0.02$ m·s^{-1} and $v_y = v_z = 0$ m·s^{-1} for castor oil and ethanol fluids. This correspond to a laminar flow regime with a Reynolds number (Re) = 2. At the outlet, a constant pressure condition (P=0) was imposed and no-slip boundary conditions were applied at all walls. It should be noted that castor oil was modeled through previous physicochemical studies (Martínez, 2010), in order to characterize fluid properties. The ANSYS CFX 11.0 solver was used to solve the momentum and continuity equations in the steady state for the fluid flow in the micromixers. The advection terms in each equation were discretized using a bounded second-order differencing scheme. Simulations were typically considered converged when the normalized root mean square (RMS) residuals for the velocities fell below 1x10^{-4}.

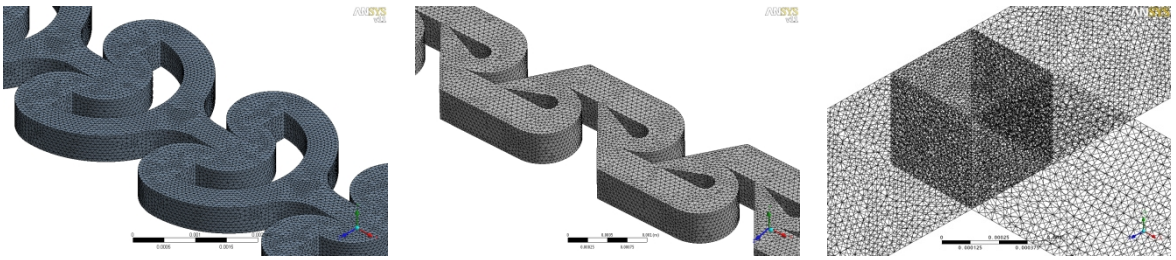

(a) (b) (c)

Figure 3. Geometry and mesh of the numerical model for: (a), Omega-shaped (b) Tesla-shaped and (c) T-shaped microreactors.

3. Results and Discussion

3.1 Liquid-liquid two-phase flow patterns in microreactors

The study of immiscible fluids flow and the formation process of flow patterns at the T-, Omega-, and Tesla-shaped microreactors were carried out. Shooting points were chosen elaborately to show the formation processes of flow pattern, and can be seen in Figures 4-5. In the microreactors tested, castor oil and ethanol system leads to a parallel flow with “sandwich” and “side by side” flow pattern for all volumetric flow rates studied.

Mixing has long been a significant area of research in chemical engineering, the pharmaceutical industry, bioengineering, food engineering, and polymer engineering, among others. If the mixing process is poor, the reaction process may be slowed down by local shortage of one of the reactants, uneven catalyst distribution, thermal nonuniformities, or ignition delays. The dominant effect of micromixing is molecular diffusion, where the mixing length is proportional to the mixing time and diffusion coefficient.

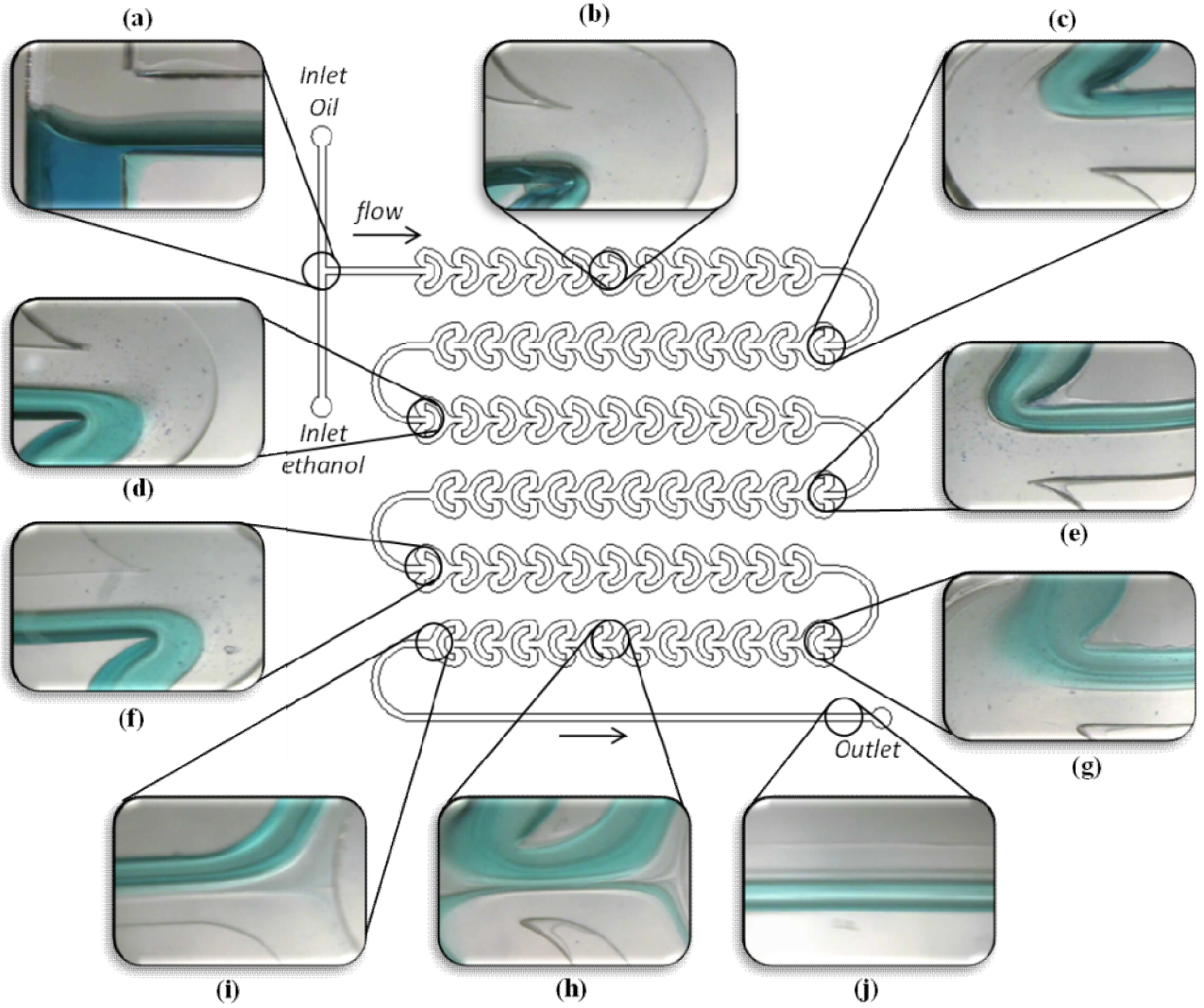

Figure 4. Flow pattern for the Omega-shaped microreactor at volumetric castor oil flow of 7.5 mL/h and volumetric ratio Ethanol/Oil of 1.51. Organic phase = castor oil. Aqueous phase = ethanol with solvatochromatic dye. (a) T-junction; (b) $2.2x10^4$ µm; (c) $4.6x10^4$ µm; (d) $8.5x10^4$ µm; (e) $1.2x10^5$ µm; (f) $1.6x10^5$ µm; (g) $2.0x10^5$ µm; (h) $2.2x10^5$ µm; (i) $2.3x10^5$ µm; (i) $2.7x10^5$ µm.

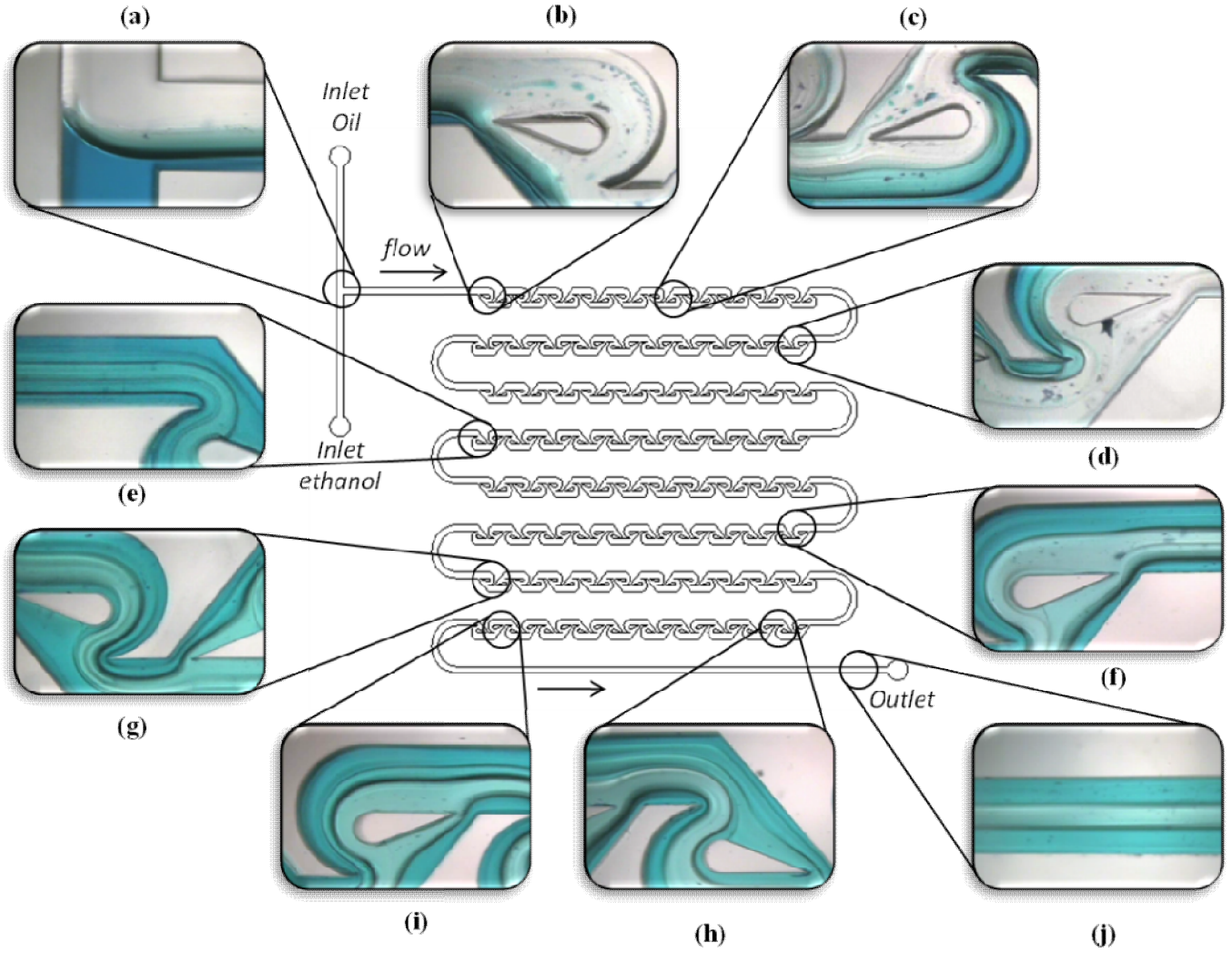

Figure 5. Flow pattern for the Tesla-shaped microreactor at volumetric castor oil flow of 7.5 mL/h and volumetric ratio Ethanol/Oil of 1.51. Organic phase = castor oil. Aqueous phase = ethanol with solvatochromatic dye. (a) T-junction; (b) $1.0x10^4$ µm; (c) $2.2x10^4$ µm; (d) $4.3x10^4$ µm; (e) $1.3x10^5$ µm; (f) $1.8x10^5$ µm; (g) $2.1x10^5$ µm; (h) $2.4x10^5$ µm; (i) $2.7x10^5$ µm; (i) $3.1x10^5$ µm.

In a microreactor, mixing in a straight microchannel is relatively poor. Therefore, it is important in designing a microreactor to create microchannels that lead to chaotic and turbulent flow, which rapidly increase the mixing efficiency. The mixing in T-shaped microreactor was first studied. In this configuration two inlets channels merge into a common mixing channel where mixing of the two co-flowing fluid streams occurs. A simple mixing mechanism via diffusion between co-flowing fluid "side by side" was observed. Obviously, complex convection-dominated mixing mechanisms (for example driven by swirls or recirculating flows) are absent in the T-mixer for the range of Reynolds numbers studied.

The performance of T-microreactor is usually not sufficient for liquid-mixing applications, since corresponding diffusion constants are of the order of 10^{-9} m^2/s or smaller and longer mixing times are required. As described above, mixing in straight channels occurs mainly by diffusion between co-flowing streams with a characteristic time contact of $\tau_d=l^2/D$ where τ_d is the molecular diffusion time, l is the characteristic scale and D is the diffusion coefficient. A reduction of the mixing time scale can be achieved if diffusion is superposed by convective transport.

In this context, it was believed that a chaotic flow has a great potential for speeding up mixing. Chaotic advection is synonymous with complex flow patterns in which extreme stretching and back-folding of fluid volumes occurs. In order to improve the mixing performance, an Omega-shaped microreactor consisting of a series of omega structures was fabricated. The Omega configuration produces flow obstacles that lead to high velocities. The obstacles formed by the omega channel force the flow to commingle back and forth between the center and the channel wall. The velocity of flow in the omega channel varies significantly from point to point and its variance is large, which improves the interfacial mass transfer (Yu *et al.*, 2008).

In the Omega-shaped microreactor, the channel shape and structure lead to changes in flow direction that cause non uniform flow velocities and generate vortices in the flow. Each omega channel has a curve that impedes the oncoming flow and separates it into two streams, which converge with other flows in adjacent omega channels. In addition, this flow behavior within the channel is created without moving parts or external sources.

Omega channels generate higher vorticity than that of the straight T-shaped microreactor. Vortices are known to enhance mixing, where straight channel of T-shaped microreactor do not have such an advantage. In the omega channel, the streamlines of the fluid flowing through the channel show back flow and some rotational movement at intermediate Reynolds numbers (Yu *et al.*, 2008). This flow characteristic does not exist in straight channels. Besides, the back flow can enhance mixing and increase the residence time. This flow phenomenon, along with an increased chance of contact between fluids, can lead to an increase in the conversion rate of a chemical reaction. However, as shown in Figure 4, complete mixing of ethanol/oil system was not achieve at low Reynolds number used in this study, such as 1.0 to 7.5 mL/h and 0.5 to 11.3 mL/ h for castor oil and ethanol dyed, respectively.

On the other hand, in the Tesla-shaped micromixer the fluids are first bi-laminated in a T-type configuration and then pass a so-called Tesla structure which comprises angled surfaces (Hong *et al.*, 2004). By flowing along the latter, splitting and redirection of the flow are achieved, which leads to a kind of collision. While one stream passes the major angled passage, the neighboring stream approaches both this major passage and a smaller secondary passage, set in a Y-type flow configuration. This stream splits into two sub-streams according to the different pressure losses of both passages. The flow of both passages is so oriented that collision results. Thus, a larger stream with predominantly one fluid collides with a smaller stream of the pure other liquid. Mixing is said to take place by turbulence.

The Tesla structure is repeated many times in a row so that a sequential mixing is achieved (Figure 5). Results show that the largest contribution to the mixing process is exerted by the Tesla structure and not by diffusion owing to the lamination beforehand. A colorimetric experiment with solvatochromatic dye reveals the formation of a central mixed zone in the initial units, as evident from Figure 5(b)-(d). Further, downstream the degree of mixing is further increased (Figure 5(e)-(j)), where a mixing mechanism via “sandwich” flow pattern was observed.

3.2 Mixing measurements

For experimental mixing measurement, the intensity of the solvatochromatic dye solution was associated as proportional to the concentration of the dye molecules. Thus, the

concentration field can be measured indirectly as the intensity field of solvatochromatic dye. In this procedure, after recording the images acquired with a CCD camera on the PC, the concentrations profiles were evaluated using a customized program written in MATLAB using the functions available in the Image Processing Toolbox (Gonzalez *et al.*, 2004). Figures 4 and 5 show digital images of a solvatochromatic dye taken in several points along of the microreactors. First, the program removes the noise in the measured image with an adaptive noise-removal filter. For each pixel, a local mean value is calculated for a window of 5 x 5 pixels. The noise distribution is assumed to be the Gaussian distribution. Subsequently, a path with a known position across the channel is evaluated.

The position across the channel is normalized against the channel width $x^*=x/W$, while the measured pixel intensity I is normalized against the maximum I_{max} and minimum I_{min} of the intensity at the inlet:

$$I^* = \frac{I - I_{min}}{I_{max} - I_{min}} \quad (1)$$

The measured dimensionless intensity is assumed to be equal to the dimensionless concentration of the solvatochromatic dye ($I^*=c^*$). Furthermore, because good mixing is understood as the homogeneity of mixing results, the distribution of the intensity values of the histogram $H(I)$ of an image can be used for evaluating the degree of mixing. The gray scale histogram represents the probability distribution function (PDF) of the concentration, which can be obtained by normalizing the pixel number of each intensity value by the total number of the pixels in the evaluated region:

$$P(c^*) = P(I^*) = P(I) = \frac{N(I)}{\sum_{I_{min}}^{I_{max}} N(I)} \quad (2)$$

Figure 6-8 shows the distribution of concentration and probability distribution function (PDF) of the concentration across the mixing channel at different lengths for T-, Omega-, and Tesla-shaped microreactors, respectively. The larger surface-to-volume ratios of microfluidic devices render surface effects increasingly important, particularly when free surfaces of two immiscible fluids are present (Squires and Quake, 2005). It has been confirmed that liquid-liquid two-phase flow structures in microchannel are more seriously affected by the wettability between the channel wall and the fluids. Depending of the microchannel design, input volume fraction, Reynolds number and the dimensions of the

microchannel, different liquid-liquid flow regimes are encountered. In our experiments, the castor oil has smaller contact angle than the ethanol phase in the PDMS microchannel, therefore, the dispersed flow regimes that includes slug flow, monodispersed droplets flow, and droplets populations flow are difficult to form. Indeed, we only can identify three flow patterns form our experiments (Figures 4-5), the parallel flow with smooth interface, the parallel flow with wavy interface, and the chaotic thin striations flow, as shown in Figure 6-8. These flow patterns were also observed by Zhao *et al.* (2007), where the mass transfer characteristics of immiscible fluids in the T-junction microchannels was investigated. As can be seen from Figure 7-9, contact area between the immiscible phases in the Tesla-shaped microreactor is larger than that in the Omega- and T-shaped microreactor.

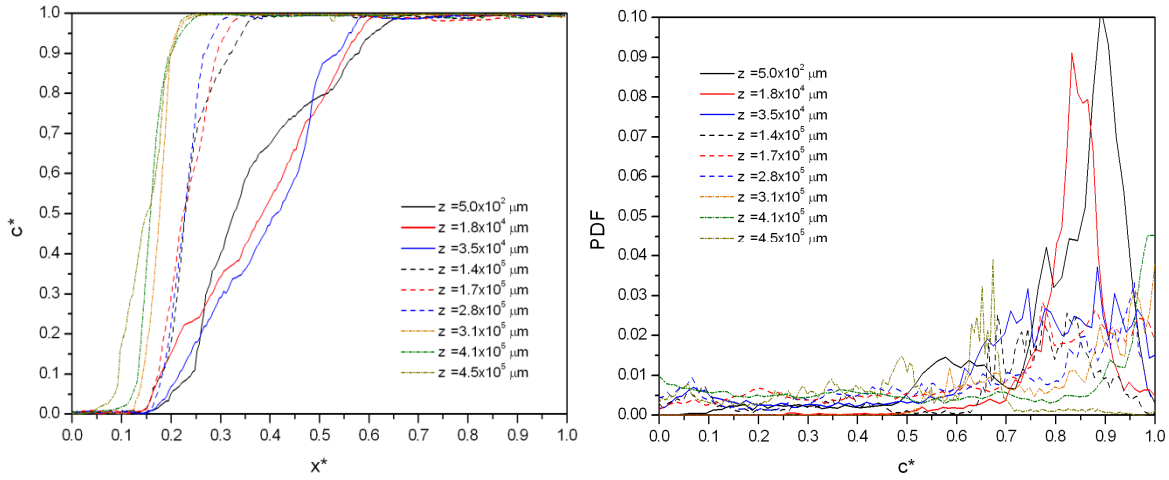

Figure 6. Distribution of concentration and probability distribution function (PDF) of the concentration across the mixing channel of the T-shaped microreactor.

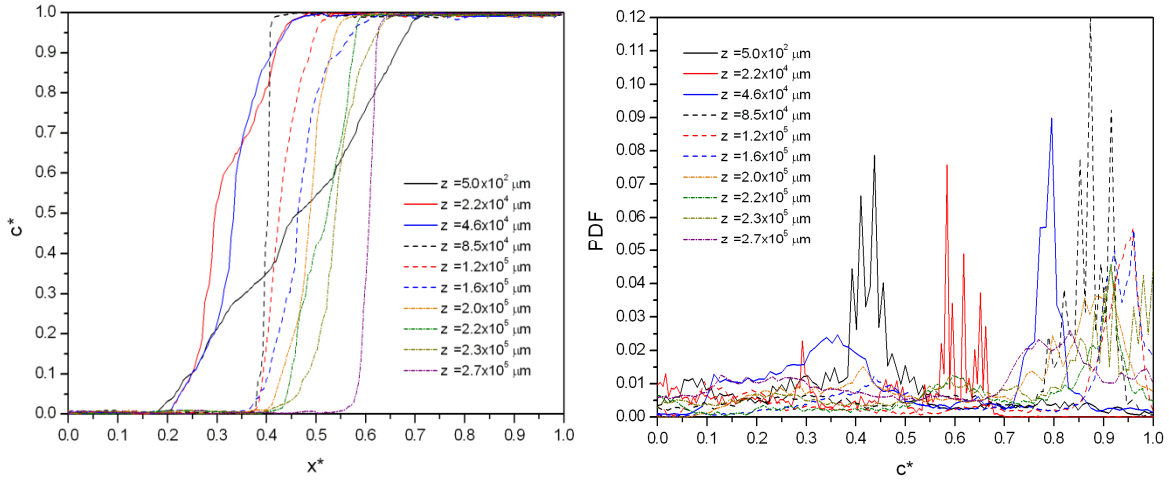

Figure 7. Distribution of concentration and probability distribution function (PDF) of the concentration across the mixing channel of the Omega-shaped microreactor.

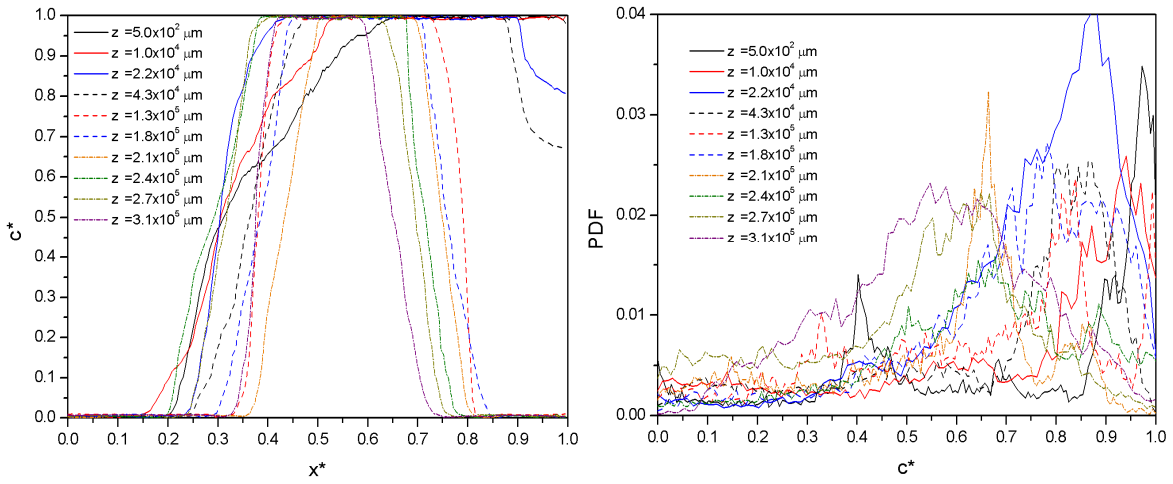

Figure 8. Distribution of concentration and probability distribution function (PDF) of the concentration across the mixing channel of the Tesla-shaped microreactor.

3.3 Effect of geometry

The three designs proposed were compared for their mixing performance. An analysis of flow patterns at volumetric castor oil flow of 7.5 mL/h and volumetric ratio Ethanol/Oil of 1.51 by colorimetric experiment clearly reveals a better mixing with Tesla structure, whereas all two other designs do not give any visual hint of mixing.

Previous work by Zhao *et al.* (2006) with similarly investigated range of Reynolds numbers only three flow patterns can be observed. At low and medium *Re* numbers, the parallel flow with smooth interface and the parallel flow with wavy interface can be observed, with either streams flow “side by side” or “sandwich” through the mixing channel (Figure 4-5). The disturbance in the interface of the two phases results in a subtle increase in the interfacial mass transfer area between the two immiscible phases per unit volume of the microchannel system in a way. As mentioned previously, in the Omega- and T-shaped microreactors “side by side” flow pattern was observed at low Reynols numbers, thererefore the main mass transfer principle is still diffusion in the interface of the two phases in these flow pattern. However, the chaotic thin striations flow pattern which is more efficient for the laminar mixing was induced at the Tesla-shaped microreactor by the impinging of the flow immiscible fluids and centrifugal forces. The interfacial area between two immiscible fluids stretches, deforms, and folds, as well as the surface renewal velocity is enhanced, making the interphase mass transfer more effective, which significantly intensifies mass transfer process and increases the overall volumetric mean mass transfer coefficient. Thus, convection effects and the enlargement of the interfacial area are between

the two phases play the dominant role on mass transfer in this geometry, thus obtaining a "sandwich" flow pattern at the end of the mixing channel.

3.4 Effect of the volumetric flux ratio based on dimensionless numbers

According to Zhao *et al.* (2006), surface effects become dominant due to the small size of microsystem devices. In fact, interfacial tension and inertial force are competing stresses that could distort the interface in these particular devices. The interfacial tension tends to reduce the interfacial area, while inertia force is inclined to extend and drag the interface downstream.

Within the range of flow rates used in this work our experiments suggest that interfacial tension dominates compared to inertial force analyzing the parallel flow. In the T- and Omega-shaped microreactor was seen that the castor oil and ethanol system leads to a parallel "side by side" flow for all volumetric flow rates. On the other hand, the Tesla-shaped leads to a parallel "sandwish" flow. The fluids properties used during the present work are summarized in the Table 2.

Table 2. Physical Properties of Castor oil and Ethanol (at 293K and atmospheric pressure)

Fluid	Density	Viscosity	Interfacial Tension
	ρ [kg/m^3]	μ [Pa·s]	σ [kg/s^2]
Castor Oil	957.3	0.689	0.0345
Ethanol	789	0.0012	0.0223

In order to define quantitatively the influence of the linear velocity on the flow patterns, the Capillary, Weber and the Reynolds numbers were calculated for all the experiments (Table 3). These numbers were calculated for each phase and the mean between the two phases was considered. Mean dimensionless numbers were used to take in consideration the influence of the properties and velocities of both phases on flow patterns.

Table 3. Dimensionless numbers

Reynolds number	$\frac{Inertial\ forces}{Viscous\ forces}$	$Re = \frac{\rho \cdot u \cdot d_H}{\mu}$
Weber number	$\frac{Inertial\ forces}{Liquid - liquid\ surface\ tension}$	$We = \frac{u^2 \cdot d_H \cdot \rho}{\sigma}$
Capillary number	$\frac{Viscous\ forces}{Liquid - liquid\ surface\ tension}$	$Ca = \frac{\mu \cdot u}{\sigma}$

As can be seen in the Table 4, an increase of linear velocity leads to an increase on the inertial forces and produces change from the parallel flow with smooth interface turns to the parallel flow with wavy inrterface on Omega-shaped microreactor, where vortices are formed at the interface of the two phases. For the T-shaped microreactor, vortices can be formed at the interface of the two phases in the T-junction with increase of linear velocity, but the energy of these vortices can be consumed in the downstream, and eventually results in vanishing of the these vortices. Therefore, the interface of two phases at the T-junction can be wavy, but it eventually evolves into a smooth interface in the fully developed flow. In the Tesla-shaped microreactor the stream of the castor oil flows between streams of the ethanol and is geometrically focused into a narrow jet in the center of the microchannel. The chaotic thin striations flow is formed due to the Tesla geometry, which this flow evolves eventually to parallel "sandwish" flow at the downstream. So, the observed flow patterns can be explained by competition between the main forces due to interfacial tension and viscosity. On the other hand, comparing two graphs in Figure 6-8, it can be seen that stability domains of flow patterns depend on the geometry of the microreactor.

In this context, at low *Re* numbers, the volumetric flux ratio is found to have a weak effect on the overall volumetric mass transfer coefficient. This is mainly due to the low interfacial mass transfer area formed at the T-shaped microreactor by the parallel flow with smooth interface. However, the intensity of disturbance in the interface of two-phase fluids at the Omega-shaped microreactor or the chaotic thin striations flow at the Tesla-shaped microreactor is more dramatically increased and as a consequence the interfacial mass transfer area and the surface renewal velocity are enlarged, which enhance mass transfer performance.

Table 4. Reynolds number and flow conditions for experimental tests

Volumetric rate (mL/h)		Dimensionaless numbers		
castor oil	ethanol dyed	Re_{mean}	We_{mean}	Ca_{mean}
1	0.5	0.0917	1.129E-05	0.0111
	0.7	0.1282	1.391E-05	0.0111
	1.0	0.1830	1.948E-05	0.0111
	1.5	0.2743	3.313E-05	0.0112
3	1.6	0.2934	1.050E-04	0.0334
	2.2	0.4030	1.299E-04	0.0334
	3.1	0.5673	1.820E-04	0.0334
	4.5	0.8230	2.982E-04	0.0335
7.5	4.1	0.7517	6.653E-04	0.0834
	5.4	0.9891	8.002E-04	0.0835
	7.7	1.4092	1.129E-03	0.0835
	11.3	2.0667	1.876E-03	0.0836

3.6. CFD Simulations

The three-dimensional simulation with ANSYS CFX provided the mixing tendencies of the different geometries, as shown in Figure 9. Using the contours and stream lines, the degrees of mixing of micro-flows could be estimated from their shapes. In the case of the T-shaped microreactor, the ethanol/oil phases flowed parallel. Because of its simple geometry, there was no mixing and the solutions just straightly flowed parallel with the microreactor. On the other hand, in the other two microreactors, Tesla- and Omega-shaped microreactors more effective dispersion was simulated than in the T-shaped microreactor. The three types of mixers had different dispersion tendencies in their contours and are shown in Figure 9. The driving force of mixing in the Tesla and Omega type was based on the variations of the flow direction, as shown path lines in Figure 9(a) and 9(c). The no slip boundary condition influenced the direction and velocity of flow near the surfaces.

For T-shaped microreactor simulation, the flow was laminar with straight streamlines. In Figure 9(f) can be seen vortices produced at the T-junction of the mixing channel. This vortex is due that portion of the entrance castor oil (with larger viscosity) going to the opposite side of the T-junction (Figure 9(e)) collides with ethanol flow (with smaller viscosity) on the opposite side, forming a vortex (Figure 9(f)). However, these vortices are damped by viscous forces and the flow become laminar again downstream, which mass transfer between the two fluids is controlled by diffusion.

Among the various microreactors, the Omega- and Tesla-shaped microreactors were expected to have the best mixing performance that the T-shaped microreactor in the simulations. The Omega configuration produces flow obstacles that lead to high velocities as show in the Figure 9(b), the streamlines of the fluid flowing through the channel show back flow and some rotational movement at intermediate Reynolds numbers. The obstacles formed by the Omega channel force the flow to come back and forth between the center and the channel wall. The velocity of flow in the Omega channel varies significantly from point to point and its variance is large, which improves the interfacial mass transfer.

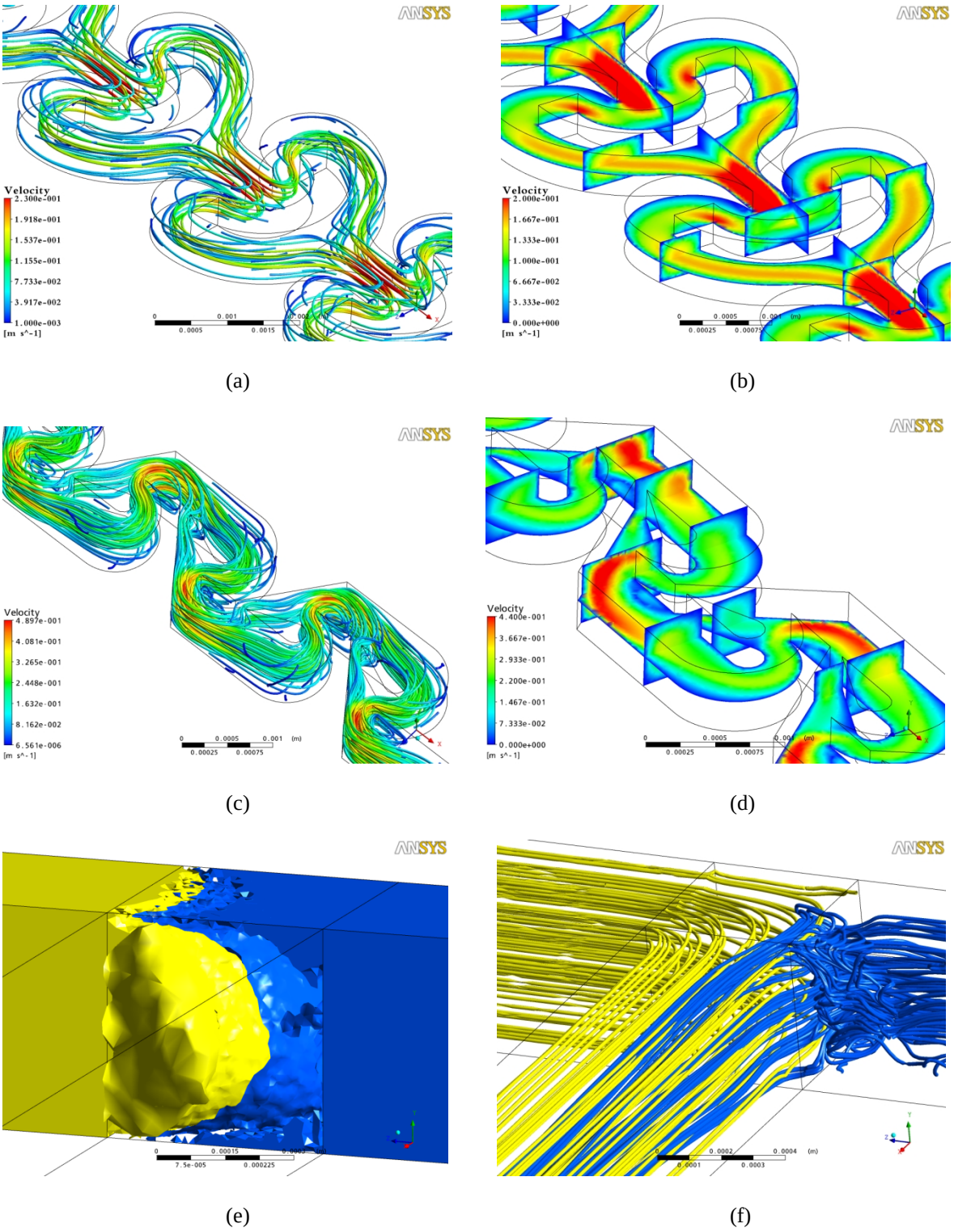

Figure 9. Numerical simulation of the fluid flow and mixing in microreactors with different geometries; Omega-shaped microreactor: (a) stream lines in the channel, (b) velocity profiles developed in the channel; Tesla-shaped microreactor: (c) stream lines in the channel (d) velocity profiles developed in the channel; T-shaped microreactor: (e) distribution of phases in the T-junction, (f) stream lines in the channel.

On the other hand, in the Tesla-shaped microreactor it can be seen that the fluid is splitting and one stream passes the major angled passage, while the neighboring stream approaches both this major passage and a smaller secondary passage splitting into two sub-streams according to the different pressure losses of both passages. The flow of both passages is so oriented that collision results (Figure 9(c)). Thus, a larger stream with predominantly one fluid collides with a smaller stream of the pure other liquid. The small vortices are characterized by a strong stretching and folding of the fluidic elements and are therefore the key regions for the mixing enhancement.

4. Conclusions

Three types of micromixers were fabricated by conventional soft-lithography. The micromixers with the different geometries for continuous and simultaneous splitting and recombination of fluids proceeds in each mixing element were evaluated. Flow patterns and the process of formation mechanism of the dispersed phase with oil-ethanol in different geometric microreactor were studied by simulation and experimentally procedures. Distinct flow patterns could be identified at the structures in the microreactors: parallel flows that have smooth interface at the T-shaped microreactor, parallel flows that have wavy interface at the Omega-shaped microreactor, and chaotic thin striations flow formed with “sandwich” patter flow in the Tesla-shaped microreactor.

Visualization test showed the improvement mixing mechanism in the microreactor with more complex geometry channel and with increase of Reynolds number, which was mainly determined by shear forces and chaotic flows. In other hand, the CFD simulation results showed good agreement of the mixing tendencies observed in the experiments with castor oil and ethanol dyed with solvatometric dye. The colorimetric observations of the mixing effects with the devices was very simple, economic and time saving, because it demanded just a few hundred micro-liters of inputs solutions, without the need for any fluorescent equipment.

The results obtained are important for the design of microreactors to carry out transesterification reaction between vegetable oil and ethanol aiming on process intensification.

Acknowledgements

The author gratefully acknowledges the financial support provided by The Scientific Research Foundation for the State of São Paulo (FAPESP) and research support by The Brazilian Synchrotron Light Laboratory (LNLS).

Bibliography

Aubin, J.; Fletcher, D. F.; Bertrand, J.; Xuereb, C. Characterization of the mixing quality in micromixers. Chemical Engineering & Technology, 26 (2003), 1262-1270.

Beebe, D. J.; Adrian, R. J.; Olsen, M. G.; Stremler, M. A.; Aref, H.; Jo, B. H. Passive mixing in microchannels: fabrication and flow experiments, Mecanique & Industries, 2 (2001), 343-348.

Ehrfeld, W.; Golbig, K.; Hessel, V.; Lowe, H.; Richter, T. Characterization of mixing in micromixers by test reaction: single mixing units and mixers arrays, Industrial and Engineering Chemistry Research, 38 (1999), 1075-1082.

Ehrfeld, W.; Hessel, V.; Löwe, H. Microreactors: New Technology for Modern Chemistry, Wiley-VCH, Weinheim, 2000.

El Moctar, A. O.; Aubry, N.; Batton, J. Electro-hydrodynamic micro-fluidic mixer, Lab on Chip, 3 (2003), 273-280.

Fredrickson, C. K.; Fan, Z. H. Macro-to-micro interfaces for microfluidic devices, Lab on a Chip, 4 (2004), 526-533.

Glasgow, A.; Aubry, N. Enhancement of microfluidic mixing using time pulsing, Lab on Chip, 3 (2003), 114-120.

Gonzalez, R. C.; Woods, R. E.; Eddins, S. L. Digital Image Processing using MATLAB, Pearson Prentice Hall, Upper Saddle River, New Jersey, 2004.

Hardt, S.; Schönfeld, F. Laminar mixing in different interdigital micromixers. II. Numerical simulations, American Institute of Chemical Engineers Journal, 49 (2003), 578-584.

Hardt, S.; Drese, K. S.; Hessel, V.; Schönfeld, F. Passive micromixers for applications in the microreactor and μTAS fields, Microfluidics and Nanofluidics, 1 (2005), 108-118.

Hessel, V.; Löwe, H. Microchemical Engineering: Components, Plants Concepts, User Acceptance – Part 1, Chemical Engineering and Technology, 26 (2003a), 13-24.

Hessel, V.; Löwe, H. Microchemical Engineering: Components, Plants Concepts, User Acceptance – Part 2, Chemical Engineering and Technology, 26 (2003b), 391-408.

Hessel, V.; Löwe, H. Microchemical Engineering: Components, Plants Concepts, User Acceptance – Part 3, Chemical Engineering and Technology, 26 (2003c), 531-544.

Hessel, V.; Hardt, S.; Löwe, H.; Schönfeld, F. Laminar mixing in different interdigital micromixers. I. Experimental characterization, American Institute of Chemical Engineers Journal, 49 (2003d), 566-577.

Hessel, V.; Löwe, H.; Schönfeld, F. Micromixers – a review on passive and active mixing principes, Chemical Engineering Science, 60 (2005), 2479-2501.

Hong, C.-C.; Choi, J.-W.; Ahn, C. H. A novel in-plane passive microfluidic mixer with modified Tesla structures, Lab on Chip, 4 (2004), 109-113.

Jeona, W.; Shin, C. H. Design and Simulation of Passive Mixing in Microfluidic Systems with Geometric Variations, Chemical Engineering Journal, 152 (2009), 575-582.

Jo, B. H.; Van Leberghe, L. M.; Motsegood K. M.; Beebe, D. J. Three-Dimensional Micro-Channel Fabrication in Polydimethylsiloxane (PDMS) Elastomer, Journal of Microelectromechanical Systems, 9 (2000), 76-81.

Kashid, M. N.; Gerlach, I.; Goetz, S.; Franzke, J.; Acker, J. F.; Platte, F.; Agar, D. W.; Turek, S. Internal circulation within the liquid slugs of a liquid-liquid slug-flow capillary microreactor, Industrial and Engineering Chemistry Research, 44 (2005), 5003-5010.

Kockmann, N.; Kiefer, T.; Engler, M.; Woias, P. Convective mixing and chemical reactions in microchannels with high flow rates, Sensors and Actuators B: Chemical, 117 (2006), 495-508.

Kuswandi, B.; Nuriman, Huskens, J.; Verboom, W. Optical sensing systems for microfluidic devices: a review, Analytical Chimica Acta, 601 (2007), 141-155.

Liu, R. H.; Yang, J.; Pindera, M. Z., Athavale, M.; Grodzinski, P. Bubble-induced acoustic micromixing, Lab on Chip, 2 (2002), 151-157.

Löwe, H.; Hessel, V.; Muller, A. Microreactors, prospects already achieved and possible misuse, Pure Applied Chemistry, 74 (2002), 2271-2276.

Martínez, E. L. Development and Assessment of Microreactors Applied to Biodiesel Production, University of Campinas, M.Sc. Thesis, Campinas, São Paulo, Brazil, 2010.

Martínez, E. L. Desenvolvimento e Avaliação de Microreatores: Aplicação para Produção de Biodiesel, University of Campinas, M.Sc. Thesis, Campinas, São Paulo, 2010.

Nauman, E. B. Residence Time Distributions. In: Paul, E. L.; Atiemo-Obeng. V. A., Kresta, S. M. (Eds.). Handbook of Industrial Mixing, Science and Practice, Wiley, New York, 2004, 1-17.

Nguyen, N. T.; Wu, Z. Micromixers - a review, Journal of Micromechanics and Microengineering, 15 (2005), R1-R16.

Panić, S.; Loebbecke, S.; Tuercke, T.; Antes, J.; Bošković, D. Experimental approaches to a better understanding of mixing performance of microfluidic devices, Chemical Engineering Journal, 101 (2004), 409-419.

Schwesinger, N.; Frank, T.; Wurmus, H. A modular microfluid system with an integrated micromixer, Journal of Micromechanics and Microengineering, 6 (1996), 99-102.

Sinton, D. Microscale flow visualization, Microfluidic and Nanofluidic, 1 (2004), 2-21.

Soleymani, A.; Kolehmainen, E.; Turunen, I. Numerical and experimental investigations of liquid mixing in T-type micromixers, Chemical Engineering Journal, 1355 (2008), S219-S228.

Squires, T. M.; Quake S. R. Microfluidic: fluid physics at the nanoliter scale, Reviews of Modern Physics, 77 (2005), 977-1026.

Stroock, A. D.; Dertinger, S. K.; Ajdari, A.; Mezic, I.; Stone, H. A.; Whitesides, G. M. Chaotic mixer for microchannels, Science, 295 (2002), 647-651.

Sudarsan, A. P.; Ugaz, V. M. Multivortex micromixing, PNAS, 103 (2006), 7228-7233.

Trachsel, F.; Gunther, A.; Khan, S.; Jensen, K. F. Measurement of residence time distribution in microfluidic systems, Chemical Engineering Science, 60 (2005), 5729-5737.

Yang, Z.; Goto, H.; Matsumoto, M.; Maeda, R. Ultrasonic micromixer for microfluidic systems, Sensor and Actuators A: Physical, 93 (2001), 266-272.

Yu, L.; Nassar, R.; Fang, J.; Kuila, D.; Varahramyan, K. Investigation of a Novel Microreactor for Enhancing Mixing and Conversion, Chemical Engineering Communication, 195 (2008), 745-757.

West, J.; Karamata, B.; Lillis, B.; Gleeson, J. P.; Alderman, J.; Collins, J. K.; Lane, W.; Mathewson, A.; Berney, H. Application of manetohydrodynamic actuation to continuous flow chemistry, Lab on Chip, 2 (2002), 224-230.

Zhao, Y. C.; Chen, G. W.; Yuan, Q. Liquid-liquid two-phase flow patterns in a rectangular microchannel, AIChE Journal, 52 (2006), 4052-4060.

7.3. Conclusões

Neste capítulo os micro-misturadores fabricados utilizando o processo de litografia macia, descrito no capítulo anterior, foram avaliados na sua eficiência para a mistura do sistema óleo de mamona - etanol. Para a análise dos padrões de fluxo e o mecanismo de formação da fase dispersa nas diferentes geométricas foram usados procedimentos experimentais e simulação fluidodinâmica CFD.

A partir dos resultados obtidos puderam-se identificar vários padrões de fluxo tais como: fluxo paralelo com interface suave no microreator em T, fluxo paralelo com interface ondulado no microreator Omega e fluxo caótico no final do canal no microreator Tesla.

Os testes de visualização mostraram uma melhoria no mecanismo de mistura nos micro-reatores com geometrias mais complexas e com o aumento do número de Reynolds, causado principalmente pelas forças de cisalhamento e fluxos caóticos dentro dos micro-dispositivos. As simulações CFD mostraram uma boa concordância com as tendências da mistura obtidas nos experimentos com o óleo de mamona e etanol com corante.

As observações colorimétricas realizadas permitiram identificar os padrões de fluxo da mistura do óleo/etanol com dispositivos simples, econômicos e de forma rápida, já que exigiu só alguns micro-litros de solução, sem necessidade de qualquer equipamento fluorescente convencionalmente usado neste tipo de análises.

Os resultados obtidos são importantes para a concepção de micro-reatores com geometrias ótimas para a realização da reação de transesterificação entre óleo vegetal e etanol visando à intensificação do processo.

Capítulo 8.

Síntese Contínua de Biodiesel Usando Microreatores com Diferentes Geometrias

8.1. Introdução

A intensificação de processos utilizando microtecnologia apresenta um conceito inovador na geração de produtos e especialidades químicas, principalmente para produtos farmacêuticos, alimentícios e cosméticos, pois utiliza no processo produtivo uma nova geração de equipamentos e suas respectivas técnicas de fabricação, como mencionado no Capítulo 2 e 6. Nesse novo conceito, os processos utilizam sistemas modulares de reação e de processos de separação, composto de sistemas modulares seqüenciais de equipamentos miniaturizados, instalados num grande conjunto de pequenos sistemas de produção operando em paralelo.

Por outra parte, a miniaturização de processos permite obter uma série de vantagens sobre os processos convencionais, tais como:

- Os processos miniaturizados viabilizam a mudança de processamento em batelada para processamento contínuo, tendo como resultado melhor aproveitamento de insumos e redução de custos de produção.
- O escalonamento do processo (*scale-up*) é muito mais fácil e rápido que nos processos convencionais, pois, além de evitar a etapa de testes em escala piloto, o escalonamento é feito pelo aumento de unidades produtivas básicas.
- A miniaturização de reatores químicos oferece o controle do ambiente de reação de forma muito precisa, permitindo produção contínua com melhores características, tais como: aumento do controle do processo e conseqüente redução de subprodutos de reação; melhor aproveitamento dos insumos; redução de aditivos; aumento da pureza do produto; redução de custos de separação e diminuição de perdas de energia e de efluentes de processo.

- A intensificação de processos pela miniaturização possibilita a criação de produtos que não podem ser fabricados de forma segura ou controlada de outras maneiras, devido a taxas de reação muito elevadas, reações altamente exotérmicas ou reagentes perigosos. Por conta do tamanho dos reatores, é possível trabalhar em condições mais controladas.
- Os processos miniaturizados apresentam características mais seguras, como redução do volume total de material potencialmente perigoso e controle mais preciso de reações muito rápidas ou perigosas.
- Muitas das aplicações de intensificação de processos oferecem oportunidades para economia de energia e benefícios ambientais, especialmente em termos de desenvolvimento sustentável.
- A fabricação dos sistemas miniaturizados permite o uso de materiais esterilizáveis, diminuindo o risco de contaminação.
- Devido ao seu caráter modular, a manutenção pode ser realizada pela substituição do módulo com problema, sem a necessidade de parar os demais módulos; ou seja, os custos de manutenção e as perdas por paradas forçadas são diminuídos com esta abordagem.
- Devido a sua abordagem modular, estes sistemas apresentam uma redução substancial do capital investido em edificações, estruturas de suporte de equipamentos, montagem e instrumentação, o que pode reduzir os custos de apólices de seguro, já que muitos dos sistemas são intrinsecamente seguros.
- Permite a integração de sensores, atuadores e eletrônica para realizar funções de controle do processo, diminuindo o custo da instrumentação global do sistema de produção.

Recentemente, um grande interesse na aplicação dos sistemas de microreação na produção contínua de biodiesel tem aumentado. Estes estudos mostram a tecnologia de microreação como um caminho promissor para a produção altamente eficiente de biodiesel já que teores de biodiesel superiores a 90% com um tempo de residência de só uns poucos minutos têm sido reportados. No entanto, na maioria desses estudos, a produção de biodiesel tem sido limitada na utilização de tubos capilares como reatores. Contudo, é bem conhecido que as geometrias internas dentro microreatores têm grande impacto na massa e transferência de calor.

Neste capítulo, microreatores com diferentes geometrias foram desenvolvidos a fim de melhorar a eficiência da síntese de biodiesel na presença de NaOH como catalisador. O efeito da geometria, concentração de catalisador, temperatura de reação, razão molar etanol/óleo e tempo de residência no rendimento da reação foram analisados. A diferença no desempenho entre o microreactor e dados obtidos no Capítulo 4 para o reator em batelada é também discutido em detalhe.

8.2. Desenvolvimento

O desenvolvimento deste capítulo é apresentado a seguir, no manuscrito intitulado: *Continuous Synthesis of Biodiesel Using Microreactors with Different Geometries.*

Continuous Synthesis of Biodiesel Using Microreactors with Different Geometries

Abstract

In this work, microreactors with different geometries, called Tesla-, Omega-, and T-shaped microreactors, has been fabricated and used for continuous production of biodiesel from castor oil and ethanol with NaOH as catalyst reaction. The influences of the main geometric parameters on the performance of the microchannel reactors were experimentally studied. It has been found that the oil conversion was influenced by catalyst loading, ethanol/castor oil molar ratio, residence time and temperature. It has been also found that the Tesla-shaped microreactor produces higher contact area than the Omega- and T-shaped microreactor which results in higher efficiency of biodiesel synthesis. Transesterification data by a conventional method, lab-scale batch reactor, were used for comparison with that in the microreactor. The time necessary for high ethyl ester conversion of 98.9% was achieved at the residence time of only 10 min by using the Tesla-shaped microreactor, which generates less energy composition for the same amount of biodiesel produced during lab-scale biodiesel synthesis. In these intensified systems, high conversions were achieved with the ethyl esters yield of 93.5%, 95.3%, and 96.7 % for Tesla-, Omega-, and T-shaped microreactors, respectively, using a catalyst loading of 1.0 wt.% NaOH and a reaction temperature of 50°C in a residence time of only 10 min. The results indicate that microreactors can be used as mini-fuel processing plant for distributive application.

Keywords: Biodiesel; Intensification; Microreactors; Transesterification; Mixing

1. Introduction

Concerns about petroleum supplies due the increasing demand and decreasing reserves, environmental pollution, high energy prices, energy and environment security, are drawing considerable attention to find environmentally friendly and renewable biofuels as alternative energy source. Biodiesel, a mixture of fatty acid alkyl esters derived from animal fats or vegetable oils, is rapidly moving towards the mainstream in the fuel field as an alternative. The most common way to produce biodiesel is transesterification which refers to a chemical reaction between a vegetable oil and an alcohol over a catalyst to yield fatty acid alkyl esters (biodiesel) and glycerol (Al-Zuhair, 2007). Triacylglycerol

(triglycerides), as the main component of vegetable oil and animal fat, consists of fatty acids with three long chains esterified to a glycerol back bone. When triacylglycerol reacts with an alcohol, three fatty acid chains are released from the glycerol skeleton and combine with the alcohol to yield fatty acid alkyl esters. Glycerol is produced as a by-product. Several aspects, including the type of catalyst, alcohol/vegetable oil molar ratio, temperature, water content and free fatty acid content have an influence on the course of transesterification. Alcohols like methanol and ethanol are the most commonly used alcohol because of their low cost (Sarma *et al.*, 2008). Although production ethyl esters rather than methyl esters is of considerable interest because it allows production of biodiesel from entirely renewable sources. Biodiesel can be done by non-catalyst (Warabi *et al.*, 2004 Demirbas, 2002; Kusdiana and Saka, 2001) and lipase catalyst (Marchetti *et al.*, 2007; Akoh *et al.*, 2007; Sanchez and Vasudevan, 2006; Al-Zuhair *et al.*, 2006) but to date, transesterification reactions are conventionally produced through base-catalyst and acid-catalyst (Peña *et al.*, 2009; Meneghetti *et al.*, 2006; Lotero *et al.*, 2005, Canakci and Van Gerpen, 2001).

The transesterification reaction is a typical two-phase reaction due to the immiscibility of oil and methanol. The rate of transesterification is primarily controlled by the rate of mass transfer between the alcohol and oil phases due to the immiscible of the two-phases (Guan *et al.*, 2009a). Stirred batch reactors are used commercially for biodiesel production however the development of continuous processes that will reduce production costs and increase the product uniformity for large-scale production is being investigated (Stiefel and Dassori, 2009; Peterson *et al.*, 2002; Noureddini *et al.*, 1998). Recently, the continuous synthesis of biodiesel fuel using a microreactor system has been reported as shown in the Table 1. Canter (2004, 2006) reported biodiesel yields greater than 90% and 96% with a residence time of 4 and 10 min respectively, in a microreactor of the size of a conventional credit card with channels of 100 μm thick. Sun *et al.* (2008) designed a microreaction system for the continuous production of biodiesel where the yield of methyl esters of 99.4% was obtained at the residence time of 5.89 min with KOH concentration of 1% and methanol/oil molar ratio of 6:1 at 60°C in a microtube reactor of 250 μm of diameter. Similar results were also reported by Guan *et al.* (2008) where biodiesel yield of about 100% at a residence time of 112 s and reaction temperature of 60°C in a microtube reactor of 1 mm of diameter and 160 mm of length was reported. Jachuck *et al.* (2009)

employed both slug and stratified flow behaviors in a narrow channel reactor and conversions greater 98% were achieved in a residence time of 3 min using a catalyst loading of 1% and reaction temperature of 60°C. Transesterification of sunflower oil with methanol using KOH as catalyst in a microtube reactor was investigated by Guan *et al.* (2009a,b). It was observed that sunflower oil conversion reached 100% in the microtube with an inner diameter of 0.8 mm with a residence time of 100 s, methanol/oil molar ratio of 23.9 and temperature of 60°C. Wen *et al.* (2009) used stainless steel zigzag microchannel reactors with hydraulic diameter of 240-900 μm for continuous alkali-catalyzed biodiesel synthesis from soybean oil and methanol. A methyl ester yield of 99.5% was reached in a reactor with a hydraulic diameter of 240 μm, at a residence time of 28 s, a methanol/oil molar ratio of 9:1, a KOH concentration of 1.2 wt.% and temperature of 56°C.

Table 1. Continuous biodiesel production with microreactors.

Reference	Reactants	Catalysts concentration	Residence time	Temperature	Conversion
Canter (2004, 2006)	Soybean Oil + Methanol	NaOH	10 min	Room temp.	96%
Sun *et al.* (2008)	Cottonseed Oil + Methanol	1.0% KOH	5.89 min	60°C	99.4%
Guan *et al.* (2008)	Sunflower Oil + Methanol	1.0% KOH	112 s	60°C	100%
Jachuck et al. (2009)	Canola oil + Methanol	1.0% NaOH	3 min	60°C	99.8%
Guan *et al.* (2009a)	Sunflower Oil + Methanol	1.0% KOH	93 s	25°C	92.8%
Guan *et al.* (2009b)	Sunflower Oil + Methanol	4.5% KOH	100 s	60°C	100%
Wen *et al.* (2009)	Soybean Oil + Methanol	1.2% KOH	28 s	56°C	99.5%
Sun *et al.* (2010)	Cottonseed Oil + Methanol	1.0% KOH	44 s	70°C	94.8%

Recently, transesterification of cottonsed oil and methanol with KOH as the catalyst for biodiesel production was carried out by Sun *et al.* (2010) in microstructured reactors. The reaction system included a micromixer that was connected to either a stainless steel capillary of diameter 0.6 mm or a poly(tetrafluoroethylene) (PTFE) tube with diameter of 3 mm and packed with Dixon rings. By using the stainless steel capillary the yield of biodiesel reached 94.8% under the conditions of a methanol /oil molar ratio of 8:1, a residence time of 44 s, and a reaction temperature of 70°C whereas using the PTFE tube the yield of biodiesel reached 99.5% at a residence time of 17 s. These reports show the microreactor technology as a new promising path for the high-efficiency industrial

production of biodiesel since scale-up of this technology to industrial scale could be easily implemented by numbering up, which consist in extrapolating a process by putting devices in parallel.

However, in most of these studies the biodiesel production has been limited to simple microtube reactor. It is well-known that internal geometries inside microreactors have big impact in mass and heat transfer (Günther and Jensen, 2006) and only some researchers (Wen *et al.*, 2009) have been investigated the effect of zigzag geometry on biodiesel production. In this work, microreactors with different geometries such as Omega-, Tesla-, and T-shaped have been developed in order to improve the efficiency of the homogeneously alkali-catalyzed biodiesel synthesis. The effect of geometric parameters, such as fluid path of the microreactor for biodiesel synthesis was experimentally investigated. Besides, the performances of microreactors have been investigated by examining the effects of catalyst amount, reaction temperature, molar ratio of ethanol to oil, and residence time. The difference in reaction performance between the microreactor and batch stirred reactor in the biodiesel synthesis at the same residence time is discussed.

2. Experimentation

2.1. Chemicals

Castor oil was purchased from Campestre Ind. & Com. De Óleos Vegetais Ltda. (São Bernardo do Campo, Brazil) with acid value of 1.3 mg KOH/g measured according to AOCS Ca 5a-40 method. Ethanol and sodium hydroxide were purchased from Merck (São Paulo, Brazil). The stock solution of NaOH was prepared dissolving the catalyst in the amount of ethanol necessary to give the desired alcohol/oil molar ratio. The main difficulty was in obtaining pure standards to calculate the correlation factors of mono-, di-, and triglycerides of castor oil. It would not have precise enough to reconstitute each lipid species mixture with individual standards, knowing the castor oil fatty acid composition, in particular the unusual ricinoleic acid, so a mixture standard of 1,2,4-butanetriol, diolein, monolein, tricaprin and triolein was used for calibration. In addition, tripalmitin, triolein, trilinolein, ethyl palmitate, ethyl stearate, ethyl oleate, ethyl ricinoleate and glycerol were also used.

2.2. Fabrication of microreactors

The microreactors were made of polydimethylsiloxane (PDMS) by soft lithography process. The three microrectors with different geometry were denoted as Omega-, Tesla-, and T-shaped. In the Figure 1, the three types of patterned microreactors are shown with its main dimensions. The microchannels were of rectangular cross section with height of 500 μm and length of 1 m (referred to the longitudinal direction). The sealing process was carried out by oxidizing PDMS surface through RF (radio frequency) oxygen plasma using a PLAB SE80 plasma cleaner (Plasma Technology, Wrintong, England). The plasma working parameters were obtained from Jo *et al.* (2000): 16 Pa of O_2, 70 W RF power and 20 s exposition. This process forms a watertight and irreversible seal. The reaction fluid was fed to and removed from microreactor headers via 1/16 inch tubing and fittings.

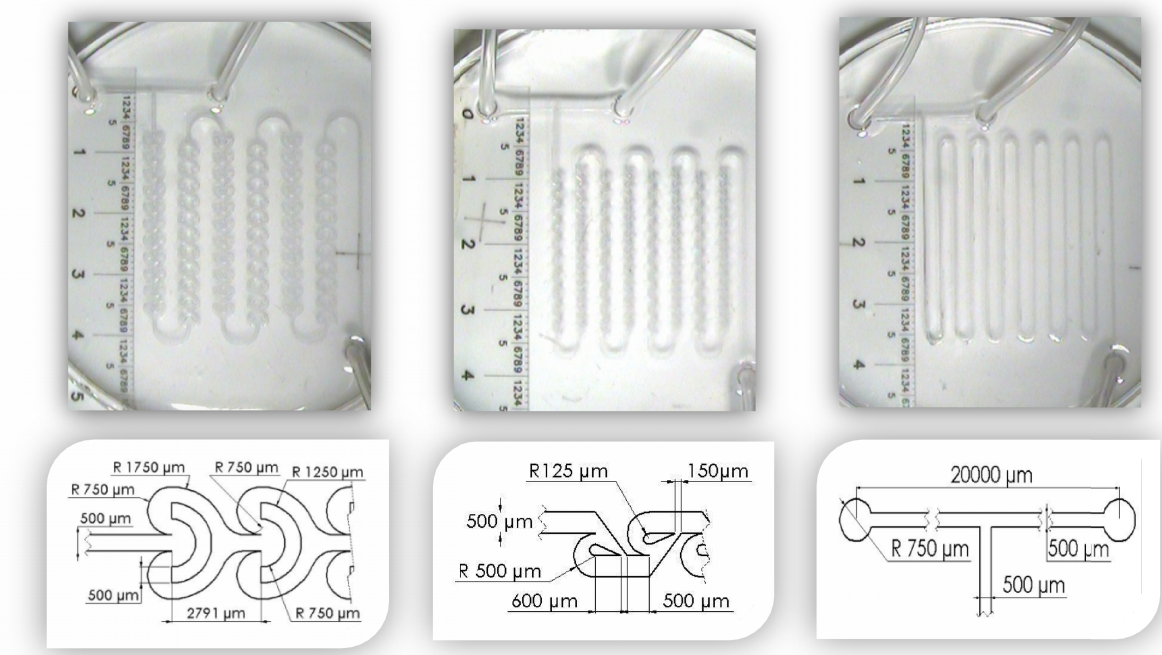

(a) (b) (c)

Figure 1. PDMS microreactors made by soft lithography process: (a) Omega- , (b) Tesla- , (c) T- design.

2.3. Transesterification reaction

Two syringe pumps ST670 (Samtronic Infusion Systems, Brazil) were used to inject the castor oil and ethanol at different flow rates ranging from 0.5 to 22.6 mL/h. The microreactors were place into HPLC furnace to ensure the accuracy of the reaction temperature. The experiments were carried out at temperatures of 30, 50, 70°C. The outlet

of the microreactor was connected with a collection flask placed in an ice-water vessel in order to terminate the transesterification reaction quickly. Experimental set-up is show in Figure 2. The catalyst amount of 0.5, 1.0, and 1.5 wt.% referred to the oil mass were prepared. The molar ratios of ethanol to castor oil were adjusted to 9:1, 12:1, and 17:1 by changing the flow rates. The molecular weight of the castor oil based in the fatty acid composition estimated according to AOCS Ce 1f-96 method (Fillières *et al.*, 1995) was assumed of 926. Ethanol/oil molar ratios of 9:1, 12:1, and 17:1 correspond to ethanol/oil volume ratios of 0.54, 0.72, and 1.03, respectively. Samples (0.1 ml) were withdrawn during the experiments at various intervals and diluted in 10 ml of tetrahydrofuran (HPLC grade) to quench immediately the reaction and immediately cooling. Samples prepared this way were ready for chemical analysis. A schematic illustration of the experimental set-up is shown in Figure 2.

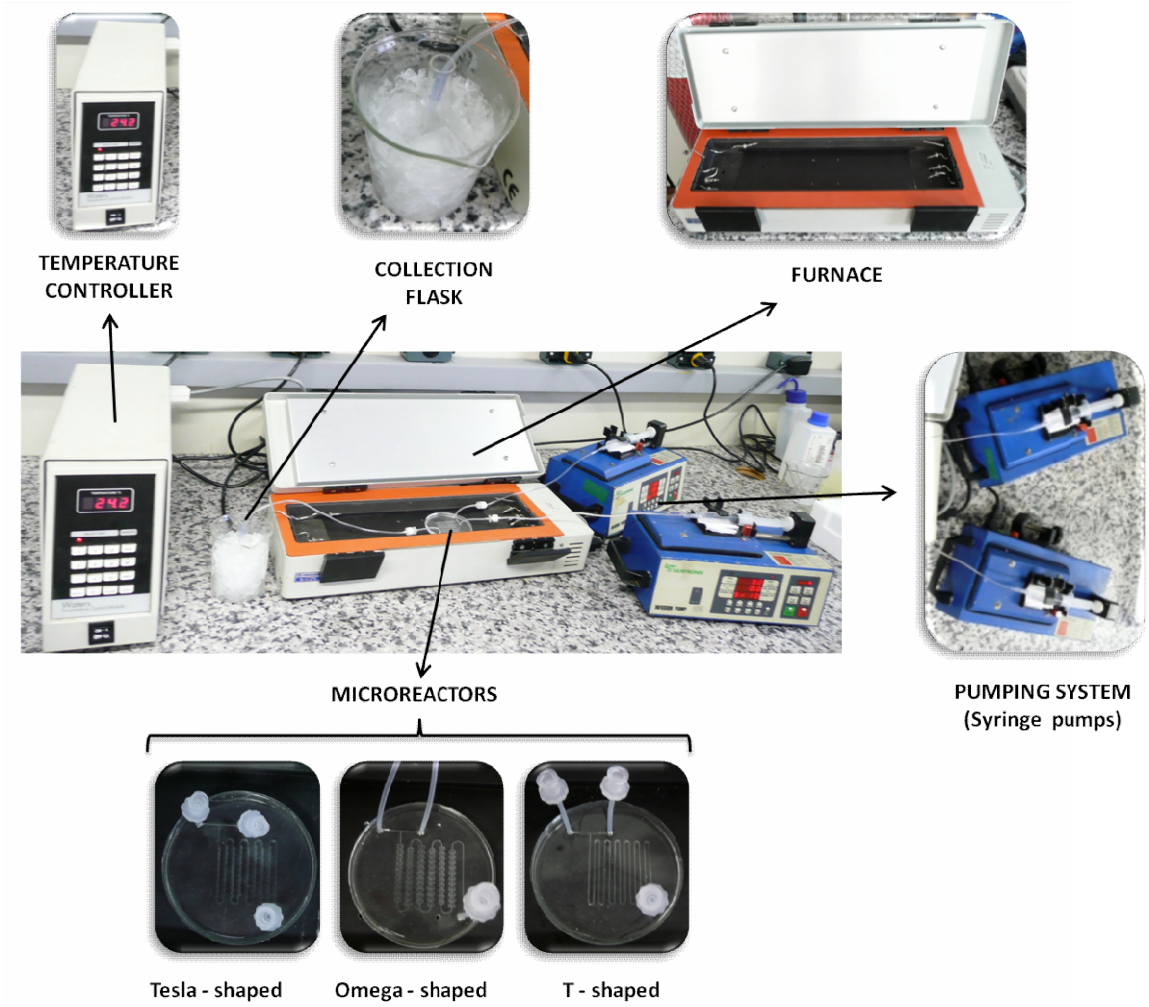

Figure 2. Experimental set-up for transesterification reaction in the microreactors

2.4. Quantitative Analysis

The size-exclusion chromatography (SEC) was used for the triglycerides, diglycerides, monoglycerides, ethyl esters and glycerol analysis according to Shoenfelder method (Schoenfelder, 2003). The system consisted of a VISCOTECK GPC/SEC TDA max^{TM} chromatograph with triple detector array: refractive index (RI), viscometer and light scattering detectors. Data collection and analysis was performed with GPC software. The mobile phase was HPLC grade THF (JT Baker, USA) at flow rate of 0.8 ml/min. Three GPC/SEC Phenogel analytical columns connected in series were used (Phenomenex, Torrance, CA), 300 mm x 7.8 mm, packed with spherical styrene divinylbenzene copolymer beads with an average particle size of 5 µm. We first placed a column with a pore size of 100 Å, corresponding to a molecular weight (MW) range of 100 - 6x10^3. This was connected in series to two columns with a pore size of 50 Å, corresponding to a MW resolving range of 50 - 3x10^3. Sample injection volume was 20 µl, and all analyses were carried out at 40°C. A mixture standard of 1,2,4-butanetriol, diolein, glycerol, monoolein, tricaprin, and triolein was used for calibration. In addition, tripalmitin, triolein, trilinolein, ethyl palmitate, ethyl stearate, ethyl oleate and ethyl ricinoleate, glycerol (99.5%) was used as reference standard as well. Identification and calibration of the GPC/SEC peaks were performed analyzing mixtures in HPLC grade THF of the above mentioned standards prepared gravimetrically within a range of concentrations as in the transesterification reactions. Standard calibration curves were obtained for each substance (triglycerides, diglycerides, monoglycerides, and fatty acid ethyl esters) and used to convert the integrated GPC/SEC areas to mass concentrations.

3. Results and Discussion

3.1. Effect of microreactors geometric parameters

To study the effect of the geometry, the ethyl ester yields in the microreactors for a catalyst amount of 1.0 wt.% (based on the castor oil weight), and temperature of 50°C were investigated. The molar ratio of ethanol to castor oil was remained 9:1 and the residence time was varied by adjusted the flow rates. The results are presented in Table 2. As shown in Figure 3, the biodiesel synthesis is greatly dependent on the geometry of the microreactor, where Tesla-shaped microreactor resulted in higher biodiesel yield than the Omega- and T-shaped microreactors. It could be seen that the yield of ethyl ester after

residence time of 15 min for Omega- and Tesla-shaped was about 1.2 fold greater than T-shaped microreactor. It is well-known that the dimension and geometry of the microchannel have strong influences on the reaction (Günther and Jensen, 2006). Therefore, it can be confirmed that the high-efficiency of reaction for biodiesel by Tesla-shaped microreactor is attributed to the higher intensification of overall volumetric mass transfer between the reactants.

Table 2. Geometry parameters and ethyl ester yield in the microreactors at molar ratio of ethanol/oil 9:1, catalyst amount 1.0 wt.% (based on oil weight) and temperature of 50°C.

Geometry	Volumetric rate of castor oil (mL/h)	Volumetric rate of ethanol (mL/h)	Residence Time (min)	Ethyl Ester Conversion (%)		
				T-shaped	Omega-shaped	Tesla-shaped
Transversal Section (µm x µm): 500 x 500	15.0	8.1	1	58.9	67.1	69.2
	7.5	4.1	2	69.4	79.3	83.8
	5.0	2.7	3	73.1	87.5	88.8
	3.8	2.1	4	74.7	88.3	91.5
Hydraulic diameter (µm): 500	3.0	1.6	5	71.1	89.7	91.1
	2.1	1.1	7	75.1	88.5	91.7
	1.5	0.8	10	73.4	87.4	92.2
	1.0	0.5	15	75.9	91.4	93.7

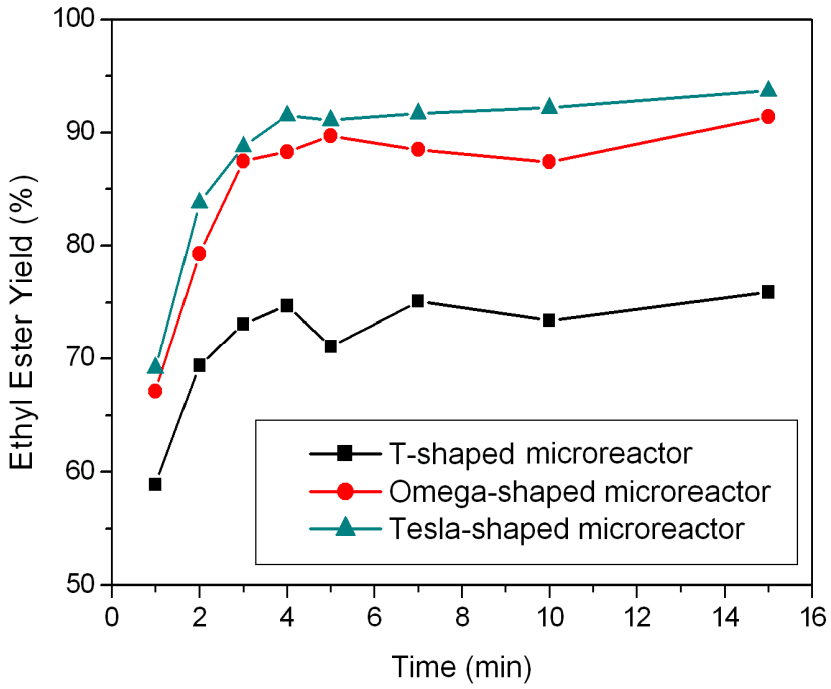

Figure 3. Ethyl ester yield of castor oil transesterification carried out in the T-, Omega-, and Tesla-shaped microreactors at different residence times at molar ratio of ethanol/oil 9:1, catalyst amount 1.0 wt.% (based on oil weight) and temperature of 50°C.

3.2. Effect of residence time

Figure 3 shows the effects of the residence time on the biodiesel synthesis in the microreactors at molar ratio of ethanol/oil 9:1, catalyst amount 1.0 wt.% (based on oil weight) and temperature of 50°C. As shown in Figure 3, the yield of ethyl ester reached a value of 75.9, 91.4 and 93.7% for T-, Omega-, and Tesla-shaped, respectively, after residence time of 15 min. It can be seen that increasing the residence time, ethyl ester yield also increases, although it was observed that too long residence time resulted in light decrease of the yield of ethyl ester in some experiments. It probably results from the saponification of biodiesel with NaOH. On the other hand, a longer reaction time leads to smaller average velocity for fixed-length microchannel, which in turn leads to weakening of the mass transfer (Dummann *et al.*, 2003), and consequently decreasing the yield of the ethyl ester.

3.3. Effect of catalyst concentration

Experiments were conducted at three different NaOH concentrations (0.5, 1.0, and 1.5 wt.% based on castor oil weight) for each microreactor. The residence time (10 min), molar ratio of ethanol to castor oil (9:1), and temperature (50°C) of reaction were held constant. Figure 4 summarizes the experimental results of the effect of catalyst amount on the performance of the T-, Omega-, and Tesla-shaped microreactor.

As shown in Figure 4, the yield of ethyl ester increased with increase of the catalyst concentration. The highest yield of ethyl ester was increased from 50.6% to 79.1%, 54.3% to 96.2%, and 56.3% to 98.9% with the increase of the catalyst concentration from 0.5% to 1.5% for T-, Omega-, and Tesla-shaped microreactor, respectively. In addition, the biodiesel synthesis was greatly increased with the complexity geometry of the microchannel, where Tesla- and Omega-shaped microreactors resulted in higher biodiesel yield than the T-shaped microreactor for a same catalyst concentration.

3.4. Effect of temperature

The effect of temperature on the biodiesel yield for three different microreactors is shown in Figure 5. The biodiesel yield increased with increasing reaction temperature up from 30 to 70°C with the ethyl ester yield of 67.3% to 89.0%, 73.9% to 92.2% and 75.9% to 92.6% for T-, Omega-, and Tesla-shaped microreactor, respectively.

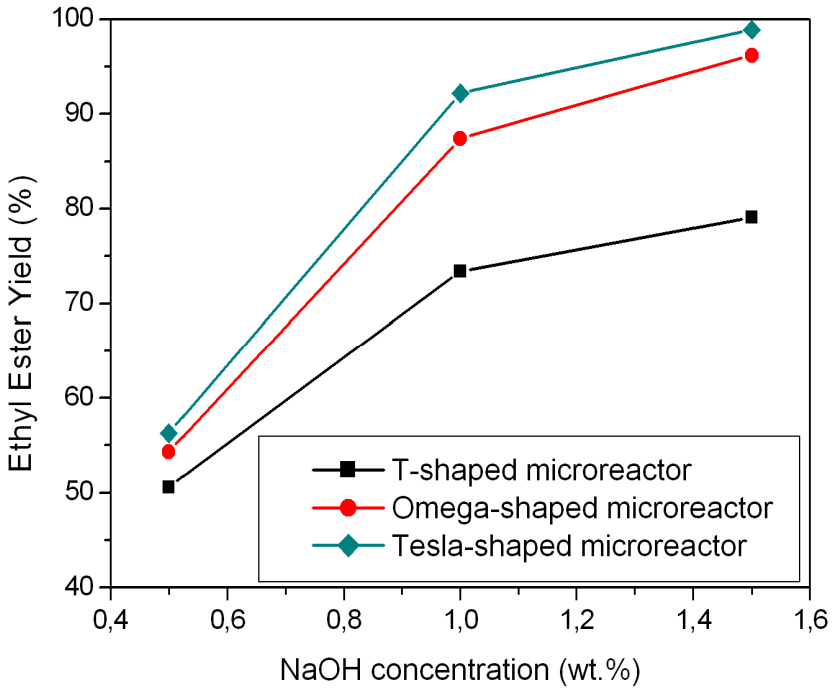

Figure 4. Influence of the NaOH concentration on the yield of ethyl ester to molar ratio of ethanol/oil 9:1, temperature of 50°C, and residence time of 10 min carried out in the T-, Omega-, and Tesla-shaped microreactors.

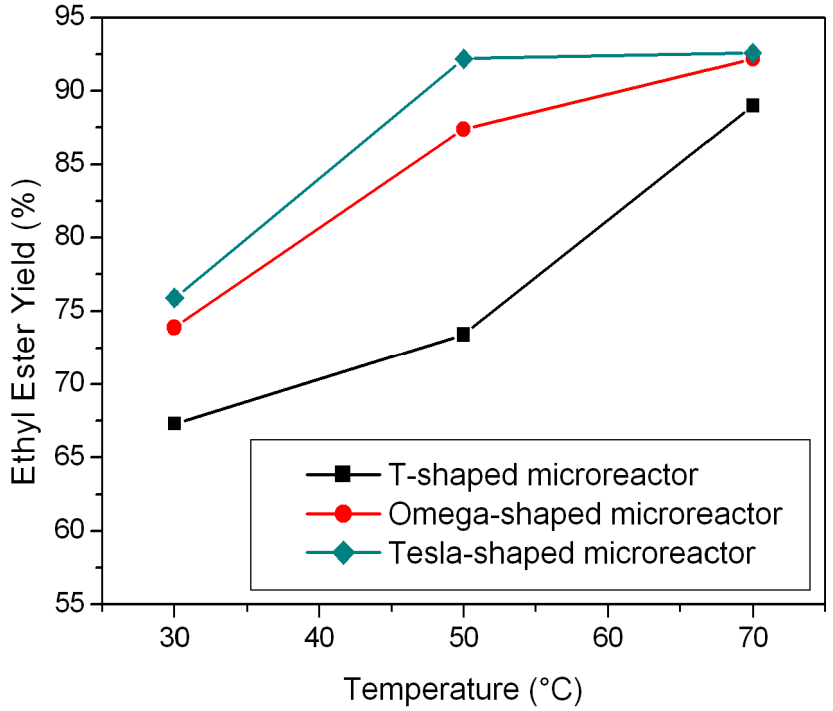

Figure 5. Influence of the reaction temperature on the yield of ethyl ester to molar ratio of ethanol/oil 9:1, NaOH concentration of 1.0 wt.%, and residence time of 10 min carried out in the T-, Omega-, and Tesla-shaped microreactors.

It is due to the mass transfer enhancement caused by the miscibility improvement of ethanol and triglyceride at high temperature (Zhou *et al.*, 2006; Cerce *et al.*, 2005). Figure 5 also shows that the conversion increases rapidly when the reaction temperature increases from 30 and 50°C, whereas this increase is not as significant for a temperature variation from 50°C to 70°C for Omega- and Tesla-shaped microreactors in comparison to T-shaped microreactor. It was owing to intensified mass transfer occasioned by internal structures inside of microchannel in the case of the Omega- and Tesla-shaped microreactors.

3.5. Effect of ethanol/castor oil molar ratio

It is well-known that according to the stoichiometry of ethanolysis reaction, it is required three moles of ethanol for each mole of oil. However, in practice, the ethanol/oil molar ratio should be higher than that of stoichiometric ratio in order to drive the reaction towards completion and produce more ethyl esters as product. The reaction results in the microreactors also exhibited the same trend, as shown in Figure 6. This trend was more obvious when the ethanol to oil molar ratio was increased from 9:1 to 12:1, where the ethyl esters yield increase about of 1.1 times. The higher ethyl esters yield of 93.5%, 95.3% and 96.7% was obtained with residence time of 10 min at the molar ratio of ethanol to oil of 25:1, catalyst amount of 1.0 wt.%, and the temperature of 50°C for T-, Omega-, and Tesla-shaped microreactor, respectively. It is the shortest time for the nearly complete ethyl esters yield at such a mild reaction condition.

Currently, the supercritical transesterification has been shown as alternative for intensified of transesterification of vegetable oils. For the supercritical transesterification without catalyst, the corresponding time is in the range of 5-12 min (Demirbas, 2008). Recently, Macneff *et al.* (2008) reported that the biodiesel yield of 92.6% was obtained at the residence time of 5.4 s using a metal oxide-based catalyst with the temperature of 455°C in a continuous fixed bed reactor. However, these new processes results in more power consumption and technical difficulties. For the case of microreactor technology, as the improvement of the throughput of biodiesel can be easily implemented by just numbering up these microreactors and the intensification of overall volumetric mass transfer can be increased by passive mixing application, the microscale appears as a promissory technology to create a compact and mini-fuel processing plant in the future.

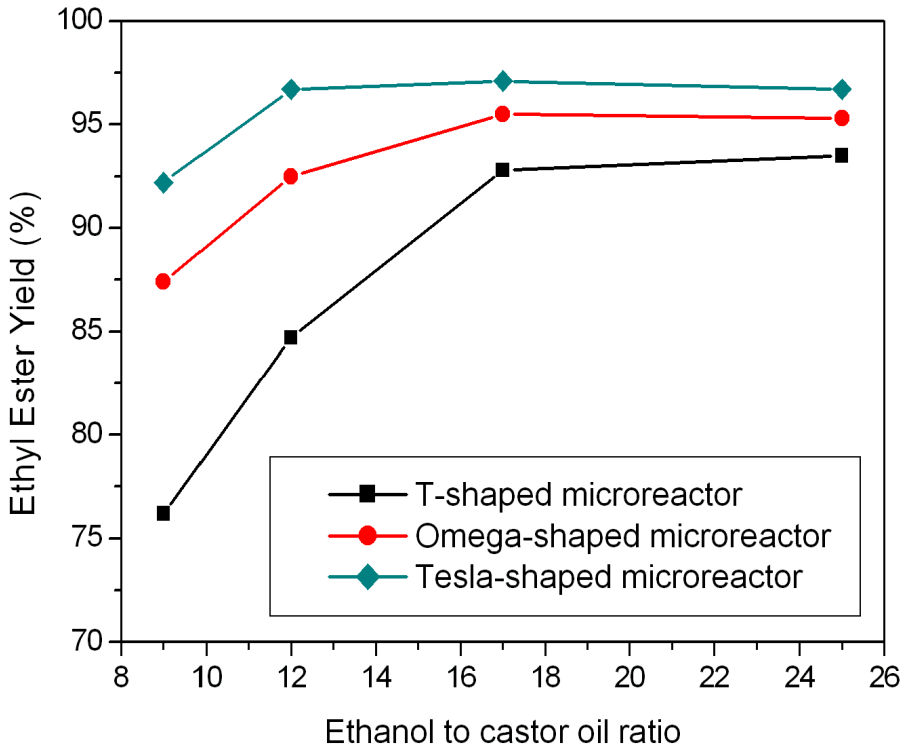

Figure 6. Influence of the ethanol/castor oil molar ratio on the yield of ethyl ester to NaOH concentration of 1.0 wt.%, temperature of 50°C, and residence time of 10 min carried out in the T-, Omega-, and Tesla-shaped microreactors.

3.6. Comparison between the microreactor and batch stirred reactor

The Figure 7 shows the comparison of the ethyl ester yield between the lab-scale batch reactor and the microreactors utilized in this study for different residence times. In both cases, the same reaction conditions were used: ethanol/oil molar ratio of 9:1, catalyst amount of 1.0 wt.% based on oil weight, and temperature of 50°C. It can be seen that increasing the residence time, the biodiesel yield increases in both kinds of reactors. However, the reaction carried out in the conventional lab-scale batch reactor reached the ethyl ester yield of 98.5%, which is higher than the obtained in the three microreactors of 75.9%, 91.4% and 93.7% for T-, Omega-, and Tesla-shaped microreactors, respectively. These yields correspond to a residence time of 15 min. The lower yields obtained by using microreactors can be justified in terms of experimental problems that were not predicted before the assays. When the experiments finished, it was observed that some catalyst particles were adhered to the walls of the microchannels, it was due to the appearance of a white film around of the microchannels, contributing to the loss of catalyst from the reacting bulk and decreasing the reaction yield in the microreactors.

In addition, microchannels geometries were damaged by catalyst particles deposition after of several reactions. It was due to the material used to build the microreactors (PDMS) was attacked by the catalyst.

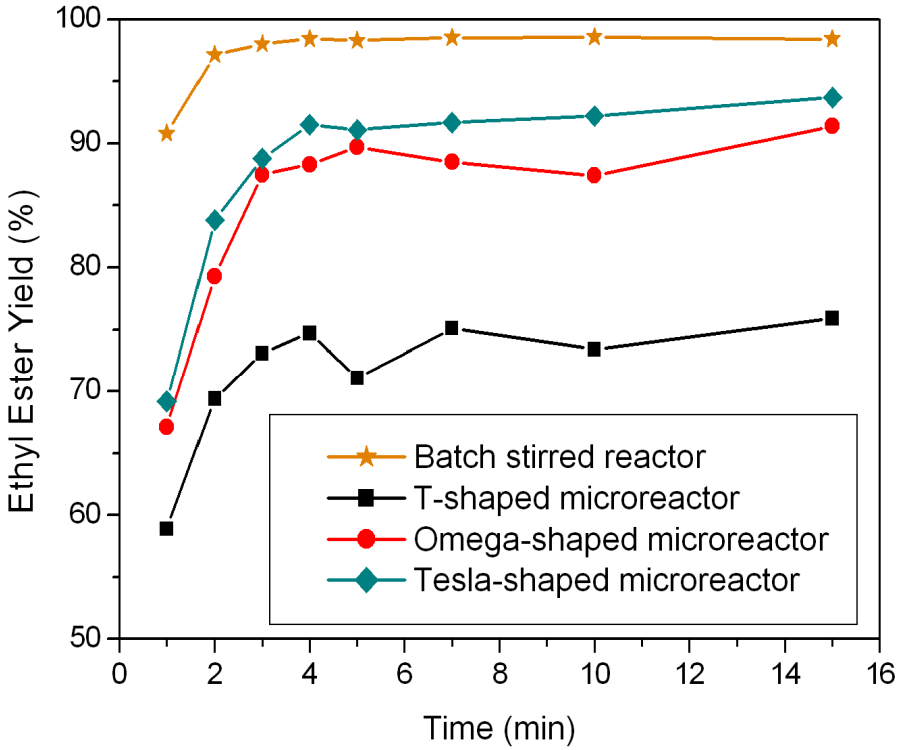

Figure 7. Comparison of ethyl ester yield oil when using microreactor and batch stirred reactor. Ethanol/castor oil molar ratio of 9:1, 1.0 wt.% NaOH, and temperature 50°C

In the Table 3 is shown a comparison of the intensified processing technique to batch and continuous biodiesel production studies done by different researchers. The comparison was done for reaction times with respect to mode of process and type of catalyst. It was found that the intensified technique is a promising means of attaining maximum conversion of triglycerides to alkyl esters in terms of residence time.

4. Conclusions

Experimental investigations on the improvement on biodiesel production process by using microreactors with different geometries were carried out. The influence of process parameters as geometry, catalyst amount, temperature, ethanol/castor oil molar ratio, and residence time were studied.

Table 3. Comparison of different processes for the production of biodiesel with microreactors

Reference	Process type	Reactants	Cat. Conc.	Residence time	Temp.	Conv.	Volume / Flow rate
Noureddini *et al.* (1997)	Batch	Soybean Oil + Methanol	0.2% NaOH	1 h	60°C	90%	217 mL
Noureddini *et al.* (1998)	Continuous	Soybean Oil + Methanol	0.4% NaOH	6.6 min	80°C	98%	300 mL/min
Darnoko *et al.* (2000a)	Batch	Palm Oil + Methanol	0.5% KOH	1 h	60°C	98%	544 mL
Darnoko *et al.* (2000b)	Continuous	Palm Oil + Methanol	1% KOH	40 min	60°C	90%	9.0 mL/min
Xu *et al.* (2003)	Batch	Soybean Oil + Methanol	30% Lipase	10 h	40°C	92%	250 mL
Dorado *et al.* (2004)	Batch	Brassica Oil + Methanol.	1.4% KOH	30 min	45°C	91.9%	250 mL
Hsu *et al.* (2004)	Continuous	oil + methanol	Lipase	48 h	50°C	96%	30 mL/min
Jachuck et al. (2009)	Batch	Sunflower Oil + Meth.	1.0% KOH	3 h	60°C	98.7%	300 mL
Jachuck et al. (2009)	Microreactor	Canola oil + Methanol	1.0% NaOH	3 min	60°C	99.8%	3.85 mL/min
Martínez (2010)	Batch	Castor Oil + Ethanol	0.5% NaOH	30 min	30°C	98.7%	1.0 L
Martínez (2010)	Microreactor	Castor Oil + Ethanol	1.5% NaOH	10 min	50°C	98.9%	1.5 mL/h

The biodiesel synthesis was greatly dependent on the geometry of the microreactor, where Tesla-shaped microreactor resulted in higher biodiesel yield than the Omega and T microreactors. The high-efficiency of reaction for biodiesel production by Tesla-shaped microreactor is attributed to the higher intensification of overall volumetric mass transfer between the reactants. It could be seen that the yield of ethyl ester after residence time of 15 min for Omega- and Tesla-shaped was about 1.2 fold greater than T-shaped microreactor for a catalyst amount of 1.0 wt.% based on the castor oil, a temperature of 50°C, and a molar ratio of ethanol/castor oil of 9:1. The enhanced rate of reaction may be attributed to specific characteristics of the intensified module employed in the experiments. It is important to note that the transesterification reaction is diffusion controlled (Noureddini and Zhu, 1997). Therefore, it can be concluded that the reason for obtaining better conversion in the Tesla- and Omega-shaped microreactor employed in this work is due to convective mixing rather than in the T-shaped microreactor which is based in diffusive and laminar mixing. Additionally, the use of an intensified process provides good control of the process parameters due to smaller volumes and shorter path lengths which contribute to higher transport rates. Thus, microreactors showed promissory

technology for biodiesel synthesis in order to design a compact and mini-fuel processing plant for the disturbed applications.

The yield of ethyl ester reached a value of 75.9, 91.4 and 93.7% after residence time of 15 min for T-, Omega-, and Tesla-shaped, respectively. It can be seen that increasing the residence time, ethyl ester yield also increases, although was also observed that long residence time led to decreasing of the yield of ethyl ester in some experiments possibly as results from the saponification reaction with NaOH. Due to the residence time was adjusted to the flow rates, a longer reaction time led to smaller average velocity for fixed-length microchannel, which in turn reduced the mass transfer and consequently decreased the yield of the ethyl ester.

Castor oil conversion in microreactors increased with the ethanol/castor oil molar ratio, catalyst amount, and reaction temperature. The highest yield of ethyl ester in this study was obtained with increase from 50.6% to 79.1%, 54.3% to 96.2%, and 56.3% to 98.9% with the increase of the catalyst concentration from 0.5% to 1.5% for T-, Omega-, and Tesla-shaped microreactor, respectively, for a residence time of 10 min, molar ratio of ethanol to castor oil of 9:1, and temperature of 50°C.

In the study of the temperature effect on the biodiesel yield, resulted that the biodiesel yield increased with increasing reaction temperature up from 30 to 70°C with the ethyl ester yield of 67.3% to 89.0%, 73.9% to 92.2% and 75.9% to 92.6% for T-, Omega-, and Tesla-shaped microreactor, respectively. It is due to the mass transfer enhancement caused by the miscibility improvement of ethanol and triglyceride at high temperature. When the ethanol/oil molar ratio was increased from 9:1 to 12:1 at 50°C in the microreactors with a hydraulic diameter of 500 µm, the ethyl esters yield increase about of 1.1 times. The ethyl esters yield of 93.5%, 95.3% and 96.7% was obtained for T-, Omega-, and Tesla-shaped microreactor, respectively, with a residence time of 10 min at the molar ratio of ethanol to oil of 25:1, catalyst amount of 1.0 wt.%, and a the temperature of 50°C.

Compared to conventional stirred reactor, the reaction carried out in the microreactors was lower than the obtained in the conventional lab-scale batch reactor. The lower yields obtained by using microreactors was attributed that some catalyst particles adhered to the walls of the microchannels, contributing to the loss of catalyst from the reacting bulk, therefore, decreasing the reaction yield in the microreactors. In addition, it

was observed that microchannels geometries were damaged by catalyst particles deposition, showing that PDMS microreactors can not used for long time transesterification reaction.

Acknowledgements

The author gratefully acknowledges the financial support provided by The Scientific Research Foundation for the State of São Paulo (FAPESP) and research support by The Brazilian Synchrotron Light Laboratory (LNLS).

Bibliography

Akoh, C. C.; Chang, S.-W.; Lee, G.-C.; Shaw, J.-F. Enzymatic Approach to Biodiesel Production, Journal of Agricultural and Food Chemistry, 55 (2007), 8995-9005.

Al-Zuhair, S.; Jayaraman, K. V.; Krishnan, S.; Chan, Y. H. The effect of fatty acid concentration and water content on the production of biodiesel by lipase, Biochemical Engineering Journal, 30 (2006), 212-217.

Al-Zuhair, S. Review: Production of biodiesel: possibilities and challenges, Biofuels, Bioproducts & Biorefining, 1 (2007), 57-66.

Canakci, M.; Van Gerpen, J. Biodiesel production from oils and fats with high free fatty acids, Transactions of the ASAE, 44 (2001), 1429-1436.

Canter, N. Scale up of a More Efficient Biodiesel Process, Tribology & Lubrication Technology, 60 (2004), 16-17.

Canter, N. Making Biodiesel in a Microreactor, Tribology & Lubrication Technology, 62 (2006), 15-17.

Cerce, T.; Peter, S.; Weidner, E. Biodiesel-Transesterification of Biological Oils with Liquids Catalyst: Thermodynamic Properties of Oil-Methanol-Amine Mixtures, Industrial & Engineering Chemical Research, 44 (2005), 9535-9541.

Darnoko, D.; Cheryan, M. Kinetics of palm oil transesterification in a batch reactor. *Journal of the American Oil Chemists Society*, 77 (2000a), 1263-1267.

Darnoko, D.; Cheryan, M. Continuous production of palm methyl esters. *Journal of the American Oil Chemists Society*, 77 (2000b), 1269-1272.

Demirbas, A. Biodiesel from vegetable oils via transesterification in supercritical methanol, Energy Conversion and Management, 43 (2002), 2349-2356.

Demirbas, A. Comparison of transesterification methods for production of biodiesel from vegetable oils and fats, Energy Conversion and Management, 49 (2008), 125-130.

Dorado, M. P.; Ballesteros, E.; Lopez, F. J.; Mittelbach, M. Optimization of alkali-catalyzed transesterification of Brassica Carinata oil for biodiesel production. *Energy and Fuels*, 18 (2004), 77-83.

Dummann, G.; Quittmenn, U.; Groschel, L.; Agar, D. W.; Worz, O.; Morgenschweis, K. The Capillary-microreactor: A New Reactor Concept for the Intensification of Heat and Mass Transfer in Liquid-Liquid Reactions, Catalysis Today, 433 (2003), 79-80.

Guan, G.; Kusakabe, K.; Sakurai, N.; Moriyama, K. Continuous Production of Biodiesel Using a Microtube Reactor, Chemical Engineering Transactions, 14 (2008), 237-244.

Guan, G.; Sakurai, N.; Kusakabe, K. Synthesis of biodiesel from sunflower oil at room temperature in the presence of various cosolvents, Chemical Engineering Journal, 146 (2009a), 302-306.

Guan, G.; Kusakabe, K.; Moriyama, K.; Sakurai, N. Transesterification of Sunflower Oil with Methanol in a Microtube Reactor, Industrial & Engineering Chemistry Research, 48 (2009b), 1357-1363.

Günther, A.; Jensen, K. F. Multiphase microfluidics: from low characteristics to chemical and materials synthesis, Lab on Chip, 6 (2006), 1487-1503.

Hsu, A. F.; Jones, K. C.; Foglia, T. A.; Marmer, W. N. Continuous production of ethyl esters of grease using an immobilized lipase. *Journal of the American Oil Chemists' Society*, 81 (2004), 749-752.

Jachuck, R.; Pherwani, G.; Gorton, S. M. Green engineering: continuous production of biodiesel using an alkaline catalyst in an intensified narrow channel reactor, Journal of Environmental Monitoring, 11 (2009), 642-647.

Jo, B. H.; Van Leberghe, L. M.; Motsegood K. M.; Beebe, D. J. Three-Dimensional Micro-Channel Fabrication in Polydimethylsiloxane (PDMS) Elastomer, Journal of Microelectromechanical Systems, 9 (2000), 76-81.

Kusdiana, D.; Saka, S. Kinetics of transesterification in rapeseed oil to biodiesel fuel as treated in supercritical methanol, Fuel, 80 (2001), 693-698.

Lotero, E.; Liu, Y.; Lopez, D. E.; Suwannakarn, K.; Bruce, D. A.; Goodwin, J. G. Synthesis of Biodiesel via Acid Catalyst, Industrial & Engineering Chemistry Research, 44 (2005), 5318-5324.

Marchetti, J. M.; Miguel, V. U.; Errazu, A. F. Possible methods for biodiesel production, Renewable and Sustainable Energy Reviews, 11 (2007), 1300-1311.

Martínez, E. L. Desenvolvimento e Avaliação de Microreatores: Aplicação para Produção de Biodiesel, University of Campinas, M.Sc. Thesis, Campinas, São Paulo, 2010.

McNeff, C. V.; McNeff, L. C.; Yan, B.; Nowlan, D. T.; Rasmussen, M.; Gyberg, A. E.; Krohn, B. J.; Fedie, R. L.; Hoye, T. R. A continuous catalytic system for biodiesel production, Applied Catalysis A: General, 343 (2008), 39-48.

Meneghetti, S. M.; Meneghetti, M. R.; Wolf C. R.; Silva, E. C.; Lima, G. E.; Coimbra, M.; Soletti, J. I.; Carvalho, S. H. V. Ethanolysis of Castor and Cottonseed Oil: A Systematic Study Using Classical Catalysts, Journal of the American Oils Chemists' Society, 83 (2006), 819-822.

Noureddini, H.; Zhu, D. Kinetics of Transesterification of Soybean Oil, Journal of the American Oil Chemists' Society, 74 (1997), 1457-1463.

Noureddini, H.; Harkey, D.; Medikonduru, V. A continuous Process for the Conversion of Vegetable Oils into biodiesel, Journal of the American Oil Chemists' Society, 75 (1998), 1775-1783.

Peña, R.; Romero, R.; Martínez, S. L.; Ramos, M. J.; Martínez, A.; Natividad R. Transesterification of Castor oil: Effect of Catalyst and Co-Solvent, Industrial & Engineering Chemistry Research, 48 (2009), 1186-1189.

Peterson, C. L.; Cook, J. L.; Thompson, J. C., Taberski, J. S. Continuous Flow Biodiesel Production, Applied Engineering in Agriculture, 18 (2002), 5-11.

Sanchez, F.; Vasudevan, P. T. Enzyme catalyzed production of biodiesel from olive oil, Applied Biochemistry and Biotechnology, 135 (2006), 1-14.

Sarma, A. K.; Sarmah, J. K.; Barbora, L., Kalita, P.; Chatterjee, S.; Mahanta, P.; Goswami, P. Recent Inventions in Biodiesel Production and Processing – A Review, Recent Patents on Engineering, 2 (2008), 47-58.

Stiefel, S.; Dassori, G. Simulation of Biodiesel Production through Transesterification of Vegetable oils, Industrial & Engineering Chemistry Research, 48 (2009), 1068-1071.

Sun, J.; Ju, J.; Ji, L.; Zhang, L.; Xu, N. Synthesis of Biodiesel in Capillary Microreactors, Industrial & Engineering Chemistry Research, 47 (2008), 1398-1403.

Sun, P.; Wang, B.; Yao, J.; Zhang, L.; Xu, N. Fast Synthesis of Biodiesel at High Throughput in Microstructured Reactors. *Industrial and Engineering Chemistry Research*, 49 (2010), 1259-1264.

Warabi, Y.; Kusdiana. D.; Saka, S. Reactivity of triglycerides and fatty acids of rapeseed oils in supercritical alcohols, Bioresource Technology, 91 (2004), 283-287.

Wen, Z.; Yu, X.; Tu, S.-T.; Yan, J.; Dahlquist, E. Intensification of biodiesel synthesis using zigzag micro-channel reactors, Bioresource technology, 100 (2009), 3054-3060.

Xu, Y.; Du, W.; Liu, D.; Zeng, J. A novel enzymatic route for biodiesel production from renewable oils in a solvent-free medium. *Biotechnology Letters*, 25 (2003), 1239-1241.

Zhou, H.; Lu, H.; Liang, B. Solubility of Multicomponent Systems in the Biodiesel Production by Transesterification of Jatropha Curcas L. Oil with Methanol, Journal of Chemical & Engineering Data, 51 (2006), 1130-1135.

8.3. Conclusões

Neste capítulo foram estudados três microreatores para avaliar a síntese contínua de biodiesel. Os microreatores diferem quanto à geometria dos microcanais, sendo identificados por microreator T, Omega e Tesla. A reação de transesterificação foi conduzida utilizando-se o óleo de mamona, etanol e NaOH como catalisador da reação. A influência dos parâmetros de processo como a geometria do microreator, massa de catalisador, temperatura de reação, razão molar etanol/óleo de mamona e o tempo de residência foram estudados.

Foi verificado que o rendimento da reação de síntese do biodiesel se mostrou dependente da geometria do microreator, sendo que o microreator Tesla apresentou o maior rendimento da reação em comparação aos microreatores T e Omega. A alta eficiência da reação para o microreator Tesla foi atribuída à geometria dos microcanais que proporciona a intensificação da transferência de massa entre os reagentes. Além disso, foi encontrado que o rendimento para o microreator Omega e Tesla, após um tempo de retenção de 15 min, foi em torno de 1,2 vezes maior do que para o microreator T. É importante notar que a reação de transesterificação é controlada pela difusão devido à imiscibilidade dos óleos vegetais com o álcool. Portanto, pode-se concluir que a obtenção dos melhores rendimentos da reação nos microreatores Tesla e Omega, empregados neste trabalho, é devido à mistura convectiva gerada pelas geometrias internas dos microcanais em comparação com o microreactor T, no qual a mistura ocorre mediante a difusão das substâncias. Por outro lado, a utilização dos microdispositivos permitiu um bom controle dos parâmetros do processo, devido aos pequenos volumes manipulados e à diminuição do caminho molecular entre as substâncias o que contribuem para o aumento das taxas de reação. Assim, os microreatores apresentam-se como uma promissora tecnologia para a síntese de biodiesel. Futuros desenvolvimentos devem contemplar o projeto de uma mini-planta compacta para o processamento de biocombustível através do acoplamento de diversos microreactores em série e/ou paralelo.

O rendimento do éster etílico atingiu um valor de 75,9%, 91,4% e 93,7% após um tempo de residência de 15 min para o microreator T, Omega e Tesla, respectivamente. Pode ser visto que, com o aumento do tempo de residência, a produção de éster etílico também aumenta. Observou-se uma leve diminuição da produção de biodiesel para tempos de

residência prolongados, possivelmente resultante da reação de saponificação com NaOH. Além disso, o tempo de residência nos microreatores foi ajustado mediante a variação do fluxo de entrada, porém, um maior tempo de reação corresponde a uma menor velocidade média dentro dos microcanais, o que diminui a transferência de massa e, conseqüentemente, reduz o rendimento da reação.

A conversão do óleo de mamona aumentou com o aumento da razão molar etanol/óleo, a quantidade de catalisador e a temperatura de reação. O aumento da concentração de catalisador de 0,5% a 1,5% levou a um aumento do rendimento da reação para todos os microreatores estudados. O rendimento passou de 50,6% para 79,1% no caso do microreator T, de 54,3% para 96,2% no microreator Omega e de 56,3% para 98,9% para o microreator Tesla. Esses dados correspondem a um tempo de residência de 10 min, uma razão molar de etanol/óleo de 9:1, e temperatura de 50 °C.

Para avaliar o efeito da temperatura sobre a produção de biodiesel foram realizados ensaios entre 30-70°C. Os resultados mostraram que a produção de biodiesel aumentou com o aumento da temperatura. Nesta faixa de temperatura, o rendimento de ésteres etílicos passou de 67,3% para 89,0% no caso do microreator T, de 73,9% para 92,2% no caso de microreator Omega e de 75,9% para 92,6% para o microreator Tesla. O aumento da temperatura proporciona o aumento da transferência de massa, pois melhora a miscibilidade entre o etanol e os triglicerídeos. Além disso, quando a razão molar de etanol/óleo foi aumentada de 9:1 para 12:1 a 50°C, a produção de ésteres etílicos aumentou em torno de 1,1 vezes. A produção de ésteres etílicos de 93,5%, 95,3% e 96,7% foi obtida para os microreatores T, Omega e Tesla, respectivamente, com um tempo de residência de 10 min, uma razão molar etanol/óleo de 25:1, uma massa de catalisador de 1,0 wt.%, e uma temperatura de 50°C.

O rendimento da reação realizada nos microreatores foi inferior ao obtido no reator batelada de bancada. O menor rendimento obtido nos microreatores foi atribuído à adesão do catalisador (NaOH) às paredes dos microcanais. Desse modo, houve a perda do catalisador da massa reacional e, portanto, o rendimento da reação nos microreatores diminuiu. Além disso, foi observado que as geometrias nos microcanais foram danificadas pela deposição de partículas de catalisador, mostrando que microreatores feitos de polidimetilsiloxano (PDMS) não podem ser usados para reações de transesterificação prolongadas, e outros tipos de materiais tais como metal ou vidro devem ser explorados.

Capítulo 9.

Monitoramento em tempo real do processo de transesterificação em microreatores por espectroscopia no infravermelho usando fibra ótica

9.1. Introdução

Como foi mencionado no Capítulo 2, a possibilidade de uso de óleos vegetais como combustível tem sido reconhecido mundialmente. Os derivados de óleos vegetais são substitutos adequados para o óleo diesel já que não requerem modificações nos motores e apresentam alto rendimento energético. Eles não contêm enxofre e sua combustão gera menores teores de gases poluentes que o óleo diesel. A alternativa mais viável de transformação dos óleos vegetais para gerar um combustível capaz de fazer funcionar um motor por compressão sem danificá-lo tem sido o biodiesel. Considerado um combustível biodegradável e ambientalmente correto, o biodiesel quimicamente é uma mistura de ésteres mono-alquílicos de ácidos graxos. O processo mais empregado para sua produção é a transesterificação, que consiste na reação de um triglicerídeo com um álcool de cadeia curta, na presença de um catalisador ácido ou básico. Como resultado, obtém-se ésteres de ácidos graxos metílicos ou etílicos (biodiesel) e glicerina.

Recentemente, um grande interesse na aplicação dos sistemas de microreação na produção contínua de biodiesel tem aumentado. Estes estudos mostram a tecnologia de microreação como um caminho promissor para a produção altamente eficiente de biodiesel já que teores de biodiesel superiores a 90% com um tempo de residência de só uns poucos minutos têm sido reportados. No Capítulo 8, os resultados obtidos na síntese de biodiesel em microreatores com diferentes geometrias e diversas condições de processo, mostraram que 98.9% de conversão podem ser obtidos em um tempo de residência de 15 min.

Não obstante, um combustível alternativo precisa ser tecnicamente competitivo, facilmente acessível e compatível com as necessidades de proteção ambiental. Atualmente

tem-se estabelecido normas de certificação da qualidade do biodiesel e para isso, há necessidade do desenvolvimento de metodologias analíticas rápidas e de baixo custo para análise e quantificação do biodiesel produzido.

Recentemente, a literatura científica apresenta relatos sobre o uso de espectroscopia no infravermelho para o monitoramento da transesterificação de óleos vegetais com metanol e etanol, determinando a taxa de conversão desta reação. Como o diesel e o biodiesel apresentam funções químicas distintas, os espectros de infravermelho desses combustíveis contêm bandas específicas. Esta técnica pode ser usada também para quantificar o percentual de biodiesel presente em misturas biodiesel:diesel. Ressalta-se o uso do infravermelho para determinar o teor de biodiesel misturado ao diesel através das técnicas de PLS (Mínimos Quadrados Parciais) com ANN (Rede Neural Artificial) e PCA (Análise de Componentes Principais), além do uso da espectroscopia de infravermelho próximo associada à Ressonância Magnética Nuclear de Hidrogênio (RMN ^{1}H), utilizando calibração multivariada para determinar o percentual de biodiesel em mistura com diesel.

Neste capítulo apresenta-se o desenvolvimento de um método para o monitoramento em tempo real do processo de transesterificação do óleo de mamona realizado em um microreator por espectroscopia no infravermelho próximo usando fibra ótica. É importante ressaltar que este novo método permite um analise rápida, não destrutiva, sem preparação previa de amostra e de baixo custo. O estudo desta montagem experimental e seus parâmetros têm implicações no desenvolvimento de mini-plantas portáteis e altamente eficientes na produção de biodiesel, reduzindo custos no consumo de energia, tempo de reação e análise, assim como um controle *"on-line"* dos produtos da reação.

9.2. Desenvolvimento

O desenvolvimento deste capítulo é apresentado a seguir, no manuscrito intitulado: *On-line Transesterification Process Monitoring in Microreactors by Infrared Spectroscopy Using Fiber-Optic.*

On-line Transesterification Process Monitoring in Microreactors by Near-Infrared Spectroscopy Using Fiber-Optic Device

Abstract

Vegetable oil esters, particularly ethyl esters, are being explored and used as alternative diesel fuel (biodiesel). The transesterification reaction which yields the ethyl esters can be monitored for completion by infrared spectroscopy using fiber-optic probe. Although the infrared spectroscopy method is less sensitive than gas chromatography for quantifying minor components, by correlation with existing gas chromatography of other analytical data, biodiesel fuel quality can be assessed through the infrared spectroscopy method. The infrared spectroscopy method is easier and faster to use than gas chromatography.

Keywords: Biodiesel; Microreactors; Transesterification; Fiber-optic; Spectroscopy

1. Introduction

The term biodiesel refers to the fatty acid alkyl esters derived from vegetable, animal or waste oil feedstock. Biodiesel is synthesized by the reaction of the triglyceride molecule (the main constituent of oils) with an alcohol over an acid or base catalyst. Due to the increasing pressure for fuel energy security, to reduce global emissions of greenhouse gases and of the finite nature of fossil fuels, alternative transport fuels such as biodiesel are being increasingly sought.

Considerable effort has also been placed in monitoring the transesterification reaction for the percent conversion of triglycerides into the corresponding methyl esters. Several methods have been developed for analyzing samples obtained by the transesterification of vegetable oils. These include techniques such as thin layer chromatography (TLC), gas chromatography (GC), high performance liquid chromatography (HPLC), gel permeation chromatography (GPC), ^{1}H nuclear magnetic resonance (^{1}H NMR), however all of these techniques rely on extensive sample preparation and are not applicable to in-vitro monitoring. An alternative analytical technique which is both non-destructive and applicable to online sensing is infrared (IR) spectroscopy (Meher *et al.*, 2006; Knothe, 2006; Chuck, 2010).

Analyses of fatty materials by near infrared (NIR) spectroscopy have become widespread (Sato, 1997). Biodiesel was determined in lubricating oil by fiber-optic Fourier transform infrared spectroscopy (Sadeghi-Jorabchi *et al.*, 1994). Studies have been conducted comparing the near infrared (NIR) spectra of soybean oil and its corresponding biodiesel methyl ester (Pimentel *et al.*, 2006). In the past decade, NIR spectroscopy has been used to monitor the transesterification reaction (Knothe, 1999). The basis for quantitation of the conversion from triglyceride feedstock to methyl ester product is differences in the NIR spectra of these classes of compounds. Knothe (1999) showed that at 6005 cm^{-1} and 4425–4430 cm^{-1}, the methyl esters display peaks, while triglycerides display only shoulders. However the absorption at 6005 cm^{-1} gave better result than the one at 4425 cm^{-1}. NIR spectra were obtained with the aid of a fiber-optic probe coupled to the spectrometer and using quantitation software, it was possible to develop a method for quantifying the conversion of triglycerides to methyl esters. In addition, Bezerrra de Lira *et al.* (2010) showed that ethyl esters could be distinguished in a similar fashion.

In this work, is presented differences between NIR spectra of castor oil and their corresponding ethyl esters in order to use these spectral differences to monitor progress and endpoint of the transesterification. Moreover, initial results on the potential use of a portable spectrometer coupled fiber-optic device for on-line transesterification process monitoring in microreactors, which presents a possibility for rapid, easy-to-handle, and cost-effective monitoring of the transesterification reaction and of biodiesel fuel quality.

2. Experimental procedures

2.1. Chemicals and Samples

Castor oil was obtained from Campestre Ind. & Com. De Óleos Vegetais Ltda. (Brazil) with acid value of 1.3 mg KOH/g measured according to AOCS Ca 5a-40 method. Ethanol and sodium hydroxide were purchased from Merck (São Paulo, Brazil).

Samples were prepared in a baker by mixing ethyl esters of castor oil (biodiesel), such as: ethanol, glycerol, and castor oil. After each addition of reaction sub-product, then mixture was stirred for 5 min and the spectrum was recorded. The ethyl ester content in these blends ranged from 81.25 to 66.66%w/w as shown in the Table 1. Additionally, spectra of the pure oils and ethyl esters samples were obtained.

Table 1. Samples prepared with defined quantities of reactions sub-products of the transesterification reaction.

Sample	Component	Composition (% v/v)
1	Ethyl Esters	100
2	Castor Oil	100
3	Glycerol	100
4	Ethanol	100
5	Ethyl Esters	81.25
	Castor Oil	18.75
6	Ethyl Esters	77.78
	Ethanol	22.22
7	Ethyl Esters	81.25
	Glycerol	18.75
8	Ethyl Esters	75.0
	Castor Oil	12.5
	Ethanol	12.5
9	Ethyl Esters	75.0
	Castor Oil	12.5
	Glycerol	12.5
10	Ethyl Esters	66.67
	Castor Oil	11.11
	Ethanol	11.11
	Glycerol	11.11

2.2. Apparatus and data pre-processing

The mixtures were checked firstly by a conventional near-infrared spectrometer (NIR). The NIR spectra (900 to 2100 nm) were obtained with a Perkin-Elmer Spectrum GX spectrometer equipped. Spectra were acquired, in the NIR region, using a quartz flow cell with a 1.0 mm path length positioned directly in front of the near-infrared radiation beam. In all cases, the spectra were recorded at room temperature with a spectral resolution of 8 cm^{-1} and 16 co-averaged scans. After recording a spectrum, the cell was cleaned by successive treatments with ethanol and acetone. The obtained spectra were digitalized and exported for subsequent analysis.

In the on-line reaction monitoring process in three microreactors with different geometries, it was made by a portable near-infrared spectroscopy using fiber-optic device is show in the Figure 1. The NIR spectra were obtained on an Ocean-Optics (NY) Spectrum 2000 spectrometer equipped with Galileo (NY) transmission-type fiber-optic probe. The transesterification reactions were conducted at room temperature with a ethanol/castor oil molar ratio of 6:1 and 1.0 wt.% NaOH refer weight oil. The reactions were analyzed in-situ

through of a fiber-optic probe coupled to the spectrometer positioned directly in front of the microchannel and the near-infrared radiation beam (Figure 1). After recording a spectrum, the fiber-optic probe was cleaned by successive treatments with ethanol and acetone by immersing into each stirred solvent for several minutes. The obtained spectra were digitalized and exported for subsequent analysis on a personal computer (Hewlett-Packard HP). Method calibrations were carried out automatically by using the corresponding software feature.

3. Results and Discussions

3.1. NIR spectra of the samples

NIR spectra of the castor oil, glycerol, and ethanol were compared with the ethyl esters, as shown in the Figure 2(a). NIR spectra of the castor oil and its corresponding ethyl esters showed significant differences. There are not absorption peaks in the region 9000 to 11000 cm^{-1}. Differences in NIR spectra of castor oil, glycerol, ethanol, and ethyl esters are shown in detail in Figure 2(b) for the region 5000 to 5500 cm^{-1} that can be assigned to C=O and C-O stretching combinations (Burns and Ciurczak, 2001). Differences in NIR spectra of sub-products blend of the transesterification reaction are show in the Figure 3.

While the mid-range infrared spectra of triglycerides (vegetable oils) and their corresponding ethyl esters are similar (Pimentel *et al.*, 2006), the NIR spectra of castor oil and the corresponding ethyl esters reveal a possibility for distinguishing them. The ethyl ester (biodiesel) presents an absorbance at wavenumber between 5000 and 5500 cm^{-1}. The Figure 2 depicts the NIR spectra of castor oil, ethanol, glycerol, and ethyl esters. In this region the ethyl esters displays peaks while castor oil, ethanol, and glycerol do not.

In order to evaluate the NIR spectra for a mixture of ethyl esters, glycerol, ethanol, and castor oil, which are compounds found during transesterification reaction, blends of ethyl esters were prepared with the compositions showed in the Table 1.

It was observed that all blends showed the ethyl esters characteristic absorbance at 5000-5500cm^{-1}. The absorbance in this region has been proposed to carry out ethyl ester quantification through multivariate calibration.

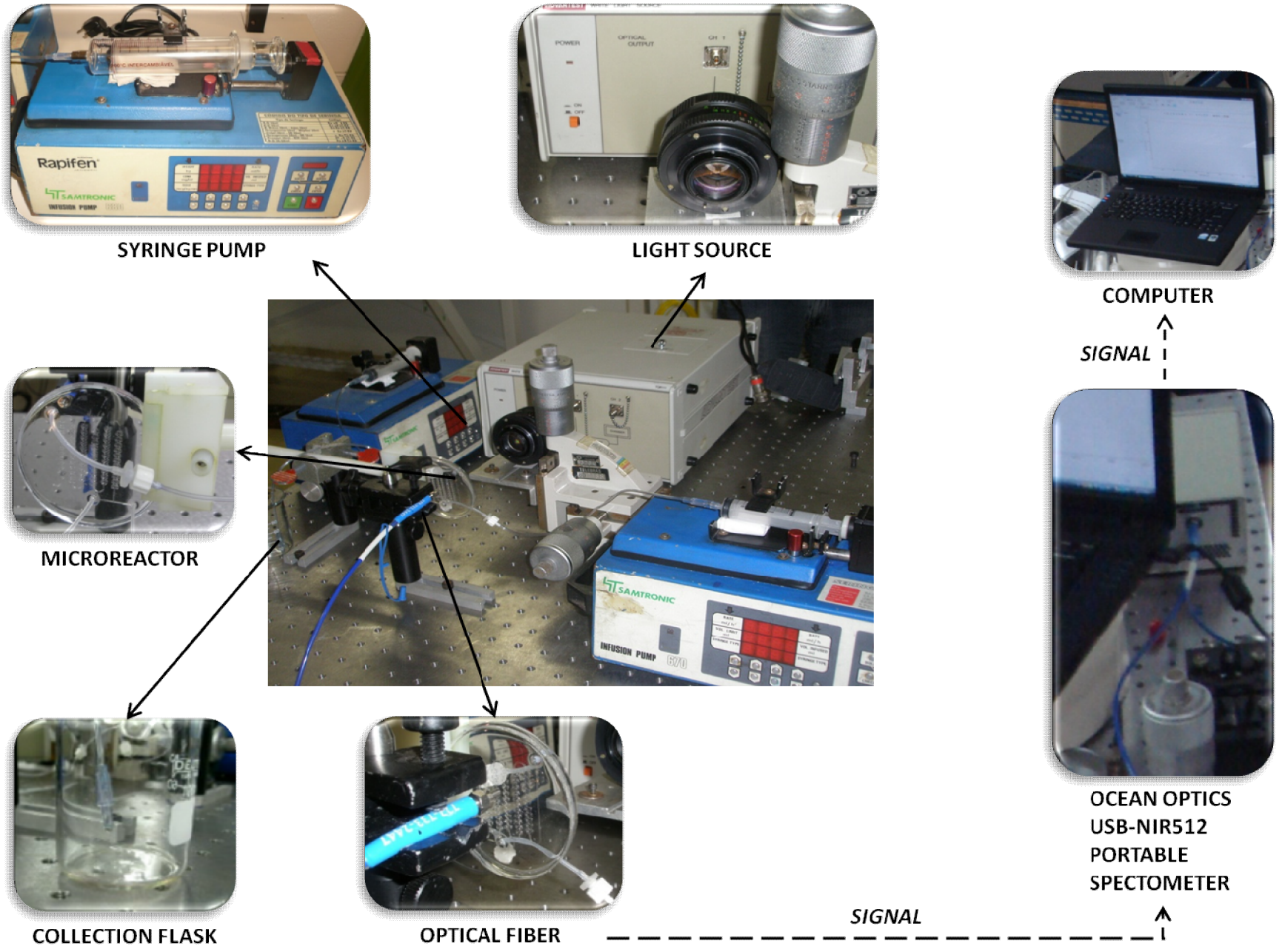

Figure 1. Experimental set-up for on-line transesterification process monitoring in a microreactor by near-infrared spectroscopy using fiber-optic device

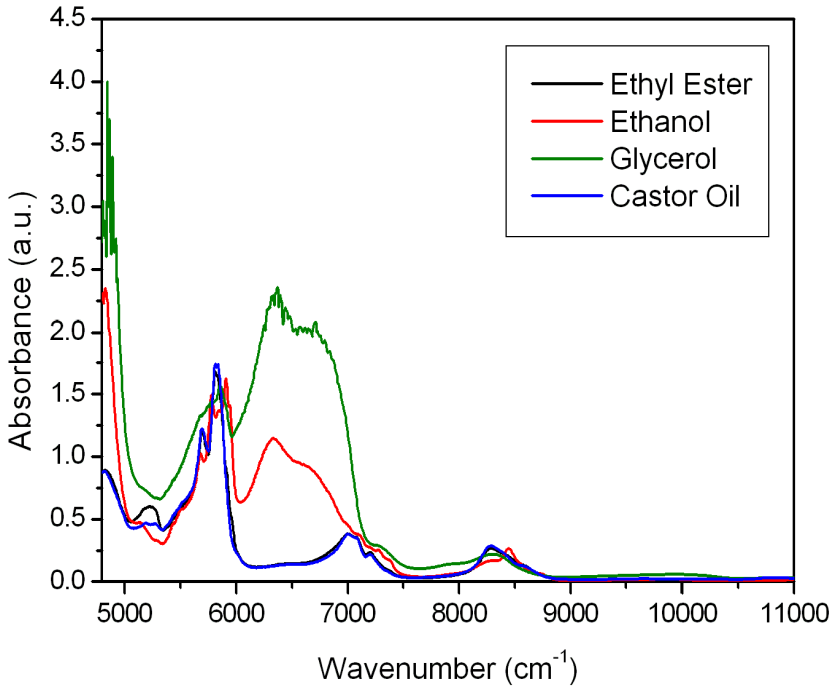

(a)

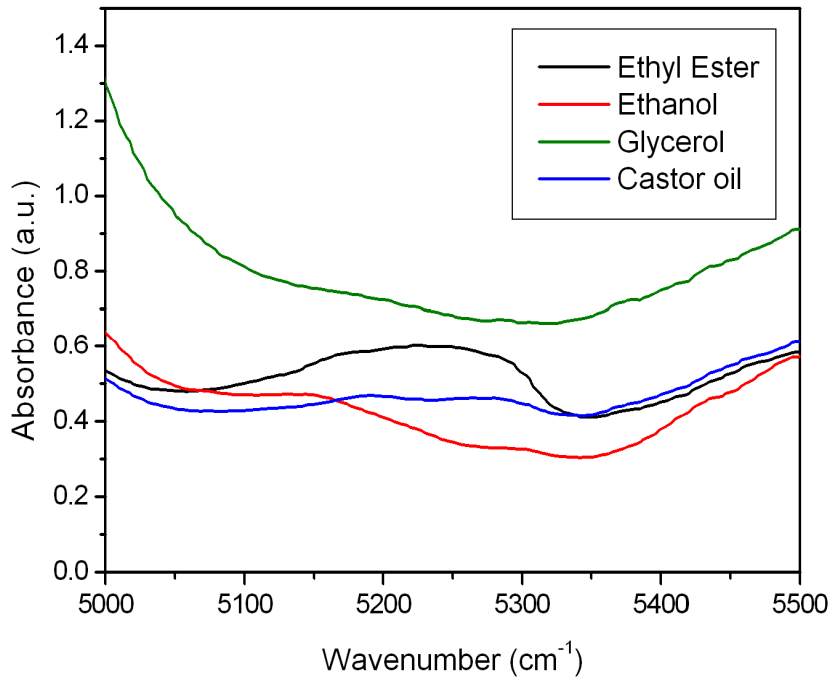

(b)

Figure 2. (a) NIR spectra from 4800 to 11000 cm^{-1} for castor oil, ethanol, glycerol, and ethyl esters; (b) Detail of the spectra in region from 5000 to 5500 cm^{-1}.

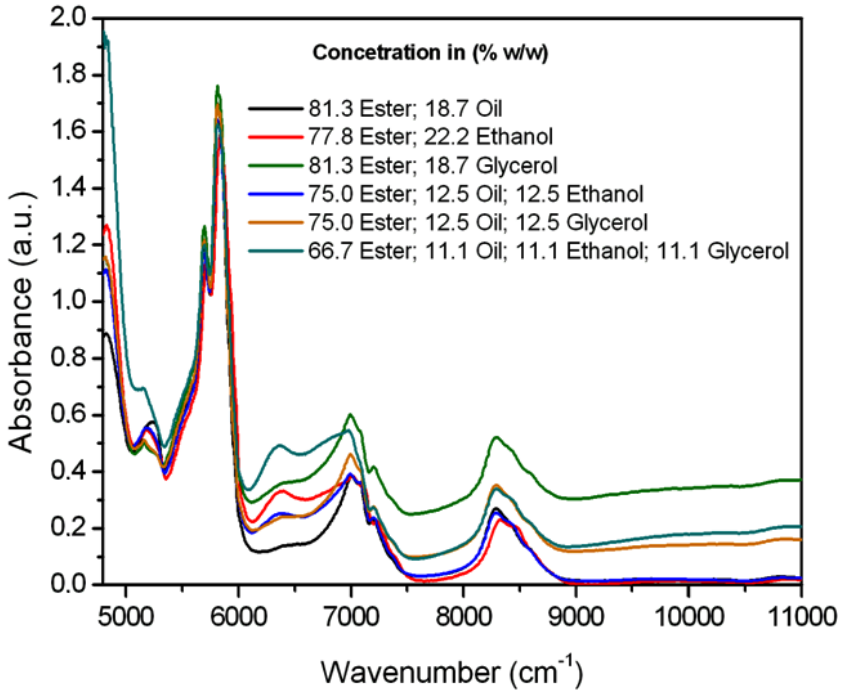

(a)

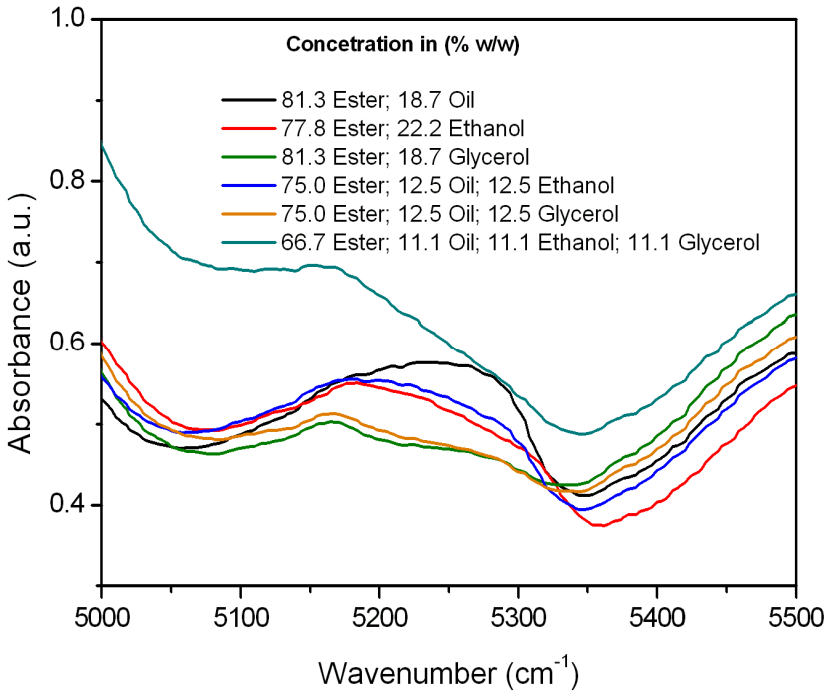

(b)

Figure 3. (a) NIR spectra from 4800 to 11000 cm^{-1} for mixtures of: 81.3%w/w ethyl ester and 18.7%w/w castor oil; 77.8%w/w ethyl ester and 22.2%w/w ethanol; 81.3%w/w ethyl ester and 18.7%w/w glycerol; 75.0%w/w ethyl ester, 12.5%w/w castor oil and 12.5%w/w ethanol; 75.0%w/w ethyl ester, 12.5%w/w castor oil and 12.5%w/w glycerol; 66.7%w/w ethyl ester, 11.1%w/w castor oil, 11.1%w/w ethanol and 11.1%w/w glycerol; (b) Detail of the spectra in region from 5000 to 5500 cm^{-1}.

3.2. On-line monitoring in a microreactors

To study the on-line monitoring of transesterification reaction performed at microreactors, a reaction was conducted at room temperature, using 1.0wt% of NaOH and a volumetric ratio (ethanol:castor oil) of 1.5. Ethanol flow rates ranged from 1.5 to 11.3 mL/h and castor oil flow rates ranged from 1 to 7.5 mL/h. NIR spectra were taken at different times and the results are presented at Figures 4, 5, and 6.

It was observed that it is possible to monitor the transesterification reaction on-line through fiber optic probe. However, the results did not show a constant base line of the NIR spectra due to the inherent continuous process. The baseline is very sensitive to any disturbance of flow inside the microchannel. The baseline variation can lead to problems in considering ethyl esters quantification, once it is done considering the area under the peak, mainly when the concentration of esters is low. Similar results were found by Knothe (1999).

In addition, it was observed that using higher volumetric flow rates produced higher ethyl esters yields. These observations are based on peak areas under the NIR spectra in the range of 5000 and 5500 cm^{-1}. Higher ethyl esters yields are due to the use of higher volumetric flow rates which favor turbulence, decreasing the mass transfer resistance, and contributing to increase biodiesel production.

More studies need to be conducted to improve the baseline stability. Probably the baseline instability is caused by the small optical path traveled by the infrared beam, due to small microreactor dimensions. One possibility that can be explored is to measure the concentration of esters out of the microchannels. It can be done increasing the diameter of the channel where the infrared beam focuses and consequently, increasing the optical way of infrared beam.

Besides the challenges involving the continuous online monitoring of biodiesel production still, this methodology appears as an attractive analytical technique to monitor the reactions in microreactors and to be used in control of portable plants because of its low cost, simplicity, and less time consuming.

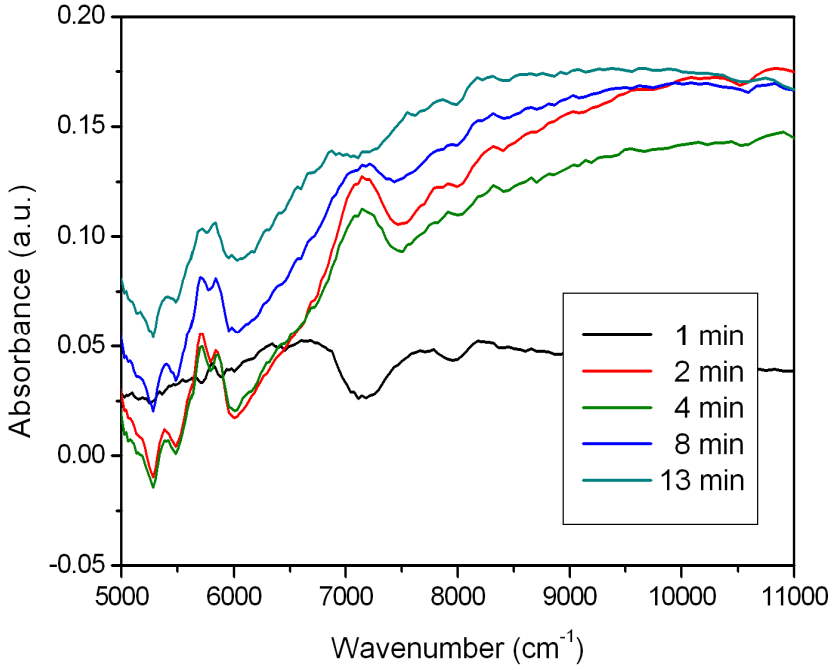

(a)

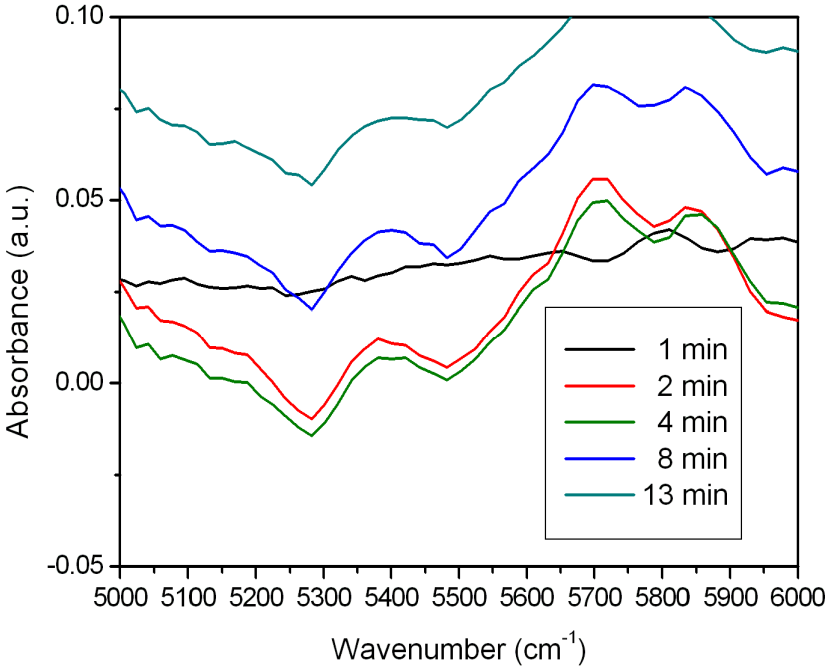

(b)

Figure 4. (a) NIR spectra from 5000 to 11000 cm^{-1} from on-line transesterification monitoring in the microreactor at different times for a volumetric rate 1.5 and 1.0 mL/h for ethanol and castor oil respectively, catalyst amount 1.0 wt.% based on castor oil weight and room temperature; (b) Detail of the spectra in region from 5000 to 5500 cm^{-1}.

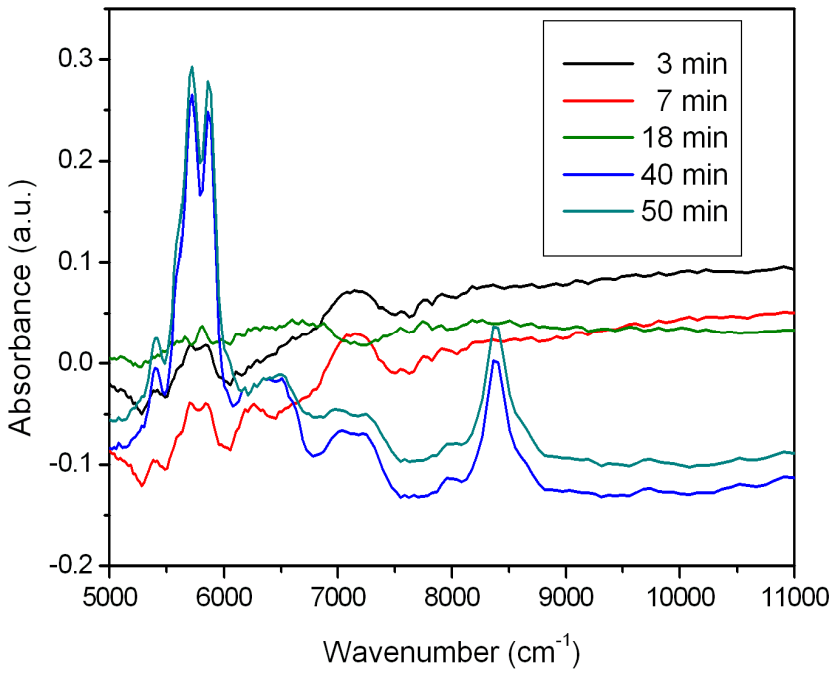

(a)

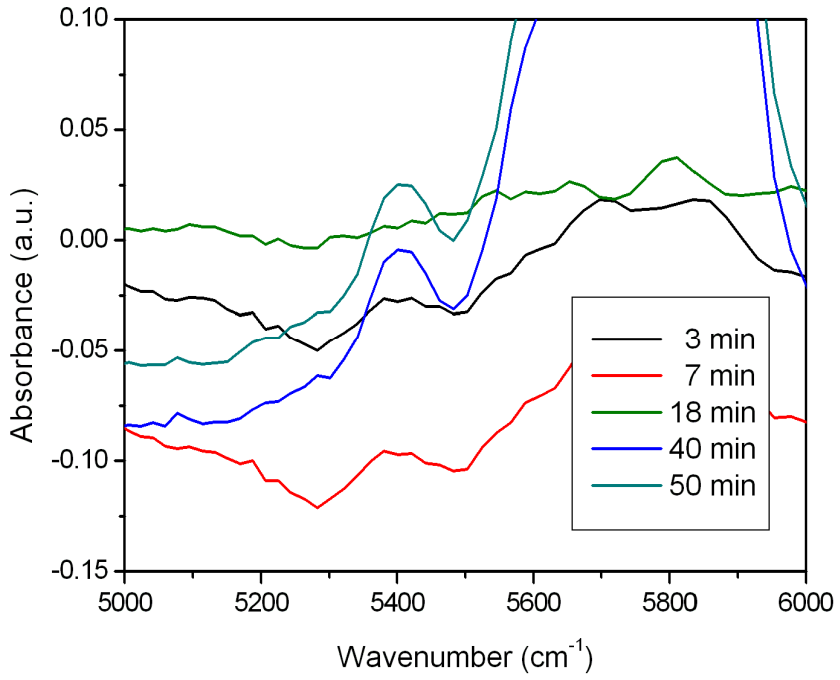

(b)

Figure 5. (a) NIR spectra from 5000 to 11000 cm^{-1} from on-line transesterification monitoring in the microreactor at different times for a volumetric rate 4.5 and 3.0 mL/h for ethanol and castor oil respectively, catalyst amount 1.0 wt.% based on castor oil weight and room temperature; (b) Detail of the spectra in region from 5000 to 5500 cm^{-1}.

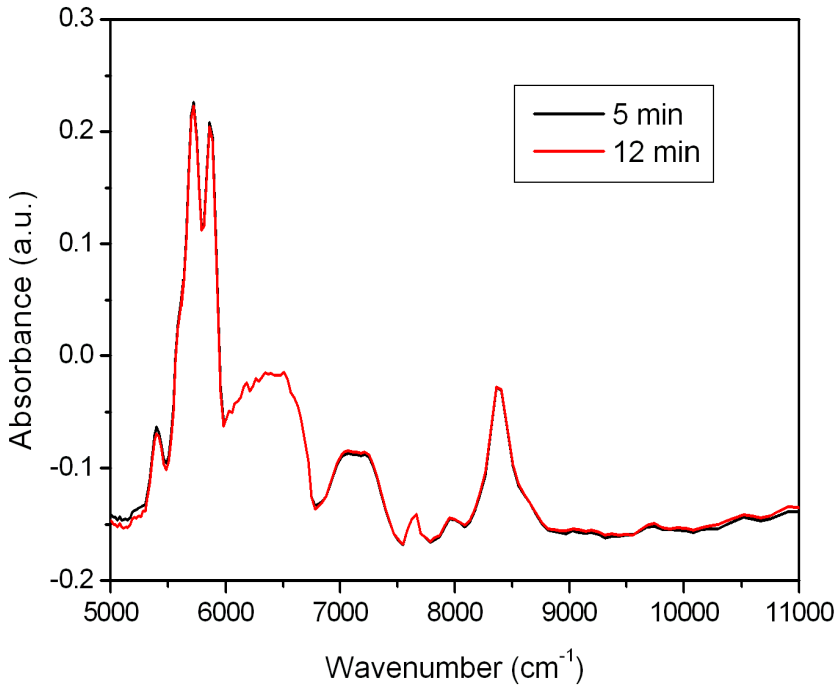

(a)

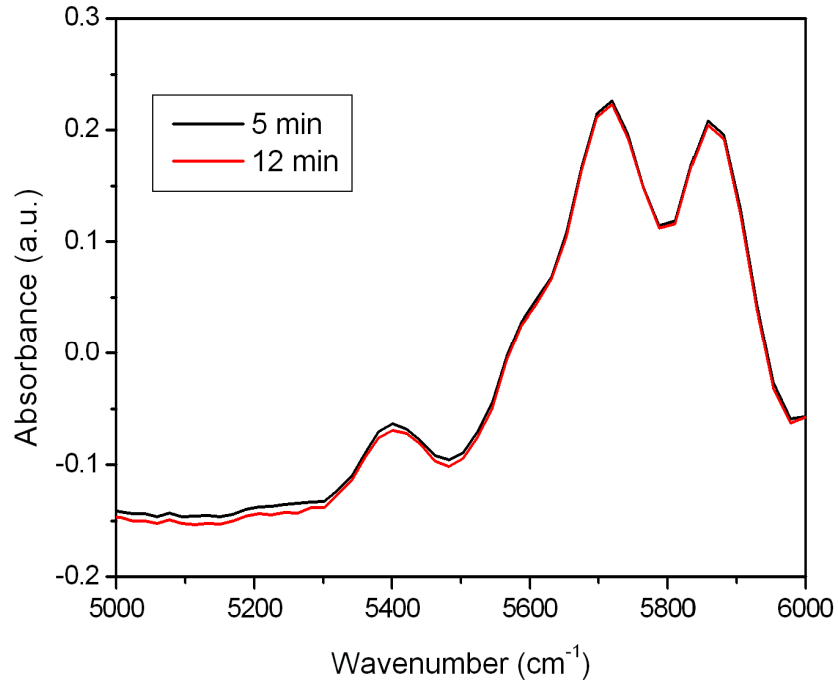

(b)

Figure 6. (a) NIR spectra from 5000 to 11000 cm^{-1} from on-line transesterification monitoring in the microreactor at different times for a volumetric rate 11.3 and 7.5 mL/h for ethanol and castor oil respectively, catalyst amount 1.0 wt.% based on castor oil weight and room temperature; (b) Detail of the spectra in region from 5000 to 5500 cm^{-1}.

4. Conclusions

Ethyl esters showed a characteristic absorbance at 5000-5500 cm^{-1}. This characteristic can be use to perform the quantification analysis of the transesterification reaction using castor oil and ethanol.

Higher ethyl esters yields was observed with the use of higher volumetric flow rates, which favor turbulence, decreasing the mass transfer resistance, and contributing to increase biodiesel production.

However, the on line monitoring of microreactors showed baseline instability and more studies should be performed to try to improve the baseline stability in order to quantify the esters concentration. Possibly baseline instability is caused by the small optical path traveled by the infrared beam, due to small microreactor dimensions. The increasing of infrared beam optical path can be made by increasing the diameter of the channel where the infrared beam focuses.

Acknowledgements

The author gratefully acknowledges the financial support provided by The Scientific Research Foundation for the State of São Paulo (FAPESP) and research support by The Brazilian Synchrotron Light Laboratory (LNLS).

Bibliography

Bezerra de Lira, L. F.; Cruz de Vasconcelos, F. V.; Pereira, C. F.; Paim, A. P. S.; Stragevitch, L.; Pimentel, M. F. Prediction of Properties of Diesel/Biodiesel Blends by Infrared Spectroscopy and Multivariable Calibration, Fuel, 89 (2010), 405-409.

Chuck, C. J.; Bannister, C. D.; Hawley, J. G.; Davidson, M. G. Spectroscopic sensor techniques applicable to real-time biodiesel determination, Fuel, 89 (2010), 457-461.

Dube, M. A.; Zheng, S.; McLean, D. D.; Kates, M. Comparison of attenuated total reflectance-FTIR spectroscopy and GPC for monitoring biodiesel production, Journal of the American Oil Chemists' Society, 81 (2004), 599-603.

Knothe, G. Rapid monitoring of transesterification and accessing biodiesel fuel quality by near-infrared spectroscopy using a fibre optic probe, Journal of the American Oil Chemists' Society, 76 (1999),795-800.

Knothe, G. Analyzing Biodiesel: Standards and Other Methods, Journal of the American Oil Chemists' Society, 83 (2006), 823-833.

Knothe G. Monitoring a progressing transesterification reaction by fiber-optic near infrared spectroscopy with correlation to ^{1}H nuclear magnetic resonance spectroscopy, Journal of the American Oil Chemists' Society, 77 (2000), 489-93.

Meher, L.C.; Vidya Sagar, D.; Naik S.N. Technical aspects of biodiesel production by transesterification – a review, Renewable and Sustainable Energy Reviews, 10 (2006), 248–268.

Pimentel, M. F.; Ribeiro, G. M. G. S.; da Cruz, R. S.; Stragevitch, L.; Pacheco Filho, J. G. A.; Teixeira, L. S. G. Determination of Biodiesel Content when Blended with Mineral Diesel Fuel Using Infrared Spectroscopy and Multivariate Calibration, Microchemical Journal, 82 (2006), 201-206.

Sato, T. Application of Near Infrared Spectroscopy for the Analysis of Fatty Acid Composition, Lipid Technology, 9 (1997), 46-49.

Sadeghi-Jorabchi, H.; Wood, V.M.E.; Jeffery, F.; Bruster Davies, A.; Loh, N.; Coombs, D. Estimation of Biodiesel in Lubricating Oil Using Fourier Transform Infrared Spectroscopy Combined with a Mid-Infrared Fiber-Optic Probe, Spectroscopy Europe, 6 (1994), 16-21.

9.3. Conclusões

Os ésteres etílicos apresentaram uma absorbância característica a 5000-5500 cm^{-1}. Esta absorbância característica pode ser utilizada para realizar a quantificação da reação de transesterificação usando óleo de mamona e etanol.

Altos rendimentos de etil ésteres foram obtidos com o uso de maiores vazões de fluxo volumétrico, o que favorece a turbulência, diminuindo a resistência a transferência de massa, e contribuindo para o aumento da produção de biodiesel.

Entretanto, o monitoramento *on-line* de microreatores revelou instabilidade na linha base. Portanto, mais estudos devem ser realizados para tentar aumentar a estabilidade da linha base, e assim, permitir que a concentração de etil ésteres seja medida. Possivelmente a instabilidade da linha base é causada pelo pequeno caminho óptico percorrido pelo feixe de raios infravermelhos, devido às reduzidas dimensões dos microreatores. O aumento do caminho ótico percorrido pelo feixe de raios infravermelhos pode ser realizado através do aumento do diâmetro do canal onde o feixe de infravermelho incide.

Apesar dos desafios que envolvem o monitoramento *on-line* da produção contínua de biodiesel ainda permanecerem, esta metodologia aparece como uma técnica analítica promissora para monitorar reações em microreatores e para ser usada no controle de plantas portáteis devido ao seu baixo custo, simplicidade, e rapidez.

Capítulo 10.

Conclusões e Sugestões de Trabalhos Futuros

10.1. Conclusões

Neste projeto de investigação foi apresentada uma breve revisão bibliográfica dos principais conceitos envolvidos na intensificação de processos, tecnologia de microreação e produção de biodiesel. Pode ser visto que a miniaturização traz fundamentais vantagens nos dispositivos de reação e análise. Com a diminuição das dimensões lineares, os gradientes e, portanto, as forças condutoras de transferência de massa e energia aumentam por unidade de volume, o que conduz a curtos tempos de reação e mais simples processos de controle. Devido à intensificação das propriedades de transporte e a diminuição do "*hold up*" nos microreatores, uma variedade de condições podem ser aplicadas, as quais não podem ser realizadas nos reatores convencionais. Além disso, a aplicação de micromisturadores favorece a mistura em sistemas multifásicos já que é diminuído o caminho difusional das moléculas permitindo uma interação maior entre as fases. Como resultado, as condições de reação podem ser manipuladas numa ampla faixa de operação, dificilmente conseguidas com equipamentos de laboratório ou plantas de produção convencionais.

Recentemente, uma crescente atenção vem sendo dada ao desenvolvimento de microreatores para a produção de biodiesel e os resultados mostram estes como um promissor método de reação, devido à grande intensificação da transferência de massa e energia e à maior relação área superficial–volume, o que conduz a um maior rendimento da reação em tempos mais curtos e espaços reduzidos. Os largos tempos de reação para atingir altas conversões no processo convencional têm sido atribuídos à grande resistência difusiva entre as fases para a formação do biodiesel. Portanto, maiores conversões são atingidas no microreator, onde a difusão se converte numa resistência menos significante para a reação.

Espera-se assim, que com o estudo destes sistemas de microreação, no futuro possam-se substituir as custosas e ineficientes usinas por plantas de menores, menos custosas, mais eficientes, promovendo assim uma maior segurança e um melhor controle dos processos (Figura 10.1).

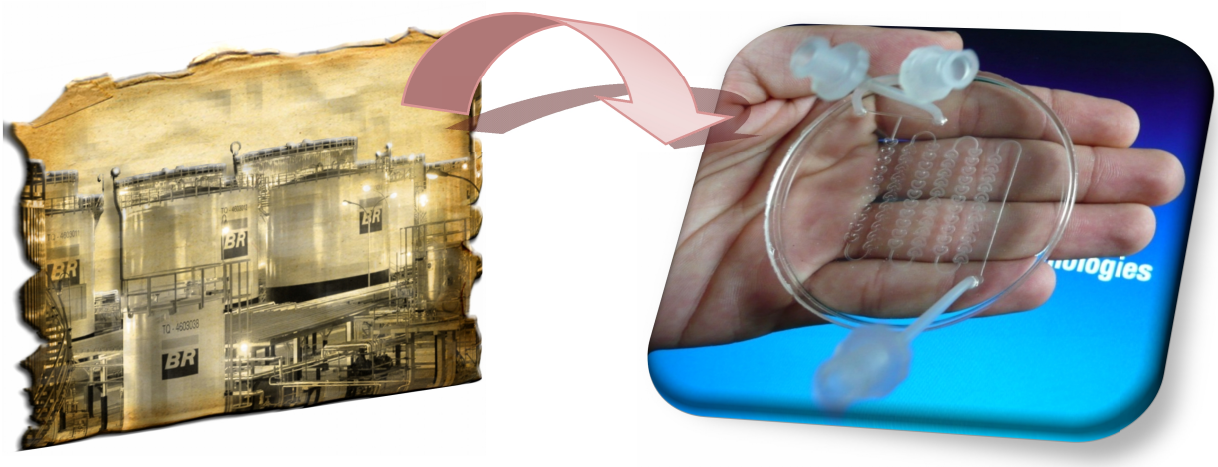

Figura 10.1. Representação das vantagens na intensificação dos processos mediante o desenvolvimento de microreatores.

Como parte da avaliação da eficiência do novo processo proposto, a caracterização físico-química da matéria prima utilizada na reação é importante. Porém, no estudo das propriedades do óleo de mamona encontrou-se que a viscosidade do óleo apresentou uma diminuição exponencial com o incremento da temperatura. Este comportamento mostra o significativo ganho na energia requerida no bombeamento do óleo a elevadas temperaturas já que um aumento da temperatura de 20 a 100°C, a viscosidade do óleo de mamona cai ao redor de 40 vezes. Por outro lado, a correlação empírica de Andrade descreveu satisfatoriamente a variação da viscosidade com a temperatura, sendo o erro padrão (SEE) da estimativa ao redor de 0.1%.

O perfil de decomposição térmica do óleo de mamona apresentou três eventos de decomposição, entre 300-405°C atribuído à decomposição dos ácidos graxos poliinsaturados, entre 405-420°C atribuído à decomposição dos ácidos graxos monoinsaturados e na faixa de 420-500°C atribuído à decomposição térmica dos ácidos graxos saturados.

Na realização da reação de transesterificação do óleo de mamona com etanol em presença de NaOH como catalisador, observou-se que o aumento da temperatura resulta num aumento na taxa de reação e num menor tempo para atingir a conversão de equilíbrio. Um efeito menos significativo foi observado a temperaturas maiores de 50°C o que produz só um pequeno aumento da conversão. Uma variação de temperatura de 50C° para 70C° provocou um aumento na conversão de 0,6% em 10 minutos de reação e de 0.2% em 60 minutos de reação. Este comportamento é devido à maior solubilidade do óleo de mamona

em álcool a temperatura ambiente em comparação com outros óleos vegetais. Portanto, o aumento de temperatura não contribui no aumento da solubilidade entre o óleo de mamona e o etanol.

Nos ensaios em que foram utilizados uma razão molar etanol:óleo de mamona de 6:1 até 12:1, verificou-se um aumento da conversão com o tempo de reação. Além disso, foi observado que a reação atinge a estabilidade em conversões inferiores às obtidas em 30 minutos de reação. Verificou-se também um aumento da conversão com o aumento da razão molar etanol:óleo de mamona para a mesma concentração de catalisador e temperatura. Foi verificado uma conversão de 87,92, 95,39 e 98,13% para razão molar álcool:óleo de 6:1, 9:1 e 12:1, respectivamente, num tempo de reação de 5 min.

O aumento da concentração de catalisador de 0,5% para 1,0% provocou um considerável aumento na conversão. Por outro lado, um aumento da concentração de catalisador de 1,0% para 1,5% não ocasiona um grande aumento na conversão. Além disso, a evolução da seletividade dos produtos da reação com o tempo foi afetada pela concentração de catalisador. Uma maior seletividade foi observada para os diglicerideos e monoglicerideos durante os primeiros minutos da reação com uma menor concentração de catalisador. Conforme avança a reação, a seletividade dos diglicerideos e monoglicerideos cai, sendo favorecida então a seletividade da glicerina.

O método analítico, baseado na cromatografia de exclusão por tamanho, foi utilizado para a determinação simultânea das concentrações dos diversos compostos envolvidos na reação de transesterificação do óleo de mamona. Este método mostrou-se de fácil execução, robusto, relativamente rápido e fornece resultados precisos e reprodutíveis.

A modelagem cinética e a análise do mecanismo de reação do óleo de mamona e etanol em presença de NaOH como catalisador em um reator batelada foi realizada entre 30-70°C. Além disso, um procedimento sistemático confiável para a obtenção dos parâmetros cinéticos da reação foi proposto.

A transesterificação do óleo de mamona ocorreu a uma taxa de reação alta onde a concentração de ésteres etílicos foram de 2,05 mol/L (94,6%), 2,11 mol/L (96,6%) e 2,14 mol/L (97,1%) a temperaturas de 30, 50 e 70°C, respectivamente, após 10 minutos de reação com uma razão molar etanol/óleo de 6:1, 0,5% de NaOH em peso de óleo. Em geral, na reação de transesterificação ocorre a formação de um sistema bifásico, já que os

reagentes, álcool o óleo vegetal, não são miscíveis. A imiscibilidade entre os reagentes diminui o contato entre os reagentes e, conseqüentemente, a conversão da reação. No entanto, o óleo de mamona e seus derivados apresentam maior solubilidade em álcool do que outros óleos vegetais devido à presença de um grupo hidroxila no carbono 12, o que leva a um aumento da transferência de massa na reação e, portanto, na conversão de éster.

O processo para a estimativa das constantes cinéticas da reação, mediante a integração de dois algoritmos de otimização, a saber, o algoritmo genético para a estimativa do chute inicial que é usado pelo método do Levenberg-Maquard para otimização final, mostrou um bom desempenho na otimização da função multivariável com um custo computacional relativamente baixo. Os resultados mostraram boa concordância entre os dados experimentais e os calculados, indicando que o modelo de segunda ordem, apresentado neste trabalho, descreveu adequadamente o avanço da reação.

Além disso, nas temperaturas de 30 e 50°C a $k_{DG\text{-}MG}$ *(k4)* e $k_{MG\text{-}G}$ (*k6*) foram superiores a $k_{TG\text{-}DG}$ (*k2*), o qual indica que a primeira etapa da reação foi a etapa limitante na reação global, enquanto que a altas temperaturas como 70°C a constante da taxa de reação $k_{MG\text{-}G}$ (*k6*) apresentou um valor inferior a $k_{TG\text{-}DG}$ (*k2*) e $k_{DG\text{-}MG}$ (*k4*). Este comportamento pode ser atribuído ao aumento da solubilidade do óleo vegetal no álcool com o aumento da temperatura. Além disso, as constantes de taxa de reação direta mostraram serem maiores que as constantes de taxa inversas para todas as temperaturas estudadas. Pode ser visto também, que a saponificação dos ésteres etílicos é mais lenta do que os glicerídeos, ilustrado pelas constantes de taxa de reação $k_{E\text{-}A}$ (*k8*), $k_{TG\text{-}A}$ (*k9*), $k_{DG\text{-}A}$ (*k10*) e $k_{MG\text{-}A}$ (*k11*). Isto significa que a maior parte do sabão formado (A) na produção de biodiesel a partir do óleo de mamona e etanol com NaOH como catalisador é causado pela hidrólise dos TG, DG e MG.

Os valores de energia de ativação para a reação de etanólise indicaram que a temperaturas elevadas é favorecido o consumo de TG e DG (para a reação DG↔TG e MG↔DG os valores da *Ea* para a reação direta são maiores que os valores correspondentes da reação inversa). Também é favorecida a formação de MG (para MG ↔ G o valor da Ea para a reação direta é menor que a Ea da reação inversa).

No entanto, algumas diferenças nos valores preditos pelo modelo para os dados experimentais não usados na otimização dos parâmetros cinéticos, foram encontradas. Estas

discrepâncias foram atribuídas ao fato que o modelo não toma em conta a heterogeneidade da mistura da reação. Contudo, o modelo poderia ajudar a otimizar o processo atual de produção de biodiesel, por exemplo, na escolha do tempo de reação ideal para uma temperatura particular, ou bem, para definir estratégias operacionais a fim de se obter no processo alto rendimento.

No processo de fabricação dos microreatores, a fotoresina SU-8 foi avaliada como material para a construção de microreatores mediante litografia UV. O aparecimento de trincas, baixa adesão, dilatação, inchação, delaminação e colapso das estruturas foram observados e atribuídos ao alto nível de stress do resiste induzido pelo processo. As possíveis causas e soluções foram discutidas em detalhe. Uma técnica simples para a selagem dos microcanais, a qual usa um delgado filme de SU-8 como adesivo, foi utilizado. O processo se mostrou simples e rápido, sem a necessidade de equipamento especial. A resistência mecânica da selagem para aplicações de microfluídica foi satisfatória, já que vazamentos não foram observados. Além disso, a obstrução dos microcanais devido ao possível escoamento do fotoresiste SU-8 para dentro dos microcanais durante a selagem não foi observado.

A litografia macia foi usada como método alternativo para a fabricação de microreatores. Neste processo, moldes de SU-8 com dimensões de 500 µm de altura e diferentes geometrias foram obtidos. Os dispositivos finais feitos de PDMS foram replicados com êxito a partir do molde fabricado onde estruturas com paredes verticais e livres de bolhas de ar foram apresentadas.

Em comparação com a fotolitografia do SU-8, a litografia macia apresenta uma grande vantagem, já que vários dispositivos podem ser produzidos rapidamente a partir de um único molde com o uso mínimo de equipamentos especializados de sala limpa, resultando em microreatores com idêntica geometria e dimensões, facilitando a reprodução dos experimentos.

Na tabela 10.1, apresenta-se uma comparação dos materiais, equipamentos e tempo aproximado de processamento entre a fotolitografia usando SU-8 e a litografia macia para a construção dos microreatores utilizados neste trabalho. Como pode ser visto a litografia macia requer um mínimo de equipamentos especializados e substâncias envolvidas, assim como um menor tempo de processamento.

Tabela 10.1. Comparação entre os métodos de microfabricação: Fotolitografia SU-8 vs. Litografia macia.

Processo	Fotolitografia	Litografia Macia
Materiais	Fotorresiste Revelador Substratos Solventes Mascaras	PDMS Agente de cura Moldes
Equipamentos	Sala limpa Spinner Chapas de aquecimento Perfilômetro Microscópio ótico Fotoalinhadora	Chapas de aquecimento Câmera de vácuo
Tempo	≈ 10 h	≈ 4 h

Um posterior estudo da eficiência de mistura dos microreatores construídos foi realizado para o sistema óleo de mamona - etanol. A partir dos resultados obtidos puderam-se identificar dois padrões de fluxo, tais como: fluxo paralelo nos microreatores T e Omega e um padrão de fluxo "sanduíche" no final do canal no microreator Tesla. Isto foi causado pela configuração geométrica dos microcanais, demonstrando a importância do estudo de geometria para um ótimo contato entre os fluidos.

Os testes de visualização mostraram uma melhoria no mecanismo de mistura nos microreatores com geometrias mais complexas. Além do mais, com aumento do número de Reynolds a mistura também foi favorecida, principalmente pelo aumento das forças de cisalhamento e fluxos caóticos dentro dos microdispositivos. As simulações CFD mostraram boa concordância com as tendências da mistura obtidas nos experimentos com o óleo de mamona e etanol com corante.

As observações colorimétricas realizadas permitiram identificar os padrões de fluxo da mistura etanol/óleo de mamona com dispositivos simples, econômicos e de forma rápida, já que exigiu apenas alguns microlitros de solução, sem necessidade de qualquer equipamento fluorescente convencionalmente usado neste tipo de análise.

No estudo da síntese contínua de biodiesel foram utilizados três microreatores com diferentes geometrias. A influência dos parâmetros de processo como a geometria do microreator, massa de catalisador, temperatura de reação, razão molar etanol/óleo de mamona e o tempo de residência foram estudados. Foi verificado que o rendimento da reação de síntese do biodiesel se mostrou dependente da geometria do microreator, sendo que o microreator Tesla apresentou o maior rendimento da reação em comparação aos

microreatores T e Omega. A alta eficiência da reação para o microreator Tesla foi atribuída à geometria dos microcanais que proporciona a intensificação da transferência de massa entre os reagentes.

Além disso, foi encontrado que o rendimento para o microreator Omega e Tesla, após um tempo de retenção de 15 min, foi em torno de 1,2 vezes maior do que para o microreator T. É importante notar que a reação de transesterificação é controlada pela difusão devido à imiscibilidade dos óleos vegetais com o álcool. Portanto, pode-se dizer que a obtenção dos melhores rendimentos da reação nos microreatores Tesla e Omega, empregados neste trabalho, é devido à mistura convectiva gerada pelas geometrias internas dos microcanais em comparação com o microreactor T, no qual a mistura ocorre mediante a difusão molecular das substâncias. Por outro lado, a utilização dos microdispositivos permitiu um bom controle dos parâmetros do processo, devido aos pequenos volumes manipulados e à diminuição do caminho molecular entre as substâncias o que contribuem para o aumento das taxas de reação.

O rendimento do éster etílico atingiu um valor de 75,9%, 91,4% e 93,7% para o microreator T, Omega e Tesla, respectivamente, após um tempo de residência de 15 min. Pode ser visto que, com o aumento do tempo de residência, a produção éster etílico também aumenta. Apesar disso, uma leve diminuição da produção de biodiesel para tempos de residência prolongados também foi observado. Possivelmente essa diminuição é resultante da reação de saponificação com NaOH. O tempo de residência nos microreatores foi ajustado mediante a variação do fluxo de entrada, porém, um maior tempo de reação corresponde a uma menor velocidade média dentro dos microcanais, o que diminui a transferência de massa e, conseqüentemente, reduz o rendimento da reação.

O aumento da concentração de catalisador de 0,5% a 1,5% levou a um aumento do rendimento da reação para todos os microreatores estudados. O rendimento passou de 50,6% para 79,1% no caso do microreator T, de 54,3% para 96,2% no microreator Omega e de 56,3% para 98,9% para o microreator Tesla. Esses dados correspondem a um tempo de residência de 10 min, uma razão molar de etanol/óleo de 9:1, e uma temperatura de 50 °C.

Para avaliar o efeito da temperatura sobre a produção de biodiesel foram realizados ensaios entre 30-70°C. Os resultados mostraram que a produção de biodiesel aumentou com o aumento da temperatura. Nesta faixa de temperatura, o rendimento de ésteres etílicos

passou de 67,3% para 89,0% no caso do microreator T, de 73,9% para 92,2% no caso de microreator Omega, e de 75,9% para 92,6% para o microreator Tesla. Além disso, quando a razão molar de etanol/óleo foi aumentada de 9:1 para 12:1 a 50°C, a produção de ésteres etílicos aumentou em torno de 1,1 vezes. A produção de ésteres etílicos de 93,5%, 95,3% e 96,7% foi obtida para os microreatores T, Omega e Tesla, respectivamente, com um tempo de residência de 10 min, uma razão molar etanol/óleo de 25:1, uma massa de catalisador de 1,0 wt.%, e uma temperatura de 50°C.

Comparando-se os rendimentos obtidos nos microreatores com o reator batelada de bancada, encontrou-se que seriam necessários 843 microreatores para obtenção da mesma quantidade de biodiesel produzido no reator em batelada (Figura 10.2). Contudo, o volume ocupado por estes microreatores resulta ser bastante menor o que resulta numa redução substancial do capital investido em edificações, estruturas de suporte de equipamentos, montagem e instrumentação.

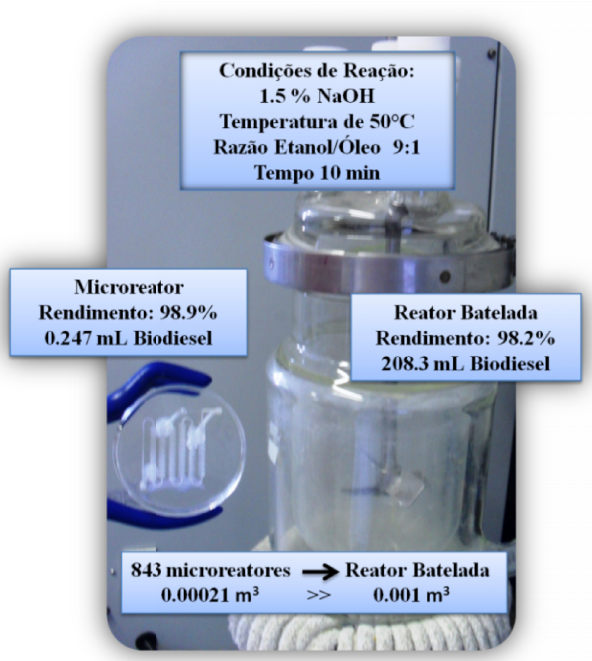

Figura 10.2. Comparação dos microreatores e o reator em batelada para a produção de biodiesel a partir do óleo de mamona e etanol com NaOH como catalisador.

A comparação dos microreatores com o reator batelada de bancada mostrou também que o rendimento da reação foi inferior quando esta foi realizada nos microreatores. O menor rendimento obtido nos microreatores foi atribuído à adesão do catalisador (NaOH) às paredes dos microcanais. Desse modo, houve a perda do catalisador da massa reacional e, portanto, o rendimento da reação nos microreatores diminuiu. Além

disso, foi observado que as geometrias dos microcanais foram danificadas pela deposição de partículas de catalisador, mostrando que microreatores feitos de polidimetilsiloxano (PDMS) não podem ser usados para reações de transesterificação prolongadas.

Na avaliação do monitoramento *on-line* da reação mediante o uso de espectroscopia no infravermelho próximo e uma fibra ótica, os ésteres etílicos apresentaram uma absorbância característica a um número de onda entre 5000-5500 cm^{-1}. Esta característica pode ser utilizada para realizar a quantificação da reação de transesterificação usando óleo de mamona e etanol.

O monitoramento da reação *on-line* permitiu observar que altos rendimentos de etil ésteres foram obtidos com o uso de maiores vazões de fluxo volumétrico, o que favorece a turbulência, diminui a resistência a transferência de massa, e contribui para o aumento da produção de biodiesel. Entretanto, o monitoramento *on-line* de microreatores revelou instabilidade na linha base. Possivelmente a instabilidade da linha base foi causada pelo pequeno caminho óptico percorrido pelo feixe de raios infravermelhos, devido às reduzidas dimensões dos microreatores. O aumento do caminho ótico percorrido pelo feixe de raios infravermelhos pode ser realizado através do aumento do diâmetro do canal onde o feixe de infravermelho incide, como apresentado na Figura 10.3.

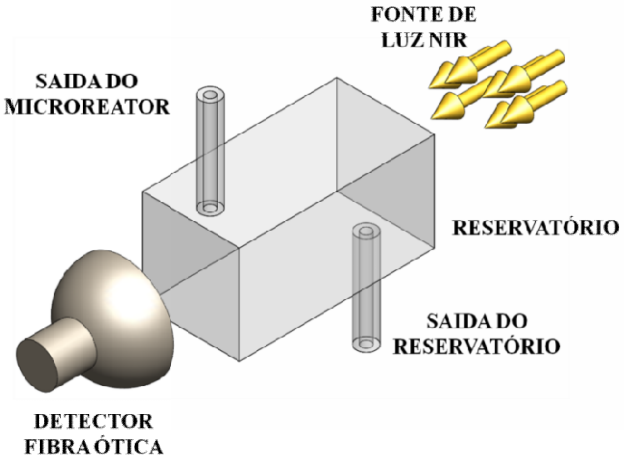

Figura 10.3. Reservatório para o monitoramento on-line da reação de transesterificação em microreatores mediante infravermelho próximo.

Apesar dos desafios que envolvem o monitoramento *on-line* da produção contínua de biodiesel ainda permanecerem, esta metodologia ainda é considerada como uma técnica analítica promissora para monitorar reações em microreatores e para ser usada no controle de plantas portáteis devido ao seu baixo custo, simplicidade, e rapidez.

10.2. Sugestão para Trabalhos Futuros

Com o desenvolvimento desta dissertação, grandes avanços no entendimento da aplicação de intensificação de processos mediante a utilização de microreatores foram realizados. No entanto, estudos ainda precisam ser realizados com o intuito de viabilizar o processo e projetar novas plantas miniaturizadas para a produção de biodiesel no futuro. A seguir são apresentadas algumas sugestões para trabalhos futuros:

- Estudar a mudança da densidade do meio reativo, o qual foi observado durante a realização das reações de transesterificação. Este fato é de importância para o desenvolvimento de processos contínuos os quais envolvem reatores tubulares, onde a mudança de densidade é refletida no rendimento do reator.
- Estender o modelo cinético a fim de se avaliar o efeito da presença de ácidos graxos livres nos óleos vegetais e gorduras animais. Isto, pelo fato que a presença dos ácidos graxos livres reagem com o íon hidroxila do catalisador básico, resultando na produção de sabão e água (reação de saponificação), o que leva a um maior consumo do catalisador e à diminuição do rendimento da reação.
- Explorar outros materiais como metal, vidro, e outros polímeros na construção dos microreatores, uma vez que o PDMS não pode ser utilizado por tempos prolongados nas reações de transesterificação.
- Avaliar a construção de microdispositivos mediante tecnologias novas tais como a prototipagem rápida, já que este tem se mostrado como um processo rápido, de custo relativamente baixo e com a possibilidade de detectar possíveis erros antes da construção destes.
- Projetar uma mini-planta compacta para o processamento de biocombustíveis através do acoplamento de diversos microreactores em série e/ou paralelo**.**
- Aprofundar os estudos para viabilizar o monitoramento *on-line* da reação de transesterificação em microreatores. Estes estudos devem contemplar a estabilização da linha base do espectro de infravermelho. Para isso pode-se utilizar um reservatório após a saída do microreator. Esse reservatório deve possuir diâmetro maior do que os apresentados pelos microcanais para aumentar o caminho óptico do feixe de raios infravermelhos. Neste caso, o feixe infravermelho incidiria sobre o reservatório ao invés de incidir sobre o microcanal.